



THE HONG KONG
POLYTECHNIC UNIVERSITY

香港理工大學

Pao Yue-kong Library

包玉剛圖書館

Copyright Undertaking

This thesis is protected by copyright, with all rights reserved.

By reading and using the thesis, the reader understands and agrees to the following terms:

1. The reader will abide by the rules and legal ordinances governing copyright regarding the use of the thesis.
2. The reader will use the thesis for the purpose of research or private study only and not for distribution or further reproduction or any other purpose.
3. The reader agrees to indemnify and hold the University harmless from and against any loss, damage, cost, liability or expenses arising from copyright infringement or unauthorized usage.

IMPORTANT

If you have reasons to believe that any materials in this thesis are deemed not suitable to be distributed in this form, or a copyright owner having difficulty with the material being included in our database, please contact lbsys@polyu.edu.hk providing details. The Library will look into your claim and consider taking remedial action upon receipt of the written requests.

**NONCLASSICAL RUTHENIUM SILYL DIHYDRIDE
COMPLEXES AND THEIR CATALYTIC ACTIVITIES.
CATALYTIC REACTIONS WITH ELECTROPHILIC
BIPYRIDINE RUTHENIUM COMPLEXES**

LEE TING YAN

Ph.D

The Hong Kong Polytechnic University

2011

The Hong Kong Polytechnic University

Department of Applied Biology and Chemical Technology

**Nonclassical Ruthenium Silyl Dihydride Complexes and
their Catalytic Activities. Catalytic Reactions with
Electrophilic Bipyridine Ruthenium Complexes**

By

Ting-Yan LEE

A Thesis Submitted in Partial Fulfillment of the Requirements for the
Degree of Doctor of Philosophy

January, 2011

Declaration

I hereby declare that this thesis is my own work and that, to the best of my knowledge and belief, it reproduces no material previously published or written, nor material that has been accepted for the award of any other degree or diploma, except where due acknowledgement has been made in the text.

Ting-Yan LEE

January, 2011

Abstract of thesis entitled “Nonclassical Ruthenium Silyl Dihydride Complexes and their Catalytic Activities. Catalytic Reactions with Electrophilic Bipyridine Ruthenium Complexes”

Submitted by Ting-Yan LEE

for the degree of doctor of philosophy

at The Hong Polytechnic University

in January, 2011

Abstract

The X-ray crystallographic study showed that it is more appropriate to describe the ruthenium-silane complexes $\text{TpRu}(\text{PPh}_3)_2\text{H}_2\text{SiR}_3$ as $\text{TpRu}(\text{PPh}_3)(\eta^3\text{-HSiR}_3\text{H})$, a static structure containing $\text{H}\cdots\text{Si}\cdots\text{H}$ bonding rather than a highly fluxional pair of σ -silane hydride species $\text{TpRu}(\text{PPh}_3)(\text{H}_a)(\eta^2\text{-H}_b\text{SiR}_3\text{H}) \rightleftharpoons \text{TpRu}(\text{PPh}_3)(\text{H}_b)(\eta^2\text{-H}_a\text{SiR}_3\text{H})$. One of the complexes, $\text{TpRu}(\text{PPh}_3)(\eta^3\text{-HSiPhMe}_2\text{H})$, was used for the catalytic hydrolytic oxidation of organosilanes to silanols. A mechanism, which does not involve the usual oxidative addition of silane to the metal center to form the silyl hydride species, is proposed; it is supported by theoretical calculations.

The ruthenium-silane complex $\text{TpRu}(\text{PPh}_3)(\eta^3\text{-HSiPhMe}_2\text{H})$ was also found to effect catalytic reduction of carbon dioxide by PhMe_2SiH to give methoxide as the ultimate reduction product. Proton NMR study of the reaction revealed that various reduced products of carbon dioxide including formoxysilane, bis(silyl)acetal, and silyl methoxide were formed during the course of the catalysis, the identities of which were further confirmed by ^{13}C NMR through the use of $^{13}\text{CO}_2$. Concurrent ^{31}P NMR monitoring indicated that the starting complex was first converted to the carbonyl-hydride species $\text{TpRu}(\text{PPh}_3)(\text{CO})\text{H}$, probably due to decarbonylation of the

initially formed formoxysilane. The carbonyl-hydride complex was then partially converted to a new species, which we suspect to be the formate complex $\text{TpRu}(\text{PPh}_3)(\text{CO})(\eta^1\text{-OCHO})$ generated by protonation of the hydride complex by formic acid in the reaction. Slow formation of the dicarbonyl-hydride complex $\text{TpRu}(\text{CO})_2\text{H}$ from the formate complex was observed at the latter stage of the monitoring experiment. A mechanism for the reduction of carbon dioxide to the various silicon-containing products was proposed after taking into consideration the NMR monitoring results.

The air stable, dicationic bipyridine ruthenium diaquo complex $\text{cis-}[\text{Ru}(6,6'\text{-Cl}_2\text{bpy})_2(\text{H}_2\text{O})_2](\text{OTf})_2$ was found to be an efficient catalyst for the β -alkylation of secondary alcohols with primary alcohols. On the other hand, the dimethyl analog $\text{cis-}[\text{Ru}(6,6'\text{-Me}_2\text{bpy})_2(\text{H}_2\text{O})_2](\text{OTf})_2$ was found to be an efficient catalyst for the transfer hydrogenation of carbonyl compounds with 1,4-butanediol. The diol, acting as both solvent and hydrogen donor, was converted to the more thermodynamically stable γ -butyrolactone upon its release of hydrogen. For each catalytic reaction a mechanistic pathway was proposed. It should be noted that both catalytic systems are insensitive to oxygen and therefore do not require the use of nitrogen or argon atmosphere for protection.

Publications

Cheung, H. W., Lee, T. Y., Lui, H. Y., Yeung, C. H., and Lau, C. P., Ruthenium-Catalyzed β -alkylation of Secondary Alcohols with Primary Alcohols, *Advanced Synthesis & Catalysis*, **2008**, 250, 2975-2983.

Lee, T. Y., Dang, L., Zhou, Z., Yeung, C. H., Lin, Z., and Lau, C. P., Nonclassical Ruthenium Silyl Dihydride Complexes $\text{TpRu}(\text{PPh}_3)(\eta^3\text{-HSiR}_3\text{H})$ (Tp = Hydrotris(pyrazolyl)borate). Catalytic Hydrolytic Oxidation of Organosilanes to Silanols with $\text{TpRu}(\text{PPh}_3)(\eta^3\text{-HSiR}_3\text{H})$, *European Journal of Inorganic Chemistry*, **2010**, 5675-5684.

Lee, T. Y., Yeung, C. H., and Lau, C. P., Ruthenium-Catalyzed Transfer Hydrogenation of Aldehydes and Ketones in 1,4-Butanediol, *12th Belgian Organic Synthesis Symposium, Namur, Belgium*, **2010**, pp P219.

Lee, T. Y., Dang, L., Zhou, Z., Yeung, C. H., Lin, Z., and Lau, C. P., Nonclassical Ruthenium Silyl Dihydride Complexes $\text{TpRu}(\text{PPh}_3)(\eta^3\text{-HSiR}_3\text{H})$ (Tp = Hydrotris(pyrazolyl)borate). Catalytic Hydrolytic Oxidation of Organosilanes to Silanols with $\text{TpRu}(\text{PPh}_3)(\eta^3\text{-HSiR}_3\text{H})$, *17th Symposium on Chemistry Postgraduate*

Research in Hong Kong, **2010**, pp I-49.

Lee, T. Y., Yeung, C. H., and Lau, C. P., Ruthenium-Catalyzed Transfer Hydrogenation of Aldehydes and Ketones in 1,4-Butanediol, *16th Symposium on Chemistry Postgraduate Research in Hong Kong*, **2009**, pp I-87.

Lee, T. Y., Yeung, C. H., and Lau, C. P., Ruthenium-Catalyzed Electrophilic β -alkylation of Secondary Alcohols with Primary Alcohols under Air, *15th Symposium on Chemistry Postgraduate Research in Hong Kong*, **2008**, pp I-59.

Ng, S. M., Lee, T. Y., Yeung, C. H., Lau, C. P., Catalytic Hydrolysis of Hydrosilanes by Tris(pyrazolyl)borate Ruthenium Complexes, *15th Symposium on Chemistry Postgraduate Research in Hong Kong*, **2008**, pp I-64.

Acknowledgements

I would like to express my deepest gratitude to my supervisor Prof. C. P. Lau for his invaluable advice, guidance, and patience throughout the course of my research study.

His smart and creative idea and enthusiasm in research have inspired me and enriched my logical thinking in my work. He has also given lots of distinctive and perceptive comments and views to my work and also my thesis. I was very delighted to be supervised by him. Working with him and his research group would be a truly beneficial and unforgettable experience in my life.

I would also like to thank to my co-supervisor Dr. C. H. Yeung, a man of everything, for his kind advice and opinion to my research work. His sharing of working experience with me is especially precious.

It is also my pleasure to say thank you to Prof. Z. Zhou for resolving the molecular structures of some new compounds by X-ray crystallography.

Special thanks are given to Prof. Z. Lin and his research group in the Department of Chemistry, The Hong Kong University of Science and Technology, for their support on theoretical calculations.

I am also indebted to my friends and colleagues, Dr. C. W. Leung, Dr. H. W. Cheung, Dr. W. N. Sit, Dr. P. Liu, and Mr. S. M. Ng, all of whom have made valuable opinion and advice making my study more smooth and pleasant. Special thanks are also given to Dr. C. M. So and Dr. K. C. Cheung, who shared their skilful experiences on chemical syntheses with me.

I would also like to show my appreciation to the staff of the Chemical Technology Section of the Department of Applied Biology and Chemical Technology, The Hong Kong Polytechnic University, for their assistance throughout my research study. In particular, thanks Mr. W. K. Kwan and Dr. S. C. Yan for their assistance in my NMR experiments, and Mr. Y. K. Au and Dr. P. K. So for their help in performing the MS experiments. Also acknowledged is the Research Degree Committee of The Hong Kong Polytechnic University for awarding a studentship and a grant for my conference presentation in the 12th Belgian Organic Synthesis Symposium (BOSSXII) held in Namur, Belgium on 11-16th July 2010.

Finally, may I also express my heartfelt thanks to my family and friends for their love and endless support, especially my beloved wife, Miss Rachel Leung, for her concern, appreciation, and support in my postgraduate study.

Table of Contents

	Page
Abstract	iii
Publications	v
Acknowledgements	vii
Table of Contents	ix
List of Figures	xiii
List of Tables	xvi
List of Schemes	xvii
Abbreviations	xix
Chapter 1	
Introduction	1
1.1 Activation of Hydrosilanes by transition metal complexes	1
1.1.1 Non-classical σ -silane complexes	1
1.1.2 Multicenter Si \cdots H interactions in Silyl Polyhydride Complexes	3
1.1.3 Catalytic processes involving silane complexes	7
1.2 Hydrolytic Hydrosilane oxidation to silanol	13
1.3 Carbon Dioxide Reduction by Silane	17
1.4 Electrophilic Transition-metal Complexes for catalytic Reactions	26
1.5 Activation of Alcohols via Borrowing Hydrogen Methodology	27
1.5.1 β -Functionalization of Alcohols	30
1.6 Transfer Hydrogenation of Carbonyl Compounds	36
1.6.1 Mechanisms of Transition-metal Catalyzed Transfer Hydrogenation	36
1.6.2 Choices of Hydrogen Donors	41

Chapter 2

Nonclassical Ruthenium Silyl Dihydride Complexes $\text{TpRu}(\text{PPh}_3)(\eta^3\text{-HSiR}_3\text{H})$ (Tp = Hydrotris(pyrazolyl)borate). Catalytic Hydrolytic Oxidation of Organosilanes to Silanols with $\text{TpRu}(\text{PPh}_3)(\eta^3\text{-HSiR}_3\text{H})$

2.1	Introduction	43
2.2	Experimental Section	
2.2.1	Materials and Instrumentation	44
2.2.2	Syntheses and Reactions	45
2.2.2.1	Synthesis of $\text{TpRu}(\text{PPh}_3)(\eta^3\text{-HSiPh}_2\text{MeH})\text{-1b}$	45
2.2.2.2	Synthesis of $\text{TpRu}(\text{PPh}_3)(\eta^3\text{-HSiPhMe}_2\text{H})\text{-1c}$	46
2.2.2.3	General Procedures for the Hydrolysis of Silanes Catalyzed by $\text{TpRu}(\text{PPh}_3)(\eta^3\text{-HSiPhMe}_2\text{H})\text{-1c}$	47
2.2.2.4	Monitoring of 1c -Catalyzed Hydrolytic Oxidation of PhMe_2SiH to PhMe_2SiOH with NMR spectroscopy	48
2.2.2.5	Monitoring of the Reaction Between 1c and EtMe_2SiH	48
2.2.2.6	Crystallographic Structure Analysis of $\text{TpRu}(\text{PPh}_3)(\eta^3\text{-HSiPh}_3\text{H})\text{-1a}$, $\text{TpRu}(\text{PPh}_3)(\eta^3\text{-HSiPh}_2\text{MeH})\text{-1b}$, and $\text{TpRu}(\text{PPh}_3)(\eta^3\text{-HSiPhMe}_2\text{H})\cdot 3\text{CH}_2\text{Cl}_2\text{-1c}$	49
2.2.2.7	Computational Details	50
2.3	Results and Discussion	51
2.3.1	Synthesis and X-ray Crystallographic Study of $\text{TpRu}(\text{PPh}_3)\text{H}_2\text{SiR}_3$	51
2.3.2	Catalytic hydrolytic oxidation of organosilanes to silanols with $\text{TpRu}(\text{PPh}_3)(\eta^3\text{-HSiPhMe}_2\text{H})$ (1c)	63
2.3.3	NMR monitoring of the 1c -catalyzed hydrolytic oxidation of PhMe_2SiH to PhMe_2SiOH	65
2.3.4	Relative stability of $\text{TpRu}(\text{PPh}_3)(\eta^3\text{-HSiPhMe}_2\text{H})\text{-1c}$ and $\text{TpRu}(\text{PPh}_3)(\eta^3\text{-HSiEtMe}_2\text{H})\text{-1d}$	67
2.3.5	Proposed mechanism for the catalytic hydrolytic oxidation of silanes to silanols	68

Chapter 3

Ruthenium-catalyzed Reduction of Carbon Dioxide by Hydrosilanes

3.1	Introduction	76
3.2	Experimental Section	79
3.2.1	Materials and Instrumentation	
3.2.2	Reactions	80
3.2.2.1	NMR Monitoring of the Reaction between CO ₂ and TpRu(PPh ₃)(η ³ -HSiPhMe ₂ H)- 1c in 1,4-dioxane- <i>d</i> ₈	80
3.2.2.2	NMR Monitoring of the Reaction between CO ₂ and PhMe ₂ SiH in the presence of TpRu(PPh ₃)(η ³ -HSiPhMe ₂ H)- 1c in 1,4-dioxane- <i>d</i> ₈	80
3.2.2.3	In Situ Preparation of TpRu(PPh ₃)(CO)(η ¹ -OCHO)- 6	80
3.3	Results and Discussion	82
3.3.1	NMR Monitoring of the reaction between TpRu(PPh ₃)(η ³ -HSiPhMe ₂ H)- 1c and CO ₂ in 1,4-dioxane- <i>d</i> ₈	82
3.3.2	NMR Monitoring of the Catalytic Reduction of CO ₂ by PhMe ₂ SiH with 1c	90
3.3.3	Suggested Mechanism of Formoxysilane Reduction	98

Chapter 4

Electrophilic Ruthenium-complexes-catalyzed β-Alkylation of Secondary Alcohols with Primary Alcohols and Transfer Hydrogenation of Carbonyl Compounds with 1,4-Butanediol

4.1	Introduction	104
4.2	Experimental Section	105
4.2.1	Materials and Instrumentation	105
4.2.2	Reactions	106
4.2.2.1	General Procedure for catalytic β-Alkylation of Secondary Alcohols with Primary Alcohols	106
4.2.2.2	3-(2-methoxyphenyl)-1-phenylpropan-1-ol	107
4.2.2.3	3-(3,4-dimethoxyphenyl)-1-phenylpropan-1-ol	107
4.2.2.4	3-(4-fluorophenyl)-1-phenylpropan-1-ol	108
4.2.2.5	1-cyclohexyl-1-phenylpropan-1-ol	108

4.2.2.6	3-(furan-2-yl)-1-phenylpropan-1-ol	108
4.2.2.7	1-phenyl-(3-thiophen-2-yl)-propan-1-ol	108
4.2.2.8	General Procedures for the transfer hydrogenation of ketones and aldehydes with 1,4-butanediol	110
4.3	Results and Discussion	111
4.3.1	β -Alkylation of Secondary Alcohols with Primary Alcohols catalyzed by <i>cis</i> -[Ru(6,6'-Cl ₂ bpy) ₂ (H ₂ O) ₂](OTf) ₂ - 10	111
4.3.2	Transfer Hydrogenation of Aldehydes and Ketones with 1,4-Butanediol Catalyzed by <i>cis</i> -[Ru(6,6'-Me ₂ bpy) ₂ (H ₂ O) ₂](OTf) ₂ - 11	118
Chapter 5		
Conclusion		125
Appendices		128
Reference		163

List of Figures

		Page
Figure 1.1	Dewar–Chatt–Duncanson model for Si···H···M bonding	3
Figure 1.2	Traditional methods for the syntheses of silanols from hydrosilanes	14
Figure 2.1	ORTEP view (30% probability) of $\text{TpRu}(\text{PPh}_3)(\eta^3\text{-HSiPh}_3\text{H})\text{-1a}$ showing the atom-labeling scheme.	54
Figure 2.2	ORTEP view (30% probability) of $\text{TpRu}(\text{PPh}_3)(\eta^3\text{-HSiPh}_2\text{MeH})\text{-1b}$ showing the atom-labeling scheme.	55
Figure 2.3	ORTEP view (30% probability) of $\text{TpRu}(\text{PPh}_3)(\eta^3\text{-HSiPhMe}_2\text{H})\text{-1c}$ showing the atom-labeling scheme.	56
Figure 2.4	NMR study of 1c -catalyzed hydrolysis of PhMe_2SiH to PhMe_2SiOH	66
Figure 2.5	Energy profile calculated for the hydrolysis reaction of HSiHMe_2 catalyzed by $\text{TpRu}(\text{PMe}_3)(\eta^3\text{-HSiHMe}_2\text{H})$ (1A). The calculated relative electronic energies are given in kJ/mol.	72
Figure 2.6	Optimized structures for the species involved in the hydrolysis reaction of HSiHMe_2 catalyzed by $\text{TpRu}(\text{PMe}_3)(\eta^3\text{-HSiHMe}_2\text{H})$ (1A) (Figure 5). Bond distances are given in angstrom.	73
Figure 2.7	^1H NMR spectrum of $\text{TpRu}(\text{PPh}_3)(\eta^3\text{-HSiPh}_2\text{MeH})\text{-1b}$	128
Figure 2.8	^{13}C NMR spectrum of $\text{TpRu}(\text{PPh}_3)(\eta^3\text{-HSiPh}_2\text{MeH})\text{-1b}$	129
Figure 2.9	^{29}Si NMR spectrum of $\text{TpRu}(\text{PPh}_3)(\eta^3\text{-HSiPh}_2\text{MeH})\text{-1b}$	130
Figure 2.10	^{31}P NMR spectrum of $\text{TpRu}(\text{PPh}_3)(\eta^3\text{-HSiPh}_2\text{MeH})\text{-1b}$	131
Figure 2.11	Infrared spectrum of $\text{TpRu}(\text{PPh}_3)(\eta^3\text{-HSiPh}_2\text{MeH})\text{-1b}$	132
Figure 2.12	^1H NMR spectrum of $\text{TpRu}(\text{PPh}_3)(\eta^3\text{-HSiPhMe}_2\text{H})\text{-1c}$	133
Figure 2.13	^{13}C NMR spectrum of $\text{TpRu}(\text{PPh}_3)(\eta^3\text{-HSiPhMe}_2\text{H})\text{-1c}$	134
Figure 2.14	^{29}Si NMR spectrum of $\text{TpRu}(\text{PPh}_3)(\eta^3\text{-HSiPhMe}_2\text{H})\text{-1c}$	135
Figure 2.15	^{31}P NMR spectrum of $\text{TpRu}(\text{PPh}_3)(\eta^3\text{-HSiPhMe}_2\text{H})\text{-1c}$	136
Figure 2.16	Infrared NMR spectrum of $\text{TpRu}(\text{PPh}_3)(\eta^3\text{-HSiPhMe}_2\text{H})\text{-1c}$	137
Figure 2.17	^1H NMR spectrum of the reaction mixture of 1c -catalyzed hydrolytic oxidation of Ph_3SiH	138
Figure 2.18	^1H NMR spectrum of the reaction mixture of 1c -catalyzed hydrolytic oxidation of Ph_2MeSiH	139

Figure 2.19	^1H NMR spectrum of the reaction mixture of 1c -catalyzed hydrolytic oxidation of PhMe_2SiH	140
Figure 2.20	^1H NMR spectrum of the reaction mixture of 1c -catalyzed hydrolytic oxidation of $^t\text{BuMe}_2\text{SiH}$	141
Figure 2.21	^1H NMR spectrum of the reaction mixture of 1c -catalyzed hydrolytic oxidation of EtMe_2SiH	142
Figure 2.22	^1H NMR spectrum of the reaction mixture of 1c -catalyzed hydrolytic oxidation of CyMe_2SiH	143
Figure 2.23	^1H NMR spectrum of the reaction mixture of 1c -catalyzed hydrolytic oxidation of $\text{CH}_3(\text{CH}_2)_{16}\text{CH}_2\text{Me}_2\text{SiH}$	144
Figure 2.24	^1H NMR spectrum of the reaction mixture of 1c -catalyzed hydrolytic oxidation of Et_3SiH	145
Figure 2.25	^1H NMR spectrum of the reaction mixture of 1c -catalyzed hydrolytic oxidation of Et_2MeSiH	146
Figure 2.26	^1H NMR spectrum of the reaction mixture of 1c -catalyzed hydrolytic oxidation of $1,4\text{-(SiMe}_2\text{H)}_2\text{C}_6\text{H}_4$	147
Figure 2.27	^1H NMR spectrum of the reaction mixture of 1c -catalyzed hydrolytic oxidation of (+)-(R)- $\text{Me}(\alpha\text{-Np})\text{PhSiH}$	148
Figure 3.1	^1H NMR monitoring of the reaction between 1c and carbon dioxide in 1,4-dioxane- d_8	85
Figure 3.2	^{31}P NMR monitoring of the 1c -catalyzed reduction of carbon dioxide by PhMe_2SiH in 1,4-dioxane- d_8	93
Figure 3.3	^1H NMR spectrum of $\text{TpRu}(\text{PPh}_3)(\text{CO})(\eta^1\text{-OCHO})\text{-8}$ in 1:1 formic acid and dioxane.	149
Figure 3.4	^{31}P NMR spectrum of $\text{TpRu}(\text{PPh}_3)(\text{CO})(\eta^1\text{-OCHO})\text{-8}$ in 1:1 formic acid and dioxane.	150
Figure 4.1	^1H NMR spectrum of 3-(2-methoxyphenyl)-1-phenylpropan-1-ol	151
Figure 4.2	^{13}C NMR spectrum of 3-(2-methoxyphenyl)-1-phenylpropan-1-ol	152
Figure 4.3	^1H NMR spectrum of 3-(3,4-dimethoxyphenyl)-1-phenylpropan-1-ol	153
Figure 4.4	^{13}C NMR spectrum of 3-(3,4-dimethoxyphenyl)-1-phenylpropan-1-ol	154
Figure 4.5	^1H NMR spectrum of 3-(4-fluorophenyl)-1-phenylpropan-1-ol	155

Figure 4.6	¹³ C NMR spectrum of	156
	3-(4-fluorophenyl)-1-phenylpropan-1-ol	
Figure 4.7	¹ H NMR spectrum of	157
	1-cyclohexyl-1-phenylpropan-1-ol	
Figure 4.8	¹³ C NMR spectrum of	158
	1-cyclohexyl-1-phenylpropan-1-ol	
Figure 4.9	¹ H NMR spectrum of	159
	3-(furan-2-yl)-1-phenylpropan-1-ol	
Figure 4.10	¹³ C NMR spectrum of	160
	3-(furan-2-yl)-1-phenylpropan-1-ol	
Figure 4.11	¹ H NMR spectrum of	161
	1-phenyl-(3-thiophen-2-yl)-propan-1-ol	
Figure 4.12	¹³ C NMR spectrum of	162
	1-phenyl-(3-thiophen-2-yl)-propan-1-ol	

List of Tables

		Page
Table 2.1	Crystal Data and Structure Refinement of $\text{TpRu}(\text{PPh}_3)(\eta^3\text{-HSiPh}_3\text{H})\text{-1a}$	57
Table 2.2	Selected bond Distance (\AA) and Angles ($^\circ$) for $\text{TpRu}(\text{PPh}_3)(\eta^3\text{-HSiPh}_3\text{H})\text{-1a}$	58
Table 2.3	Crystal Data and Structure Refinement of $\text{TpRu}(\text{PPh}_3)(\eta^3\text{-HSiPh}_2\text{MeH})\text{-1b}$	59
Table 2.4	Selected bond Distance (\AA) and Angles ($^\circ$) for $\text{TpRu}(\text{PPh}_3)(\eta^3\text{-HSiPh}_2\text{MeH})\text{-1b}$	60
Table 2.5	Crystal Data and Structure Refinement of $\text{TpRu}(\text{PPh}_3)(\eta^3\text{-HSiPhMe}_2\text{H})\text{-1c}$	61
Table 2.6	Selected bond Distance (\AA) and Angles ($^\circ$) for $\text{TpRu}(\text{PPh}_3)(\eta^3\text{-HSiPhMe}_2\text{H}).3\text{CH}_2\text{Cl}_2\text{-1c}$	62
Table 2.7	Hydrolytic Oxidation of Organosilanes to Silanols with $\text{TpRu}(\text{PPh}_3)(\eta^3\text{-HSiPhMe}_2\text{H})\text{-1c}$	64
Table 3.1	NMR-data of the organic compounds generated in the reaction between CO_2 and PhMe_2SiH in the presence of 1c in 1,4-dioxane- d_8 .	91
Table 4.1	Optimization of β -alkylation of secondary alcohols with primary alcohols	112
Table 4.2	β -alkylation of secondary alcohols with primary alcohols catalyzed by <i>cis</i> - $[\text{Ru}(6,6'\text{-Cl}_2\text{bpy})_2(\text{H}_2\text{O})_2](\text{OTf})_2$ 10	114
Table 4.3	Catalytic transfer hydrogenation of 3-pentanone with 1,4-butanediol	120
Table 4.4	Transfer hydrogenation of carbonyl compounds with 1,4-butanediol catalyzed by <i>cis</i> - $[\text{Ru}(6,6'\text{-Me}_2\text{bpy})_2(\text{H}_2\text{O})_2](\text{OTf})_2$ 11	122

List of Schemes

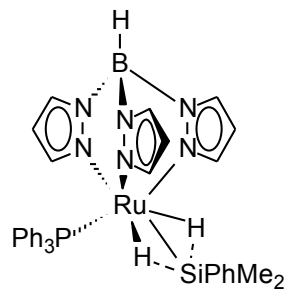
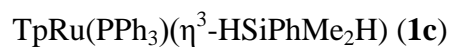
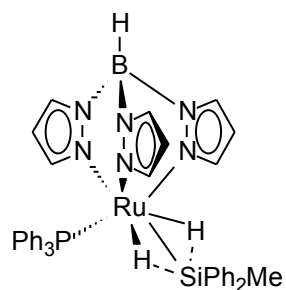
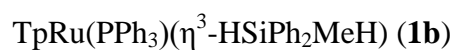
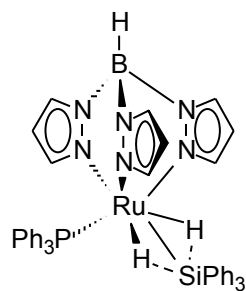
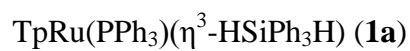
		Page
Scheme 1.1	Mechanism of the $[\text{IrH}_2(\text{S})_2(\text{PPh}_3)_2]\text{SbF}_6$ -catalyzed silane alcoholysis (S = solvent)	8
Scheme 1.2	Proposed mechanism for the iron-catalyzed silane alcoholysis	8
Scheme 1.3	Proposed mechanism for the manganese-catalyzed alcoholysis of HSiEt_3 by phenol	9
Scheme 1.4	Generation of the η^2 -silane complex $\text{RuH}(\eta^2\text{-HSiMe}_2\text{Cl})\{(\eta^3\text{-C}_6\text{H}_8)\text{PCy}_2\}(\text{PCy}_3)$ during ethylene hydrosilylation by HSiMe_2Cl	11
Scheme 1.5	Proposed mechanism for the iridium-catalyzed reduction of alkyl halides by triethylsilane	12
Scheme 1.6	Proposed mechanism for the rhenium-catalyzed hydrolytic oxidation of hydrosilanes to silanols	16
Scheme 1.7	$\text{Ir}(\text{CN})(\text{CO})\text{dppe}$ -catalyzed reduction of carbon dioxide by Me_3SiH	18
Scheme 1.8	Conversion of carbon dioxide to methane catalyzed by zirconium complex	19
Scheme 1.9	Calculated mechanism of the ruthenium-catalyzed hydrosilylation of carbon dioxide	22
Scheme 1.10	Decomposition of bis(silyl)acetal (BSA) to give disiloxane (DSO) and formaldehyde	23
Scheme 1.11	Detailed mechanism for the N-heterocyclic carbene-catalyzed reduction of carbon dioxide by silane.	24
Scheme 1.12	Reduction of carbon dioxide to methane catalyzed by a frustrated acid-base pair $[\text{TMPH}]^+[\text{HB}(\text{C}_6\text{F}_5)_3]^-$	25
Scheme 1.13	Activation of alcohols by borrowing hydrogen methodology	29
Scheme 1.14	Borrowing hydrogen in the β -functionalization of alcohols	31
Scheme 1.15	Carbon-carbon bond formation between two alcohols	32
Scheme 1.16	Proposed mechanism for the $\text{RuCl}_2(\text{DMSO})_4$ -catalyzed β -alkylation of secondary alcohols with primary alcohols	34
Scheme 1.17	Proposed mechanism of the transfer hydrogenation of carbonyl compounds involving a dihydride intermediate	39

Scheme 1.18	Catalytic cycle of (η^6 -arene)RuH((S,S)-H ₂ NCHRCHRNTs) via a concerted six-membered transition state.	40
Scheme 1.19	Lactonization of 1,4-butanediol	42
Scheme 2.1	Attack of water on [H ₂ Si(Me)(α -Np)Ph] ⁻ moiety	69
Scheme 2.2	Proposed mechanism for the hydrolytic oxidation of organosilanes to silanols	70
Scheme 2.3	Alternative mechanism for the hydrolytic oxidation of organosilanes to silanols	75
Scheme 3.1	Proposed mechanism for the TpRu(PPh ₃)(CH ₃ CN)H-catalyzed hydrogenation of carbon dioxide to formic acid	77
Scheme 3.2	Suggested pathway for the reaction between 1c and CO ₂ to give HCOOSiPhMe ₂ .	85
Scheme 3.3	Proposed mechanism for the decarbonylation of aldehyde with TpRu(PPh ₃)(CH ₃ CN)H	87
Scheme 3.4	Proposed mechanism for the decarbonylation of HCOOSiPhMe ₂ by TpRu(PPh ₃)H	87
Scheme 3.5	Sequential reduction of CO ₂ by PhMe ₂ SiH to PhMe ₂ SiOCH ₃	93
Scheme 3.6	Suggested mechanism for the conversion of the carbonyl formate complex 6 to dicarbonyl hydride complex 7 .	96
Scheme 3.7	Suggested mechanism for the 8 -catalyzed reduction of HCOOSiPhMe ₂ to (PhMe ₂ SiO) ₂ CH ₂	98
Scheme 3.8	Suggested mechanism for the 8 -catalyzed reduction of formaldehyde to PhMe ₂ SiOCH ₃	100
Scheme 4.1	Proposed mechanism for the 10 -catalyzed β -alkylation of secondary alcohols with primary alcohols	115
Scheme 4.2	Proposed mechanism for the 11 -catalyzed transfer hydrogenation of carbonyl compounds with 1,4-butanediol	122

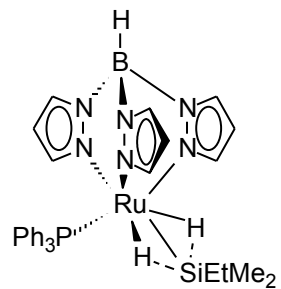
Abbreviations

δ	Chemical shift (NMR)
η	Descriptor for hapticity
μ	Descriptor for bridging
ν	Frequency
e^-	Electron
L	Generalized ligand, in particular a $2e^-$ ligand
L_nM	Generalized metal fragment with n ligands
[]	Encloses complex molecules or ions
ESI-MS	Electrospray ionization mass spectrometry
IR	Infra-red
NMR	Nuclear magnetic resonance
THF	Tetrahydrofuran
MeOH	Methanol
EtOH	Ethanol
DMSO	Dimethylsulfoxide
Tp	Hydrotris(1-pyrazolyl)borate
Cp	Cyclopentadienyl
Cp*	Pentamethylcyclopentadienyl
OTf	Trifluoromethanesulfonate
BAr_F	Tetrakis(pentafluorophenyl)borate
dmp	1,10-dimethylphenanthroline
bpy	2,2'-bipyridine
PPh_3	Triphenylphosphine
PCy_3	Tricyclohexylphosphine
dppm	Bis(diphenylphosphino)methane
dppe	Bis(diphenylphosphino)ethane
COD	1,5-Cyclooctadiene
R	Generalized alkyl group
X	Halogen group
Me	Methyl

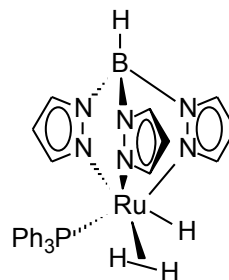
Et	Ethyl
iPr	Isopropyl
tBu	<i>t</i> -Butyl
nBu	<i>n</i> -Butyl
Ph	Phenyl
Np	Naphthyl
s	Singlet
d	Doublet
t	Triplet
q	Quartet
m	Multiplet



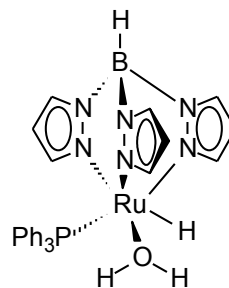
$\text{TpRu}(\text{PPh}_3)(\eta^3\text{-HSiEtMe}_2\text{H})$ (**1d**)



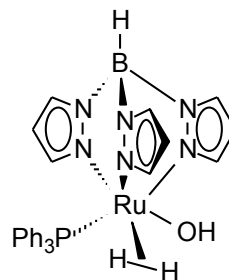
$\text{TpRu}(\text{PPh}_3)(\text{H}_2)\text{H}$ (**2**)



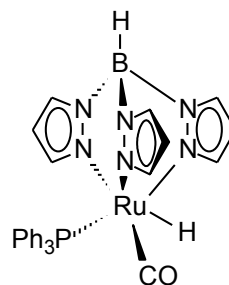
$\text{TpRu}(\text{PPh}_3)(\text{H}_2\text{O})\text{H}$ (**3**)

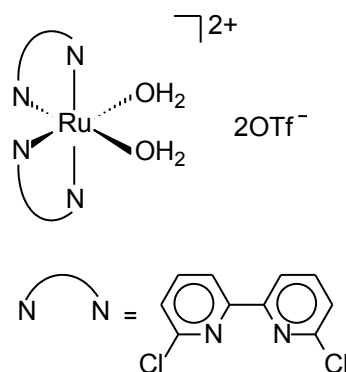
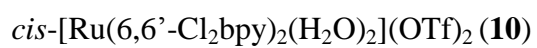
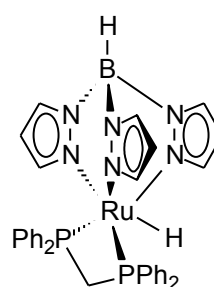
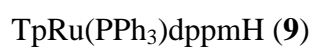
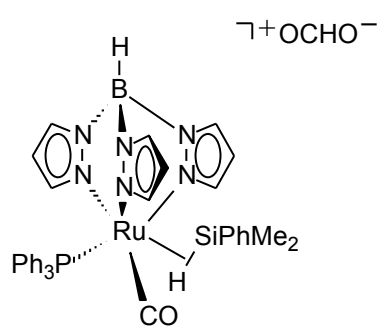
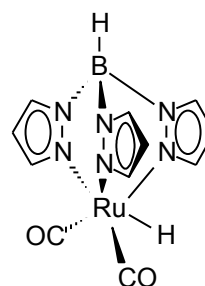
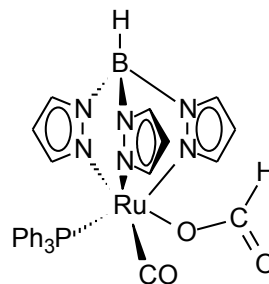


$\text{TpRu}(\text{PPh}_3)(\text{H}_2)\text{OH}$ (**4**)

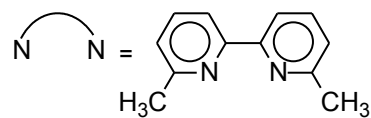
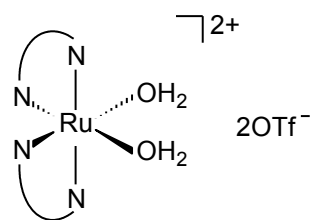


$\text{TpRu}(\text{PPh}_3)(\text{CO})\text{H}$ (**5**)

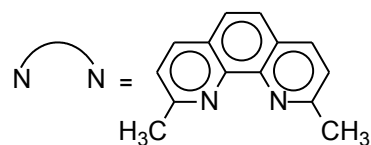
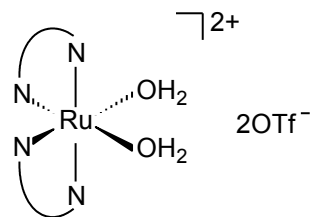




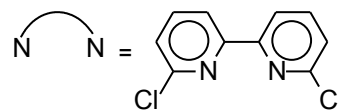
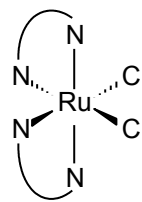
cis-[Ru(6,6'-Me₂bpy)₂(H₂O)₂](OTf)₂ (**11**)



cis-[Ru(2,9-dmp)₂(H₂O)₂](OTf)₂ (**12**)



cis-[Ru(6,6'-Cl₂bpy)₂Cl₂] (**13**)



Chapter 1 Introduction

1.1 Activation of Hydrosilanes by transition metal complexes

1.1.1 Non-classical σ -Silane complexes

Since the discovery of the first transition metal complex incorporating molecular dihydrogen ligand by Kubas *et al.*, there has been an extensively growing interest on the studies of this type of non-classical σ -coordinated compounds [1–4]. As an analogue of dihydrogen, silanes possessing silicon–hydrogen bond (hydrosilanes) are also capable of interacting with transition metal center in a non-classical manner, giving rise to σ -silane complexes (**Chart 1.1**) [5].

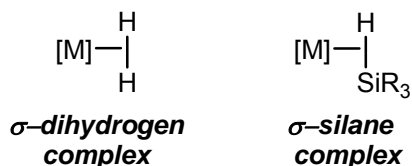


Chart 1.1

Although the bonding mode of both $\text{M}(\eta^2\text{-HSiR}_3)$ and $\text{M}(\eta^2\text{-H}_2)$ moiety can be viewed in terms of the famous Dewar–Chatt–Duncanson model (**Figure 1.1**) [6], the situation regarding the extent of the oxidative addition process is more complex in the former case for 2 major reasons. Firstly, the Si–H bond is more basic than H–H bond, and is thus a better σ -donor; moreover, back donation of electron density from metal is more

prominent in the $M(\eta^2\text{-HSiR}_3)$ moiety since the Si–H bond is also a better π acceptor than the H–H bond. Secondly, the presence of substituents at the silicon center with different steric and electronic properties, a feature not found in hydrogen, has a significant influence on the extent of oxidative addition of Si–H bond to the metal center, directly affecting the resultant strength of Si–H interaction. For these reasons, difficulties are sometimes found in discriminating a σ -silane coordination from a silyl hydride formulation [7]. In fact, the hydrogen atom in a Si–H bond of hydrosilane interacting with a metal center could be regarded as a classical hydride ligand, involved in a σ -coordination, or having a secondary interaction with a silicon atom [8–11] (see next section). X-ray crystallographic analysis and DFT calculations are particularly useful for the assignment of these different bonding modes [8]. For ruthenium complexes, the key parameters thus concerned are not only the Si–H distances, but also the Ru–Si and Ru–H distances. The Ru–Si distance diminishes for a given series of compounds as the extent of activation of the Si–H bond increases. Typically, Si–H distances of 1.7–1.8 Å can reasonably be regarded as involving in σ -bond coordination; those in the range of 1.9–2.0 Å are more controversial.

Values up to 2.4 Å, which is still much shorter than the sum of the van der Waal's radii of Si and H (3.4 Å), indicates a significant Si–H interaction.

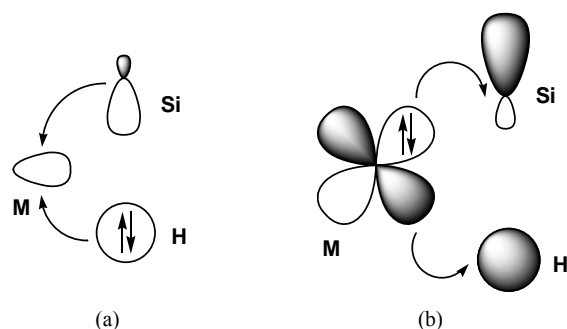


Figure 1.1 Dewar–Chatt–Duncanson model for Si...H...M bonding.

1.1.2 Multicenter Si...H interactions in Silyl Polyhydride Complexes

The term interligand interaction could be applied to complexes that incorporate a supposedly η^2 -silane and one or more *cis*-coordinated hydride ligand, and in fact there is solid evidence for the presence of multiple interligand Si...H interactions in polyhydride trialkyl/aryl silyl complexes. Crabtree and co-worker reported in 1990 the syntheses of the rhenium complexes $\text{Re}(\text{PPh}_3)_2\text{H}_6\text{SiR}_3$ (**Chart 1.2**)

[12]. Although the T_1 relaxation time measured for the hydride ligands gave small values of 76–79 ms (for 259 MHz at 209 K), they rejected the assignment of the complex as having σ -coordinated dihydrogen ligand on the basis of very small isotopic perturbation of resonance. Indeed, Hartree-Fock calculations using the model complexes $\text{Re}(\text{PPh}_3)_2\text{H}_6\text{SiH}_3$ indicated that all the H–H distances between any two *cis*-coordinated hydride ligands fall in nonbonding range (2.083–3.157 Å, 0.82–0.90 Å for σ -dihydrogen ligand). The Re–Si distance in $\text{Re}(\text{PPh}_3)_2\text{H}_6\text{SiR}_3$ was determined to be 2.474 Å. This value is considerably shorter than the sum of covalent radii of the two atoms (2.65 Å). This observation, together with the two short Si–H distances of 1.76 and 1.92 Å in the complex, led to the suggestion of a $\text{Re}(\eta^3\text{-H}_2\text{SiR}_3)$ moiety being present in $\text{Re}(\text{PPh}_3)_2\text{H}_6\text{SiR}_3$. A similar $\eta^3\text{-H}_2\text{SiR}_3$ motif was also found in the related complex $\text{Re}(\text{PPh}_3)_4(\text{CO})\text{H}_2\text{SiR}_3$ (**Chart 1.3**), which shows a rather short Re–Si distance of 2.451(3) Å and two close Si–H interactions [13].

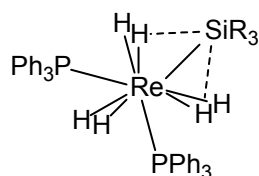


Chart 1.2

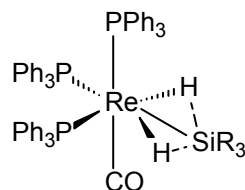


Chart 1.3

In 1999, the research group of Sabo-Etienne and Chaudret reported the synthesis and X-ray characterization of the ruthenium complex $\text{RuH}_2(\eta^2\text{-H}_2)(\eta^2\text{-HSiPh}_3)(\text{PCy}_3)_2$, which was originally formulated as a mixed dihydrogen and silane σ -complex. However, its unusual structural features including the *cis*-orientation of the two bulky phosphine ligand, the close Ru–P bond lengths despite the two phosphines are lying trans to two supposedly different ligands ($\eta^2\text{-HSiPh}_3$ and hydride), and the almost-equivalent bonding of the silicon center to the two hydride units, suggest that a special type of interligand interaction is present in the complex [14]. In a separate

report, Nikonov suggested that the unusual bonding between the silicon and the hydride in $\text{RuH}_2(\eta^2\text{-H}_2)(\eta^2\text{-HSiPh}_3)(\text{PCy}_3)_2$ could be viewed in terms of an interaction between the metal fragment $[(\text{PCy}_3)_2\text{RuH}_2]^+$ and the dihydrosilyl anion $[\text{H}_2\text{SiPh}_3]^-$, resulting in the nonclassical complex $[\eta^2\text{-H}_2](\text{PCy}_3)_2\text{RuH}(\eta^3\text{-H}_2\text{SiR}_3)$ [9] (**Chart 1.4**).

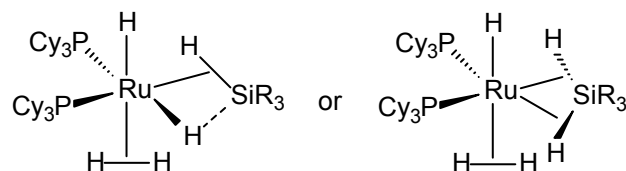


Chart 1.4

More recently, Nikonov and co-workers provided evidence via X-ray and DFT studies for the existence of $\text{H}\cdots\text{Si}\cdots\text{H}$ bonding in the complex resulting from silane activation on the $\text{CpFe}(\text{Pr}^i_2\text{MeP})\text{H}$ moiety (**Chart 1.5**). The compound can reasonably be formulated as $\text{CpFe}(\text{Pr}^i_2\text{MeP})(\eta^3\text{-HSiR}_3\text{H})$ [15].

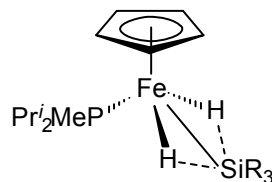
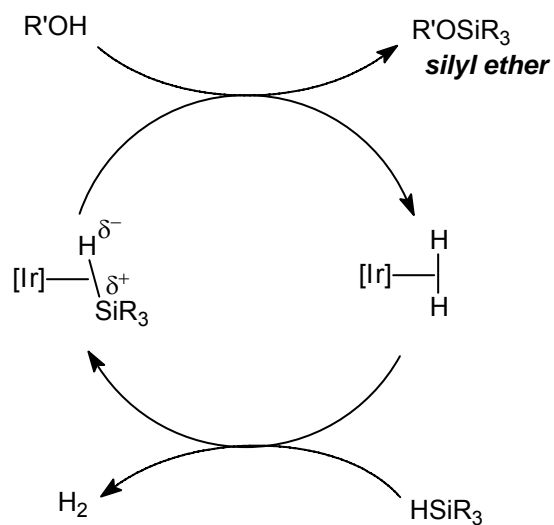


Chart 1.5

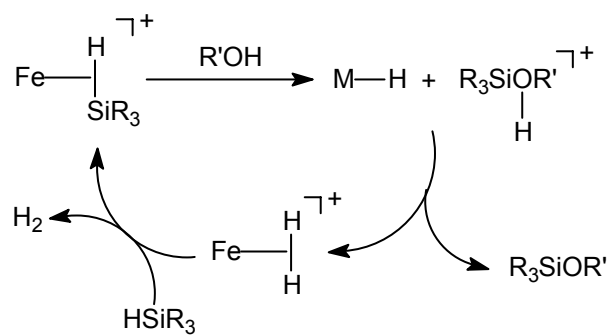
1.1.4 Catalytic processes involving silane complexes

Several σ -coordinated silane complexes have been suggested to be involved in catalytic transformations [16]. Crabtree and Luo reported highly efficient iridium-catalyzed homogeneous silane alcoholysis to silyl ethers [17]. Direct nucleophilic attack of a η^2 -Si-H bond rather than silyl hydride by oxygen of alcohol was proposed (**Scheme 1.1**). Kinetic, mechanistic, and DFT studies on an iron and a manganese catalytic systems show that the key step of the alcoholysis of silane catalyzed by these metal systems (Ir, Fe, and Mn) is the nucleophilic attack of alcohol oxygen on the silicon of η^2 -Si-H bond.

Brookhart's group found that the iron σ -silane complex $[\text{CpFe}(\text{CO})(\text{PR}_3)(\text{HSiEt}_3)][\text{BAr}_F]$ is an active catalyst for silane alcoholysis [18]. It was proposed that the alcohol oxygen attack the silicon-center of the η^2 -coordinated $\text{R}_3\text{Si-H}$ to give a protonated silyl ether which rapidly protonate the hydride to form a dihydrogen complex $[\text{M-H}_2]^+$. Displacement of coordinated dihydrogen regenerates the starting silane complex, completing the catalytic cycle. The displacement step was determined to be rate-determining (**Scheme 1.2**) [19].

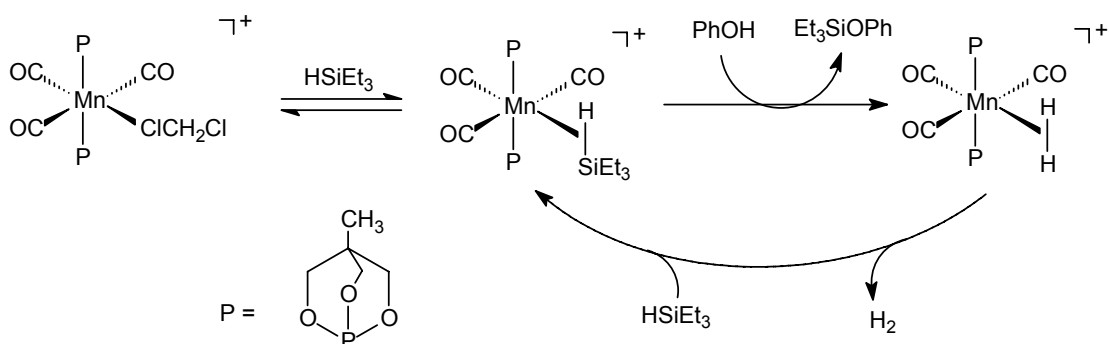


Scheme 1.1 Mechanism of the $[\text{IrH}_2(\text{S})_2(\text{PPh}_3)_2]\text{SbF}_6$ -catalyzed silane alcoholysis (S = solvent).



Scheme 1.2 Proposed mechanism for the iron-catalyzed silane alcoholysis

The cationic manganese dichloromethane complex $[\text{Mn}(\text{CO})_3(\text{P})_2(\text{CH}_2\text{Cl}_2)]^+[\text{BAr}_\text{F}]^-$ bearing tied-back phosphites was also found to catalyze the alcoholysis of triethylsilane with phenol, following a mechanism similar to that proposed for the Brookhart's iron systems (**Scheme 1.3**) [20].

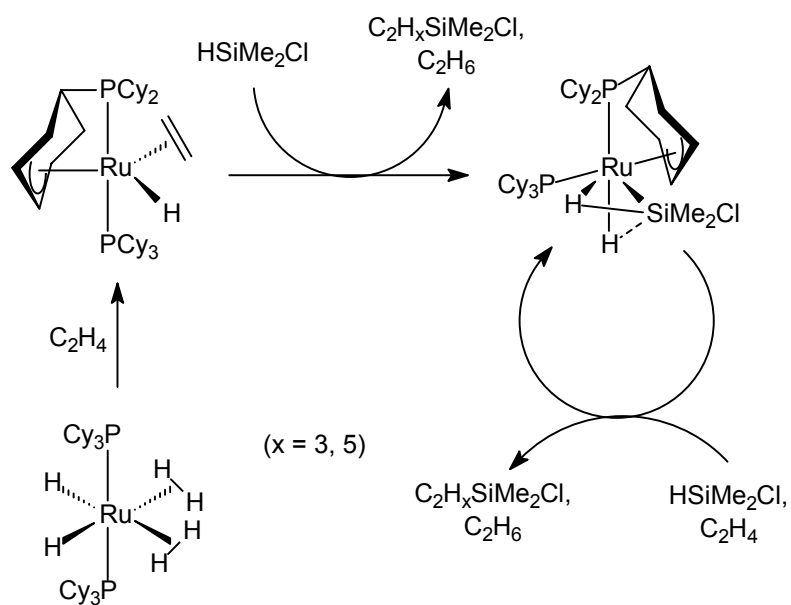


Scheme 1.3 Proposed mechanism for the manganese-catalyzed alcoholysis of HSiEt_3 by phenol

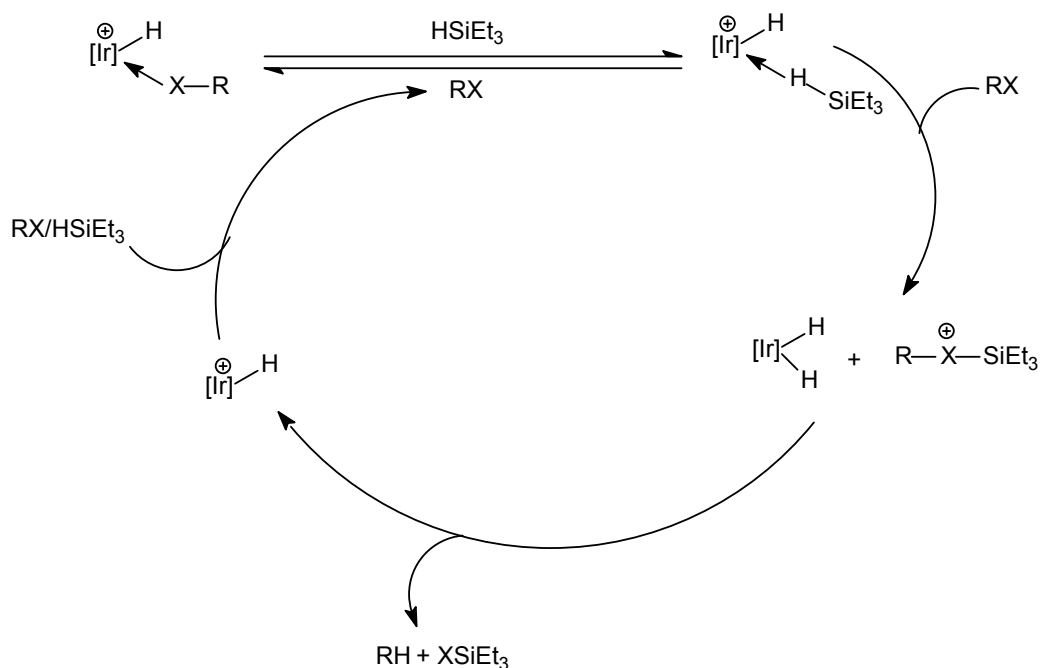
Sabo-Etienne's and Chaudret's groups showed that a silane complex $\text{Ru}^{\text{II}}\text{H}_2\text{SiMe}_2\text{Cl}^{\text{II}}\{(\eta^3\text{-C}_6\text{H}_8)\text{PCy}_2\}(\text{PCy}_3)$ was generated during the silylation of ethylene with HSiMe_2Cl catalyzed by a bis(dihydrogen) complex $\text{RuH}_2(\eta^2\text{-H}_2)_2(\text{PCy}_3)_2$ [21, 22]. The complex was fully characterized by multinuclear NMR and X-ray spectroscopies, which indicated that the silicon is almost symmetrically bound to the two

neighboring hydrogens. It is therefore more reasonable to assign the complex as having a η^3 -HSiMe₂ClH moiety rather than a η^2 -silane hydride. Independently-synthesized Ru(η^3 -HSiMe₂ClH){(η^3 -C₆H₈)PCy₂}(PCy₃) was also found to be a catalyst for ethylene silylation, albeit with lower rate. NMR monitoring indicated that the silane complex remained the only detectable organometallic species in the course of catalysis (**Scheme 1.4**).

Brookhart and coworkers reported the reduction of alkyl halides by triethylsilane based on a cationic iridium bis(phosphinite) pincer catalyst (POCOP)IrH⁺ {POCOP = 2,6-[OP(^tBu)₂]₂C₆H₃} [23, 24]. They originally proposed the formation of an η^2 -silane complex (POCOP)Ir(η^2 -HSiEt₃)H⁺ during the course of the catalysis. However, their later work on the X-ray crystallographic analysis of the silane complex showed that the complex is in fact an unprecedented η^1 -silane complex (**Scheme 1.5**).



Scheme 1.4 Generation of the η^2 -sialne complex $\text{RuH}(\eta^2\text{-HSiMe}_2\text{Cl})\{(\eta^3\text{-C}_6\text{H}_8)\text{PCy}_2\}(\text{PCy}_3)$ during ethylene hydrosilylation by HSiMe_2Cl



Scheme 1.5 Proposed mechanism for the iridium-catalyzed reduction of alkyl halides by triethylsilane

Very recently Nikonov's group reported the use of cationic ruthenium complex $[\text{Cp}(\text{P}^i\text{Pr}_3)\text{Ru}(\text{CH}_3\text{CN})_2]^+\text{BAr}_\text{F}^-$ for a number of silane-related transformations, such as hydrosilylation of aldehydes, ketones, and esters [25]. They proposed the formation of cationic silane σ -complexes from $[\text{Cp}(\text{P}^i\text{Pr}_3)\text{Ru}(\text{CH}_3\text{CN})_2]^+\text{BAr}_\text{F}^-$ during the course of the hydrosilylation of carbonyl substrates.

1.2 Hydrolytic hydrosilane oxidation to silanol

Silanols are widely utilized as building blocks for silicon-based polymeric materials [26–29] and as the nucleophilic partners in cross-coupling reactions [30–33]. Common preparative methods for silanols include hydrolysis of chlorosilanes [34–35] or reactions of siloxanes with alkali reagents. Oxidation of organosilanes with stoichiometric amounts of oxidants such as potassium permanganate [36], OsO₄ [37], and dioxiranes [38], has also been reported (**Figure 1.2**). The obvious shortcoming of these methods is the generation of large amounts of environmentally damaging wastes; moreover, these methods have limited scopes. Highly efficient and more environmentally friendly synthetic methods for the conversion of readily available organosilanes to silanols are therefore highly desirable. In recent years some promising homogeneous [39–43] and heterogeneous [44–46] systems that catalyze the oxidation of hydrosilane to silanol with the use of water as an oxygen source have been reported. This oxidation approach is deemed an environmentally benign one not only because of the use of water as a source of oxygen, but also the generation of molecular hydrogen as the only byproduct.

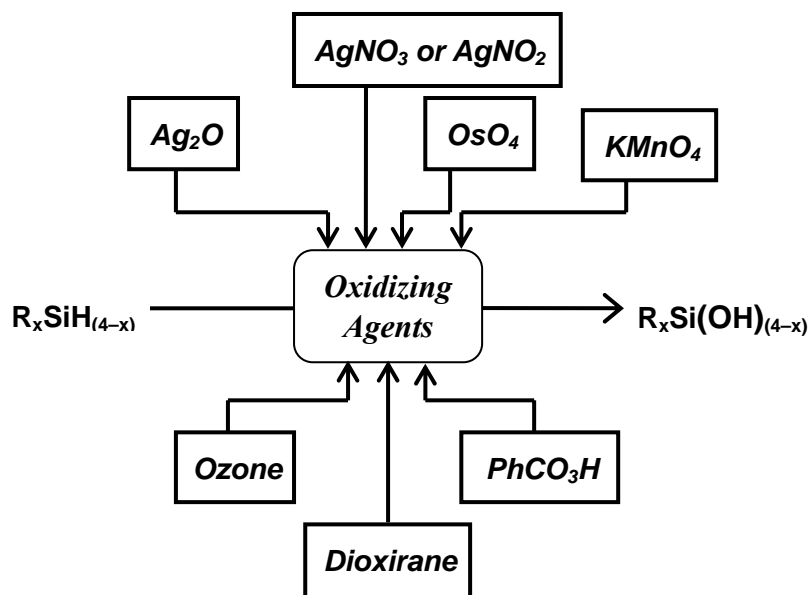
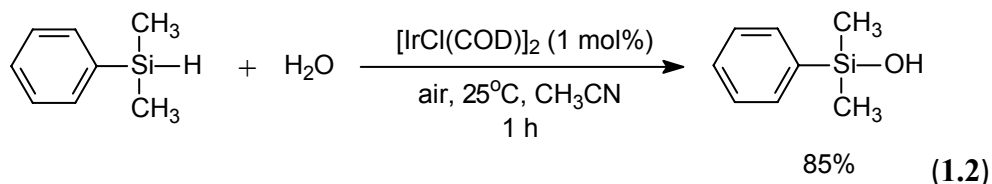
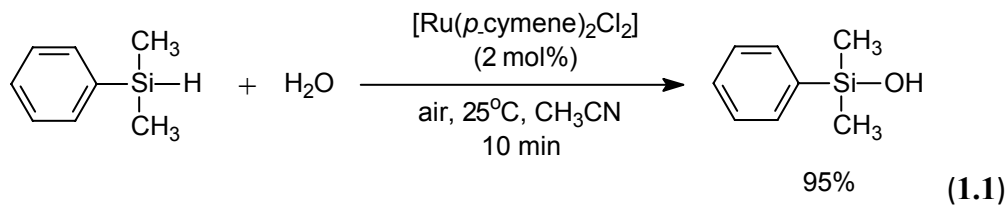
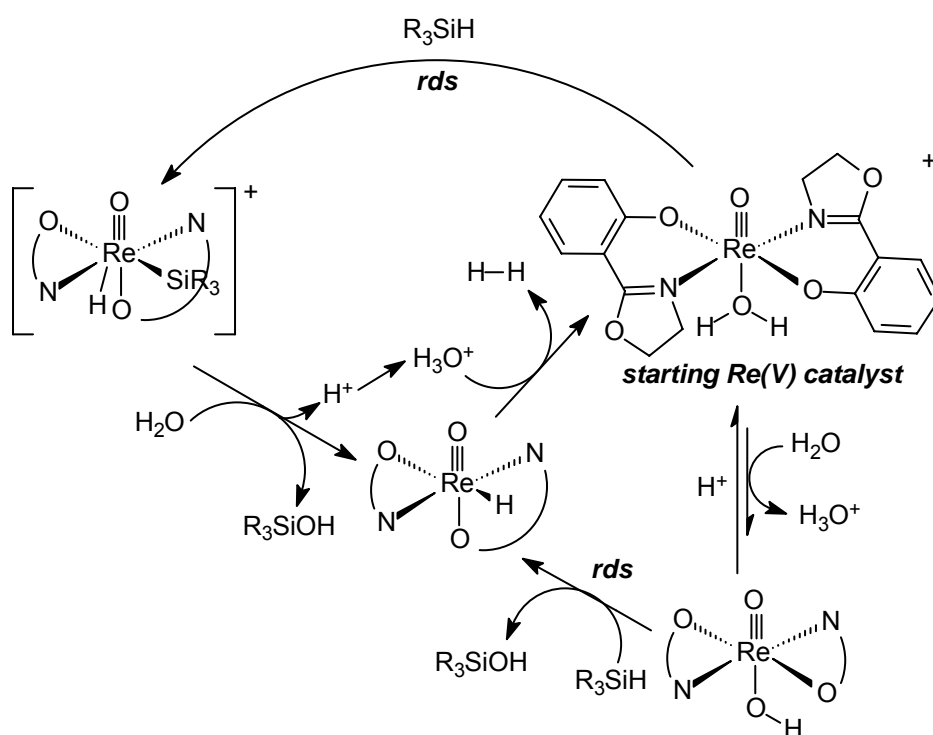
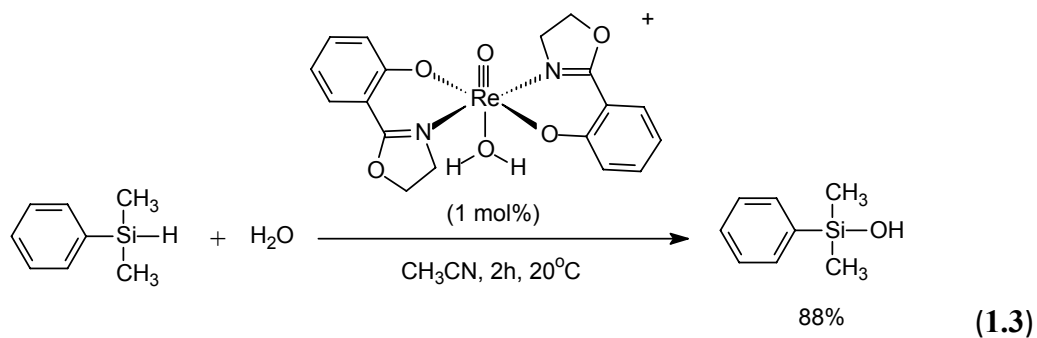


Figure 1.2 Traditional methods for the syntheses of silanols from hydrosilanes

Chang's group reported highly efficient ruthenium [40] and iridium [41] systems for the hydrolytic oxidation of hydrosilanes to silanols under very mild conditions. Dimethylphenylsilane, for instance, was hydrolyzed in the presence of $[\text{Ru}(p\text{-Cymene})_2\text{Cl}_2]$ to give high yield of dimethylphenylsilanol at 25°C in air (eq. 1.1). The same silane was also hydrolyzed to give good yield of the corresponding silanol using $[\text{IrCl}(\text{COD})]_2$ as catalyst under very similar reaction conditions (eq. 1.2). In both catalyst systems a metal silyl hydride species was suggested to be the active species.



A very recent work on silane hydrolysis reaction using cationic [2-(2'-hydroxyphenyl)-2-oxazolinato(-2)]oxorhenium(V) complex was reported by Abu-Omar [43]. The reaction between PhMe_2SiH and H_2O in the presence of the rhenium complex gives high yield of PhMe_2SiOH under ambient conditions (**e.q. 1.3**). A proposed mechanism for the hydrolysis reaction was disclosed. The coordinated H_2O in the aquorhenium(V) complex was first deprotonated to generate the corresponding hydroxo species; reaction between the R_3SiH and the hydroxo ligand affords R_3SiOH and a rhenium(V) hydride. The hydride reacts with solvated H^+ generated in the first step of the catalytic reaction to evolve H_2 and regenerate the cationic active catalyst (**Scheme 1.6**).



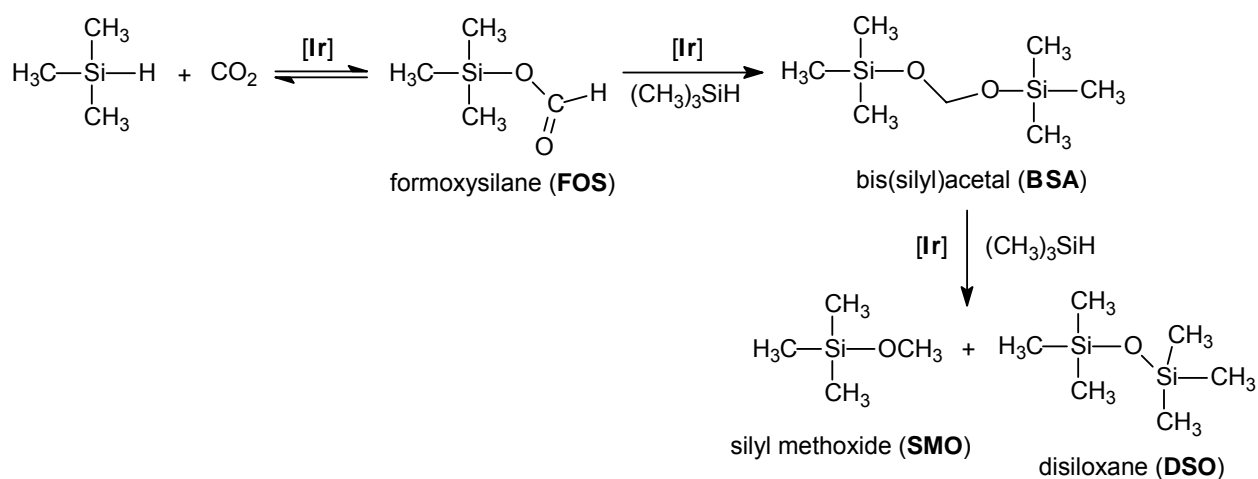
Scheme 1.6 Proposed mechanism for the rhenium-catalyzed hydrolytic oxidation of hydrosilanes to silanols

1.3 Carbon dioxide reduction by silane

Work on the use of carbon dioxide as a renewable source of carbon for the manufacture of chemicals has been extensively conducted in recent decades since CO₂ offers the advantages of being cheap, abundant, and non-toxic [47–48]. To date, however, industrial processes employing carbon dioxide as raw material are still very limited; carbon dioxide, the most oxidized form of carbon, is of high thermodynamic stability, large energy input such as the use of light, electricity, or high energy substances are required to overcome the obstacle imposed by the low-energy nature of carbon dioxide.

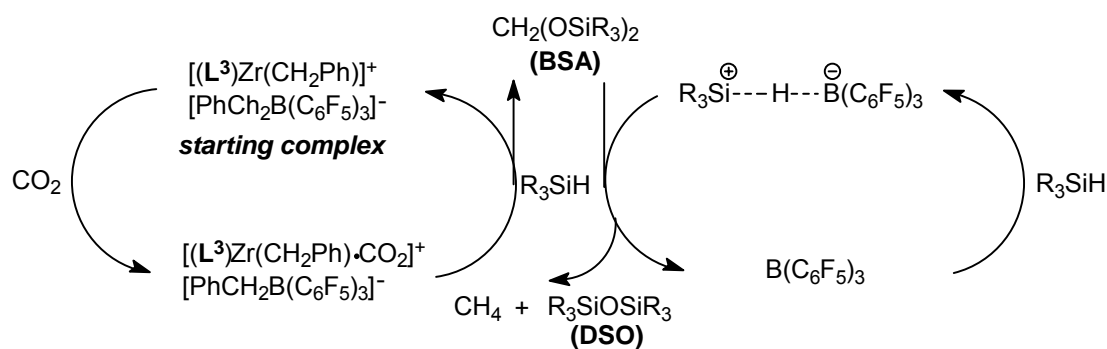
A notable example of overcoming the unfavorable thermodynamics associated with the use of carbon dioxide is to employ reducing agents such as molecular hydrogen [49–54] or hydrosilanes, R_{3-x}SiH_{1+x} [55–64]. We will focus our attention on the use of hydrosilanes, a class of relatively unexplored reagents for effecting CO₂ transformation. Silicon–hydrogen bond is of high reactivity and therefore might transfer its energy to CO₂ through the formation of the more stable Si–O bond. A number of catalytic systems were reported in recent decades for the reduction of carbon dioxide using hydrosilanes as reducing agent.

Early in the 1980's, ruthenium [55, 56] and iridium [57] complexes were known to be catalysts for the hydrosilylation of carbon dioxide. Eisenberg *et al.* reported the reduction of carbon dioxide by alkylsilanes catalyzed by the iridium complex Ir(CN)(CO)dppe at ambient temperature and pressures [57]; carbon dioxide reacts with Me₂SiH₂, Et₂SiH₂, and Me₃SiH to yield silyl methoxides as the ultimate reduction products. Monitoring of the reaction through the use of ¹³CO₂ revealed that several reduced carbon intermediates such as formoxysilane (**FOS**), bis(silyl)acetals (**BSA**), silyl methoxides (**SMO**), and disiloxane (**DSO**) are formed during the course of the reaction (**Scheme 1.7** using Me₃SiH as an example).



Scheme 1.7 Ir(CN)(CO)dppe-catalyzed reduction of carbon dioxide by Me₃SiH

Matsuo and Kawaguchi reported in 2006 that the reduction of carbon dioxide by hydrosilanes under mild conditions to afford methane was catalyzed by the zirconium–borane complexes [60]. An outline of a proposed mechanism had been described; the zirconium cationic complex first forms an adduct with CO₂; the activated CO₂ then reacts with hydrosilanes to yield **BSA**, CH₂(OSiR₃)₂, as initial reduction product. Subsequently, B(C₆F₅)₃, generated by slow decomposition of the counter-anion [PhCH₂B(C₆F₅)₃][−] during the reaction, catalyzes the reduction of the **BSA** by HSiR₃ to afford methane and (R₃Si)₂O (**DSO**) (**Scheme 1.8**).



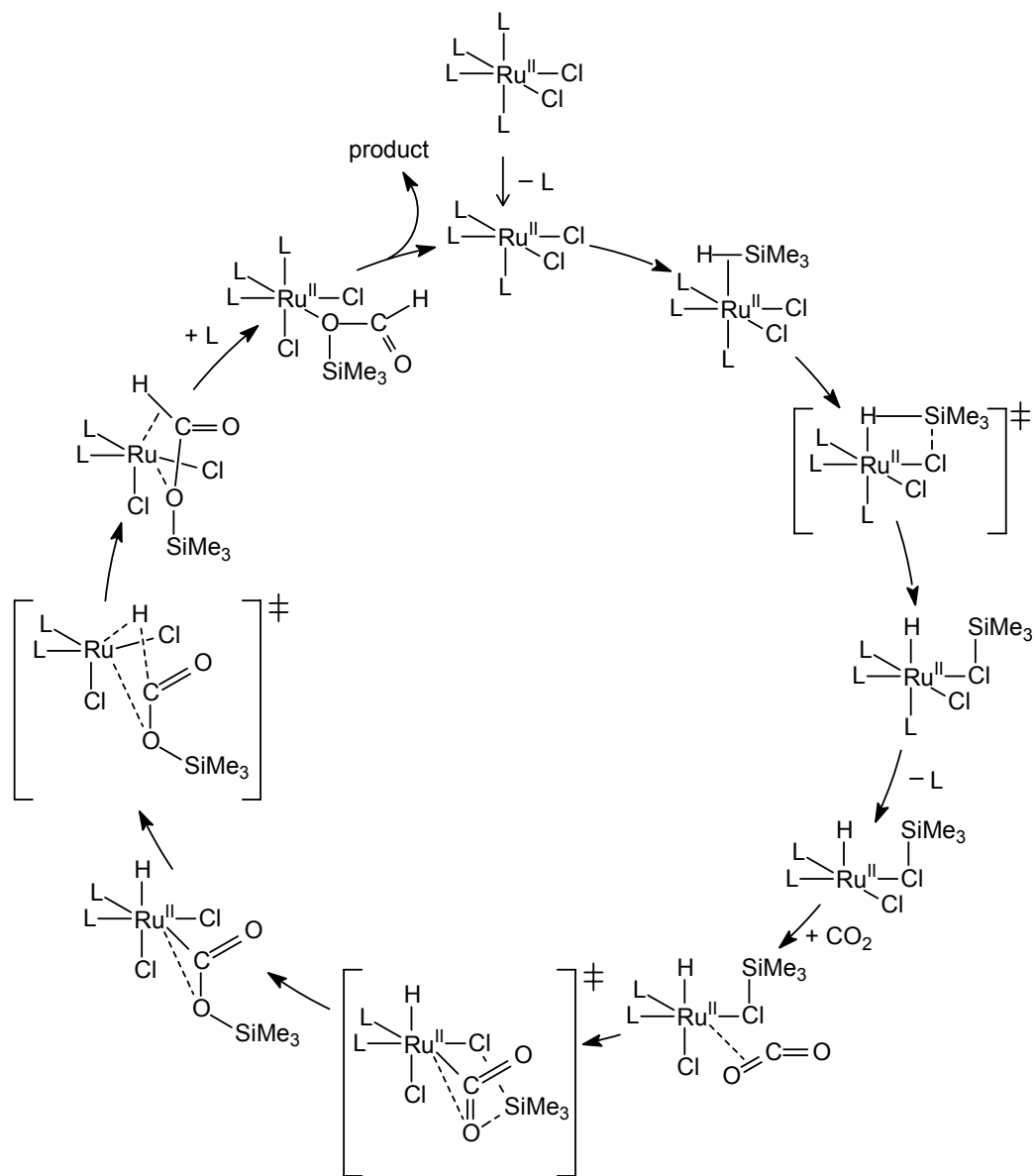
Scheme 1.8 Conversion of carbon dioxide to methane catalyzed by zirconium complex

In 2007 Deglmann reported the hydrosilylation of carbon dioxide by PhMe_2SiH catalyzed by the ruthenium nitrile complexes *mer*-($\text{RuX}_3(\text{MeCN})_3$) and *cis/trans*-($\text{RuX}_2(\text{MeCN})_4$), with $\text{X} = \text{Cl}, \text{Br}$ [61]. The major steps of the catalytic cycle were shown by theoretical calculation to be the transfer of the trimethylsilyl moiety from Me_3SiH to a coordinated halide ligand, leading to the formation of a $\text{L}_n\text{RuH}-(\text{XSiMe}_3)$ intermediate, carbon dioxide coordination to Ru center in a side-on manner, transfer of trimethylsilyl group to carbon dioxide, and finally, reductive elimination of the silyl formate product HCOOSiMe_3 . The step involving the silyl transfer from the R_3SiCl ligand to the oxygen of the coordinated carbon dioxide was found to be the highest point in the energy pathway (**Scheme 1.9**).

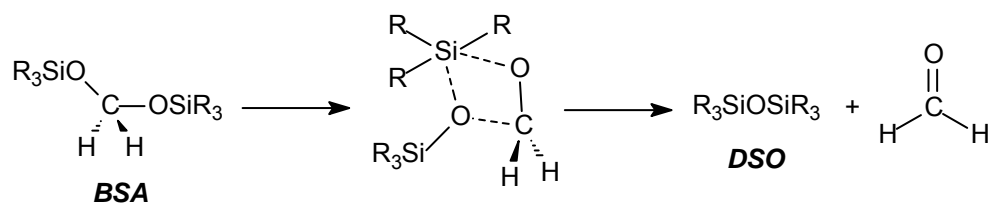
In 2009 Ying reported conversion of carbon dioxide into methanol with silanes using N-heterocyclic carbene (NHC) catalysts under ambient conditions [62]. The reactions between CO_2 and diarylsilane in the presence of 1,3-bis(2,4,6-trimethylphenyl)imidazolium carboxylate (Imes-CO_2) yield silyl methoxides (**SMO**) as the final reduction product. Various reduced carbon intermediates such as **FOS** and **BSA** were identified during the course of the catalytic reaction using $^{13}\text{CO}_2$ as a source of carbon. Density functional theory

study of the catalytic reduction of carbon dioxide by the NHC catalysts reported by Wang's group in an independent article revealed that formaldehyde, not detected in Ying's work but is believed to have been generated from the dissociation of BSA (**Scheme 1.10**), should be an inevitable intermediate [65].

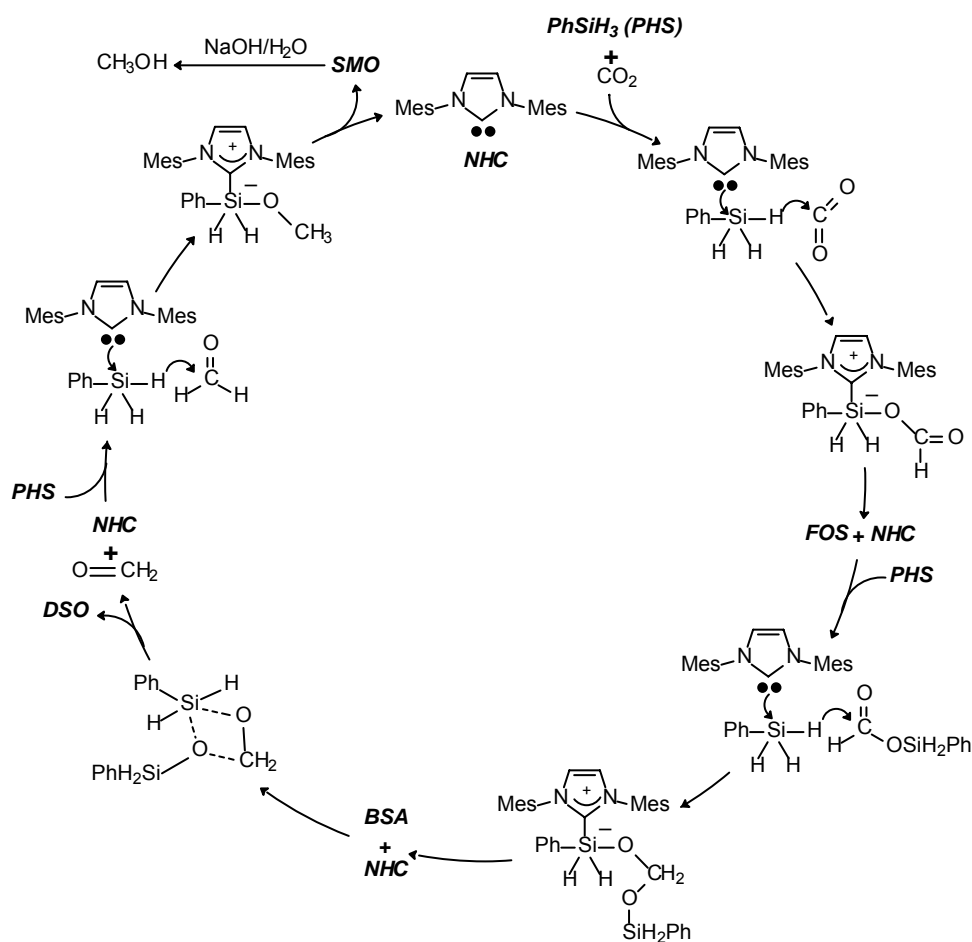
When NHC catalyzes the reduction of CO₂/**FOS**/formaldehyde by silane, it prefers to activate Si-H bonds of silane and push electron density to the hydrogen atoms in favor of prior coordination to the electrophilic carbonyl carbon of CO₂/**FOS**/formaldehyde. **Scheme 1.11** depicts the predicted mechanism of the whole catalytic cycle. It should be noted that methanol, the target reduction product from carbon dioxide, is obtained by treatment of the methoxysilanes with aqueous NaOH.



Scheme 1.9 Calculated mechanism of the ruthenium-catalyzed hydrosilylation of carbon dioxide

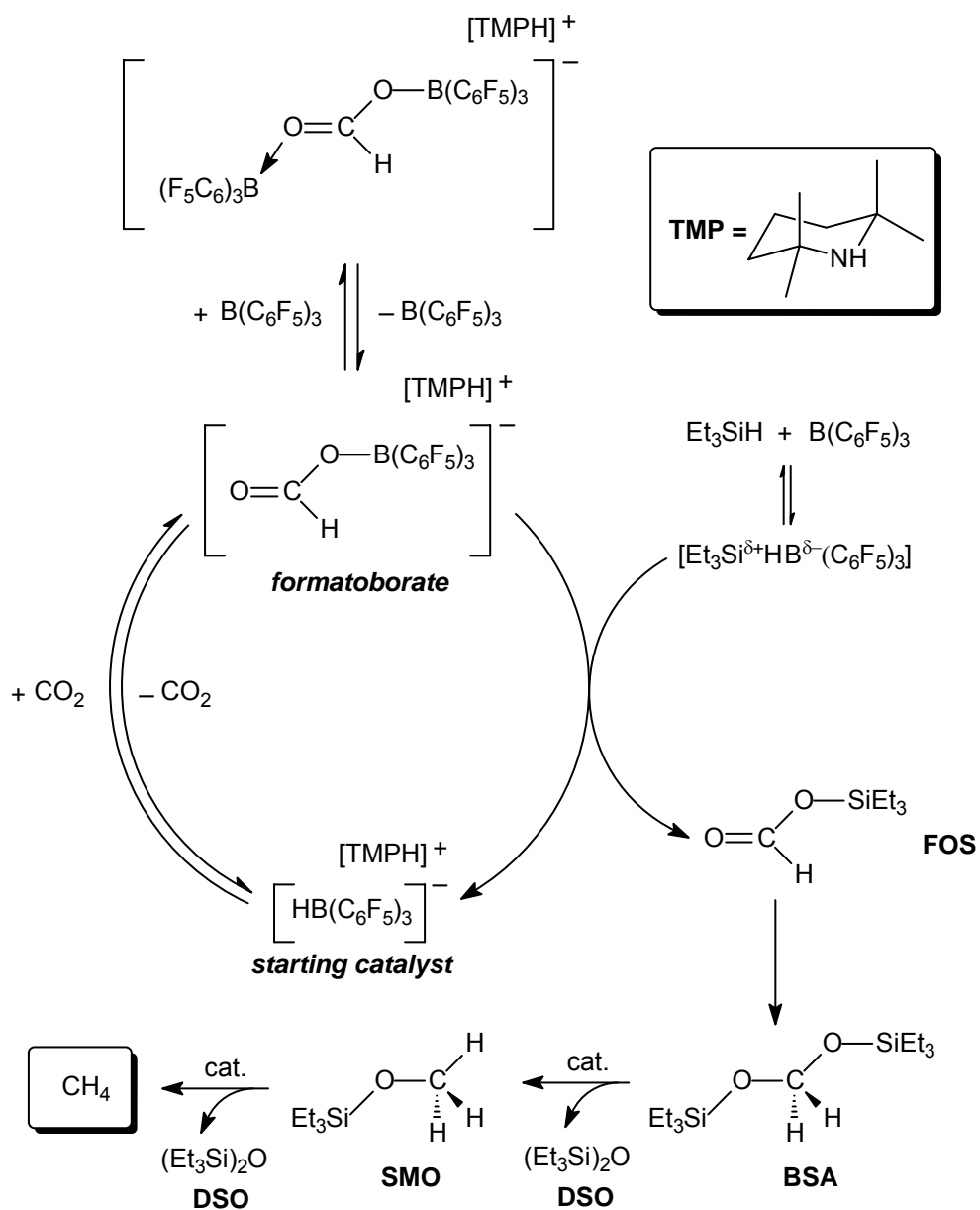


Scheme 1.10 Decomposition of bis(silyl)acetal (BSA) to give disiloxane (DSO) and formaldehyde



Scheme 1.11 Detailed mechanism for the N-heterocyclic carbene-catalyzed reduction of carbon dioxide by silane.

Very recently Piers reported the reduction of carbon dioxide to methane catalyzed by a tandem catalyst comprising of an ion pair $[\text{TMPH}]^+[\text{HB}(\text{C}_6\text{F}_5)_3]^-$ (TMP = 2,2,6,6-tetramethylpiperidine) and a Lewis acidic borane $\text{B}(\text{C}_6\text{F}_5)_3$ [64]. Carbon dioxide is first activated by the ion pair $[\text{TMPH}]^+[\text{HB}(\text{C}_6\text{F}_5)_3]^-$ to afford the formatoborate species $[\text{TMPH}]^+[\text{HCOOB}(\text{C}_6\text{F}_5)_3]^-$ (**Scheme 1.12**). In the presence of $\text{B}(\text{C}_6\text{F}_5)_3$ and triethylsilane, an adduct $[\text{Et}_3\text{Si}^{\delta+}\text{HB}^{\delta-}(\text{C}_6\text{F}_5)_3]$ is formed, the formatoborate rapidly transfer its CO_2 moiety to the adduct to give **FOS** and regenerate $[\text{TMPH}]^+[\text{HB}(\text{C}_6\text{F}_5)_3]^-$. The reactive formoxysilane is then readily reduced by the borane/triethylsilane system to afford CH_4 via **BSA** and **SMO**, with the formation of the **DSO** $(\text{Et}_3\text{Si})_2\text{O}$ as byproduct.



Scheme 1.12 Reduction of carbon dioxide to methane catalyzed by a frustrated acid-base pair $[TMPH]^+[HB(C_6F_5)_3]^-$

1.4 Electrophilic transition-metal complexes for catalytic reactions

The design and synthesis of electrophilic transition-metal complexes has been an important area of research in organometallic chemistry catalysis [66, 67]. Several types of catalytic reactions such as alkene hydrogenation [68, 69], alkene metathesis [70], and 1,3-butadiene polymerization [71] were found to have rate enhancement with increased electrophilicity of the metal centers achievable by going from neutral to cationic catalyst complexes. Brookhart's cationic dimine complexes $[\text{Pd}(\text{Me})(\text{sol})(\text{Ar}_2\text{DAB})]^+$ (Ar_2DAB = diaryldiazabutadiene, sol = coordinated solvent) (**Chart 1.6**) for ethylene and olefin polymerization represents an impressive example of utilizing electrophilic late transition metal for olefin polymerization [72–74]. On the other hand, Sen's early work on reactions such as alkene polymerization, promoted by electrophilic palladium(II) species $[\text{Pd}(\text{CH}_3\text{CN})_4](\text{BF}_4)_2$ (**Chart 1.7**) and other electrophilic solvent complexes have also contributed to the development of electrophilic transition–metal catalysis [75, 76].

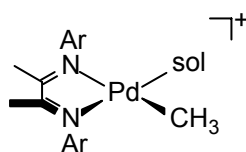


Chart 1.6

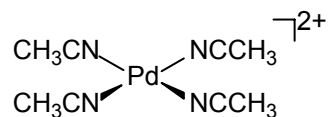


Chart 1.7

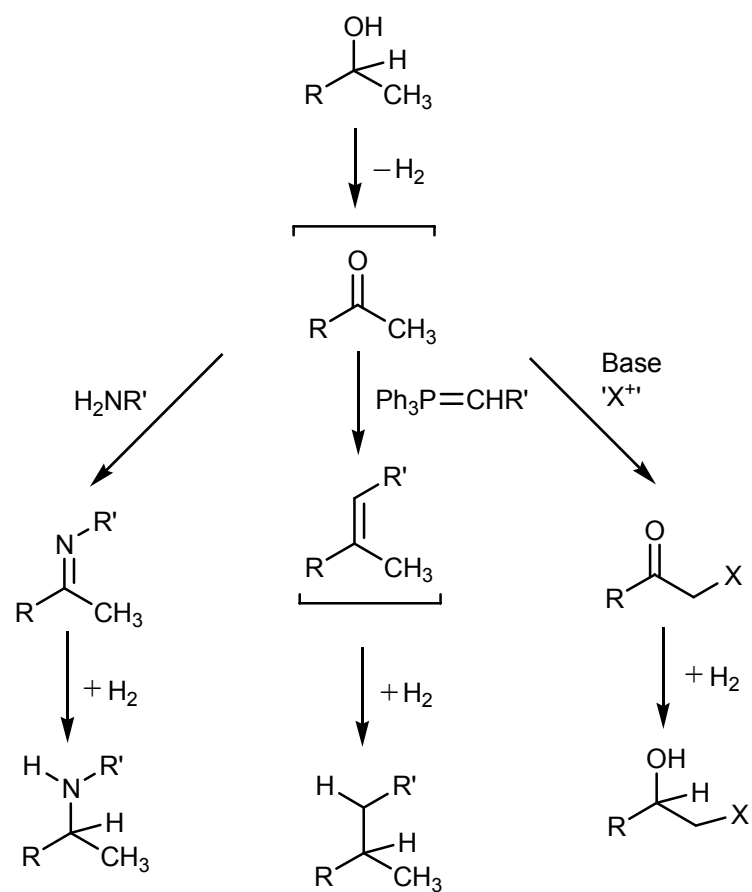
It is suggested that with the use of the above-mentioned catalysts, the electrophilicity of the coordinated alkenes can be strongly enhanced by increasing the net positive charge, resulting in high carbocationic properties. This concept of increasing the positive charge on the complex is believed to be useful for the development of catalysts for reactions where activation of alkenes or other unsaturated compounds are involved.

1.5 Activation of alcohols via borrowing hydrogen methodology

Alcohols are generally of limited reactivity unless activated by several means, including the conversion to a nucleophilic alkoxide by addition of a base, or to an electrophilic species by the addition of an acid. Alternatively, they can be temporarily oxidized into the corresponding aldehydes or ketones, taking advantages of the latter being able to participate in nucleophilic addition reactions as well as acting as nucleophiles by themselves (in the form of the corresponding enol or enolate). This activation mode can become a catalytic

process when the oxidation product is subsequently subjected to reduction under the reaction conditions. **Scheme 1.13** shows the major reactions in which this mode of alcohol activation, named borrowing hydrogen methodology, was employed. The greater reactivity of the ketone over that of the alcohol is utilized for (i) imine formation and its subsequent reduction to an amine, (ii) alkene formation and its reduction to a carbon–carbon bond and (iii) enolisation with electrophile and subsequent reduction to afford a functionalized alcohol. It should be emphasized that, in all the cases mentioned above there is no net hydrogen loss or gain during the reaction.

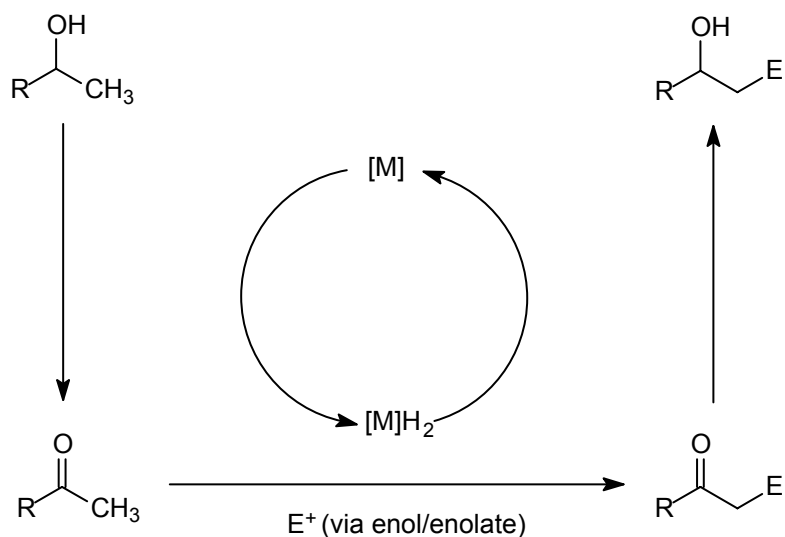
Recent research on the area of borrowing hydrogen methodology had benefited from the advancement in transfer hydrogenation chemistry [109–112]. Late transition complexes have been shown to affect imine and alkene reduction using alcohol as hydrogen donor.



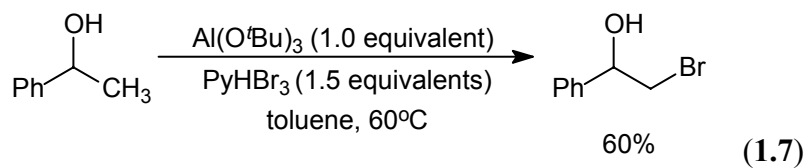
Scheme 1.13 Activation of alcohols by borrowing hydrogen methodology

1.5.1 β -functionalization of alcohols

As discussed, when an alcohol is temporarily oxidized to the corresponding aldehyde or ketone, nucleophilic addition process can take place more readily and, with amine or Wittig reagent as nucleophile, imine and alkene can be formed respectively which were then reduced to give C–N and C–C bonds. Another possible manipulation of this temporary oxidation of an alcohol to a carbonyl compound is reacting the carbonyl compound via enol/enolate chemistry. The possibility for the β -functionalisation of alcohols by temporarily oxidation using borrowing hydrogen methodology is shown in **Scheme 1.14**. The alcohol oxidation is followed by addition of an electrophile to the generated enol or enolate, and this allows the overall reaction to proceed. This β -functionalisation strategy has been applied to the bromination of alcohols [113]. Thus, in the presence of an aluminium alkoxide and pyridium tribromide, bromination occurred giving 2-bromo-1-phenylethanol as the product (**eq. 1.7**). The reaction conditions also result in some irreversible oxidation of the alcohol by its direct interaction with the brominating agent.

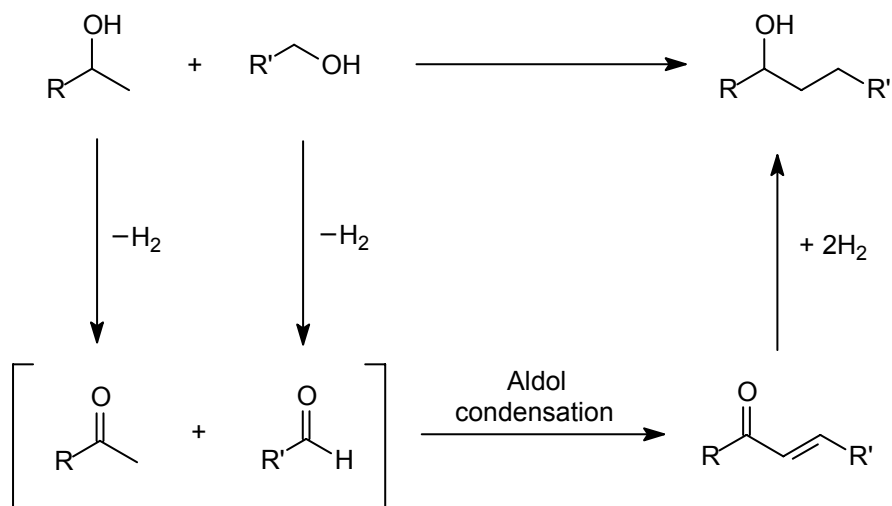


Scheme 1.14 Borrowing hydrogen in the β -functionalization of alcohols.



The activation of a primary alcohol and a secondary alcohol simultaneously by borrowing hydrogen methodology can result in an interesting C–C bond coupling process [114–120]. Such processes are believed to involve temporary oxidation of both alcohols to the corresponding ketone and aldehyde, which undergo an aldol condensation in the presence of base to give an α,β -unsaturated ketone.

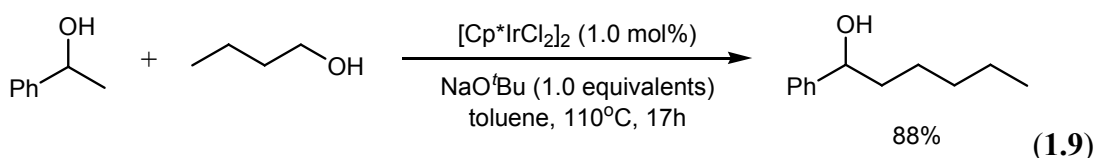
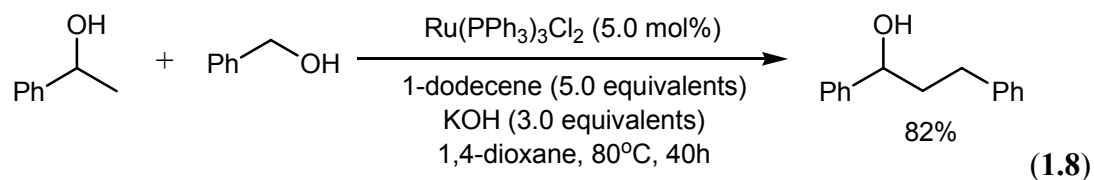
Reduction of this ketone affords the saturated alcohol as the final product (**Scheme 1.15**).

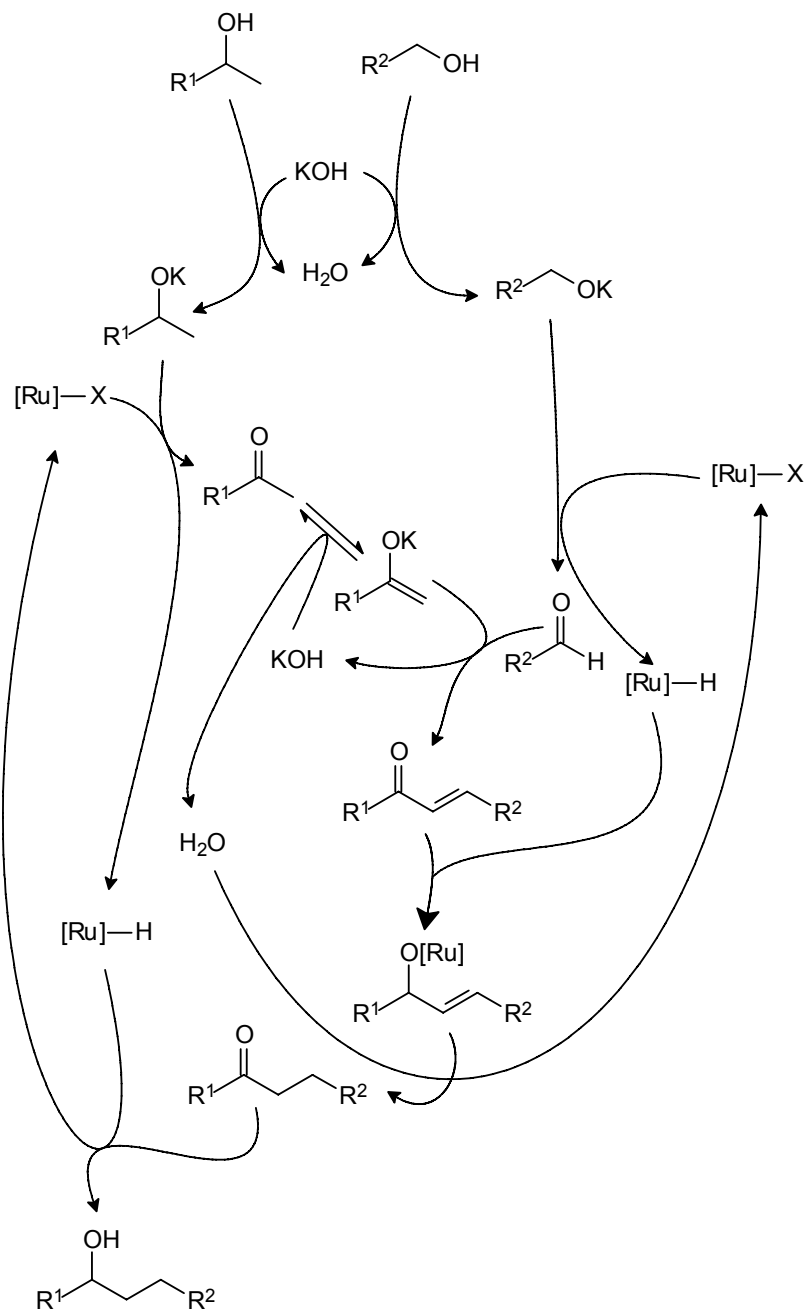
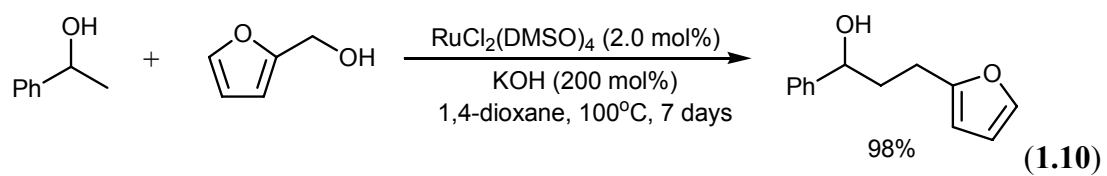


Scheme 1.15 Carbon-carbon bond formation between two alcohols.

Cho et al. reported in 2003 the first example of one-pot β -alkylation of secondary alcohol with primary alcohol [114]. The coupling process involves the addition of 1-dodecene as a sacrificial hydrogen acceptor, which allows 1-phenylethanol to be β -alkylated by benzyl alcohol giving high yield of product (**eq. 1.8**). In 2005 Yamaguchi reported the β -alkylation of secondary alcohols with primary alcohols using the dimeric iridium complex $[\text{Cp}^*\text{IrCl}_2]_2$ as catalyst [115]. As an example, the reaction between 1-phenylethanol

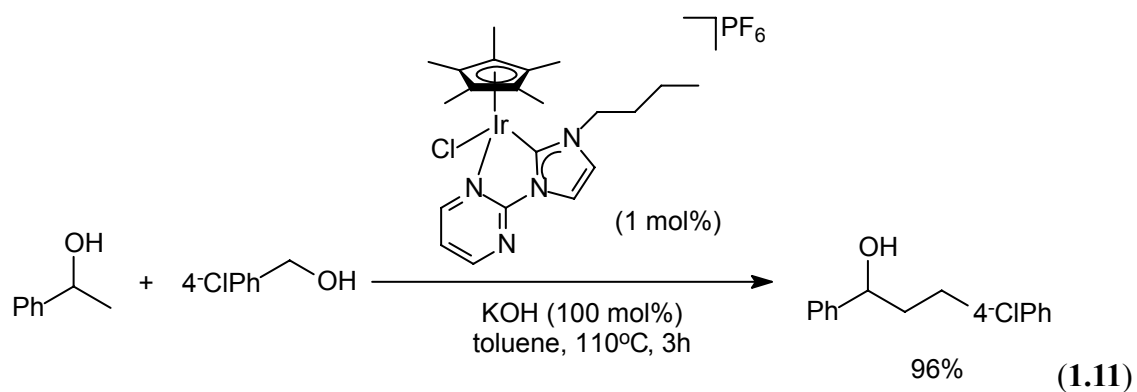
and a slight excess of *n*-butanol afforded 1-phenyl-1-hexanol in good yield (**eq. 1.9**). Ramon and Yus reported in 2006 the use of dimethylsulfoxide ruthenium complex $\text{RuCl}_2(\text{DMSO})_4$ as a catalyst for the coupling reaction between primary alcohol and secondary alcohol [116]. For instance, 1-phenylethanol was successfully β -alkylated with 2-furfuryl alcohol in the presence of KOH to give 3-(2-furyl)-1-phenylethanol in 98% yield, although a relatively longer reaction time is required (**eq. 1.10**). In the report they suggested a mechanism for the coupling reaction (**Scheme 1.16**). The alcohols are first oxidized to the corresponding aldehyde and ketone, which then undergo an aldol condensation in the presence of base to afford an unsaturated ketone. Subsequent reduction of the ketone gives the saturated alcohol as the final product.





Scheme 1.16 Proposed mechanism for the $\text{RuCl}_2(\text{DMSO})_4$ -catalyzed β -alkylation of secondary alcohols with primary alcohols

The most efficient β -alkylation of secondary alcohols with primary alcohols to date is reported in 2009 by Crabtree and coworkers using iridium complexes supported by chelating N-Heterocyclic carbenes [120]. As an example, 1-phenylethanol reacted with 4-chlorobenzyl alcohol in refluxing toluene to afford 96% conversion to 3-(4-chlorophenyl)-1-phenylethanol (**eq. 1.11**).



1.6 Transfer hydrogenation of carbonyl compounds

Transfer hydrogenation refers to a process in which a hydrogen donor releases its hydrogen to an unsaturated bond, such as C=C, C=O, and C=N. The reaction is now widely investigated in both academic and industrial sectors since the use of potentially hazardous pressurized hydrogen can be avoided. Many transition-metal complexes of rhodium, iridium and ruthenium have been found to be active in catalyzing transfer hydrogenation of polar functional groups [77–80]. In particular, ruthenium(II) complexes supported by either tridentate, cyclometalated PCP- [81–84], NCN- [81], CNN-[85, 86], NNN- [87, 88] pincer, or bidentate PC- [89], NC- [90, 91], and NN-[92] ligands are found to be highly active for such reaction.

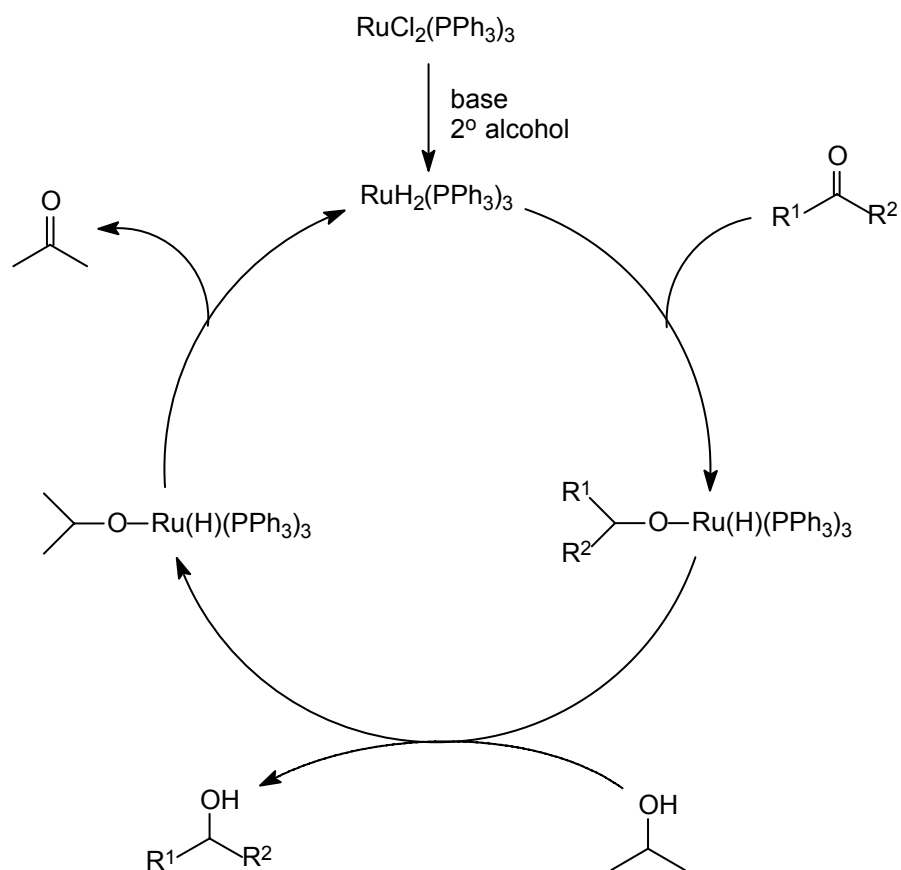
1.6.1 Mechanisms of transition metal-catalyzed transfer hydrogenation

Generally, transition-metal complexes catalyze transfer hydrogenation of unsaturated compounds through the formation of metal monohydride or dihydride as key intermediates [79, 93–94]. In some cases, the hydride species are stable enough to be isolated or observed spectroscopically. The $\text{RuCl}_2(\text{PPh}_3)_3$ -catalyzed reduction of carbonyl compounds reported in the 1960s represents an early example of

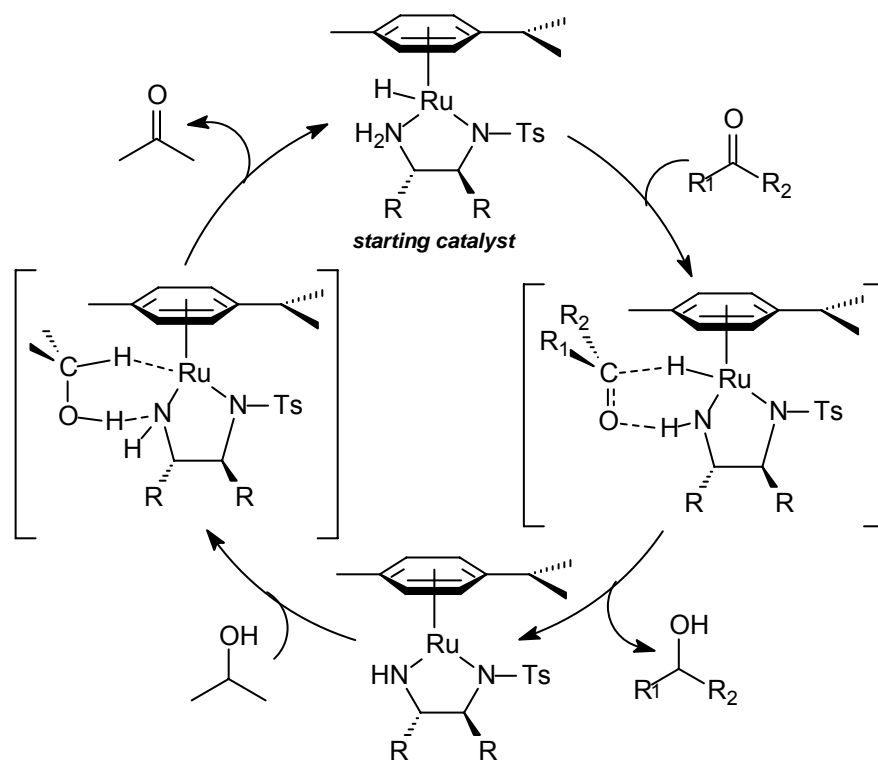
transition metal-catalyzed hydrogen transfer reaction [95–97]. In the presence of base, the rate of the transfer reaction was found to be enhanced dramatically [98, 99] and this was later shown by Backvall to be a result of the formation of a highly active dihydride species $\text{RuH}_2(\text{PPh}_3)_2$ (**Scheme 1.13**) [100].

Noyori reported the use of metal-ligand bifunctional catalysts, such as $(\eta^6\text{-arene})\text{RuH}((\text{S,S})\text{-H}_2\text{NCHRCHRNTs})$, for the asymmetric transfer hydrogenation of unsaturated compounds [101–103]. They suggested that the key feature of these catalysts is the presence of a basic site in the ligand, which interacts with the alcohol or other hydrogen donor through hydrogen bond and thereby facilitates the hydride transfer (from the hydrogen donor to the metal). The proposed mechanism of the transfer hydrogenation of ketones in 2-propanol catalyzed by these complexes involves a concerted transfer of the proton and the hydride from the catalyst to the substrate via a cyclic six-membered transition state to give the alcohol and $(\eta^6\text{-arene})\text{Ru}((\text{S,S})\text{-HNCHRCHRNTs})$ (**Scheme 1.14**). The proton and the hydride from 2-propanol are then transferred to the nitrogen and metal, respectively, forming acetone and

regenerating the active catalyst. It is noted that the catalytic reaction is suggested to proceed without coordination of either alcohol or ketone to the metal. Other examples of metal-ligand bifunction catalysts for transfer hydrogenation reactions include $\text{RuH}(\text{NHCOMe})(\text{OHCHMe}_2)(\text{PCy}_3)_2(\text{CO})$ (**Chart 1.8**) reported by Yi [104] and $[(\text{Ph}_4\text{C}_4\text{COHOCC}_4\text{Ph}_4)(\mu\text{-H})(\text{CO})_4\text{Ru}_2]$ (**Chart 1.9**) by Shvo [105].



Scheme 1.17 Proposed mechanism of the transfer hydrogenation of carbonyl compounds involving a dihydride intermediate



Scheme 1.18 Catalytic cycle of $(\eta^6\text{-arene})\text{RuH}((S,S)\text{-H}_2\text{NCHRCHRNTs})$ via a concerted six-membered transition state.

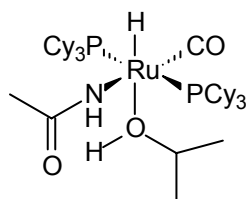


Chart 1.8

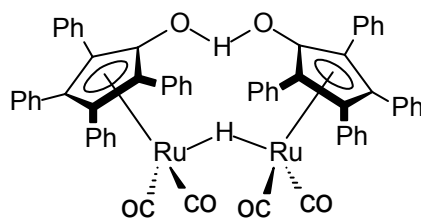
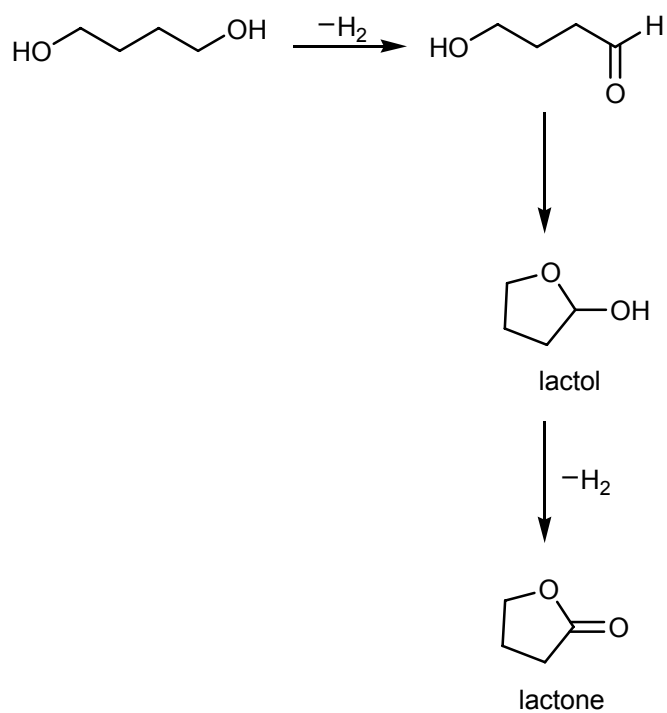


Chart 1.9

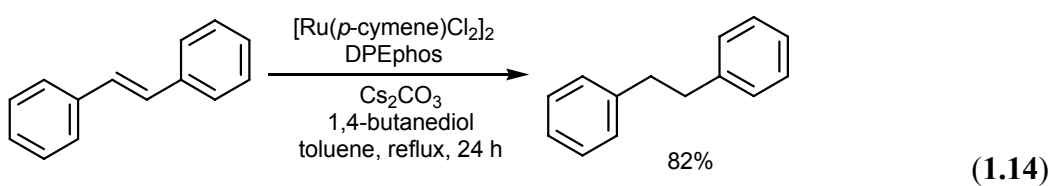
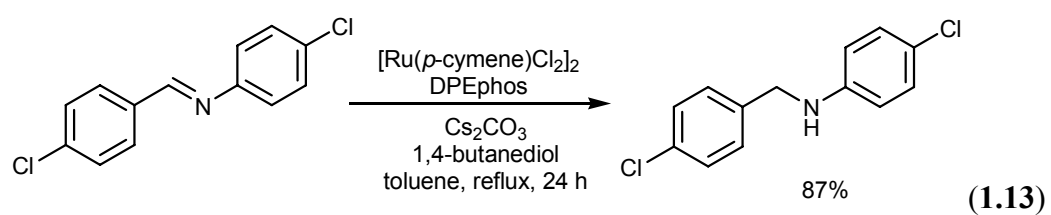
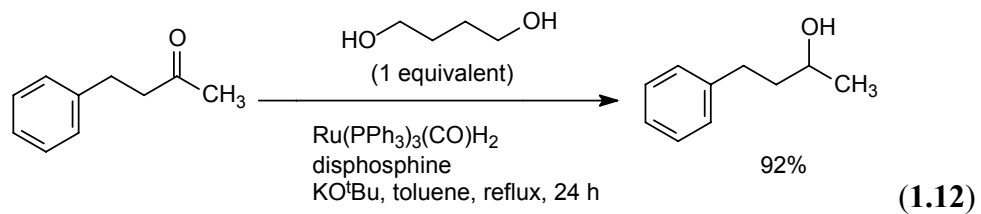
1.4.2 Choices of hydrogen donors

It is well known that 2-propanol is conventionally used as a hydrogen donor in hydrogen transfer reactions because of its valuable properties: it is of high stability, easy to handle, non-toxic, environmentally benign, inexpensive, and is good solvent for most organic compounds [106]. The oxidized product acetone has a low boiling point and is therefore readily removable. However, due to the very similar thermal stabilities of the 2-propanol and acetone, large excess of the former is required in order to push the hydrogen transfer reaction to the product. Therefore, an alternative hydrogen donor other than 2-propanol is desirable.

William has investigated the possibility of using 1,4-butanediol as an alternative source of hydrogen donor in ruthenium-catalyzed transfer hydrogenation of unsaturated compounds. The diol, after its double hydrogen release, is converted irreversibly to a lactone, rendering stoichiometric reduction possible (**Scheme 1.19**). In addition to aldehydes and ketones, imines and alkenes were also successfully reduced with 1 equivalent of 1,4-butanediol under similar reaction conditions (**eq. 1.12-1.14**) [107, 108].



Scheme 1.19 Lactonization of 1,4-butanediol



**Chapter 2 Nonclassical Ruthenium Silyl Dihydride Complexes
TpRu(PPh₃)(η³-HSiR₃H) (Tp = Hydrotris(pyrazolyl)borate).
Catalytic Hydrolytic Oxidation of Organosilanes to Silanols with
TpRu(PPh₃)(η³-HSiR₃H)**

2.1 Introduction

Our research group has previously reported the syntheses of a series of ruthenium complexes TpRu(PPh₃)“H₂SiR₃” (Tp = hydrotris(pyrazolyl)borate); on the basis of NMR and DFT studies, we formulated these complexes as the σ-silane hydride species which rapidly exchange between the two forms: TpRu(PPh₃)(H_a)(η²-H_bSiR₃) ⇌ TpRu(PPh₃)(H_b)(η²-H_aSiR₃) [121]. We have now successfully obtained single crystals of three of these complexes and carried out X-ray crystallographic studies, the results of which are more consistent with a static structure TpRu(PPh₃)(η³-HSiR₃H) containing H⋯Si⋯H bonding. In addition to the X-ray structures of three Ru-(η³-HSiR₃H) complexes, we report here catalytic hydrolytic oxidation of organosilanes to silanols with one of these complexes.

2.2 Experimental section

2.2.1 Materials and Instrumentation

All manipulations were carried out under an inert nitrogen atmosphere using standard Schlenk techniques. Solvents were dried, degassed, and distilled prior to use: THF, 1,4-dioxane, and diethyl ether from Na benzophenone ketyl, *n*-hexane and toluene from Na, acetonitrile and dichloromethane from CaH₂. All chemicals were commercially available (Aldrich, Acros, Strem and International Laboratory) and used without further purification. The chiral silane *R*-(+)-Me(α -Np)PhSiH (98% ee) [122], and the complexes TpRu(PPh₃)(CH₃CN)H [123] and TpRu(PPh₃)(η^3 -HSiPh₃H) [121] were prepared according to literature methods. Deuterated NMR solvents, purchased from Armar and Cambridge Isotope Laboratories, were dried with P₂O₅ prior to use. ¹H NMR spectra were obtained from a Varian (500 MHz) or Bruker DPX (400 MHz) spectrometer; chemical shifts were reported relative to residual protons of the deuterated solvents. ¹³C NMR spectra were recorded with a Bruker DPX 400 spectrometer at 100.61 MHz; chemical shifts were internally referenced to CD₂Cl₂ (δ = 53.8 ppm). ³¹P NMR spectra were recorded on a Bruker DPX 400 spectrometer at 161.70 Mz; chemical shifts were externally referenced to 85% H₃PO₄ in D₂O (δ =

0.00 ppm). ^{29}Si NMR spectra were obtained from a Bruker DPX 400 spectrometer at 79.50 MHz; chemical shifts were externally referenced to Me_4Si in CDCl_3 ($\delta = 0.00$ ppm). Infrared spectra were obtained from a Bruker Vector 22 FT-IR spectrophotometer. Optical rotations were recorded on a Perkin-Elmer 341 polarimeter in a 10 cm cell. Electrospray ionization mass spectrometry was carried out with a Finnigan MAT 95S mass spectrometer with the samples dissolved in dichloromethane. Elemental analyses were performed by M-H-W Laboratories, Phoenix, AZ.

2.2.2 Syntheses and Reactions

2.2.2.1 Synthesis of $\text{TpRu}(\text{PPh}_3)(\eta^3\text{-HSiPh}_2\text{MeH})$

A sample of $\text{TpRu}(\text{PPh}_3)(\text{CH}_3\text{CN})\text{H}$ (0.20 g, 0.32 mmol) was loaded into a 50 mL two-necked pear-shaped flask, which was evacuated and filled with nitrogen for four cycles. Freshly distilled toluene (10 mL) and Ph_2MeSiH (0.8 mL, 4 mmol) were then added to the flask via syringes, and the resulting solution was heated at 90°C with stirring for 4 h. The solution was cooled to room temperature, the volume of which was reduced to 1 mL in vacuo, and 10 mL of pre-cooled hexane was added to precipitate out the product as orange solid. The solid was collected and washed with

pre-cooled hexane (5 mL), it was dried under vacuum. Yield: 0.14 g (55%).

Anal. Calcd (%) for $C_{40}H_{40}BN_6PRuSi$: C 61.93, H 5.20, N 10.83. Found: C

61.93, H 5.25, N 10.85. IR (KBr): $\nu(Ru-H) = 1942$ (m), $\nu(B-H) = 2468$ (m).

1H NMR (400.13 MHz, CD_2Cl_2 , $25^\circ C$): $\delta -9.93$ (d, 2H, Ru-H, $^1J_{SiH} = 25.0$

Hz, $^2J_{HP} = 22.6$ Hz); 0.70 (s, 3H, Si- CH_3); 5.48 (t, 1H of Tp), 5.77 (t, 2H of

Tp), 7.52 (d, 1H of Tp), 7.68 (d, 2H of Tp), 7.82 (d, 1H of Tp), 8.35 (d, 2H

of Tp), 6.93–7.60 (m, 25H of Ph). $^{13}C\{^1H\}$ NMR (100.61 MHz, CD_2Cl_2 ,

$25^\circ C$): $\delta 9.49$ (s, Si- CH_3). $^{31}P\{^1H\}$ NMR (161.7 MHz, CD_2Cl_2 , $25^\circ C$): δ

70.3. $^{29}Si\{^1H\}$ NMR (79.50 MHz, CD_2Cl_2 , $25^\circ C$): $\delta 16.8$ (s). ESI-MS (m/z):

576, $[M - Ph_2MeSiH]^+$.

2.2.2.2 Synthesis of $TpRu(PPh_3)(\eta^3-HSiPhMe_2H)$ (**1c**) This complex was

synthesized by using the same procedure as for the preparation of **1b**,

except that $PhMe_2SiH$ was used in place of Ph_2MeSiH . Yield: 0.11 g (48%).

Anal. Calcd (%) for $C_{35}H_{38}BN_6PRuSi$: C 58.90, H 5.37, N 11.78. Found: C

58.91, H 5.41, N 11.80. IR (KBr): $\nu(Ru-H) = 2013$ (m), $\nu(B-H) = 2464$ (m).

1H NMR (400.13 MHz, CD_2Cl_2 , $25^\circ C$): $\delta -11.06$ (d, 2H, Ru-H, $^1J_{SiH} = 19.2$

Hz, $^2J_{HP} = 22.8$ Hz); 0.36 (s, 6H, Si(CH_3) $_2$); 5.33 (t, 1H of Tp), 5.77 (t, 2H

of Tp), 5.88 (d, 1H of Tp), 7.58 (d, 2H of Tp), 7.66 (d, 1H of Tp), 7.93 (d,

2H of Tp), 6.03–7.30 (m, 20H of Ph). $^{13}\text{C}\{^1\text{H}\}$ NMR (100.61 MHz, CD_2Cl_2 , 25°C): δ 13.05 (s, $\text{Si}(\text{CH}_3)_2$). $^{31}\text{P}\{^1\text{H}\}$ NMR (161.7 MHz, CD_2Cl_2 , 25°C): δ 71.0. $^{29}\text{Si}\{^1\text{H}\}$ NMR (79.50 MHz, CD_2Cl_2 , 25°C): δ 15.1 (s). ESI-MS (m/z): 576, $[\text{M} - \text{PhMe}_2\text{SiH}]^+$.

2.2.2.3 General Procedures for the Hydrolysis of Silanes Catalyzed by $\text{TpRu}(\text{PPh}_3)(\eta^3\text{-H}_2\text{SiPhMe}_2)$ (**1c**).

The catalyst **1c** (7.1 mg, 0.01 mmol) was loaded into a 25 mL two-necked pear-shaped flask, which was then evacuated and flushed with nitrogen for four cycles. Silane (0.5 mmol), water (0.36 mL, 20 mmol), and 1,4-dioxane (2 mL) were then added to the flask via syringes and needles (In the case of Ph_3SiH , the solid was loaded into the flask prior to system evacuation and nitrogen-flushing), and the resulting solution was stirred under constant nitrogen flow in a preheated 90°C silicone oil bath for the pre-designated times. At the end of the reaction, the flask was cooled to room temperature; a 0.1 mL aliquot of the solution was withdrawn and analyzed by ^1H NMR spectroscopy (in CD_3COCD_3 or CD_3CN). Conversions were determined by comparison of the integrations of the characteristic peaks of the product and the unreacted silane.

2.2.2.4 Monitoring of 1c-Catalyzed Hydrolytic Oxidation of PhMe₂SiH to PhMe₂SiOH with NMR spectroscopy. A sample of **1c** (31.2 mg) was loaded into a J. Young valved NMR tube. The tube was evacuated and filled with nitrogen for four cycles. PhMe₂SiH (33 μ L, 5 equiv), water (157 μ L, 200 equiv), and 1,4-dioxane-*d*₈ (1 mL) were added via syringes and needles. The resulting solution was heated to 90°C. At different time intervals, the tube was cooled to room temperature. ¹H and ³¹P NMR spectra of the solution were then taken.

2.2.2.5 Monitoring of the Reaction Between 1c and EtMe₂SiH. A sample of **1c** (31.2 mg) was loaded into a J. Young valved NMR tube. The tube was evacuated and filled with nitrogen for four cycles. EtMe₂SiH (28 μ L, 5 equiv) and 1,4-dioxane-*d*₈ (1 mL) were added via syringes and needles. The solution was heated to 90°C for 3h. The tube was cooled to room temperature, ¹H and ³¹P NMR spectra of the solution were taken.

2.2.2.6 Crystallographic Structure Analysis of $\text{TpRu}(\text{PPh}_3)(\eta^3\text{-HSiPh}_3\text{H})$ (**1a**),

$\text{TpRu}(\text{PPh}_3)(\eta^3\text{-HSiPh}_2\text{MeH})$ (**1b**), and

$\text{TpRu}(\text{PPh}_3)(\eta^3\text{-HSiPhMe}_2\text{H})\cdot 3\text{CH}_2\text{Cl}_2$ (**1c**).

Orange crystals of **1a-c** suitable for X-ray diffraction study were obtained by layering of *n*-hexane on a dichloromethane solution of the complexes. A suitable crystal of **1a** with dimensions $0.32 \times 0.3 \times 0.28$ mm, or **1b** with dimensions $0.50 \times 0.48 \times 0.32$ mm, or **1c** with dimensions $0.42 \times 0.36 \times 0.30$ mm was mounted on a Bruker CCD area detector diffractometer and subjected to Mo $K\alpha$ radiation ($\lambda = 0.71073$ Å) from a generator operating at 50kV and 30 mA. The intensity data of **1a**, **1b**, and **1c** were collected in the range $\theta = 1.94\text{--}27.39^\circ$, $2.09\text{--}27.33^\circ$, and $1.17\text{--}27.46^\circ$, respectively, with oscillation frames of Ψ and ω and in the range $0\text{--}180^\circ$. A total of 1728 frames in **1a**, 800 in **1b**, and 988 in **1c**, were taken in four shells. An empirical absorption correction of the SADABS (Sheldrick, 1996) program based on Fourier coefficient fitting was applied. The crystal structures were solved by Patterson function methods and expanded by difference Fourier synthesis, and refined by full-matrix least-squares on F2 using the Bruker smart and Bruker SHELXTL program packages. All non-hydrogen atoms were refined anisotropically. Hydrogen atoms were placed in ideal positions

and refined as rigid atoms. The R and R_w values of **1a**, **1b** and **1c** are 0.0335 and 0.0528, 0.0320 and 0.0758, and 0.0437 and 0.1069, respectively. CCDC-763941 (**1a**), CCDC-763942 (**1b**) and CCDC-763943 (**1c**) contain the supplementary crystallographic data for this paper. These data can be obtained free of charge from The Cambridge Crystallographic Data Centre via www.ccdc.cam.ac.uk/data_request/cif.

2.2.2.7 Computational Details

Molecular geometries of the model complexes were optimized without constraints via DFT calculations using the mPW1K [124] functional. Frequency calculations at the same level of theory have also been performed to identify all the stationary points as minima (zero imaginary frequencies) or transition states (one imaginary frequency). Transition states were located using the Berny algorithm. Intrinsic reaction coordinates (IRC) [125, 126] were calculated for the transition states to confirm that such structures indeed connect two relevant minima. The effective core potentials (ECPs) of Hay and Wadt with double- ζ valence basis sets (LanL2DZ) [127] were used to describe Ru, P and Si. Polarization functions were also added for Ru ($\zeta_f = 1.235$), P ($\zeta_d = 0.387$), Si ($\zeta_d = 0.284$). [128, 129] The 6-311G (d,

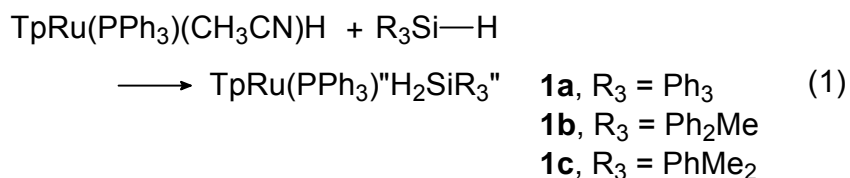
p) Pople basis set was used for water molecule and those H atoms that were directly bonded to the metal center.[130] The 6-311G basis set was used for all the other atoms.[131–133] All of the DFT calculations were performed with the Gaussian 03 package.[134]

2.3 Results and Discussion

2.3.1 Synthesis and X-ray Crystallographic Study of $\text{TpRu}(\text{PPh}_3)\text{H}_2\text{SiR}_3$

The complex $\text{TpRu}(\text{PPh}_3)\text{H}_2\text{SiPh}_3$ (**1a**) is one of the members of the series of complexes $\text{TpRu}(\text{PPh}_3)\text{H}_2\text{SiR}_3$ which we had previously reported [121]. Complexes $\text{TpRu}(\text{PPh}_3)\text{H}_2\text{SiPh}_2\text{Me}$ (**1b**) and $\text{TpRu}(\text{PPh}_3)\text{H}_2\text{SiPhMe}_2$ (**1c**) are new members of the series; they were synthesized according to our previously reported procedure, i.e. by reacting the solvent hydride precursor $\text{TpRu}(\text{PPh}_3)(\text{CH}_3\text{CN})\text{H}$ with the corresponding organosilanes (eq 1). Similar to those of other complexes in the series, the ^1H NMR spectra of **1b** and **1c** each shows a doublet hydride signal, which integrates for two hydrogens and does not show sign of decoalescence down to -100°C in the upfield region (for **1b**, at $\delta -9.93$ ppm, $J(\text{HP}) = 22.6$ Hz; for **1c**, at $\delta -11.06$ ppm, $J(\text{HP}) = 22.8$ Hz). The hydride signals of **1b** and **1c** are flanked by ^{29}Si satellites; the observed $J(\text{SiH})$ value

for **1b** is 25.0 Hz and that for **1c** is 19.2 Hz. These values are comparable to those of the other complexes in the series.



Crystals of **1a-c** suitable for X-ray crystallographic studies were obtained by layering *n*-hexane on dichloromethane solutions of the complexes. The molecular structures of **1a-c** are shown, respectively in Figures 1-3. The crystal data and refinement details are given in Table 1. Selected bond distances and angles are listed in Table 2. It is noted that the two hydrogen atoms HM1 and HM2 in each of the structures are located and refined. A common feature of the structures of **1a-c** is that the silicon atom interacts almost symmetrically with the two hydrogen atoms HM1 and HM2; the Si-H bond distances lie at the long end of the 2 Å limit normally admitted for σ -Si-H bonds [135, 136]. The ruthenium-hydrogen (Ru-HM1 and Ru-HM2) bond lengths (1.49 Å–1.568 Å) are within the normal range of classical ruthenium-hydride bond distances. In addition, the two H-Ru-Si angles in each of the complexes are very close to each other (53.9° and

57.3° in **1a**; 52.6° and 54.8° in **1b**; 53.9° and 54.8° in **1c**). The X-ray structures of **1a-c** therefore reveal that these complexes are more appropriately formulated as $\text{TpRu}(\text{PPh}_3)(\eta^3\text{-HSiR}_3\text{H})$ containing a nearly symmetrical $\text{H}\cdots\text{Si}\cdots\text{H}$ bonding in the $[\text{HSiR}_3\text{H}]^-$ moiety. On the basis of our model previously used in the B3LYP calculations, it was shown that the rapidly interchanging σ -silane hydride enantiomeric pair $\text{TpRu}(\text{PPh}_3)(\text{H}_a)(\eta^2\text{-H}_b\text{SiR}_3) \rightleftharpoons \text{TpRu}(\text{PPh}_3)(\text{H}_b)(\eta^2\text{-H}_a\text{SiR}_3)$ are slightly lower in energy (2.1 kJ/mol) than the corresponding symmetrical structure, which was regarded as the transition state for the interchange of the enantiomeric pairs. The B3LYP calculation was performed on a model complex in which the Tp, PPh₃, and SiR₃ moieties were replaced by (H₂C=NNH)₃BH, PH₃, and SiH₃, respectively [121].

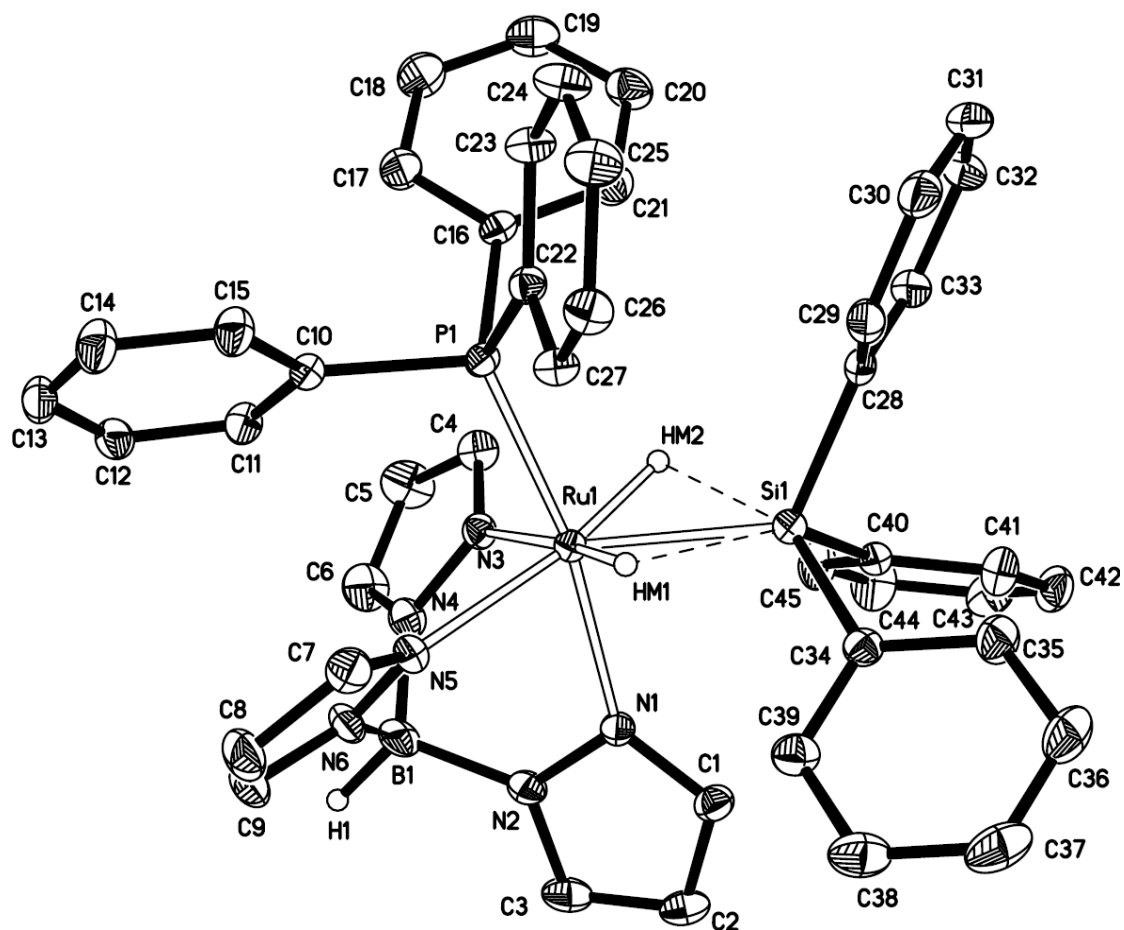


Figure 2.1 ORTEP view (30% probability) of $\text{TpRu}(\text{PPh}_3)(\eta^3\text{-HSiPh}_3\text{H})$ showing the atom-labeling scheme.

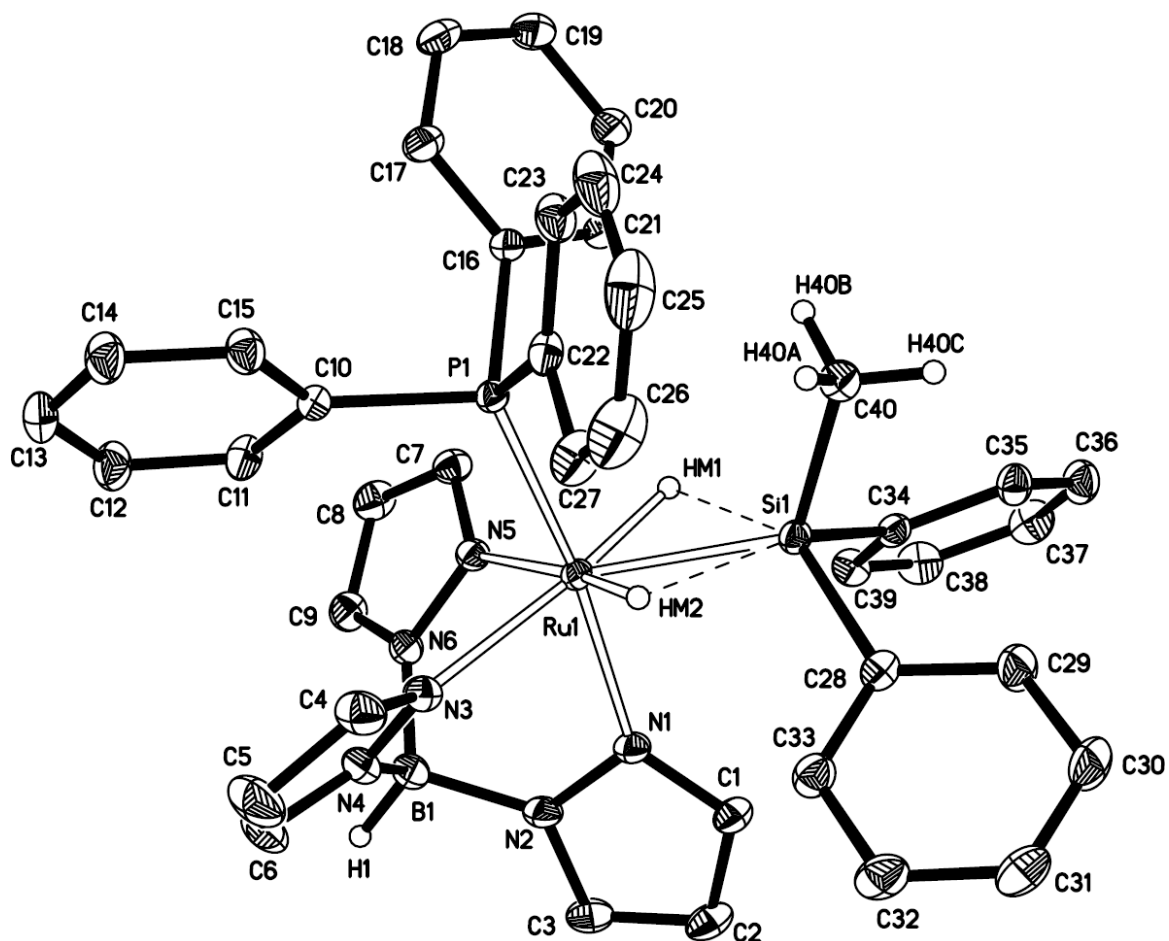


Figure 2.2 ORTEP view (30% probability) of TpRu(PPh₃)(η³-HSiPh₂MeH) showing the atom-labeling scheme.

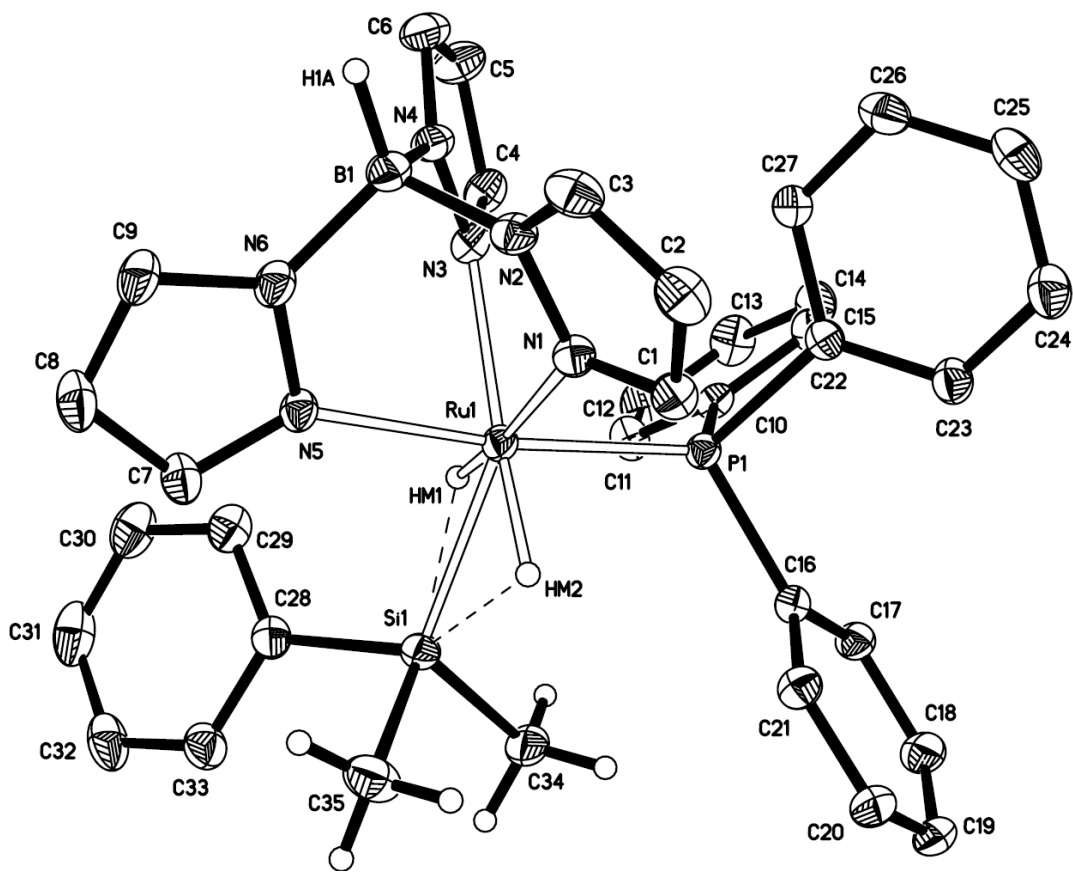


Figure 2.3 ORTEP view (30% probability) of $\text{TpRu}(\text{PPh}_3)(\eta^3\text{-HSiPhMe}_2\text{H})$ showing the atom-labeling scheme.

Table 2.1 Crystal Data and Structure Refinement of $\text{TpRu}(\text{PPh}_3)(\eta^3\text{-HSiPh}_3\text{H})$

Empirical formula	$\text{C}_{45}\text{H}_{42}\text{BN}_6\text{PRuSi}$
Formula weight	837.79
Temperature / K	296(2)
Wavelength / Å	0.71073
Crystal system	Monoclinic
Space group	$P2_1/c$
Unit cell dimensions:	$a = 16.1421(3)\text{Å}$ $\alpha = 90^\circ$ $b = 12.2111(2)\text{Å}$ $\beta = 105.2180(10)^\circ$ $c = 21.2219(4)\text{Å}$ $\gamma = 90^\circ$
Volume / Å ³	4036.42(13)
Z	4
Density (calculated) / g cm ⁻³	1.379
Absorption coefficient mm ⁻¹	0.498
F(000)	1728
Crystal size / mm ³	$0.32 \times 0.3 \times 0.28$
Theta range for data collection / °	1.94 to 27.39
Index ranges / °	$-20 \leq h \leq 20$, $-15 \leq k \leq 15$, $-27 \leq l \leq 27$
Reflection collected	87540
Independent reflections	9136 [$R(\text{int}) = 0.3921$]
Completeness to theta = 27.39° / %	99.8
Absorption correction	Semi-empirical from equivalents
Max. transmission	1.000
Min. transmission	0.840
Refinement method	Full-matrix least-squares on F^2
Data/restraints/parameters	9136 / 0 / 508
Goodness-of-fit on F^2	0.735
Final R indices [$I > 2\sigma(I)$]	$R_1 = 0.0335$, $wR_2 = 0.0528$
R indices (all data)	$R_1 = 0.2735$, $wR_2 = 0.0645$
Largest diff. peak and hole / e Å ⁻³	0.409 and -0.303

Table 2.2 Selected bond Distance (Å) and Angles (°) for **TpRu(PPh₃)(η³-HSiPh₃H) (1a)**

Bond distances (Å)			
Ru(1)–N(1)	2.2087(13)	Ru(1)–HM(2)	1.502(15)
Ru(1)–N(3)	2.1668(16)	Si(1)–HM(1)	2.016(14)
Ru(1)–N(5)	2.1576(15)	Si(1)–HM(2)	1.928(14)
Ru(1)–P(1)	2.2973(4)	Ru(1)–Si(1)	2.3816(5)
Ru(1)–HM(1)	1.491(15)		

Bond angles (°)			
N(5)–Ru(1)–N(3)	88.81(6)	N(3)–Ru(1)–HM1	173.6(5)
N(5)–Ru(1)–N(1)	80.45(5)	N(1)–Ru(1)–HM1	97.1(5)
N(3)–Ru(1)–N(1)	82.32(5)	P(1)–Ru(1)–HM1	87.1(5)
N(5)–Ru(1)–P(1)	90.69(4)	Si(1)–Ru(1)–HM1	57.3(5)
N(3)–Ru(1)–P(1)	92.54(4)	N(5)–Ru(1)–HM2	168.7(5)
N(1)–Ru(1)–P(1)	169.81(4)	N(3)–Ru(1)–HM2	81.5(6)
N(5)–Ru(1)–Si(1)	137.33(4)	N(1)–Ru(1)–HM2	103.8(5)
N(3)–Ru(1)–Si(1)	128.81(4)	P(1)–Ru(1)–HM2	84.0(5)
N(1)–Ru(1)–Si(1)	85.19(4)	Si(1)–Ru(1)–HM2	53.9(5)
P(1)–Ru(1)–Si(1)	104.829(18)	HM1–Ru(1)–HM2	104.9(8)
N(5)–Ru(1)–HM1	84.8(5)		

Table 2.3 Crstal Data and Structure Refinement of TpRu(PPh₃)(η³-HSiPh₂MeH)

Empirical formula	C ₄₀ H ₄₀ BN ₆ PRuSi
Formula weight	775.72
Temperature / K	296(2)
Wavelength / Å	0.71073
Crystal system	Triclinic
Space group	<i>P</i> 1
Unit cell dimensions:	a = 10.4776(2)Å α = 77.8800(10)° b = 11.3027(2)Å β = 74.1180(10)° c = 11.1167(4) Å γ = 72.9730(10)°
Volume / Å ³	1845.54(6)
Z	2
Density (calculated) / g cm ⁻³	1.396
Absorption coefficient mm ⁻¹	0.539
F(000)	800
Crystal size / mm ³	0.50 × 0.48 × 0.32
Theta range for data collection /°	2.09 to 27.33
Index ranges /°	-13 ≤ <i>h</i> ≤ 13, -14 ≤ <i>k</i> ≤ 14, -22 ≤ <i>l</i> ≤ 21
Reflection collected	25782
Independent reflections	8282 [<i>R</i> (int) = 0.0347]
Completeness to theta = 27.39° / %	99.1
Absorption correction	Semi-empirical from equivalents
Max. transmission	1.000
Min. transmission	0.819
Refinement method	Full-matrix least-squares on <i>F</i> ²
Data/restraints/parameters	8282 / 0 / 459
Goodness-of-fit on <i>F</i> ²	1.004
Final R indices [<i>I</i> > 2σ(<i>I</i>)]	<i>R</i> ₁ = 0.0320, <i>wR</i> ₂ = 0.0758
R indices (all data)	<i>R</i> ₁ = 0.0416, <i>wR</i> ₂ = 0.0812
Largest diff. peak and hole / e Å ⁻³	0.505 and -0.525

Table 2.4 Selected bond Distance (Å) and Angles (°) for **TpRu(PPh₃)(η³-HSiPh₂MeH) (1b)**

Bond distances (Å)			
Ru(1)–N(1)	2.1866(13)	Ru(1)–HM(2)	1.492(16)
Ru(1)–N(3)	2.1691(13)	Si(1)–HM(1)	1.903(15)
Ru(1)–N(5)	2.1689(12)	Si(1)–HM(2)	1.955(16)
Ru(1)–P(1)	2.2997(4)	Ru(1)–Si(1)	2.3905(4)
Ru(1)–HM(1)	1.568(16)		

Bond angles (°)			
N(3)–Ru(1)–P(1)	91.31(4)	P(1)–Ru(1)–HM1	88.5(6)
N(1)–Ru(1)–P(1)	172.88(3)	Si(1)–Ru(1)–HM1	52.6(5)
N(5)–Ru(1)–Si(1)	133.20(3)	N(5)–Ru(1)–HM2	172.0(6)
N(3)–Ru(1)–Si(1)	136.94(4)	N(3)–Ru(1)–HM2	84.9(6)
N(1)–Ru(1)–Si(1)	88.34(3)	N(1)–Ru(1)–HM2	97.0(7)
P(1)–Ru(1)–Si(1)	97.640(13)	P(1)–Ru(1)–HM2	83.4(6)
N(5)–Ru(1)–HM1	83.1(5)	Si(1)–Ru(1)–HM2	54.8(6)
N(3)–Ru(1)–HM1	170.3(5)	HM1–Ru(1)–HM2	104.7(8)
N(1)–Ru(1)–HM1	98.3(6)		

Table 2.5 Crstal Data and Structure Refinement of **TpRu(PPh₃)(η³-HSiPhMe₂H)**

Empirical formula	C ₃₈ H ₄₄ BCl ₆ N ₆ PRuSi
Formula weight	968.43
Temperature / K	296(2)
Wavelength / Å	0.71073
Crystal system	Triclinic
Space group	<i>P</i> 1
Unit cell dimensions:	a = 10.8951(2)Å α = 87.5410(10)° b = 12.6105(2)Å β = 79.7450(10)° c = 17.6399(3) Å γ = 69.5820(10)°
Volume / Å ³	2234.56(7)
Z	2
Density (calculated) / g cm ⁻³	1.439
Absorption coefficient mm ⁻¹	0.807
F(000)	988
Crystal size / mm ³	0.42 × 0.36 × 0.30
Theta range for data collection /°	1.17 to 27.46
Index ranges /°	-14 ≤ <i>h</i> ≤ 14, -16 ≤ <i>k</i> ≤ 16, -22 ≤ <i>l</i> ≤ 22
Reflection collected	48788
Independent reflections	10102 [<i>R</i> (int) = 0.0558]
Completeness to theta = 27.39° / %	98.8
Absorption correction	Semi-empirical from equivalents
Max. transmission	1.000
Min. transmission	0.805
Refinement method	Full-matrix least-squares on <i>F</i> ²
Data/restraints/parameters	10102 / 499
Goodness-of-fit on <i>F</i> ²	1.004
Final R indices [<i>I</i> > 2σ(<i>I</i>)]	<i>R</i> ₁ = 0.0437, <i>wR</i> ₂ = 0.1069
R indices (all data)	<i>R</i> ₁ = 0.0649, <i>wR</i> ₂ = 0.1181
Largest diff. peak and hole / e Å ⁻³	0.695 and -0.609

Table 2.6 Selected bond Distance (Å) and Angles (°) for **TpRu(PPh₃)(η³-HSiPhMe₂H).3CH₂Cl₂ (1c)**

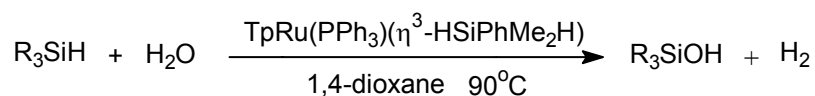
Bond distances (Å)			
Ru(1)–N(1)	2.1648(15)	Ru(1)–HM(2)	1.49(2)
Ru(1)–N(3)	2.1807(17)	Si(1)–HM(1)	1.94(2)
Ru(1)–N(5)	2.1976(17)	Si(1)–HM(2)	1.965(18)
Ru(1)–P(1)	2.2750(5)	Ru(1)–Si(1)	2.4006(5)
Ru(1)–HM(1)	1.49(2)		

Bond angles (°)			
N(1)–Ru(1)–N(3)	87.22(6)	N(3)–Ru(1)–HM1	84.3(8)
N(1)–Ru(1)–N(5)	82.82(6)	N(5)–Ru(1)–HM1	98.7(9)
N(3)–Ru(1)–N(5)	82.33(6)	P(1)–Ru(1)–HM1	85.5(9)
N(1)–Ru(1)–P(1)	92.17(5)	Si(1)–Ru(1)–HM1	53.9(8)
N(3)–Ru(1)–P(1)	92.65(5)	N(1)–Ru(1)–HM2	82.7(7)
N(5)–Ru(1)–P(1)	173.05(4)	N(3)–Ru(1)–HM2	169.9(7)
N(1)–Ru(1)–Si(1)	134.96(5)	N(5)–Ru(1)–HM2	95.7(8)
N(3)–Ru(1)–Si(1)	134.60(4)	P(1)–Ru(1)–HM2	88.4(8)
N(5)–Ru(1)–Si(1)	86.91(4)	Si(1)–Ru(1)–HM2	54.8(7)
P(1)–Ru(1)–Si(1)	100.04(2)	HM1–Ru(1)–HM2	105.8(11)
N(1)–Ru(1)–HM1	171.1(8)		

2.3.2 Catalytic hydrolytic oxidation of organosilanes to silanols with $\text{TpRu}(\text{PPh}_3)(\eta^3\text{-HSiPhMe}_2\text{H})$ (**1c**).

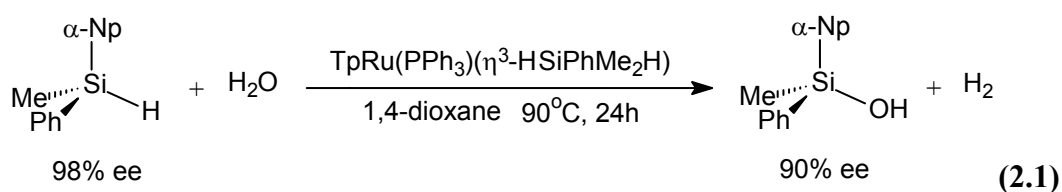
Complexes **1a-1c** can be readily synthesized; we suspect that it would make no difference using any one of them for the catalytic hydrolytic oxidation of silanes (eq 2). Table 3 shows the results of the **1c**-catalyzed hydrolytic oxidation of silanes to silanols. The reactions did not proceed at room temperature and were performed at 90°C. Trialkyl silanes (entries 4–9) were oxidized more readily than the silanes bearing aryl substituents (entries 1-3, 10). In all the reactions reported, disiloxanes resulting from condensation of silanols were basically not detected (See appendices). Formation of undesirable side products such as disiloxane and polymeric siloxanes were often observed in the catalytic hydrolytic oxidation of hydrosilanes reported in the literature. It is important to note that the optically active silane *R*-(+)-Me(α -Np)PhSiH (98% ee) was hydrolyzed to yield *S*-(+)-Me(α -Np)PhSiOH with retention (entry 11 & eq. 2.1).

Table 2.7 Hydrolytic Oxidation of Organosilanes to Silanols with $\text{TpRu}(\text{PPh}_3)(\eta^3\text{-HSiPhMe}_2\text{H})$ (1c**).^[a]**



entry	Silane	time(h)	conversion (%) ^[b]
1	Ph_3SiH	24	84
2	Ph_2MeSiH	24	99
3	PhMe_2SiH	20	96
4	$t\text{BuMe}_2\text{SiH}$	4	96
5	EtMe_2SiH	2	97
6	CyMe_2SiH	2	94
7	$\text{CH}_3(\text{CH}_2)_{16}\text{CH}_2\text{Me}_2\text{SiH}$	4	94
8	Et_3SiH	4	97
9	Et_2MeSiH	4	85
10	$1,4\text{-(SiMe}_2\text{H)C}_6\text{H}_4$	24	65
11	$R\text{-}(+)\text{-Me}(\alpha\text{-Np})\text{PhSiH}$	24	91 ^[c]

[a] Reaction conditions: silane (0.5 mmol), H_2O (40 equivalents), **1c** (10 μmol , 2 mol% with respect to silane), 1,4-dioxane (2 mL), 90°C , under nitrogen flow. [b] Determined by ^1H NMR spectroscopy. [c] product : $S\text{-}(+)\text{-Me}(\alpha\text{-Np})\text{PhSiOH}$, isolated yield, 90 % ee.



2.3.3 NMR monitoring of the **1c**-catalyzed hydrolytic oxidation of PhMe₂SiH to PhMe₂SiOH.

Five equiv of PhMe₂SiH and 200 equiv of water were added to a 1,4-dioxane-*d*₈ solution of **1c** in a J. Young valved NMR tube and the tube was heated in an oil bath at 90 °C. Figure 4 shows the ³¹P{¹H} and ¹H NMR spectra of the solution taken at different times; the column at the far right shows the percent conversions (estimated from the integrations of the methyl peaks of the PhMe₂SiH and PhMe₂SiOH in the ¹H NMR spectra) to the products. The ³¹P{¹H} NMR spectrum of the solution taken after 10 min of heating showed that **1c** was present as the overwhelming species; around 2% of the dihydrogen-hydride complex TpRu(PPh₃)(H₂)H (**2**) [137] was also formed. As the reaction proceeded, the amount of **2** increased at the expense of that of **1c**; at the end of the reaction, **1c** was nearly all converted to **2**. The presence of **1c** and **2** and the variation of their amounts at different times were corroborated by the ¹H NMR spectra of the solution which showed the hydride signals of **1c** and **2** in the upfield region. It should be pointed out that in this experiment, the H₂ by-product was trapped in the NMR tube.

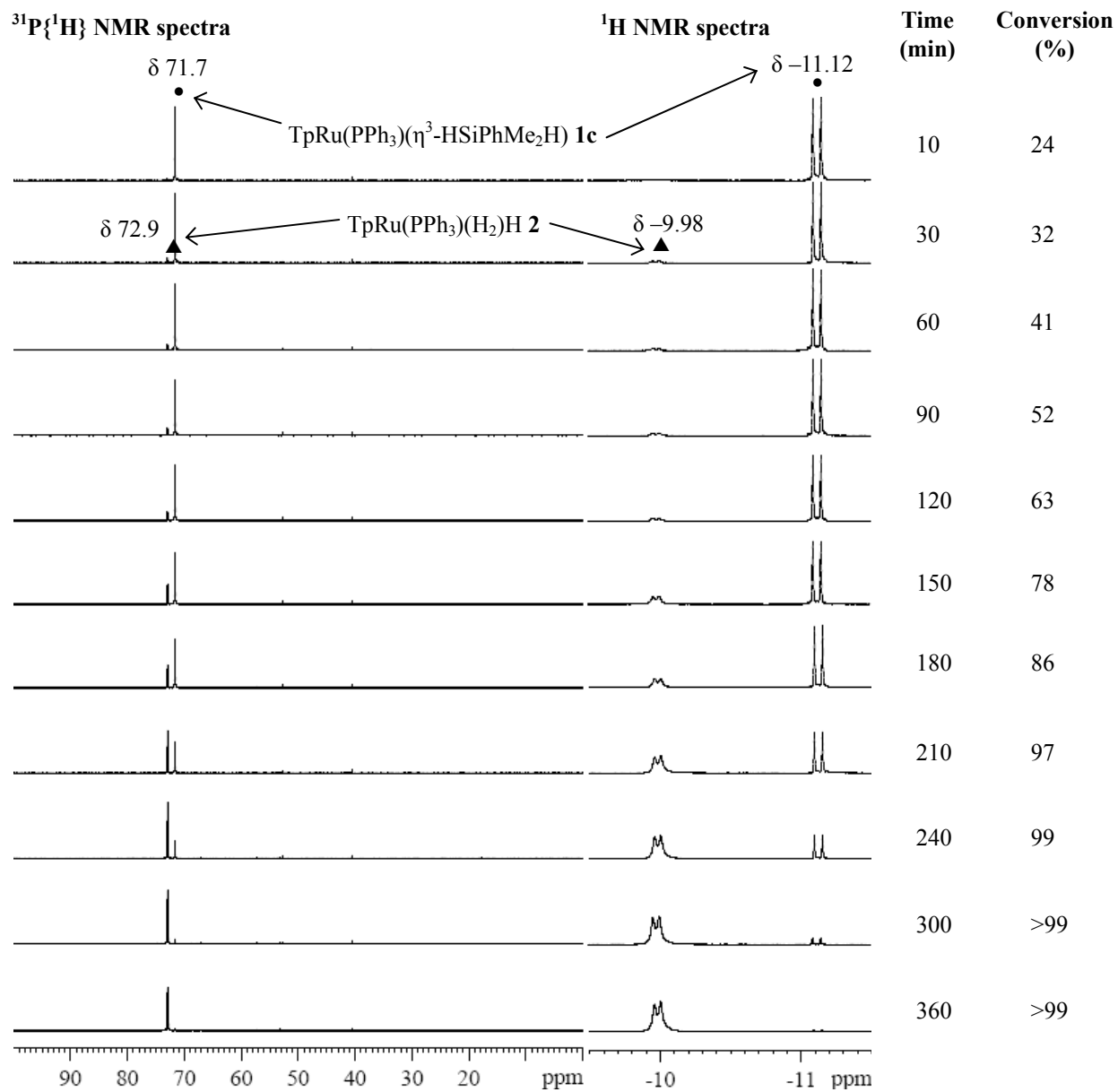
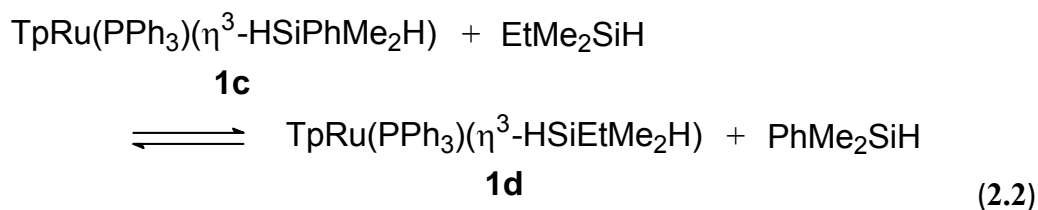


Figure 2.4 NMR study of **1c**-catalyzed hydrolysis of PhMe₂SiH to PhMe₂SiOH

2.3.4 Relative stability of $\text{TpRu}(\text{PPh}_3)(\eta^3\text{-HSiPhMe}_2\text{H})$ (**1c**) and $\text{TpRu}(\text{PPh}_3)(\eta^3\text{-HSiEtMe}_2\text{H})$ (**1d**)

In the course of growing single crystals for X-ray crystallographic studies, we learned that the complexes containing trialkyl silanes are less stable than those containing silanes with aryl groups; the trialkyl silane complexes undergo decomposition more readily; and we have not been able to obtain single crystals of them. We therefore carried out ligand substitution of **1c** with HSiEtMe_2 (eq. 2.2) to gain a more quantitative comparison of the thermal stability of **1c** and **1d**. It was learned that after heating a 1,4-dioxane- d_8 solution of **1c** in the presence of 5 equiv of HSiEtMe_2 at 90 °C for 3h, the relative equilibrium concentrations of **1c** : **1d** was ~ 50 : 50; the equilibrium constant K_{eq} is estimated to be 1.1×10^{-1} . This experiment therefore shows that the thermal stability of **1c** is about 9 times that of **1d**. The $[\text{H}_2\text{SiR}_3]^-$ moiety, in bonding to the metal fragment, transfers electron-density from the occupied orbitals ψ_1 and ψ_2 to the metal-center orbitals; on the other hand, the metal back-donates a lone pair into the empty ψ_3 orbital of $[\text{H}_2\text{SiR}_3]^-$ [9, 138] Here, ψ_1 is the all-in-phase combination of the two H 1s orbitals and the SiR_3 sp^3 -hybridized orbital, ψ_2 is the out-of-phase combination of the two H 1s orbitals only, and ψ_3 is the

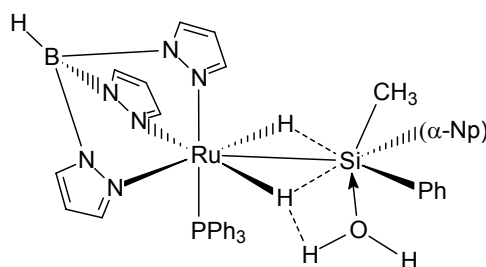
all-out-of-phase combination of the two H 1s orbitals and the SiR₃ sp³-hybridized orbital. The higher stability of **1c** vs **1d** is probably due to the phenyl group of the silane ligand in the former being able to invite more back-donation from the metal.



2.3.5 Proposed mechanism for the catalytic hydrolytic oxidation of silanes to silanols

The NMR monitoring experiment above shows that in the course of catalysis, the silane complex **1c** and TpRu(PPh₃)(H₂)H (**2**) were the only detectable organometallic complexes; these two complexes are interconvertible via ligand exchange. We believe that **1c** is the key species reacting directly with water to generate the silanol. The fact that hydrolytic oxidation of the chiral silane *R*-(+)-Me(α-Np)PhSiH to give the silanol product *S*-(+)-Me(α-Np)PhSiOH with retention is a strong indication that the water molecule attacks the silicon center in a manner shown in Scheme

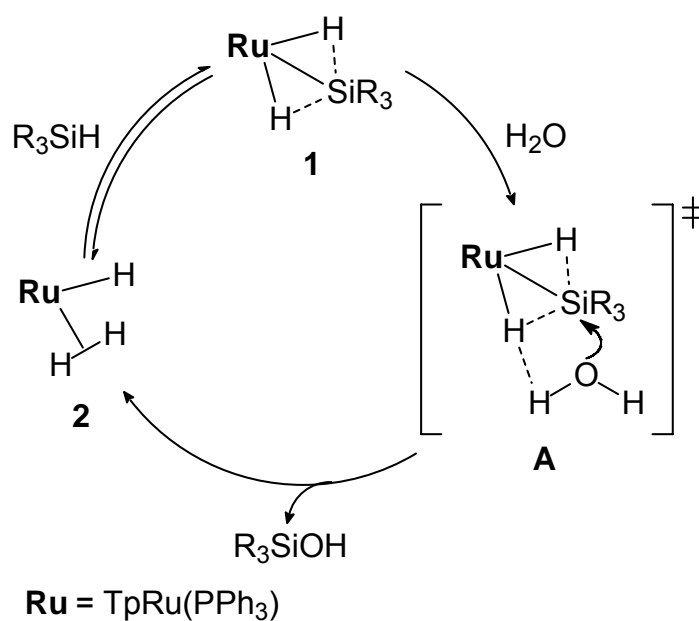
2.1. Dihydrogen-bonding interaction between the proton of the attacking water molecule and the hydride of the $(\text{H}_2\text{Si}(\text{Me})(\alpha\text{-Np})\text{Ph})^-$ moiety is expected to be present. We have reported similar dihydrogen-bonding interaction between the hydride ligand and the proton of the attacking water molecule in hydration of nitriles catalyzed by Ru-H complexes [139, 140].



Scheme 2.1 Attack of water on $[\text{H}_2\text{Si}(\text{Me})(\alpha\text{-Np})\text{Ph}]^-$ moiety.

Scheme 2.2 shows a possible mechanism for the hydrolytic oxidation of silanes to silanols. We propose the existence of dihydrogen-bonding interaction between one of the hydrides of the $[\text{H}_2\text{SiR}_3]^-$ moiety and a water proton during nucleophilic attack of the water molecule at the silicon center. Several studies of metal-silane interactions indicate that silane is a strong σ^* -accepting ligand because of the weaker H—Si σ -bonding. The metal ($d\pi$)-to-silane (σ^*) back-bonding is deemed very important for the metal-(η^2 -silane) interaction [141–143]. The lower activity of the aryl

silanes in comparison to the trialkyl silanes in the hydrolytic oxidation reactions can be explained in terms of the diminished electrophilicity of the silicon center resulting from more back bonding from the metal and the stronger Ru–Si bond in **A** when R₃ contains one or more phenyl groups. The lower electrophilicity at the silicon center renders the nucleophilic attack by the water more sluggish, and the strong Ru–Si bond would slow down the extrusion of the silanol product from the metal center.



Scheme 2.2 Proposed mechanism for the hydrolytic oxidation of organosilanes to silanols

To study the feasibility of the proposed reaction mechanism shown in Scheme 2.2 for the catalytic hydrolytic oxidation of silanes, DFT

calculations were performed to examine the catalytic cycle using $\text{TpRu}(\text{PMe}_3)(\eta^3\text{-HSiHMe}_2\text{H})$ (**1A**) as the model catalyst. The potential energy profile is shown in Figure 2.5 with the calculated relative electronic energies. The reaction of **1A** with water occurred by a nucleophilic attack of the water oxygen on the silicon center of the η^2 -silane ligand in a six-membered-ring transition state to give silanol and the dihydrogen complex **2A**. From the dihydrogen complex **2A**, a ligand substitution with silane occurs to regenerate **1A** and release a dihydrogen molecule, completing the catalytic cycle. The overall reaction barrier shown in Figure 2.5 is 90.0 kJ/mol and the hydrolysis reaction is thermodynamically favorable. These results support the proposed mechanism discussed above.

Figure 2.6 presents the optimized structures with selected structural parameters for the species shown in Figure 2.5. The bond distances calculated for the Ru–Si, Si–H and Ru–H bonds in **1A** are similar to those in $\text{TpRu}(\text{PPh}_3)(\eta^3\text{-HSiR}_3\text{H})$ determined experimentally. In **1A**, both hydride ligands maintain strong interaction with the silicon center of the silyl ligand, indicating the hypervalency around the silicon center [136]. The double silyl-hydrido interactions have been also found in $\text{Cp}(\text{Pr}^i_2\text{MeP})\text{FeH}_2\text{SiR}_3$

reported recently [15]. **2A** is a dihydrogen complex with an H–H distance of 0.90Å. The transition structure **TS_{A(1-2)}** displays a strong dihydrogen bonding with an H---H distance of 1.29 Å.

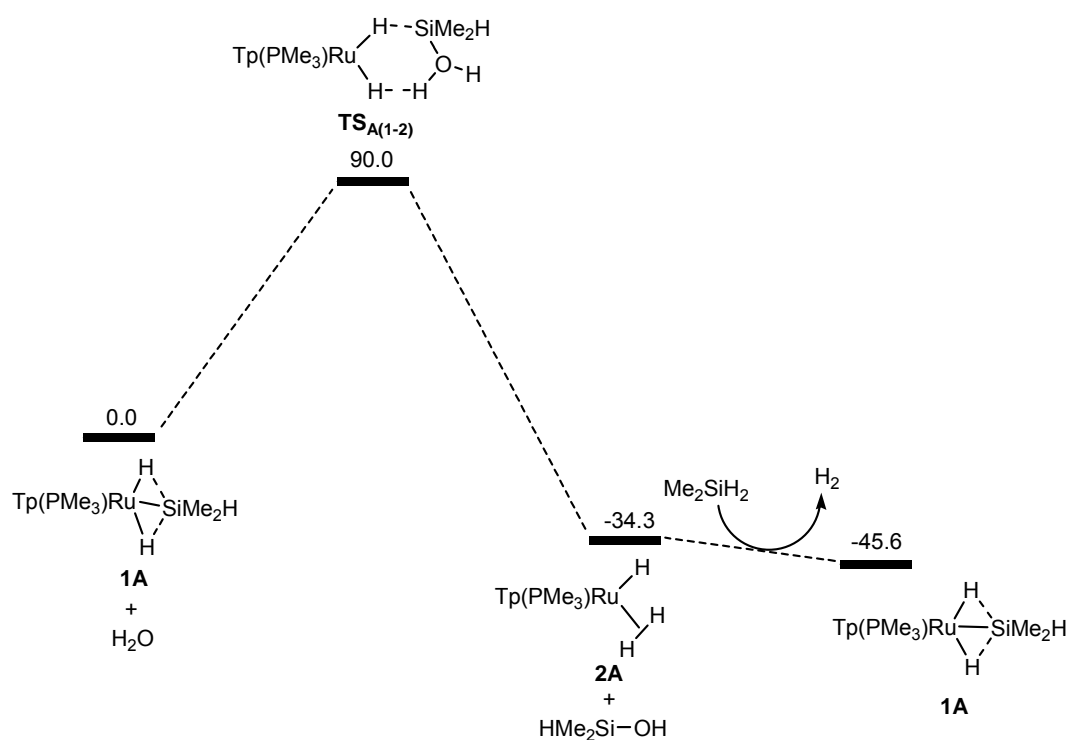


Figure 2.5 Energy profile calculated for the hydrolysis reaction of HSiHMe₂ catalyzed by TpRu(PMe₃)(η^3 -HSiHMe₂H) (**1A**). The calculated relative electronic energies are given in kJ/mol.

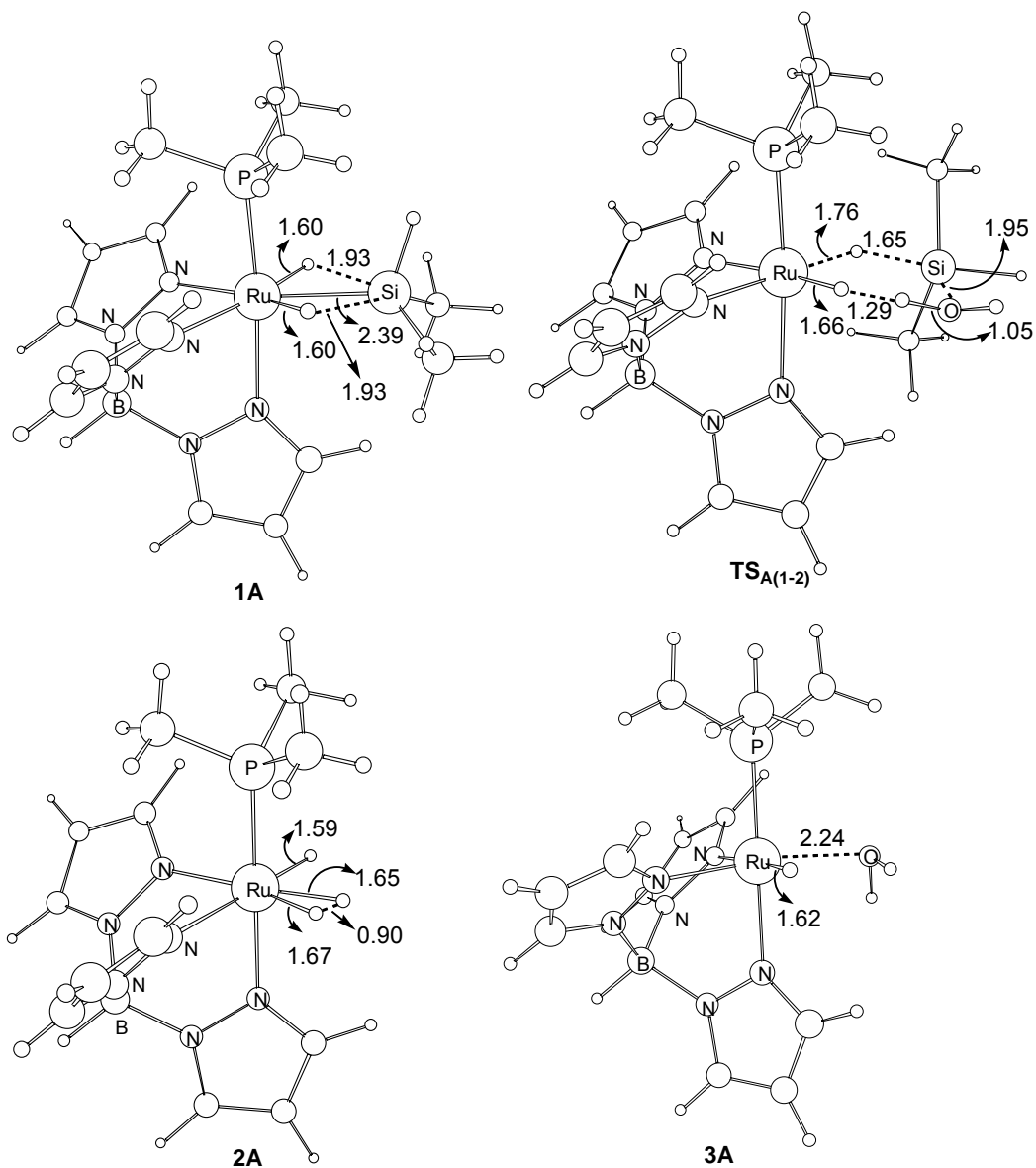
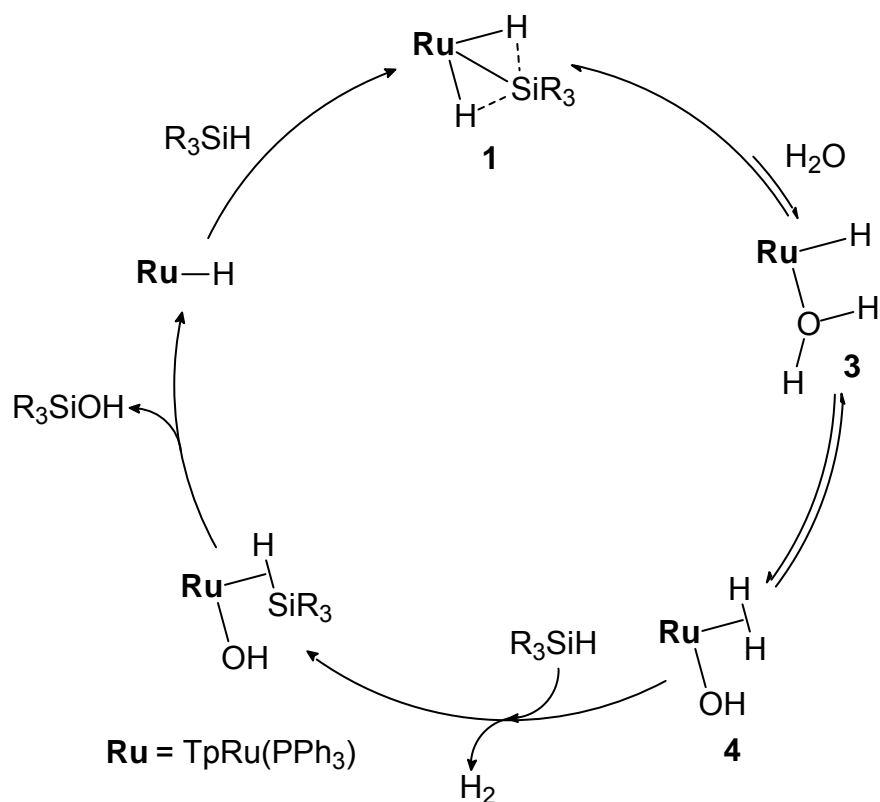


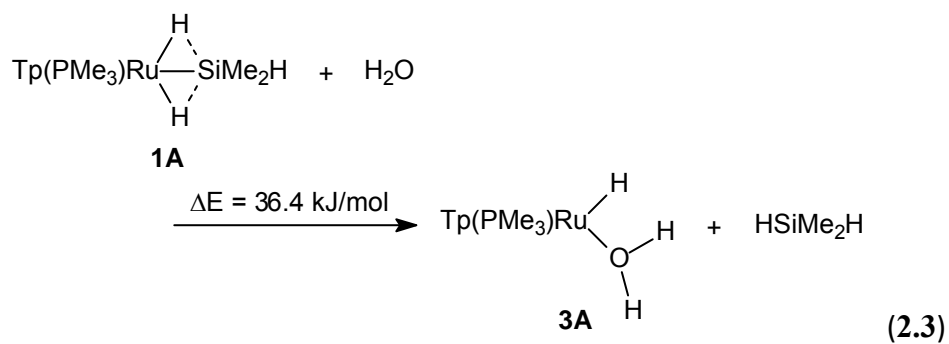
Figure 2.6 Optimized structures for the species involved in the hydrolysis reaction of HSiHMe₂ catalyzed by TpRu(PMe₃)(η^3 -HSiHMe₂H) (1A) (Figure 5). Bond distances are given in angstrom.

An alternate mechanism for the **1**-catalyzed hydrolytic oxidation of silanes is shown in Scheme 2.3. The cycle begins with the generation of the aquo-hydride complex **3** via H₂O/silane exchange, **3** then generates the hydroxo species **4**, probably via σ -bond metathesis [144–150]. Displacement of the dihydrogen ligand in **4** by silane, and subsequent intramolecular hydroxylation of the silane ligand yields the product and metal hydride. Although we have not observed the aquo-hydride complex **3** in the NMR monitoring experiment, we cannot, however, exclude the possibility that it might be present in trace amount therefore eluding NMR detection.

Our theoretical calculations show that the substitution of HSiHMe₂ by a water molecule is endothermic (eq. 2.3). **3A** is less stable than **1A** by 36.4 kJ/mol, consistent with the experiment results that the aquo-hydride complex **3A** was not observed. The energy required to dissociate a silane molecule from **1A** was estimated to be 124.3 kJ/mol, indicating that the substitution of water for silane is relatively difficult to occur.



Scheme 2.3 Alternative mechanism for the hydrolytic oxidation of organosilanes to silanols



Chapter 3 Ruthenium-catalyzed Reduction of Carbon Dioxide by hydrosilane

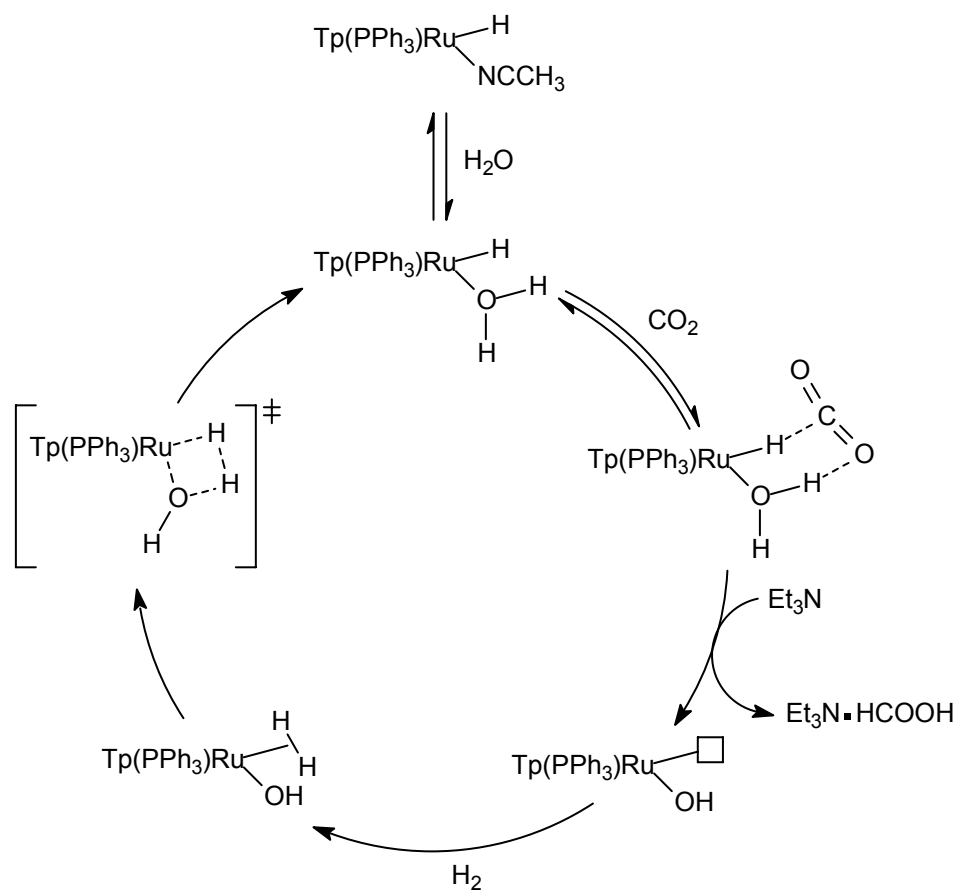
3.1 Introduction

Our group had previously reported the water-promoted hydrogenation of carbon dioxide to formic acid catalyzed by ruthenium solvento-hydride complex $\text{TpRu}(\text{PPh}_3)(\text{CH}_3\text{CN})\text{H}$ [151]. It is proposed that the key species, an aquo hydride species $\text{TpRu}(\text{PPh}_3)(\text{H}_2\text{O})\text{H}$, is generated by ligand displacement reaction of $\text{TpRu}(\text{PPh}_3)(\text{CH}_3\text{CN})\text{H}$ with H_2O ; the aquo hydride complex acts as a metal ligand bifunctional catalyst, transferring the hydride and a proton of the H_2O ligand in a concerted manner to CO_2 to yield formic acid, and itself being converted to a transient hydroxo species, which is reverted to $\text{TpRu}(\text{PPh}_3)(\text{H}_2\text{O})\text{H}$ by reaction with H_2 (**Scheme 3.1**).

Several years later, we reported that alcohols also exhibit a promoting effect in the $\text{TpRu}(\text{PPh}_3)(\text{CH}_3\text{CN})\text{H}$ -catalyzed CO_2 hydrogenation reactions [152]. It is believed that the active species in the catalysis is the analogous alcohol-hydride $\text{TpRu}(\text{PPh}_3)(\text{ROH})\text{H}$; the reaction proceeds via a reaction sequence similar to that shown in **Scheme 3.1**.

We have learned that the solvento-hydride complex $\text{TpRu}(\text{PPh}_3)(\text{CH}_3\text{CN})\text{H}$ reacts with silanes HSiR_3 ($\text{R}_3 = \text{Ph}_3, \text{Ph}_2\text{Me}, \text{PhMe}_2$) to yield non-classical silyl

dihydride complexes $\text{TpRu}(\text{PPh}_3)(\eta^3\text{-HSiR}_3\text{H})$. It is of interested to investigate if the electrophilic silyl group and the hydridic hydrogen in the complex can also be transferred in a concerted manner to CO_2 to yield a silyl formate HCOOSiPhMe_2 . Several catalytic reductions of carbon dioxide by silane have been reported in recent decades as means of CO_2 -transformation [55–64]. Reported here is a study of the reduction of carbon dioxide by PhMe_2SiH in the presence of the complex $\text{TpRu}(\text{PPh}_3)(\eta^3\text{-HSiPhMe}_2\text{H})$. The initial product silyl formate HCOOSiPhMe_2 was found to be further reduced by PhMe_2SiH to give silyl methoxide as the ultimate reduction product.



Scheme 3.1 Proposed mechanism for the $\text{TpRu(PPh}_3\text{)(CH}_3\text{CN)H}$ -catalyzed hydrogenation of carbon dioxide to formic acid

3.2 Experimental Section

3.2.1 Materials and Instrumentation

All manipulations were carried out under an inert nitrogen atmosphere using standard Schlenk techniques. Solvents were dried, degassed, and distilled prior to use: THF, 1,4-dioxane, and diethyl ether from Na benzophenone ketyl, *n*-hexane and toluene from Na, acetonitrile and dichloromethane from CaH₂. All chemicals were commercially available (Aldrich, Acros, Strem and International Laboratory) and used without further purification. The complex TpRu(PPh₃)(η³-HSiPhMe₂H) was synthesized using the method reported in section 2.2.2.1. The complexes TpRu(PPh₃)(CO)H [153] and TpRu(dppm)H [123] were prepared according to literature methods. Deuterated NMR solvents, purchased from Armar and Cambridge Isotope Laboratories, were dried with P₂O₅ prior to use. ¹H NMR spectra were obtained from a Varian (500 MHz) or Bruker DPX (400 MHz) spectrometer; chemical shifts were reported relative to residual protons of the deuterated solvents. ¹³C NMR spectra were recorded with a Bruker DPX 400 spectrometer at 100.61 MHz; chemical shifts were internally referenced to CD₂Cl₂ (δ = 53.8 ppm). ³¹P NMR spectra were recorded on a Bruker DPX 400 spectrometer at 161.70 Mz; chemical shifts were externally referenced to 85% H₃PO₄ in D₂O (δ = 0.00 ppm).

3.2.2 Reactions

3.2.2.1 NMR-monitoring of the reaction between CO₂ and TpRu(PPh₃)(η³-HSiPhMe₂H) in 1,4-dioxane-d₈

The complex TpRu(PPh₃)(η³-HSiPhMe₂H) (0.016 g, 26 μmol) was dissolved in 1,4-dioxane-*d*₈ (0.4 mL) in a pressure-valved NMR tube, which was then pressurized with 9 bar of CO₂. At different time intervals, the tube was cooled to room temperature and ¹H and ³¹P NMR spectra of the solution were taken.

3.2.2.2 NMR-monitoring of the reaction between CO₂ and PhMe₂SiH in the presence of TpRu(PPh₃)(η³-HSiPhMe₂H) 1c in 1,4-dioxane-d₈

The complex TpRu(PPh₃)(η³-HSiPhMe₂H) (0.016 g, 26 μmol) and PhMe₂SiH (70 μL, 5 equivalence) were dissolved in 1,4-dioxane-*d*₈ (0.4 mL) in a pressure-valved NMR tube. The resulting solution was heated at 110°C under 9 bar of CO₂. At different time intervals, the tube was cooled to room temperature and ¹H and ³¹P NMR spectra of the solution were taken.

3.2.2.3 In Situ Preparation of TpRu(PPh₃)(CO)(η¹-OCHO) (6)

The complex TpRu(PPh₃)(CO)H (0.016 g, 26 μmol) was loaded into a 5 mm pressure-valved NMR tube, which was then evacuated and flushed with nitrogen

for four cycles. 1,4-dioxane- d_8 (0.2 mL) and formic acid (0.2 mL) were added to the tube via syringes and needles. The tube was sealed and heated at 100°C in a silicone oil bath for 30 mins; it was cooled down to room temperature, and subjected to NMR analysis. ^1H NMR (400.13 MHz, 1,4-dioxane- d_8 , 25°C): δ 7.87 (s, 1H, -OCHO) 7.74 (d, 1H; Tp-H), 7.71 (d, 1H; Tp-H), 7.60 (d, 1H; Tp-H), 7.58 (d, 1H; Tp-H), 7.27–7.31 (m, 3H; PPh₃-H), 7.14–7.18 (m, 6H; PPh₃-H), 7.10 (d, 1H; Tp-H), 6.93–6.97 (m, 6H; PPh₃-H), 6.28 (d, 1H; Tp-H), 6.08 (t, 1H; Tp-H), 5.87 (t, 1H; Tp-H), 5.80 (t, 1H; Tp-H). $^{31}\text{P}\{^1\text{H}\}$ NMR (161.7 MHz, 1,4-dioxane- d_8 , 25°C): δ 44.4 ppm. $^{13}\text{C}\{^1\text{H}\}$ NMR (100.61 MHz, 1,4-dioxane- d_8 , 25°C): δ 205.10 (d, $^2J_{\text{P-C}} = 15.1$ Hz, Ru-CO), δ 167.83 (d, $^1J_{\text{C-H}} = 197$ Hz, Ru-OCHO)

3.3 Results and Discussion

3.3.1 NMR monitoring of the reaction between $\text{TpRu}(\text{PPh}_3)(\eta^3\text{-HSiPhMe}_2\text{H})$ (**1c**) and CO_2 in 1,4-dioxane- d_8

The reaction between the complex $\text{TpRu}(\text{PPh}_3)(\eta^3\text{-HSiPhMe}_2\text{H})$ (**1c**) and CO_2 was first studied. It is learned that the structurally analogous solvent hydride complex $\text{TpRu}(\text{PPh}_3)(\text{CH}_3\text{CN})\text{H}$ reacts with CO_2 to give a solvent formate species $\text{TpRu}(\text{PPh}_3)(\text{CH}_3\text{CN})(\eta^1\text{-OCHO})$ by insertion of CO_2 into the Ru–H bond [151]; we are curious if CO_2 -insertion also occurs for the structurally-similar complex **1c** with CO_2 .

A 1,4-dioxane- d_8 solution of **1c** in a 5-mm Wilmad pressure-valved NMR tube was pressurized with 9 bar CO_2 . After heating the tube for 5 mins, the ^1H NMR spectrum of the solution revealed that the methyl peak of $\text{TpRu}(\text{PPh}_3)(\eta^3\text{-HSiPhMe}_2\text{H})$ at δ 0.30 ppm was diminished (**Figure 3.1**). Two signals were observed at δ 0.55 and 0.28 ppm; they were identified as the methyl peaks of formoxysilane, HCOOSiPhMe_2 and silanol, HOSiPhMe_2 . The concurrent ^{31}P NMR spectrum indicated that small amounts of hydrido-dihydrogen complex $\text{TpRu}(\text{PPh}_3)(\text{H}_2)\text{H}$ (**2**) and carbonyl-hydride complex $\text{TpRu}(\text{PPh}_3)(\text{CO})\text{H}$ (**5**) were formed; **1c**, however, remained the most abundant metal-containing species in the reaction. Trace amount of H_2 was

generated as evidenced by the observation of a very small signal at δ 4.58 ppm in the ^1H NMR spectrum. After heating the solution for another 5 mins, more HCOOSiPhMe_2 and HOSiPhMe_2 were formed; the amounts of both complexes **3** and **5** increase at the expense of **1c**, with the rate of increase of **5** being more prominent. Further heating the solution for 5 mins, not only was the amount of **1c** decreased but also that of HCOOSiPhMe_2 , and HOSiPhMe_2 became the most abundant silicon containing species. More hydrogen was produced at this stage.. Trace amount of formic acid HCOOH was also observed. At the end of the heating process, **1c** and HCOOSiPhMe_2 totally disappeared and HOSiPhMe_2 was the only detectable silicon containing species. The major ruthenium containing species is **5**.

The results of the NMR monitoring experiment show that **1c** is probably the active species in the hydrosilylation of carbon dioxide by HSiPhMe_2 to HCOOSiPhMe_2 (see next section). The CO_2 reacts with the Si-H bond in **1c** without prior coordination to the Ru center (**Cycle A, Scheme 3.2**). In other words, **1a** may act as a bifunctional catalyst, transferring its hydride and SiMe_2Ph moiety in a concerted manner, respectively, to the carbon and oxygen of CO_2 to afford HCOOSiPhMe_2 . Another route that might be operative is that the CO_2 might have displaced silane in **1c** and coordinate to ruthenium center and

inserted into the Ru–H bond to form a ruthenium formate. Re-coordination of silane and σ -metathesis between the η^3 -silane and formate ligand results in the formation of HCOOSiPhMe₂ (**Cycle B, Scheme 3.2**).

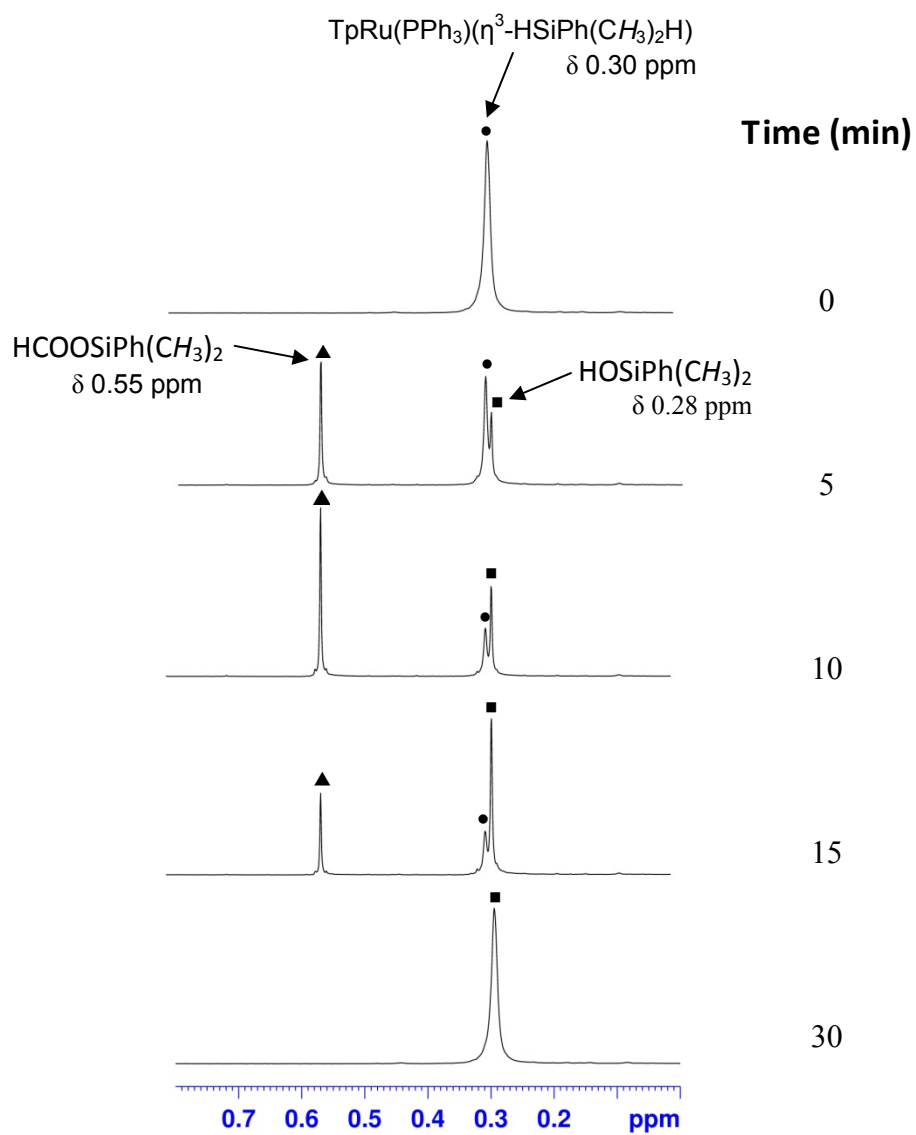
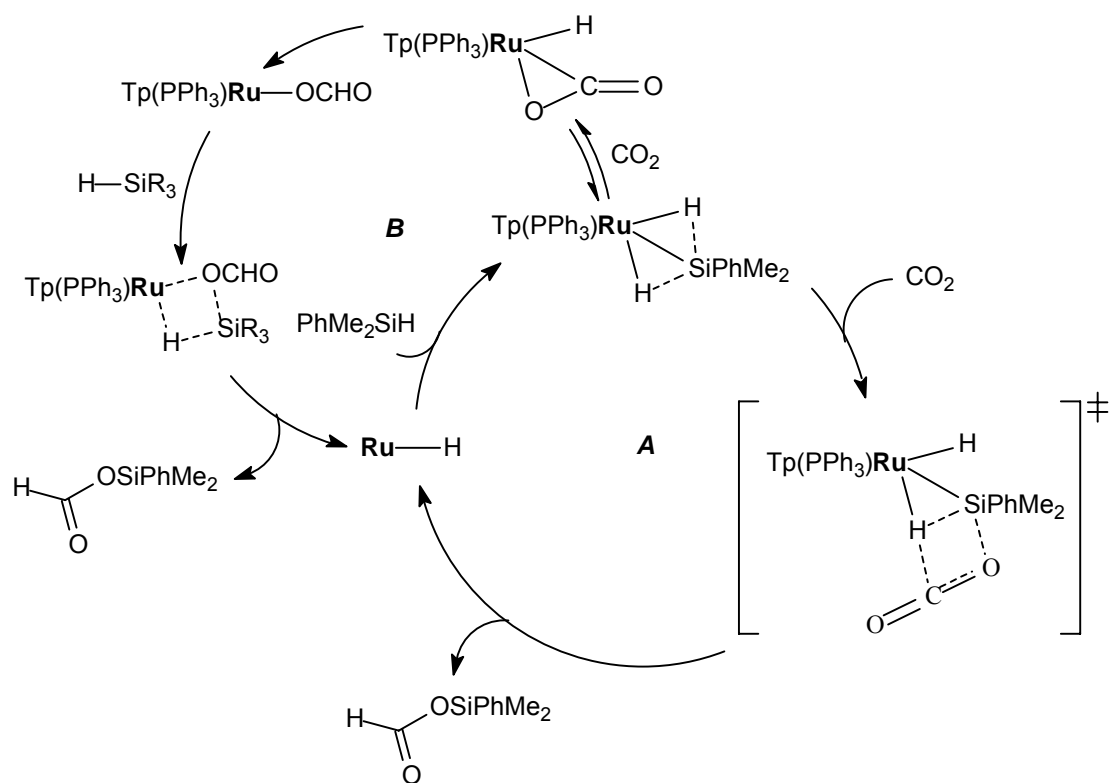
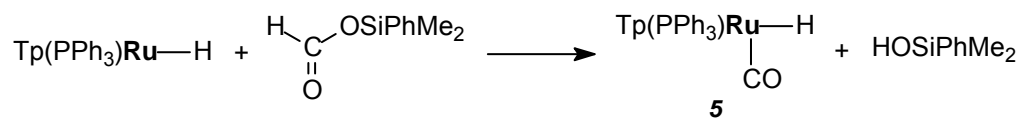


Figure 3.1. ^1H NMR monitoring of the reaction between **1c** and carbon dioxide in 1,4-dioxane- d_8

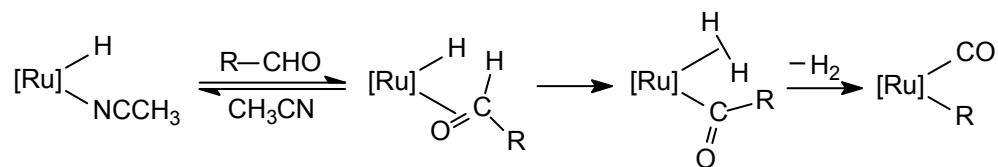


Scheme 3.2 Suggested pathways for the reaction between 1c and CO_2 to give HCOOSiPhMe_2 .

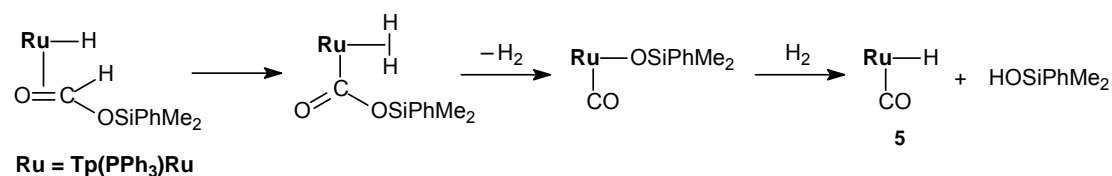
The formoxysilane HCOOSiPhMe_2 , which has never been isolated, is probably a highly reactive species. Its $-\text{CHO}$ group reacts further with the $\text{TpRu}(\text{PPh}_3)\text{H}$ fragment to give the carbonyl hydride complex **5**, and itself is converted into a silanol HOSiPhMe_2 (**eq. 3.1**). Decarbonylation of formyl group by transition metal complexes to form carbonyl complexes is well-established [154-160]. The identity of HOSiPhMe_2 was confirmed by adding an authentic sample of the silanol into the reaction mixture at the end of the monitoring experiment. The mechanism of the decarbonylation of $-\text{CHO}$ group in HCOOSiPhMe_2 might be similar to the one proposed by our group in an earlier report for the reaction between $\text{TpRu}(\text{PPh}_3)(\text{CH}_3\text{CN})\text{H}$ and aldehyde (RCHO) to give $\text{TpRu}(\text{PPh}_3)(\text{CO})\text{R}$ (**Scheme 3.3**) [137]. We propose in **Scheme 3.4** a possible pathway for the decarbonylation of HCOOSiPhMe_2 by $\text{TpRu}(\text{PPh}_3)\text{H}$ to give HOSiPhMe_2 and **5**. The hydrogen produced during the carbonylation of $\text{TpRu}(\text{PPh}_3)\text{H}$ by HCOOSiPhMe_2 to give **5** might react with $\text{TpRu}(\text{PPh}_3)\text{H}$ to give small amount of the hydrido-dihydrogen species **2** (**eq. 3.2**). In the reaction, the formic acid produced may be due to the reduction of CO_2 by H_2 catalyzed by $\text{TpRu}(\text{PPh}_3)(\eta^3\text{-HSiPhMe}_2\text{H})$ or $\text{TpRu}(\text{PPh}_3)\text{H}$ fragment.



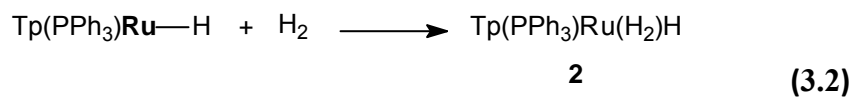
(3.1)



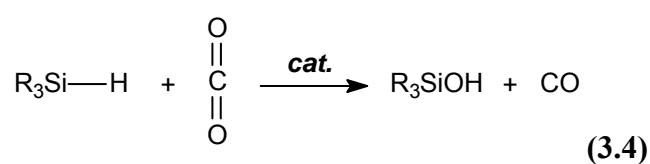
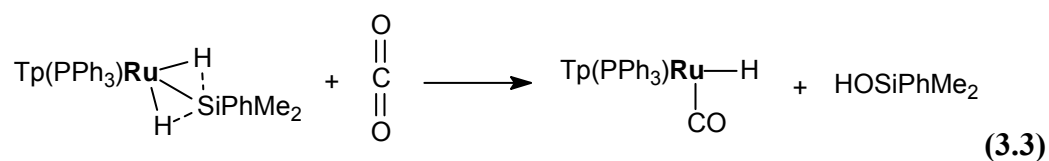
Scheme 3.3 Proposed mechanism for the decarbonylation of aldehyde with $\text{TpRu}(\text{PPh}_3)(\text{CH}_3\text{CN})\text{H}$



Scheme 3.4 Proposed mechanism for the decarbonylation of HCOOSiPhMe_2 by $\text{TpRu}(\text{PPh}_3)\text{H}$



The overall equation for the reaction between complex **1c** and carbon dioxide is represented in **eq. 3.3**. Noteworthy of this reaction is to view it as transfer of an oxygen atom from CO₂ to PhMe₂SiH (coordinated) to afford HOSiPhMe₂; the CO₂ is reduced to CO (coordinated). It is believed that such a reaction (**e.q. 3.4**) might be turned into a catalytic process if appropriate catalytic system was employed. Zhang *et. al.* reported organocatalytic oxidation of aldehydes to carboxylic acids using carbon dioxide as a source of oxygen [161]; the CO₂ is reduced to CO.



3.3.2 NMR monitoring of the catalytic reduction of CO₂ by PhMe₂SiH with **1c**.

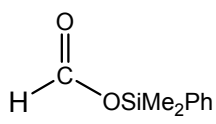
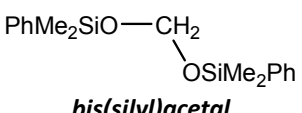
The monitoring experiment in the previous section implies the possibility of using **1c** as a catalyst for the hydrosilylation of carbon dioxide by PhMe₂SiH. We therefore monitored the reaction between PhMe₂SiH and CO₂ in the presence of **1c**. Surprisingly, it is learned that, the CO₂ reduction did not stop at the formoxysilane stage, further reduced products were also observed, despite low turnover.

A solution of **1c** and PhMe₂SiH (20 equiv relative to **1c**) in 1,4-dioxane-*d*₈ was pressurized with 9 bar of CO₂. The ¹H NMR spectrum taken after heating the solution at 110°C for 15 mins revealed that approximately 25% of PhMe₂SiH was converted to HCOOSiPhMe₂ (15%) and HOSiPhMe₂ (10%), also present were hydrogen gas and formic acid. About 90% of **1c** was converted to the carbonyl-hydride complex **5** as indicated in the concurrent ³¹P{¹H} spectrum. A small phosphorus peak at δ 41.2 ppm was also seen. The solution was then heated for a further 45 mins. At the end of this period the conversion of PhMe₂SiH to HCOOSiPhMe₂ and HOSiPhMe₂ were increased to about 25% and 15%, respectively. Except for the unknown species which showed the signal at δ 41.2 ppm in the ³¹P{¹H} spectrum, **5** was the only detectable metal-containing

species. After heating the solution for further 60 mins, the ^1H and ^{13}C NMR spectra of the resulting solution showed the formation of a new ruthenium species (appearance of a new set of Tp peaks) and a silyl methoxide $\text{PhMe}_2\text{SiOCH}_3$ (~5%). Also observed were trace amounts of formaldehyde, bis(silyl)acetal $(\text{PhMe}_2\text{SiO})_2\text{CH}_2$, hemi(silyl)acetal $\text{PhMe}_2\text{SiOCH}_2\text{OH}$, and methanol. The NMR chemical shifts and splitting patterns of all the organic species generated in this experiment are tabulated in **Table 3.1**. $^{31}\text{P}\{^1\text{H}\}$ NMR spectrum indicated that about half of **5** was converted to a new species **6** showing a signal at δ 44.4 ppm. Analysis of the NMR spectra of the solution taken at different time indicated that the amount of silyl methoxide $\text{PhMe}_2\text{SiOCH}_3$ gradually increased, while the quantity of HCOOSiPhMe_2 remains fairly constant; and those of HCOOH and PhMe_2SiH decrease slowly. The peaks due to $(\text{PhMe}_2\text{SiO})_2\text{CH}_2$, $\text{PhMe}_2\text{SiOCH}_2\text{OH}$, and methanol were kept visible, although in minute amounts. A new phosphorus peak at δ -5.7 ppm characteristic of free PPh_3 was observed and grew in intensity, accompanied by diminish of the amount of **6** and development of a new ruthenium species **7** which exhibits a new set of six peaks due to Tp ligand and a singlet hydride signal at δ -10.1 ppm in the ^1H spectrum. At the end of the monitoring experiment, the amount of $\text{PhMe}_2\text{SiOCH}_3$ was increased to about 20%; the phosphorus peak at δ 44.4 ppm

due to **6** almost vanished; **5** and **7** are the two dominant ruthenium-containing species in the reaction mixture. The conversion to **Figure 3.1** shows the $^{31}\text{P}\{^1\text{H}\}$ NMR spectra of the reaction solution taken at different time interval.

Table 3.1 NMR-data of the organic compounds generated in the reaction between CO_2 and PhMe_2SiH in the presence of **1c in 1,4-dioxane-*d*₈.**

organic compounds	NMR data
$\text{PhMe}_2\text{Si-OH}$	^1H : δ 0.28 ppm, s, 3H; Si- CH_3
 <i>formoxysilane</i>	^1H : δ 8.06 ppm, s, 1H; Si- OCHO δ 0.55 ppm, s, 3H; Si- CH_3 ^{13}C : δ 160.7 ppm, Si- OCHO , split into a doublet ($^1J_{\text{C-H}} = 224.3$ Hz) in ^1H -coupled spectrum
 <i>bis(silyl)acetal</i>	^1H : δ 5.05 ppm, s, 2H; O- CH_2 -O ^{13}C : δ 84.3 ppm, O- CH_2 -O, split into a triplet ($^1J_{\text{C-H}} = 162.3$ Hz) in ^1H -coupled spectrum
$\text{PhMe}_2\text{Si-OCH}_3$ <i>Silyl methoxide</i>	^1H : δ 3.39 ppm, s, 3H; Si- OCH_3 ^{13}C : δ 49.8 ppm, Si- OCH_3 , split into a quartet ($^1J_{\text{C-H}} = 141.0$ Hz) in ^1H -coupled spectrum
$\text{PhMe}_2\text{SiO-CH}_2\text{-OH}$ <i>hemi(silyl)acetal</i>	^1H : δ 4.78 ppm, d, $^3J = 6$ Hz, 2H; O- CH_2 -OH ^{13}C : δ 91.0 ppm, O- CH_2 -O, split into a triplet ($^1J_{\text{C-H}} = 160.0$ Hz) in ^1H -coupled spectrum
HCOOH	^1H : δ 7.93 ppm, s, 1H; HCOOH ^{13}C : δ 161.6 ppm, split into a doublet in ^1H -coupled spectrum ($^1J_{\text{C-H}} = 218.0$ Hz),
HCHO	^1H : δ 9.50 ppm, s, 1H; HCHO ^{13}C : δ 194.7 ppm, split into a triplet in ^1H -coupled spectrum ($^1J_{\text{C-H}} = 177.2$ Hz), HCHO
CH_3OH	^1H : δ 3.29 ppm, d, $^3J = 6$ Hz, 3H; CH_3OH

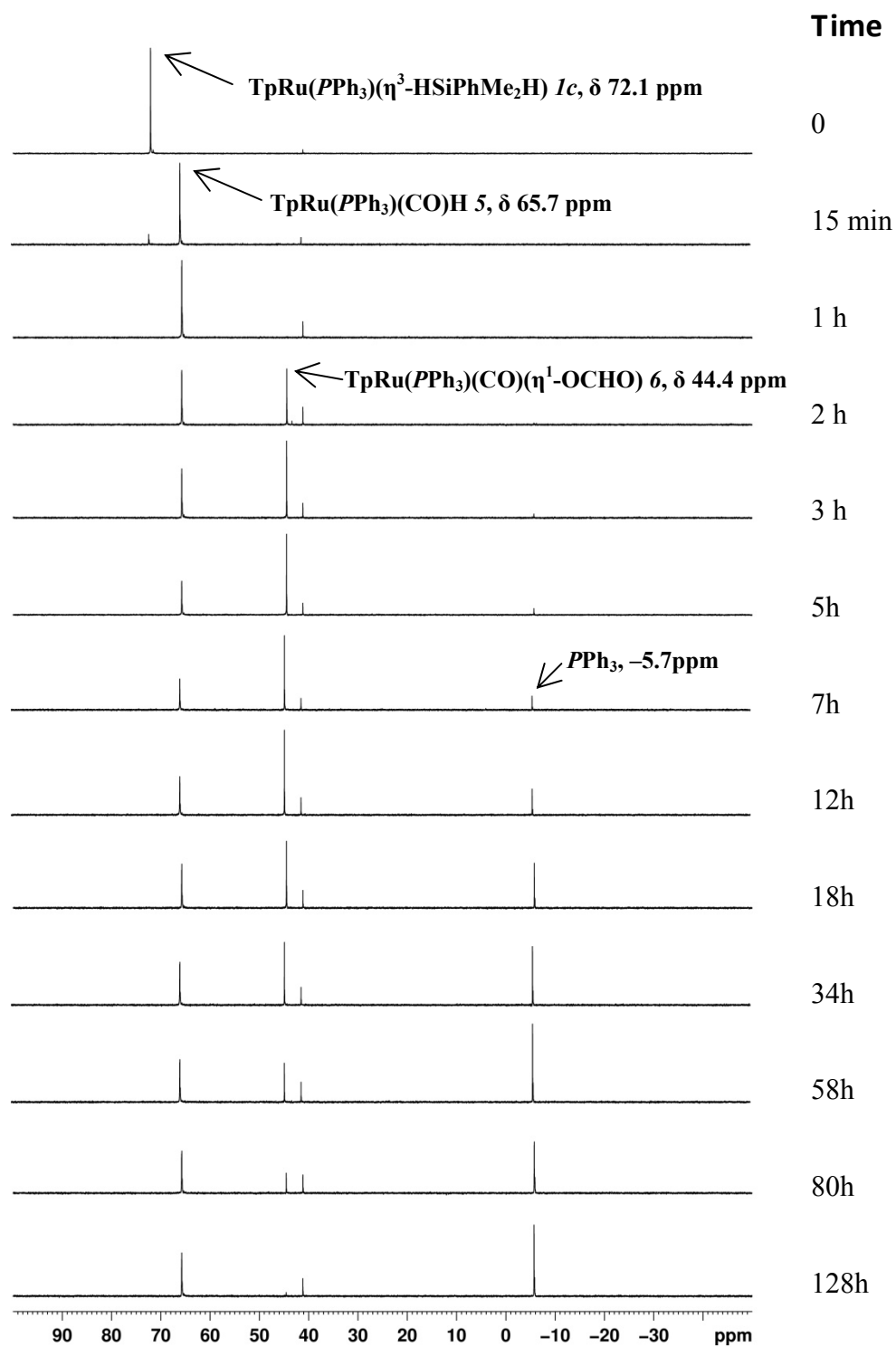
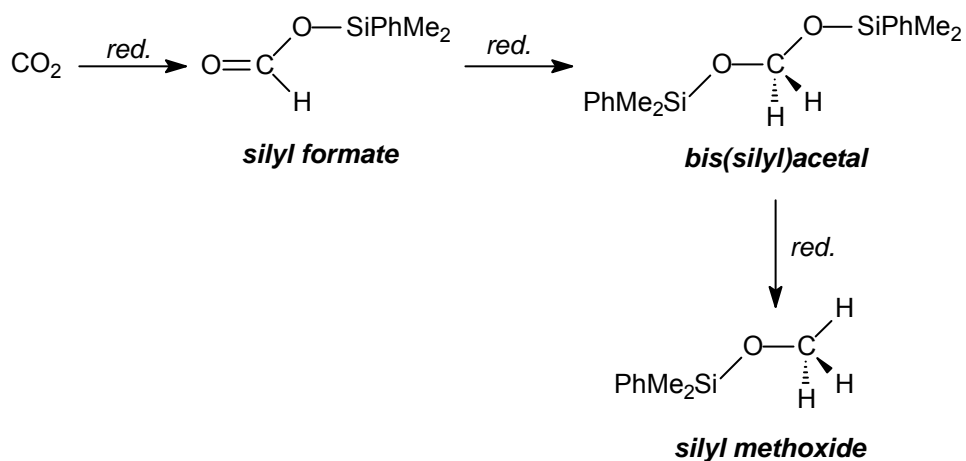


Figure 3.2 ^{31}P NMR monitoring of the 1c-catalyzed reduction of carbon dioxide by PhMe_2SiH in 1,4-dioxane- d_8

The monitoring result showed that the reduction of carbon dioxide by PhMe_2SiH in the presence of **1c** leads to the formation of silyl methoxide $\text{PhMe}_2\text{SiOCH}_3$ as the ultimately-reduced product. The silyl formate HCOOSiPhMe_2 and bis(silyl)acetal $(\text{PhMe}_2\text{SiO})_2\text{CH}_2$ were the intermediates in the sequential reduction of CO_2 (**Scheme 3.5**).



Scheme 3.5 Sequential reduction of CO_2 by PhMe_2SiH to $\text{PhMe}_2\text{SiOCH}_3$

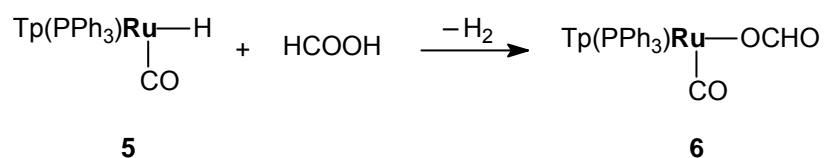
In the first hour of the monitoring experiment carbon dioxide reacts with PhMe_2SiH to afford about 25% of HCOOSiPhMe_2 in the presence of **1c** (See **Scheme 3.2**). The HCOOSiPhMe_2 then reacts with $[\text{Ru}]-\text{H}$ to give quantitative yield of the silanol HOSiPhMe_2 and $\text{Tp}(\text{PPh}_3)\text{Ru}(\text{CO})\text{H}$ (**5**), which alone did not catalyze CO_2 hydrosilylation. It is proposed that the reaction sequence depicted

in **Scheme 3.4** lead to the formation of the silanol and **5**. The formation of hydrogen gas might be a result of the decarbonylation of HCOOSiPhMe_2 by $\text{Tp}(\text{PPh}_3)\text{RuH}$ moiety. The generated H_2 then reduces CO_2 in the presence of **1c** to formic acid. It should be noted that, the amount of the silanol PhMe_2SiOH detected in this period, which should be the same as that of **1c**, was slightly higher than expected and this is probably a result of the oxidation of PhMe_2SiH by trace amount of water in the presence of **1c** as we reported in the previous section. Decarbonylation of $-\text{CHO}$ group forming metal-carbonyl species often causes catalyst deactivation [162-164], and this resulted in low conversion of PhMe_2SiH to HCOOSiPhMe_2 in our catalytic system. To investigate the possibility of raising the yield of HCOOSiPhMe_2 , we repeated our monitoring experiment under identical reaction conditions except the addition of an equivalent amount (relative to **1c**) of a bis(diphenylphosphino)methane complex $\text{TpRu}(\text{dppm})\text{H}$ **9**, which does not undergo deactivation by carbonylation due to chelating effect of the bidentate dppm ligand. The new monitoring experiment showed that the conversion of PhMe_2SiH to HCOOSiPhMe_2 was increased to about 80%.

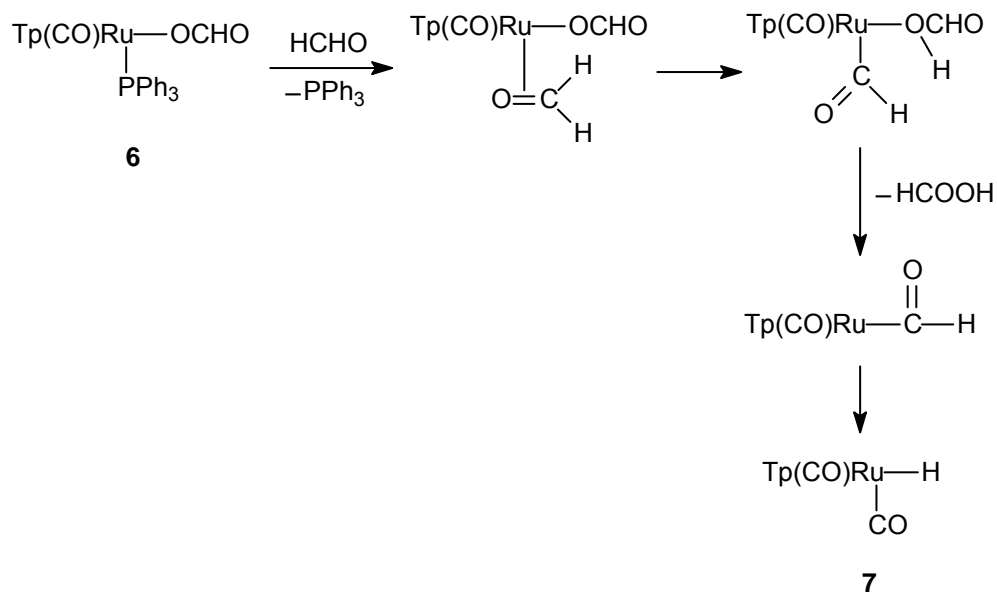
Complex **6**, observed after heating the solution for 2 hrs, is suggested to be

a ruthenium carbonyl formate species $\text{TpRu}(\text{PPh}_3)(\text{CO})(\eta^1\text{-OCHO})$. The ^1H NMR spectrum of the solution taken after this 2-hr period showed, in addition to the peaks pertaining to the Tp ligand of **6**, a singlet at δ 7.88 ppm integrated for 1H. This peak could be ascribed to a formate hydrogen. In the $^{13}\text{C}\{^1\text{H}\}$ NMR spectrum of the solution using labeled $^{13}\text{CO}_2$, a singlet signal is observed at δ 168 ppm, and is splitted into a doublet with $^1J_{\text{C-H}} = 197.0$ Hz in the ^1H -coupled spectrum. This signal is assignable to the formate carbon. In addition, a doublet was observed at 205.1 ppm; this peak is attributable to the carbon of a CO ligand. The doublet nature of the peak is a result of the coupling of the carbon with the phosphorus of the PPh_3 ligand ($^2J_{\text{C-P}} = 15.1$ Hz). Formation of the formate complex **6** is probably due to protonation of the carbonyl hydride complex **5** by formic acid (eq. 3.5). Although attempt to isolate **6** was frustrated by its decarboxylation back to **5** during workup, the formate complex was obtained in a highly pure form in solution by treatment of **5** with a large excess of formic acid and is characterized by ^1H and ^{31}P NMR spectroscopies. The fact that the further-reduced products of CO_2 , i.e. $(\text{PhMe}_2\text{SiO})_2\text{CH}_2$ and $\text{PhMe}_2\text{SiOCH}_3$, were observed as long as **6** was present might imply that the formate complex **6**, or species derived from it but not visible in the NMR spectra, is the active catalyst for the further-reduction of HCOOSiPhMe_2 by PhMe_2SiH .

Complex **7** is likely to be a ruthenium dicarbonyl-hydride $\text{TpRu}(\text{CO})_2\text{H}$ [165]. The proton NMR spectrum taken in the monitoring experiment showed a set of six peaks due to Tp ligand, which implies that two of the three legs *trans* to the Tp ligand in an octahedral configuration are equivalent. In addition to these Tp-peaks, a singlet hydride signal at $\delta -10.1$ ppm was also observed. The fact that this singlet hydride signal is splitted into a triplet when $^{13}\text{CO}_2$ is used strongly rents support to the identity of **7**. Formation of the dicarbonyl-hydride complex **7** is probably a result of dissociation of the PPh_3 ligand in the formate complex **6** followed by carbonylation. The source of the second CO ligand is probably formaldehyde generated in the reaction. **Scheme 3.6** depicts the suggested pathway for the carbonylation reaction. Complete conversion of **6** to **7** takes days, and this suggest that the PPh_3 ligand in **6** is not so substitutionally labile.



(3.5)

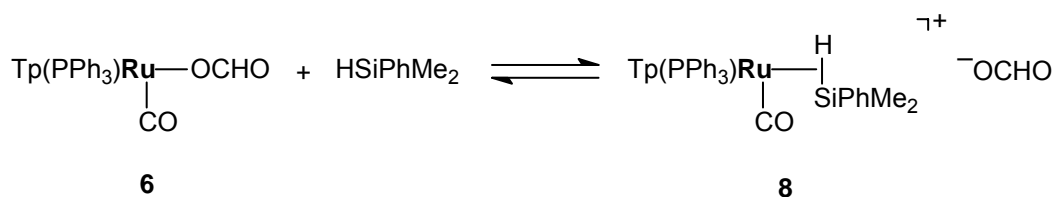


Scheme 3.6. Suggested mechanism for the conversion of the carbonyl formate complex (6) to dicarbonyl hydride complex (7).

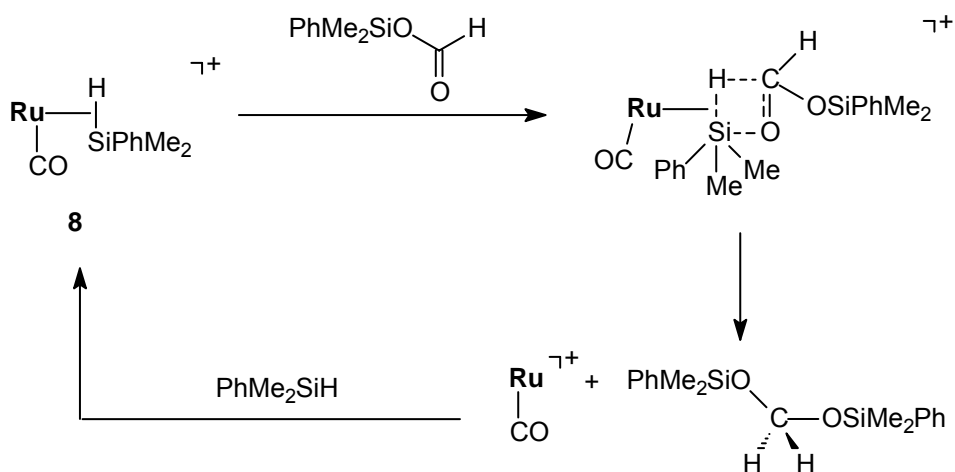
3.3.3 Suggested Mechanism of Formoxsilane Reduction

There is no information from NMR spectra on how the carbonyl-formate complex **6** catalyzes the reduction of HCOOSiPhMe_2 by PhMe_2SiH , we can therefore only speculate the route by which the reduction takes place. The formate ligand might have been displaced by silane to give a cationic silane complex $[\text{TpRu}(\text{PPh}_3)(\text{CO})(\eta^2\text{-HSiPhMe}_2)](\text{OCHO})$ (**8**) (eq. 3.6). The highly electrophilic silicon center in this complex might be having some interaction with the oxygen of the formate anion. We suggest that the cationic silane

complex **8** catalyzes the reduction of HCOOSiPhMe_2 via a 4-center intermediate as proposed in **Scheme 3.7**; transfer of the hydride and silyl group of the silane to, respectively, the carbon and oxygen of the carbonyl group in HCOOSiPhMe_2 affords bis(silyl)acetal $(\text{PhMe}_2\text{SiO})_2\text{CH}_2$. The suggested mechanism is similar to that of the rhenium-catalyzed hydrosilylation of aldehydes/ketones proposed by Abu-Omar [166]. In this reaction, the silane coordinates to the metal in an η^2 fashion and is then attacked by the aldehyde/ketone to give silyl ether; coordination of the carbonyl compound to the metal center is not required.



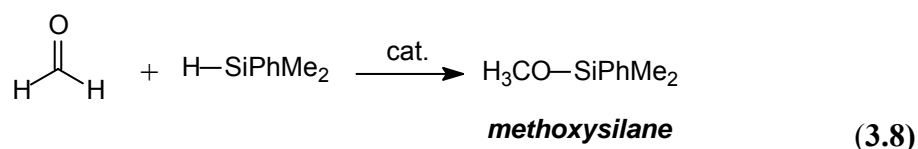
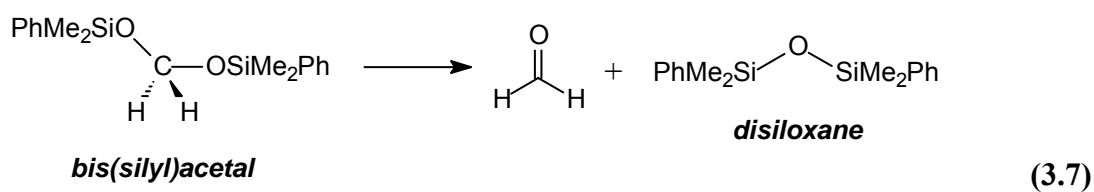
(3.6)

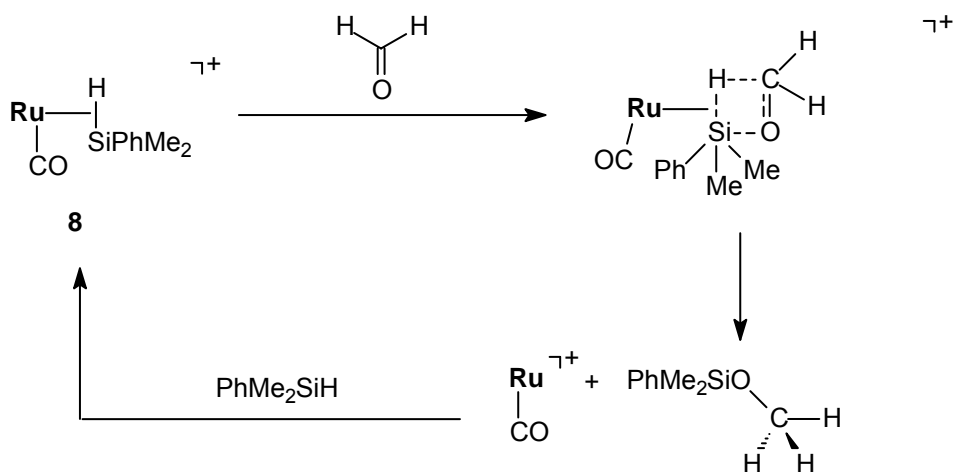


Scheme 3.7 Suggested mechanism for the **8-catalyzed reduction of HCOOSiPhMe_2 to $(\text{PhMe}_2\text{SiO})_2\text{CH}_2$**

The ability of the bis(silyl)acetal $(\text{PhMe}_2\text{SiO})_2\text{CH}_2$ to undergo further reduction by PhMe_2SiH to methoxide $\text{PhMe}_2\text{SiOCH}_3$ is probably a result of its decomposition to formaldehyde along with disiloxane $(\text{PhMe}_2\text{Si})_2\text{O}$ (eq. 3.7). The formaldehyde was then hydrosilylated by PhMe_2SiH to $\text{PhMe}_2\text{SiOCH}_3$ with the carbonyl-formate complex **6** (eq. 3.8), presumably via the formation of the cationic silane species **8** and a mechanism similar to that for the reduction of HCOOSiPhMe_2 by PhMe_2SiH (Scheme 3.8). Hydrosilylation of aldehydes to silyl ethers is a well-known reaction and is catalyzed by large number of transition metal complexes. Although we were unable to identify the disiloxane

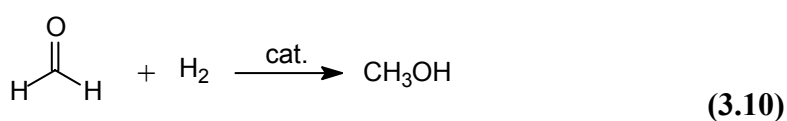
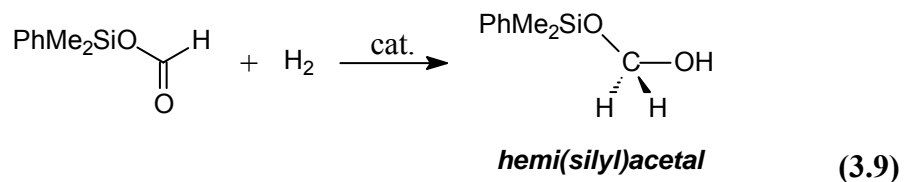
in the reaction mixture because its methyl peak probably overlaps with that of $\text{PhMe}_2\text{SiOCH}_3$ (identified by the more upfield Si-OCH_3 but not Si-CH_3) in the ^1H NMR spectrum, we did confirm the presence of formaldehyde by observation of its characteristic peaks in the ^1H and ^{13}C NMR spectra (see **Table 4.1**). The density function theory study performed by Wang *et al.* for the N-heterocyclic carbene-catalyzed reduction of CO_2 into methanol with silane revealed that formaldehyde is an indispensable intermediate in the course of reduction [65]. We believe that we are the first group to detect formaldehyde during the reduction of carbon dioxide by silane.



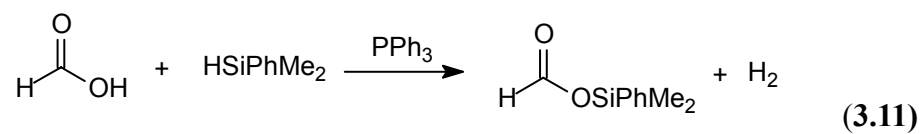


Scheme 3.8. Suggested mechanism for the 8-catalyzed reduction formaldehyde to PhMe₂SiOCH₃

The formation of trace amount of hemiacetal PhMe₂SiOCH₂OH might be due to the reduction of HCOOSiPhMe₂ by hydrogen in the reaction mixture (eq. 3.9), whereas the formation of methanol might be a result of the reduction of formaldehyde by hydrogen (eq. 3.10).



The PPh_3 dissociated from **1c** may be responsible for the consumptions of HCOOH and PhMe_2SiH at the later stage of the NMR monitoring experiment [167]. Independently performed experiment confirmed that HCOOH reacts with PhMe_2SiH to form HCOOSiPhMe_2 in the presence of PPh_3 in 1,4-dioxane (eq. 3.11).



Chapter 4 Electrophilic Ruthenium-complexes-catalyzed β -Alkylation of Secondary Alcohols with Primary Alcohols and Transfer Hydrogenation of Carbonyl Compounds with 1,4-Butanediol

4.1 Introduction

Transition metal-catalyzed transfer hydrogenation of carbonyl compounds and β -alkylation of secondary alcohols with primary alcohols are two actively investigated reactions [77–80, 109–112]. Known catalytic systems for affecting these organic transformations are mainly based on electroneutral complexes; the use of electrophilic complexes for these reactions are, however, relatively unexplored [77–92, 114–120]. Continuing our interest on the use of Lewis acidic ruthenium complexes for catalytic reactions, we report here that the air-stable, bipyridine supported dicationic ruthenium complexes *cis*-[Ru(6,6-X₂bpy)₂(H₂O)₂](OTf)₂ (X = Cl, Me) are active catalysts towards β -alkylation of secondary alcohols with primary alcohols and transfer hydrogenation of carbonyl compounds with 1,4-butanediol. Both catalytic processes require no inert atmosphere for protection as a result of the high air stabilities of the complexes.

4.2 Experimental Section

4.2.1 Materials and Instrumentation

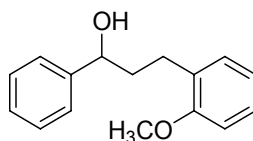
All syntheses of complexes were carried out under an inert nitrogen atmosphere using standard Schlenk techniques. Solvents were dried, degassed, and distilled before using: diethyl ether from Na/benzophenone, n-hexane and toluene from Na. All organic and inorganic compounds were commercially available (Aldrich, Acros, Strem and International Laboratory) and used without further purification. The complex *cis*-[Ru(6,6'-Cl₂bpy)₂(H₂O)₂](OTf)₂ was prepared according to literature methods [168]. The complex *cis*-[Ru(6,6'-Me₂bpy)₂(H₂O)₂](OTf)₂ was synthesized using the same method as for the synthesis of *cis*-[Ru(6,6'-Cl₂bpy)₂(H₂O)₂](OTf)₂ except 6,6'-Me₂bpy was used instead of 6,6'-Cl₂bpy. Deuterated NMR solvents, purchased from Armar and Cambridge Isotope Laboratories, were dried with P₂O₅ prior to use. ¹H NMR spectra were obtained from a Varian (500 MHz) or Bruker DPX (400 MHz) spectrometer; chemical shifts were reported relative to residual protons of the deuterated solvents. Electrospray ionization mass spectrometry was carried out with a Finnigan MAT 95S mass spectrometer with the samples dissolved in dichloromethane.

4.2.2 Reactions

4.2.2.1 General Procedure for catalytic β -Alkylation of Secondary Alcohols with Primary Alcohols

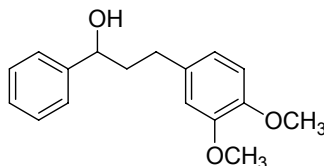
The reactions were carried out in 11-mm Schlenk tubes equipped with Teflon screw caps. In a typical run, ruthenium complex (0.005 mmol) and NaOH (0.25 mmol) were loaded into the tube equipped with a magnetic stirrer. Secondary alcohol (1.25 mmol) and primary alcohol (1.5 mmol) were then added to the tube via syringes. The tube was sealed with the screw cap and the solution was stirred in a 120°C silicon oil bath for 24 h. At the end of the reaction, the tube was cooled to room temperature; a 0.1 mL aliquot of the solution was removed and analyzed by proton NMR spectroscopy (in CDCl₃). Comparison of the integrations of the characteristic peaks of the product and the unreacted secondary alcohol gave the conversion of the reaction. In cases where the products are new compounds, they were isolated by flash column chromatography on silica gel or with preparative thin layer chromatography (silica gel).

4.2.2.2 3-(2-methoxyphenyl)-1-phenylpropan-1-ol:



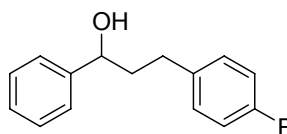
pale yellow oil; ^1H NMR (400 MHz, CDCl_3) δ 7.38-6.87 (m, 9H), 4.64 (t, $J = 6$ Hz, 1H), 3.84 (s, 1H), 2.80-2.76 (t, $J = 8$ Hz, 2H), 2.49 (s, 1H), 2.11-2.01 (m, 2H); ^{13}C NMR (100 MHz, CDCl_3) δ 157.4, 144.7, 130.1, 128.4, 127.4, 127.3, 126.0, 120.7, 110.4, 73.6, 55.4, 39.4, 26.5; HRMS (+ESI): m/z : calcd for $\text{C}_{16}\text{H}_{18}\text{O}_2\text{Na}^+$: 265.1204; found: 265.1216 $[\text{M}+\text{Na}]^+$.

4.2.2.3 3-(3,4-dimethoxyphenyl)-1-phenylpropan-1-ol:



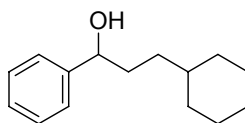
pale yellow oil; ^1H NMR (400 MHz, CDCl_3) 7.38-7.30, 6.82-6.76 (m, 8H), 4.68 (t, $J = 6$ Hz, 1H), 3.86 (s, 6H), 2.90 (s, 1H), 2.74-2.65 (m, 2H), 2.15-2.04 (m, 2H); ^{13}C NMR (100 MHz, CDCl_3) δ 148.8, 147.1, 144.8, 134.5, 128.4, 127.5, 126.0, 120.3, 111.9, 111.4, 73.7, 55.9, 55.8, 40.7, 31.7; HRMS (+ESI): m/z : calcd for $\text{C}_{17}\text{H}_{20}\text{O}_3\text{Na}^+$: 295.1310; found: 295.1313 $[\text{M}+\text{Na}]^+$.

4.2.2.4 3-(4-fluorophenyl)-1-phenylpropan-1-ol:



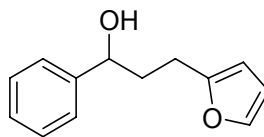
colorless oil; ^1H NMR (400 MHz, CDCl_3) δ 7.37-6.94 (m, 9H), 4.61 (t, $J = 6\text{Hz}$, 1H), 2.69-2.60 (m, 2H), 2.48 (s, 1H), 2.08-1.95 (m, 2H); ^{13}C NMR (100 MHz, CDCl_3) δ 162.5, 160.1, 144.5, 137.5, 137.4, 129.8, 128.6, 127.7, 126.0, 115.2, 115.0, 73.7, 40.6, 31.2; HRMS (+ESI): m/z : calcd for $\text{C}_{15}\text{H}_{15}\text{OFNa}^+$: 253.1005; found: 253.1017 $[\text{M}+\text{Na}]^+$.

4.2.2.5 1-cyclohexyl-1-phenylpropan-1-ol:



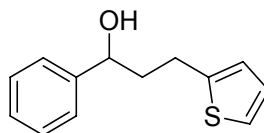
white solid; ^1H NMR (400 MHz, CDCl_3) δ 7.36-7.25 (m, 5H), 4.62 (t, $J = 6\text{ Hz}$, 1H), 1.88 (s, 1H), 1.73-1.67 (m, 6H), 1.26-1.13 (m, 7H), 0.87-0.85 (m, 2H); ^{13}C NMR (100 MHz, CDCl_3) δ 145.6, 129.1, 127.9, 126.6, 75.7, 38.3, 37.0, 34.1, 34.0, 27.3, 27.0. HRMS (+ESI): m/z : calcd for $\text{C}_{15}\text{H}_{22}\text{ONa}^+$: 241.1568; found: 241.1559 $[\text{M}+\text{Na}]^+$.

4.2.2.6 3-(furan-2-yl)-1-phenylpropan-1-ol:



pale yellow oil; ^1H NMR (400 MHz, CDCl_3) δ 7.34-7.27 (m, 6H), 6.28 (d, $J = 2$ Hz, 1H), 5.99 (d, $J = 2$ Hz, 1H), 4.65 (t, $J = 6$ Hz, 1H), 2.72-2.67 (m, 2H), 2.40 (s, 1H), 2.09-2.02 (m, 2H). ^{13}C NMR (100 MHz, CDCl_3) δ 155.6, 144.4, 141.0, 128.5, 127.7, 126.0, 110.2, 105.1, 73.6, 37.1, 24.4. HRMS (+ESI): m/z : calcd for $\text{C}_{15}\text{H}_{22}\text{ONa}^+$: 241.1568; found: 241.1559 $[\text{M}+\text{Na}]^+$.

4.2.2.7 1-phenyl-(3-thiophen-2-yl)-propan-1-ol:



colorless oil; ^1H NMR (400 MHz, CDCl_3) δ 7.35-7.27 (m, 5H), 7.13 (d, $J = 5$ Hz, 1H), 6.93 (dd, $J = 5, 3$ Hz, 1H), 6.81 (d, $J = 3$ Hz, 1H), 4.67 (t, $J = 6$ Hz, 1H), 2.94-2.88 (m, 2H), 2.46 (s, 1H), 2.18-2.05 (m, 2H). ^{13}C NMR (100 MHz, CDCl_3) δ 144.7, 144.4, 128.6, 127.7, 126.9, 126.0, 124.4, 123.2, 73.5, 40.7, 26.3. HRMS (+ESI): m/z : calcd for $\text{C}_{13}\text{H}_{14}\text{ONaS}^+$: 241.0663; found: 241.0663 $[\text{M}+\text{Na}]^+$.

4.2.2.8 General Procedures for the transfer hydrogenation of ketones and aldehydes with 1,4-butanediol

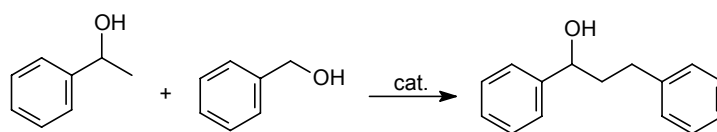
The reactions were carried out in Schlenk tubes equipped with Teflon screw caps. In a typical run, ruthenium complex (0.01 mmol) and NaOH (0.25 mmol) were loaded into the tube equipped with a magnetic stirrer. The carbonyl compound (1 mmol) was then added to the tube (via syringe in case the compound is a liquid), followed by addition of 1,4-butanediol (0.089 mL, 1 mmol) and toluene (1 mL) via syringes. The tube was sealed with the screw cap and the solution was refluxed in a silicon oil bath for 24 h. At the end of the reaction, the tube was cooled to room temperature; a 0.1 mL aliquot of the solution was removed and analyzed by proton NMR spectroscopy (in CDCl₃). Comparison of the integrations of the characteristic peaks of the product and the unreacted carbonyl compound gave the conversion of the reaction.

4.3 Results and Discussion

4.3.1 β -Alkylation of Secondary Alcohols with Primary Alcohols catalyzed by *cis*-[Ru(6,6'-Cl₂bpy)₂(H₂O)₂](OTf)₂ (**10**)

We first studied the catalytic β -alkylation of 1-phenylethanol with benzyl alcohol to give 1,3-diphenyl-1-propanol with bipyridine ruthenium complexes. It can be seen from **Table 4.1** that the dichloro-substituted bipy-ruthenium complex *cis*-[Ru(6,6'-Cl₂bpy)₂(H₂O)₂](OTf)₂ **10** demonstrates higher catalytic activity towards the alkylation reaction than the analogous dimethyl bipy-ruthenium complex *cis*-[Ru(6,6'-Me₂bpy)₂(H₂O)₂](OTf)₂ **11** under identical reaction conditions (entries 1–2). The closely related 2,9-dimethylphenanthroline complex *cis*-[Ru(2,9-dmp)₂(H₂O)₂](OTf)₂ **12** was also found to be less active than the dichloro bpy complex (entry 3). *cis*-[Ru(6,6'-Cl₂bpy)₂Cl₂] **13**, the precursor complex of **10**, also shows lower catalytic activity. Among the bases examined NaOH was found to give the highest yield of product (entries 5–6). The reaction proceeds at a faster rate under solventless condition (entries 7–9). Performing the reaction at lower temperatures resulted in significant reduction of product conversions (entries 10–12).

Table 4.1. Optimization of β -alkylation of secondary alcohols with primary alcohols^[a]



entry	Catalyst	base	solvent	conversion ^[b]
1	<i>cis</i> -[Ru(6,6'-Cl ₂ bpy) ₂ (H ₂ O) ₂](OTf) ₂ 10	NaOH	none	87(7)
2	<i>cis</i> -[Ru(6,6'-Me ₂ bpy) ₂ (H ₂ O) ₂](OTf) ₂ 11	NaOH	none	45(2)
3	<i>cis</i> -[Ru(2,9-dmp) ₂ (H ₂ O) ₂](OTf) ₂ 12	NaOH	none	34(0)
4	<i>cis</i> -[Ru(6,6'-Cl ₂ bpy) ₂ Cl ₂] 13	NaOH	none	55(23)
5	10	CS ₂ CO ₃	none	35(2)
6	10	KO ^t Bu	none	78(4)
7	10	NaOH	toluene ^[c]	80(4)
8	10	NaOH	dioxane ^[c]	42(5)
9	10	NaOH	THF ^[c]	40(5)
10 ^[d]	10	NaOH	none	3(2)
11 ^[e]	10	NaOH	none	28(2)
12 ^[f]	10	NaOH	none	68(2)

[a] Reaction conditions: catalyst (0.005 mmol, 0.4 mol% relative to 2° alcohol), 2° alcohol (1.25 mmol), 1° alcohol (1.5 mmol), NaOH (0.25 mmol, 20 mol% referred to 2° alcohol), 120°C, 24 h.

[b] Conversion (based on 1-phenylethanol) determined by ¹H NMR spectroscopy. Values in parenthesis indicate the conversion of corresponding ketone.

[c] 0.3 mL of solvent was used.

[d] The reaction was performed at 60°C.

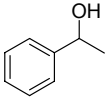
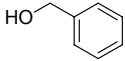
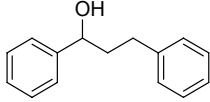
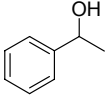
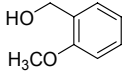
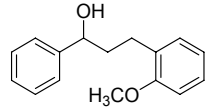
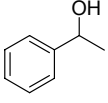
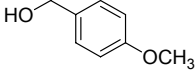
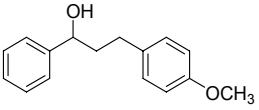
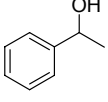
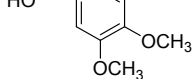
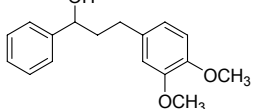
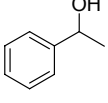
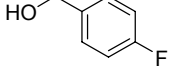
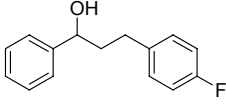
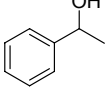
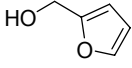
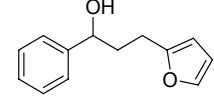
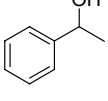
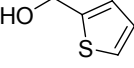
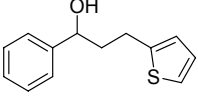
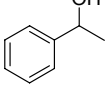
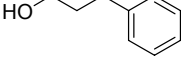
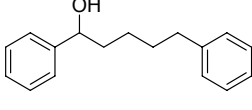
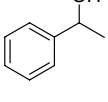
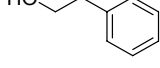
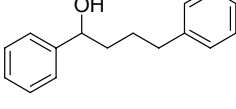
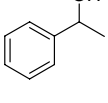
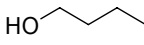
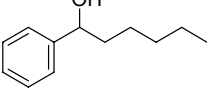
[e] The reaction was performed at 80°C.

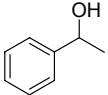
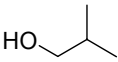
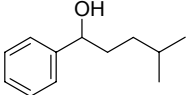
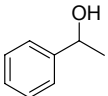
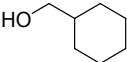
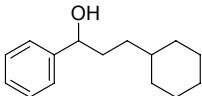
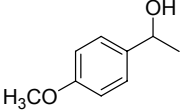
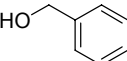
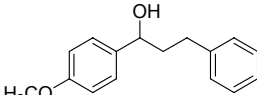
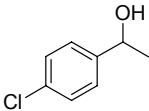
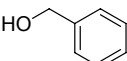
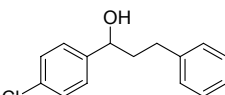
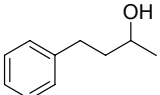
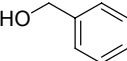
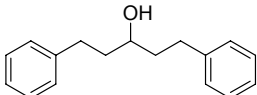
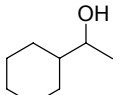
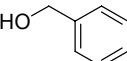
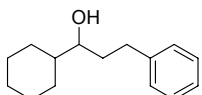
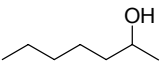
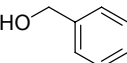
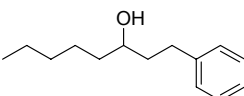
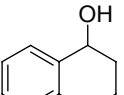

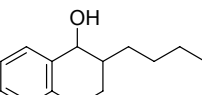
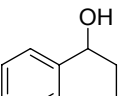
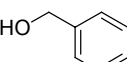
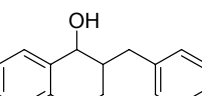
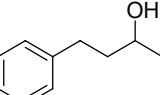

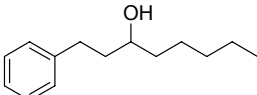
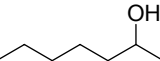

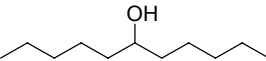
[f] The reaction was performed at 100°C.

Subsequently, we apply the optimized reaction conditions to a variety of secondary alcohols and primary alcohols, and the results are listed in Table 4.2. In a few cases (entries 2, 4–7, 12) where the β -alkylation

products are new compounds, they were isolated and characterized, and their yields are reported. Aryl methyl carbinols can be alkylated with various primary alcohols. The reactions with benzyl alcohols and heterocyclic alcohols (entries 2–7) give higher conversions than with primary aliphatic alcohols (entries 8–12). The lowering of the conversion in alkylation reactions with primary alkyl alcohols is not attributable to self-condensation of these alcohols because no self condensation products were detected in the reactions; it might be the result of the diminished electrophilicity of the carbonyl carbon atoms of the aldehydes generated via oxidation of the primary alkyl alcohols. Alkyl methyl carbinols seem to be less active than their aryl analogues toward the alkylation reaction (entries 15–17). 1-Phenyl-1-propanol, however, does not undergo alkylation. The dichloro bpy complex is basically inactive for the β -alkylation of alkyl methyl carbinols with primary alkyl alcohols (entries 20–21). Alkylation of 1,2,3,4-tetrahydro-1-naphthol gives mixtures of diastereomers (entries 18–19).

Table 4.2 β -alkylation of secondary alcohols with primary alcohols catalyzed by *cis*-[Ru(6,6'-Cl₂bpy)₂(H₂O)₂](OTf)₂ 10^[a]

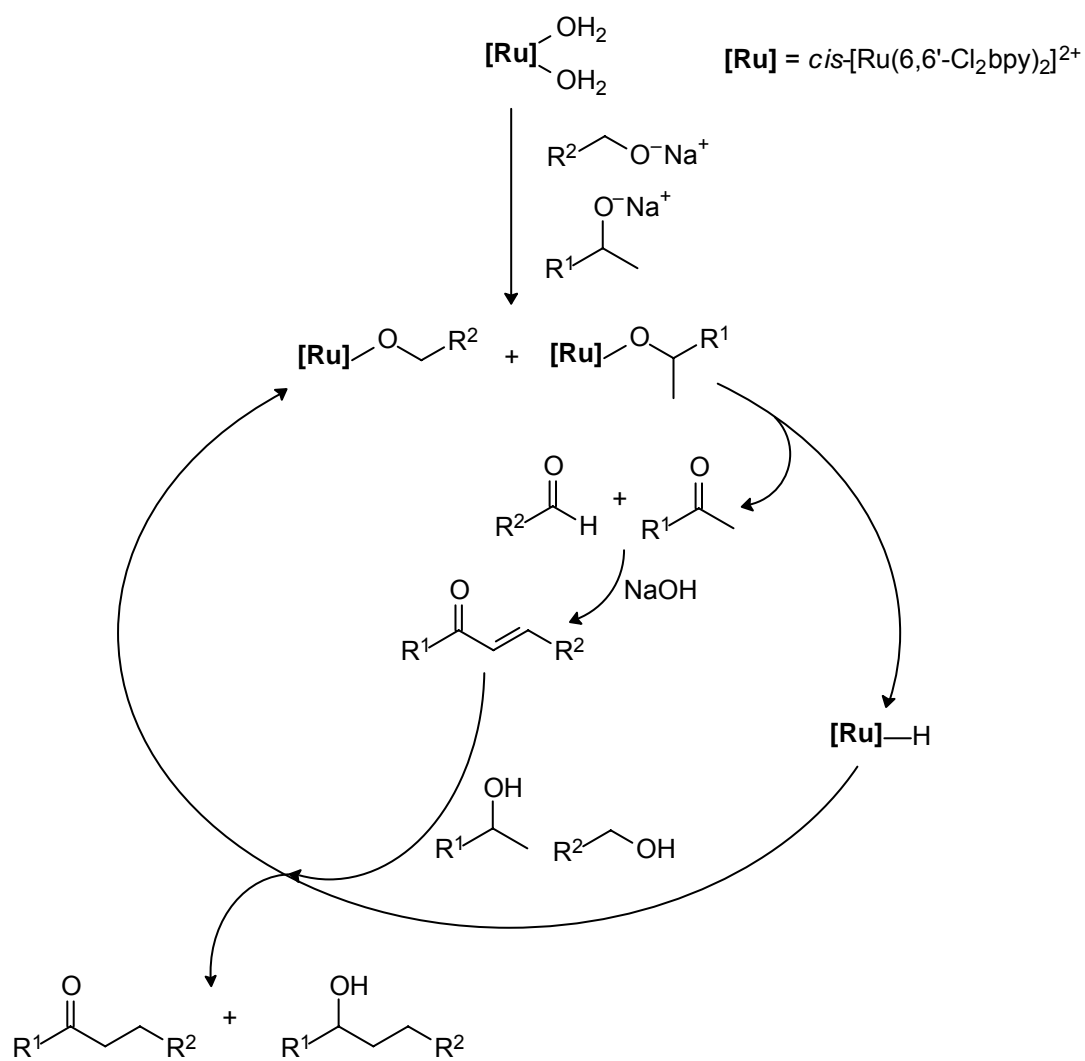
entry	2° alcohol	1° alcohol	product	conversion (%) ^[b]
1				92 (8)
2				89(11) [83]
3				88(8)
4				86(14) [83]
5				86(9) [76]
6				84(13) [76]
7				90(6) [85]
8				88(9)
9				75(4)
10				46(3)

11				32(7)
12				77(23) [71]
13				64(29)
14				86(10)
15				72(9)
16				64(14)
17				60(8)
18				63(21) (<i>Z:E</i> = 40:60)
19				70(27) (<i>Z:E</i> = 44:56)
20				trace
21				trace

[a] Reaction conditions: catalyst (0.005 mmol, 0.4 mol% referred to 2° alcohol), 2° alcohol (1.25 mmol), 1° alcohol (1.5 mmol), NaOH (0.25 mmol, 20 mol% referred to 2° alcohol), 120°C, 24 h.

[b] Conversion (based on 2° alcohol) determined by ¹H NMR spectroscopy. Values in parenthesis indicate the conversion of corresponding ketone, whereas those in square bracket indicate the isolated yield of the higher alcohol.

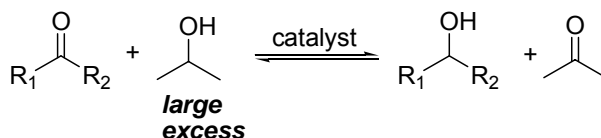
It is seen from Table 4.2 that the dichloro-bpy complex **10** is capable of catalyzing the β -alkylation of secondary alcohols to give good yield of higher alcohols in many cases, and in fact its catalytic activity is superior to most of the other systems reported in the literature. The catalytic system comprising **10**, however, does not render much information regarding the mechanistic pathway of the reaction. Complex **10** is devoid of phosphine ligand, and it is therefore not possible to monitor the **10**-catalyzed reactions with ^{31}P NMR spectroscopy. In addition, the ^1H NMR spectrum of the recovered complex after catalysis exhibits many unidentified and chaotic peaks, which further frustrated our mechanistic investigation on this catalytic system. Depicted in **Scheme 4.1** is a possible mechanism for the alkylation reaction that is parallel to those reported in the literature. The primary and secondary alcohols were temporarily oxidized in the presence of catalyst and base to the corresponding aldehyde and ketone, respectively; they undergo an aldol condensation in the presence of base to give an α,β -unsaturated ketone. Reduction of the ketone by the ruthenium-hydride species generated affords the saturated alcohol as the final product.



Scheme 4.1. Proposed mechanism for the 10-catalyzed β -alkylation of secondary alcohols with primary alcohols

4.3.2 Transfer Hydrogenation of Aldehydes and Ketones with 1,4-butanediol catalyzed by *cis*-[Ru(6,6'-Me₂bpy)₂(H₂O)₂](OTf)₂ (11)

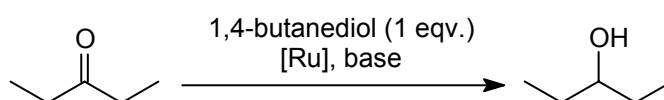
Catalytic transfer hydrogenation is a widely employed method for the reduction of aldehydes and ketones to their corresponding alcohols. 2-Propanol is one of the most frequently used hydrogen donor for this reaction, but is required in large excess to shift the reduction equilibrium to the product side (Scheme 4.2). It is therefore desirable to identify an alcohol that releases hydrogen irreversibly and thus overcomes the equilibrium problem. 1,4-Butanediol has recently been demonstrated by Willam *et al.* to be a stoichiometric hydrogen donor due to its irreversible conversion to γ -butyrolactone upon release of hydrogen (Scheme 1.19, page 42) [107–108].



Scheme 4.2. Transfer hydrogenation of carbonyl compounds with 2-propanol

It is learned from the previous section of bpy-ruthenium-complexes-catalyzed alkylation reaction that transfer hydrogenation might be a step in the catalytic process for giving saturated alcohol as the final product. We therefore anticipated that the bpy complexes are active in catalyzing reduction of carbonyl compounds, and we investigated the reaction using these complexes and with 1,4-butanediol as hydrogen donor. Optimization of the reaction conditions were found using 3-pentanone as a model substrate, and the results are shown in **Table 4.3**. The controlled experiment, in which no complex was present, shows that transfer hydrogenation of 3-pentanone only proceeds to a small extent. Among the complexes investigated the dimethyl substituted bpy-ruthenium complex *cis*-[Ru(6,6'-Me₂bpy)₂(H₂O)₂](OTf)₂ **9** was found to exhibit the highest catalytic activity towards the transfer hydrogenation reaction. Toluene is the preferred choice of solvent, although the catalysis also proceeds but at slower rate in 1,4-dioxane or water.

Table 4.3 Catalytic transfer hydrogenation of 3-pentanone with 1,4-butanediol^[a]



entry	Catalyst	base	solvent	conversion (%) ^[b]
1	–	NaOH	toluene	33
2	<i>cis</i> -[Ru(6,6'-Cl ₂ bpy) ₂ (H ₂ O) ₂](OTf) ₂ 10	NaOH	toluene	82
3	<i>cis</i> -[Ru(6,6'-Me ₂ bpy) ₂ (H ₂ O) ₂](OTf) ₂ 11	NaOH	toluene	92
4	<i>cis</i> -[Ru(2,9-dmp) ₂ (H ₂ O) ₂](OTf) ₂ 12	NaOH	toluene	66
5	11	–	Toluene	2
6	11	NaOH	dioxane	55
7	11	NaOH	water	37
8	11	KOtBu	toluene	49
9	11	Cs ₂ CO ₃	toluene	7
10 ^[c]	11	NaOH	toluene	41
11 ^[d]	11	NaOH	toluene	74
12 ^[e]	11	NaOH	toluene	78

[a] Unless otherwise noted, the reactions were carried out with 3-pentanone (1.0 mmol), 1,4-butanediol (1.0 mmol), catalyst (1.0 mol% with respect to 3-pentanone), and base (0.2 mmol) in 1 mL solvent under reflux for 20 h.

[b] 2,9-dmp: 2,9-dimethyl-1,10-phenanthroline

[c] The reaction was carried out at 100°C

[d] 16 h reaction time

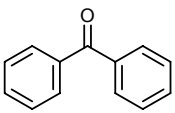
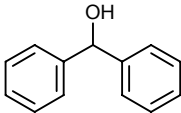
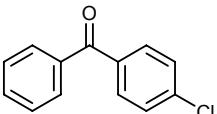
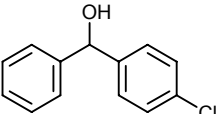
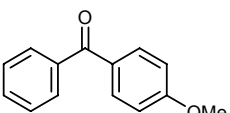
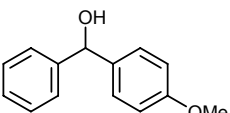
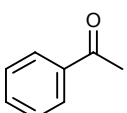
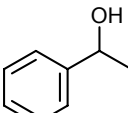
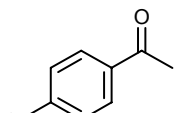
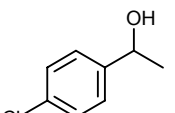
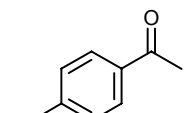
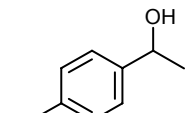
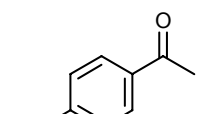
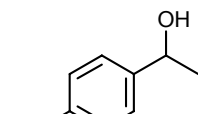
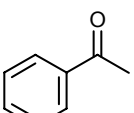
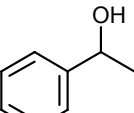
[e] The reaction was carried out using 0.5 mol% catalyst.

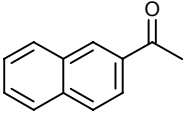
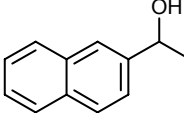
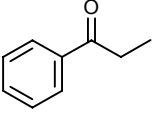
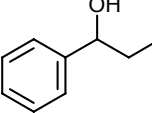
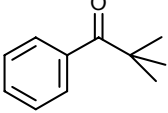
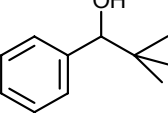
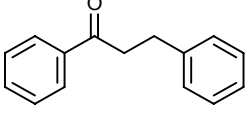
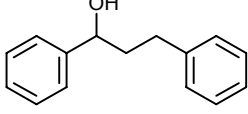
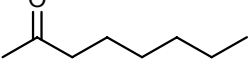
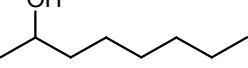
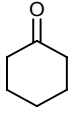
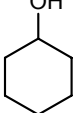
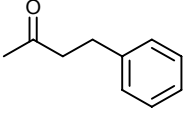
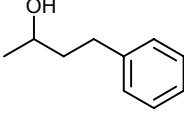
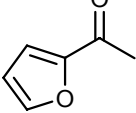
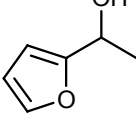
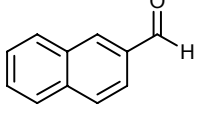
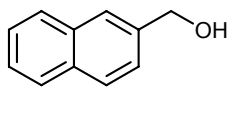
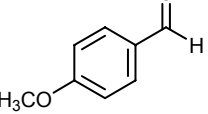
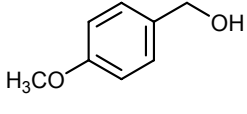
The catalytic transfer hydrogenation of carbonyl compounds with 1,4-butanediol was examined for more substrates in the presence of NaOH in refluxing toluene, and the results are listed in **Table 4.4**. Acetophenone, benzophenone, and acetophenone were reduced to give good yields of their corresponding alcohols (entries 1, 4, 9). The presence of electron-releasing group made the substrates more thermodynamically stable due to resonance effect; they give poorer results in the reduction process (entries 3, 7). Sterically hindered substrates also give less satisfactory results (entries 10-11). Aliphatic and heterocyclic ketones were reduced to give moderate to good yields of alcohols (entries 13-16). Catalytic reduction of aldehydes to primary alcohols was also found to be successful using complex **11** as the catalyst (entries 17-18).

A possible mechanism of the transfer hydrogenation reaction is depicted in **Scheme 4.2**. A ruthenium hydride complex, which is believed to be the active species, is generated from **11** and 1,4-butanediol in the presence of base. The ketone substrate coordinates to the metal center and undergoes insertion into the Ru-H bond. Protonation of the alkoxide by new 1,4-butanediol (or the lactol

formed from cyclization of 4-hydroxybutanal) afford the alcohol product.

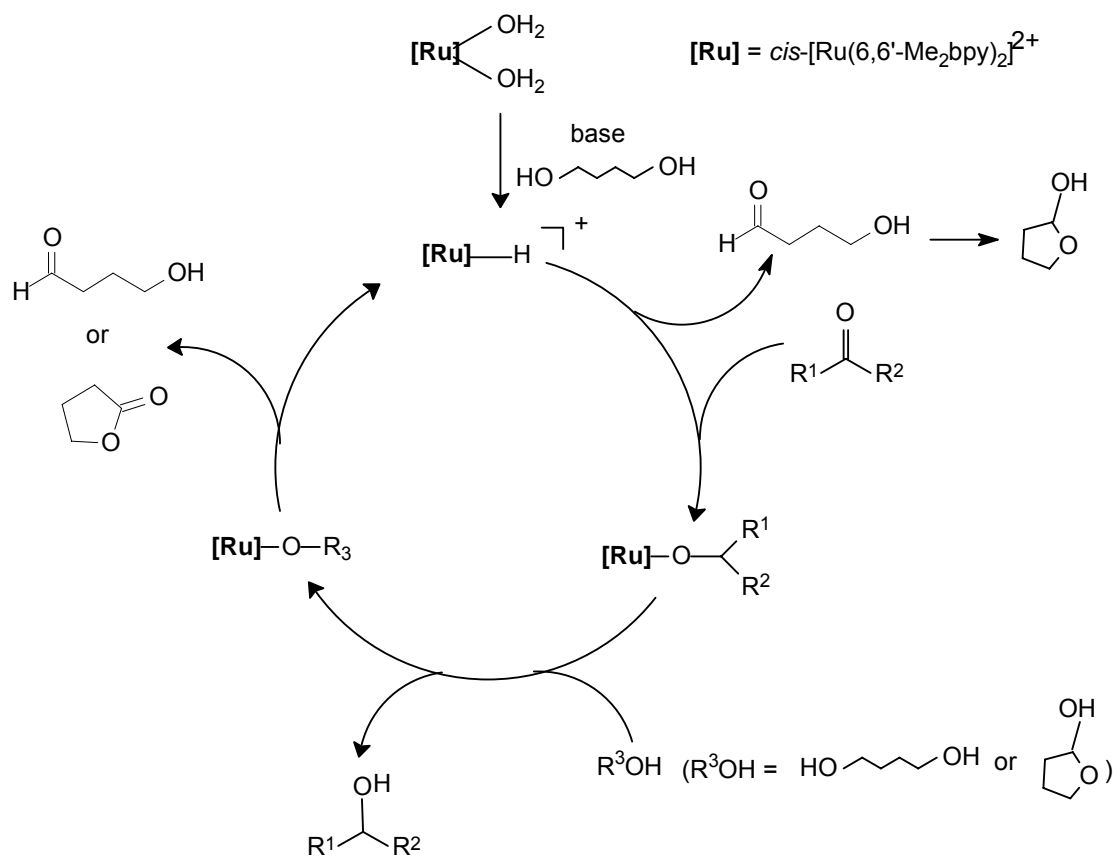
Table 4.4 Transfer hydrogenation of carbonyl compounds with 1,4-butanediol catalyzed by *cis*-[Ru(6,6'-Me₂bpy)₂(H₂O)₂](OTf)₂ 11^[a]

entry	ketone	alcohol	time	conversion (%) ^[b]
1			20	94
2			20	98
3			40	89
4			20	89
5			20	87
6			20	97
7			40	70
8			20	89

9			20	89
10			20	78
11			40	98
12			20	94
13			40	73
14			20	93
15			20	83
16			40	84
17			16	95
18			16	97

[a] Reaction conditions: catalyst (0.01 mmol, 1 mol% referred to carbonyl substrate), NaOH (0.25 mmol, 20% referred to carbonyl substrate), 1,4-butanediol (1 eq. referred to carbonyl substrate), toluene (1 mL), reflux.

[b] Conversion determined by ^1H NMR spectroscopy.



Scheme 4.2. Proposed mechanism for the 11-catalyzed transfer hydrogenation of carbonyl compounds with 1,4-butanediol

Conclusion

Based on the X-ray crystallographic structures of **1a-c**, it is more appropriate to describe this class of Ru–silane complexes $\text{TpRu}(\text{PPh}_3)(\text{H}_2\text{SiR}_3)$ as having a static structure $\text{TpRu}(\text{PPh}_3)(\eta^3\text{-HSiR}_3\text{H})$ containing $\text{H}\cdots\text{Si}\cdots\text{H}$ bonding, rather than a highly fluxional pair of σ -silane hydride complexes $\text{TpRu}(\text{PPh}_3)(\text{H}_a)(\eta^2\text{-H}_b\text{SiR}_3) \rightleftharpoons \text{TpRu}(\text{PPh}_3)(\text{H}_b)(\text{H}_a\text{SiR}_3)$. The complex $\text{TpRu}(\text{PPh}_3)(\eta^3\text{-HSiPhMe}_2\text{H})$ (**1c**) was used to catalyze the hydrolytic oxidation of silanes to silanols. Although the catalytic activity of **1c** might not be as high as some of the catalytic systems reported by others, we have, however, been able to present a much clearer picture of the mechanistic aspects of the reaction. More importantly, this is a rare example employing complex, which contains the $[\text{H}_2\text{SiR}_3]^-$ moiety, for catalytic study. For most of the previously studied catalytic systems, the reaction mechanisms had not been studied in detail; it was generally suggested that the catalysis involves oxidative addition of the silane molecule to the metal to form the silyl hydride species. In our study, a new mechanism was revealed. Theoretical calculations show that the crucial step of the catalytic process is the nucleophilic attack of water oxygen at the silicon center of the $[\text{H}_2\text{SiR}_3]^-$ moiety; strong dihydrogen-bonding interaction between one of the hydrides of $[\text{H}_2\text{SiR}_3]^-$ and a water proton is present in the transition state. This work not only provides experimental evidence, which is still scarce, for the presence of the

$[\text{H}_2\text{SiR}_3]^-$ ligand, it also establishes a unique mechanism for the transition metal-catalyzed hydrolytic oxidation of silanes to silanols. An alternative mechanism, which involves intramolecular hydroxo attack at the silane ligand is also proposed. However, theoretical calculations indicate that this alternative mechanism is less favorable.

We have also demonstrated that the silane complex **1c** is capable of catalyzing the reduction of carbon dioxide by hydrosilane to give silyl methoxide as the ultimate reduction product. Although the turnovers of the catalytic system comprising **1c** are not as high as those reported in the literature, we are able to identify most the chemical species generated in the catalytic reaction, including the CO_2 -reduction products such as formoxysilane and bis(silyl)acetal, as well as the ruthenium complexes $\text{TpRu}(\text{PPh}_3)(\text{CO})\text{H}$ (**5**), $\text{TpRu}(\text{PPh}_3)(\text{CO})(\eta^1\text{-OCHO})$ (**6**), and $\text{TpRu}(\text{CO})_2\text{H}$ (**7**). In addition, we are probably the first group to detect formaldehyde, an indispensable intermediate according to density function theory study, during the CO_2 -reduction by silane. This work also gives a demonstration of the possibility of using hydrosilane as a reducing agent for affecting CO_2 -transformation.

The dicationic bpy-ruthenium complexes were found to be active catalysts for

β -alkylation of secondary alcohols with primary alcohols and transfer hydrogenation of aldehydes and ketones with 1,4-butanediol. The work demonstrated a relatively rare example of using electrophilic transition-metal complexes for the two reactions. Moreover, the use of stoichiometric amount of 1,4-butanediol in transfer hydrogenation reaction provides an alternative for the reduction of carbonyl compounds

Appendices

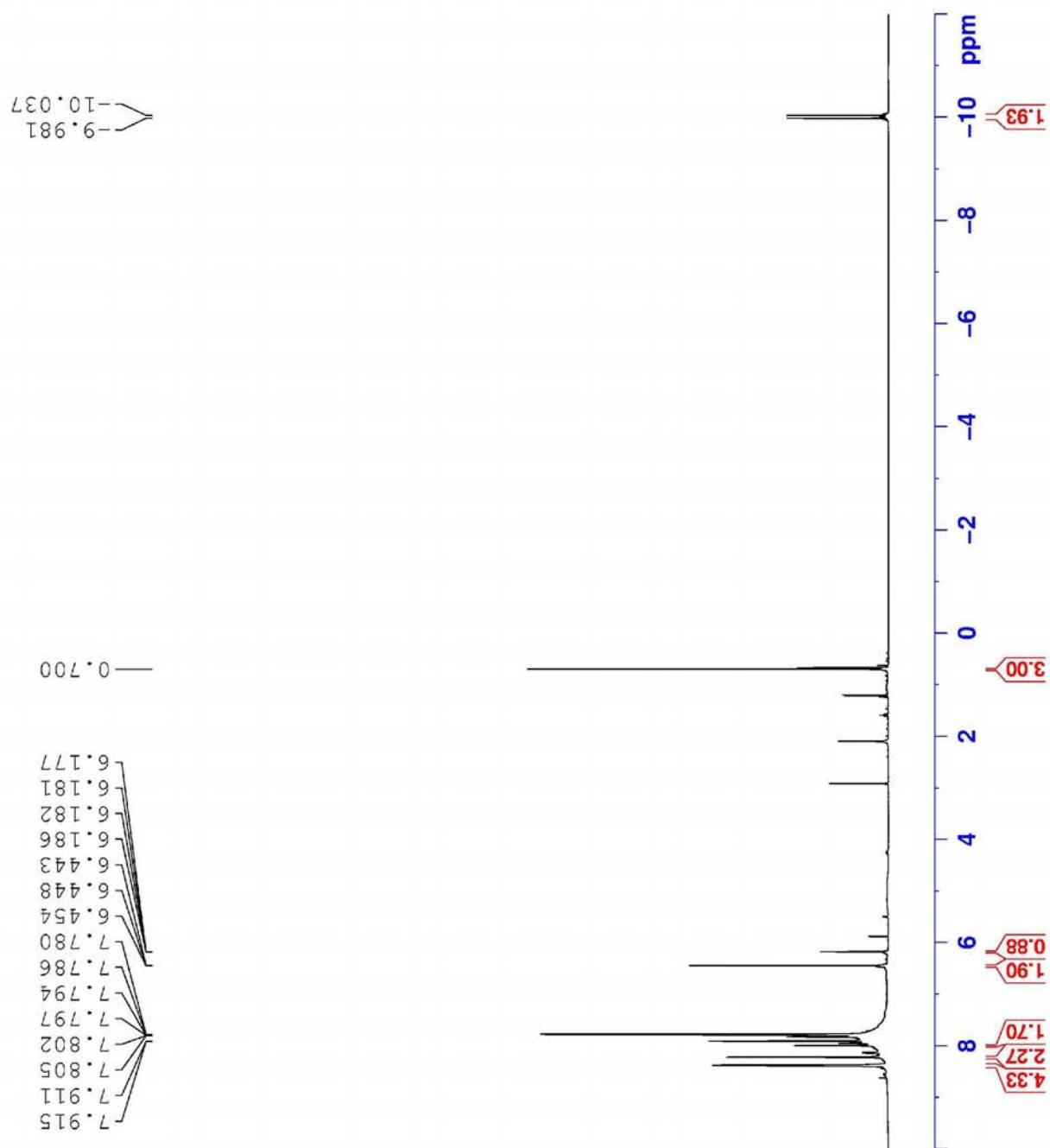


Figure 2.7. ^1H NMR spectrum of $\text{TpRu}(\text{PPh}_3)(\eta^3\text{-HSiPh}_2\text{MeH})\text{-1b}$

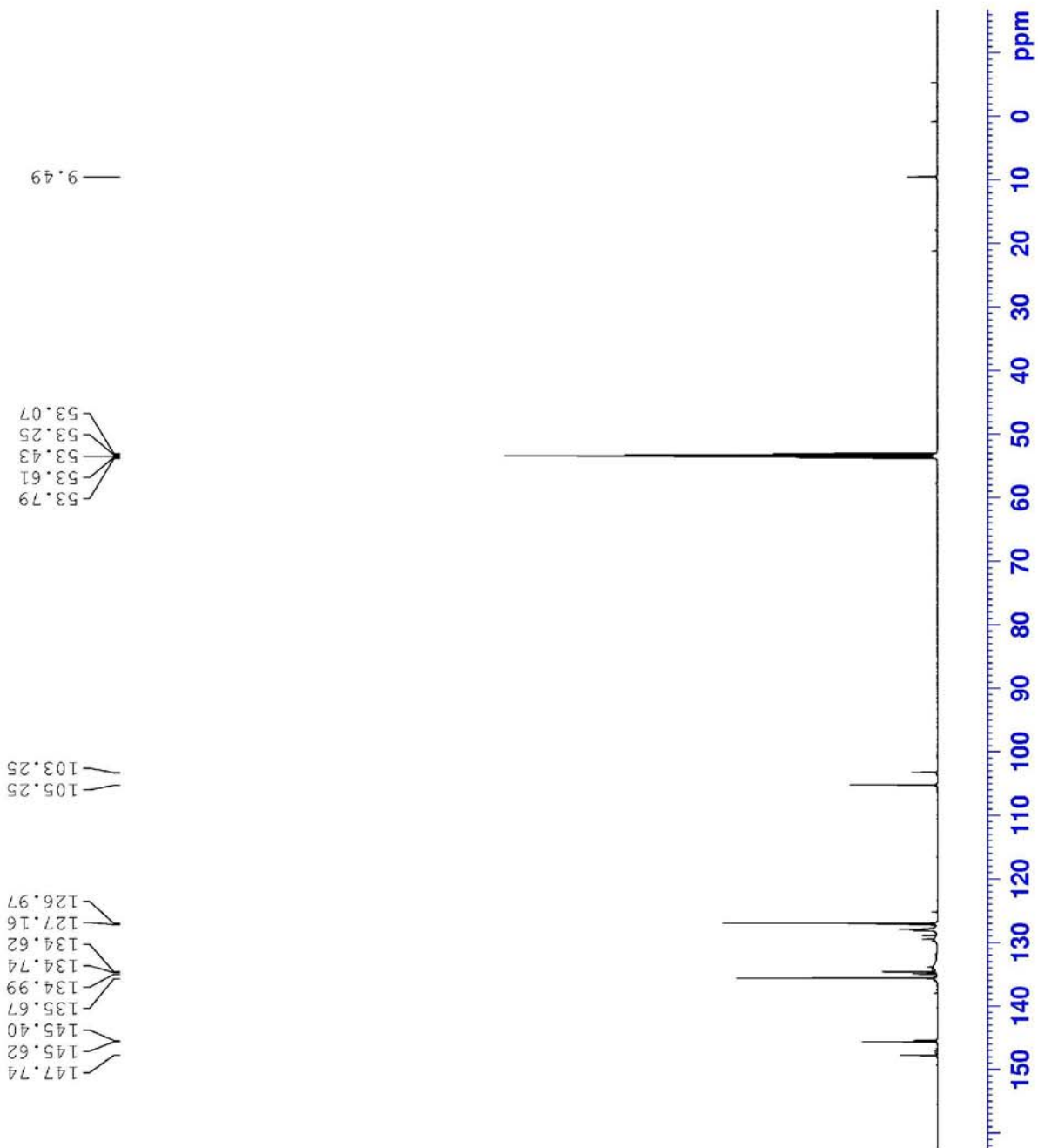


Figure 2.8 ^{13}C NMR spectrum of $\text{TpRu}(\text{PPh}_3)(\eta^3\text{-HSiPh}_2\text{MeH})\text{-1b}$

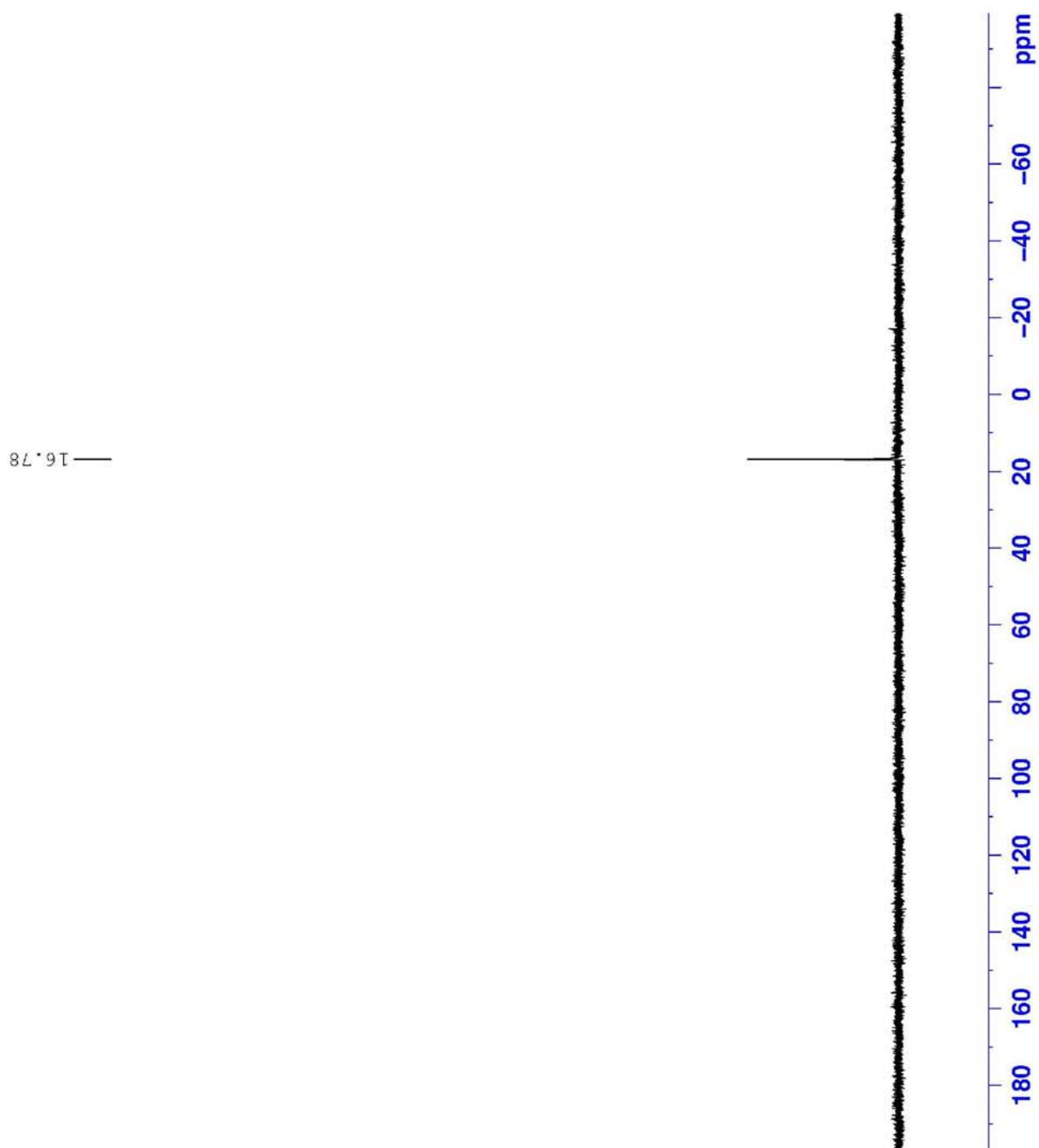


Figure 2.9 ^{29}Si NMR spectrum of $\text{TpRu}(\text{PPh}_3)(\eta^3\text{-HSiPh}_2\text{MeH})\text{-1b}$

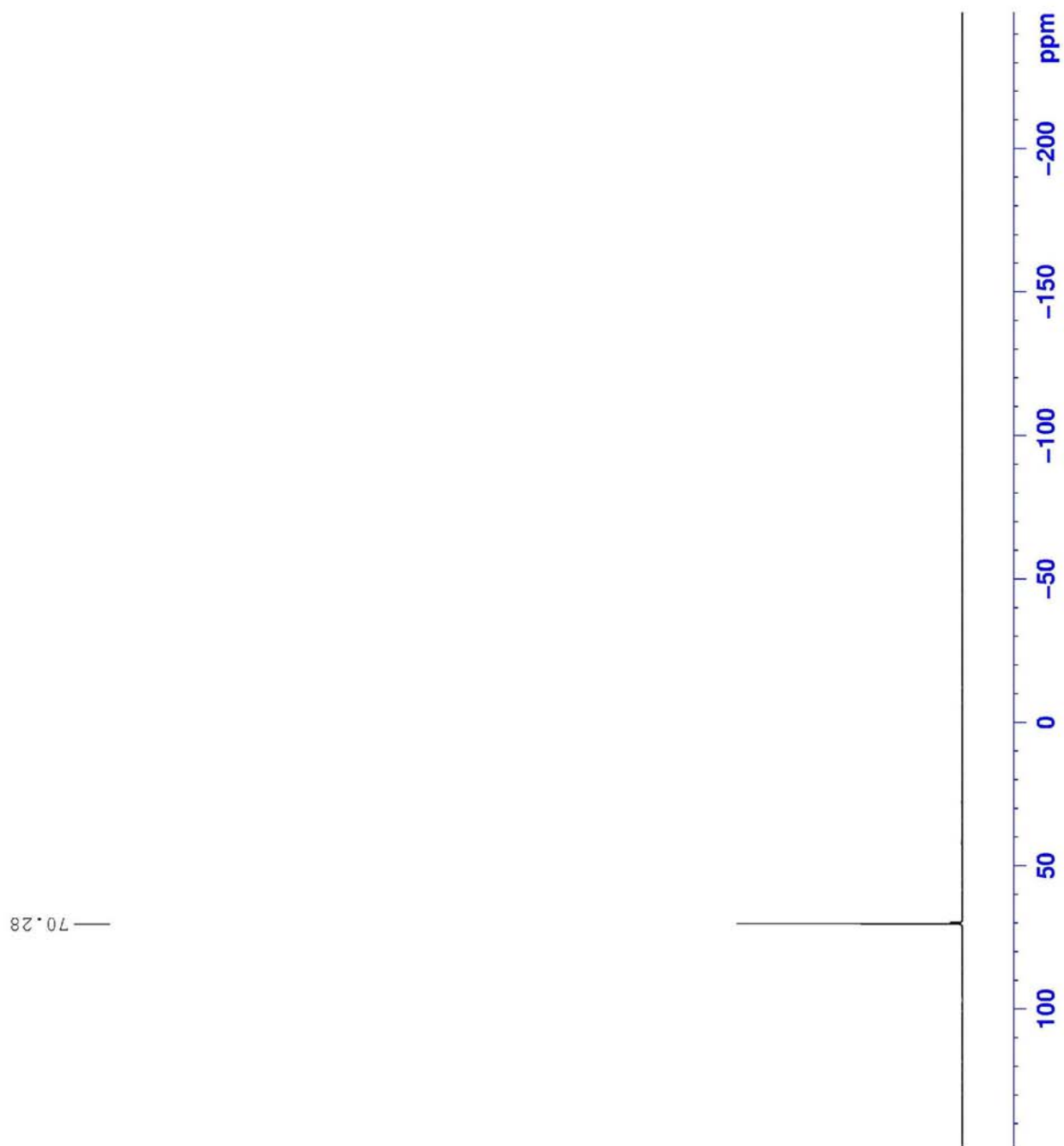


Figure 2.10 ^{31}P NMR spectrum of $\text{TpRu}(\text{PPh}_3)(\eta^3\text{-HSiPh}_2\text{MeH})\text{-1b}$

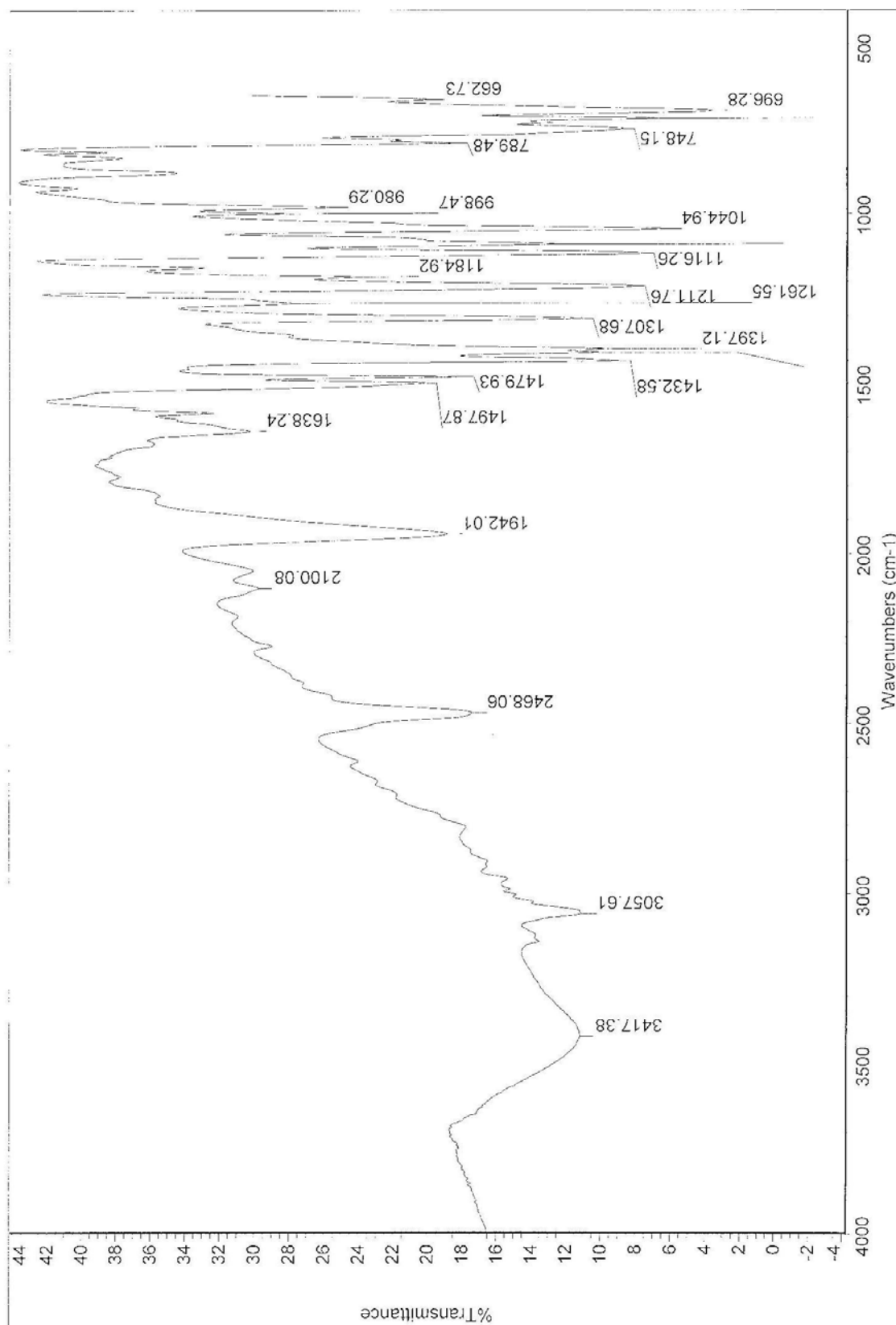


Figure 2.11 Infrared spectrum of $\text{TpRu}(\text{PPh}_3)(\eta^3\text{-HSiPh}_2\text{MeH})\text{-1b}$

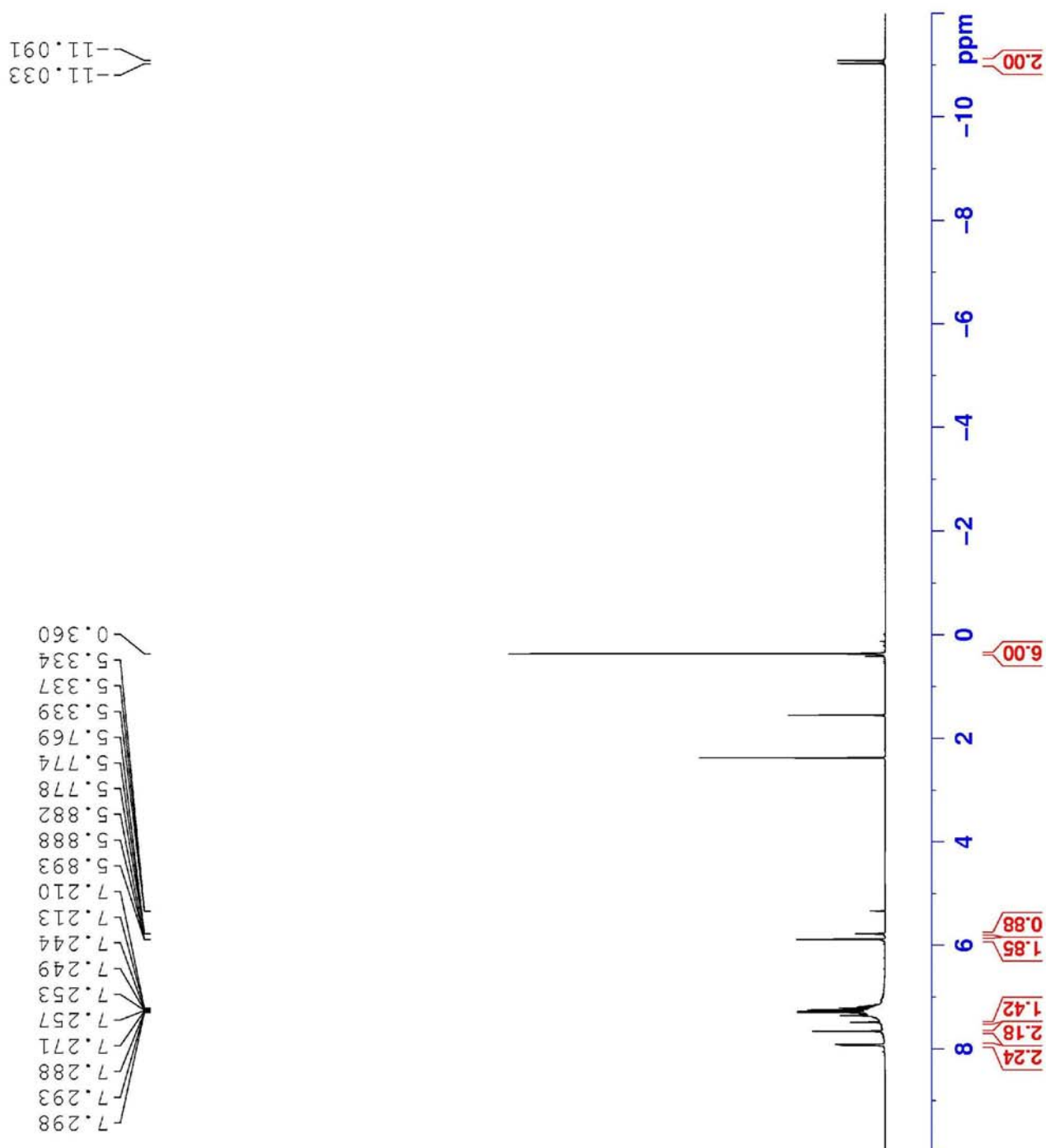


Figure 2.12 ^1H NMR spectrum of $\text{TpRu}(\text{PPh}_3)(\eta^3\text{-HSiPhMe}_2\text{H})\text{-1c}$

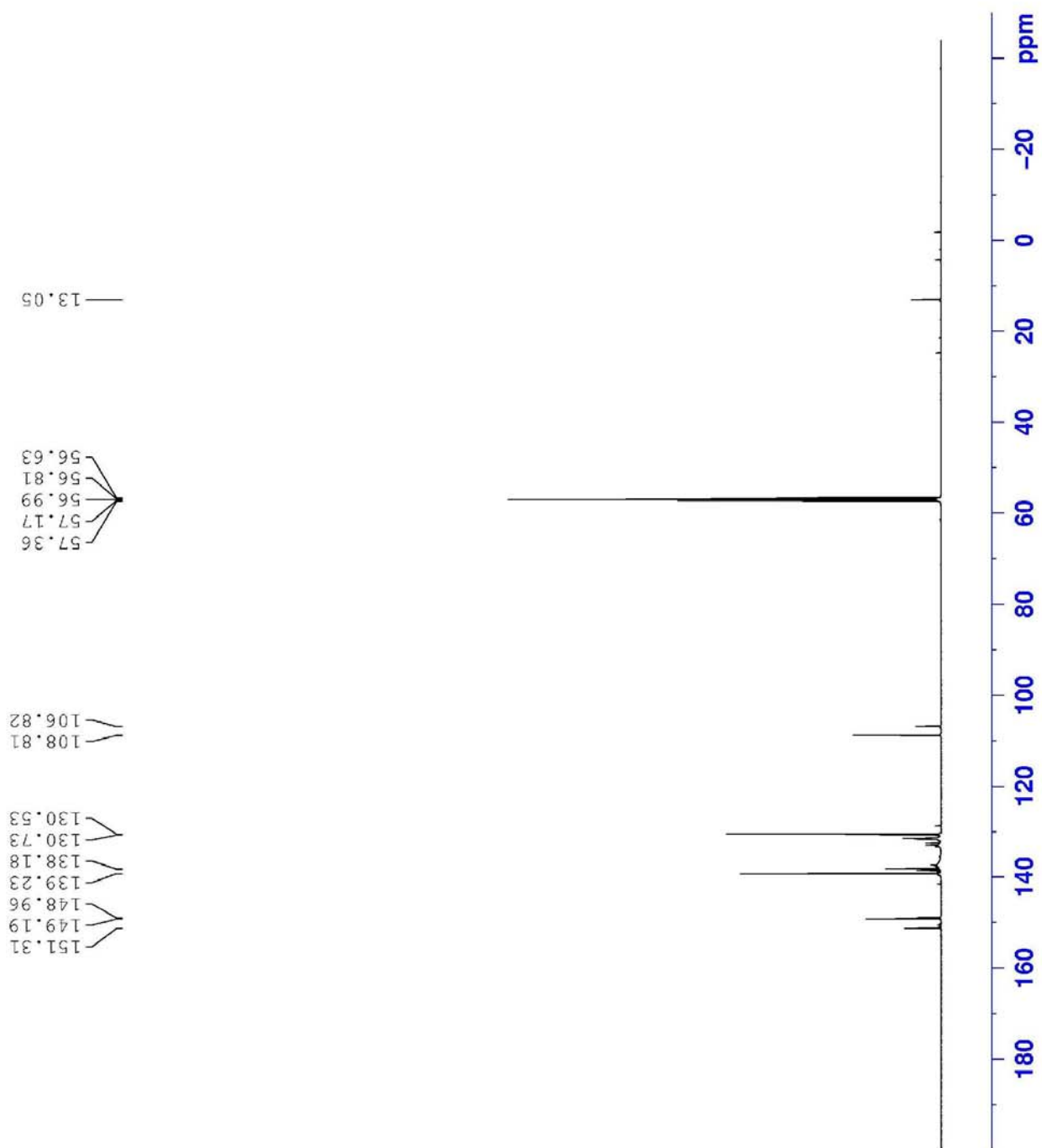


Figure 2.13 ^{13}C NMR spectrum of $\text{TpRu}(\text{PPh}_3)(\eta^3\text{-HSiPhMe}_2\text{H})\text{-1c}$

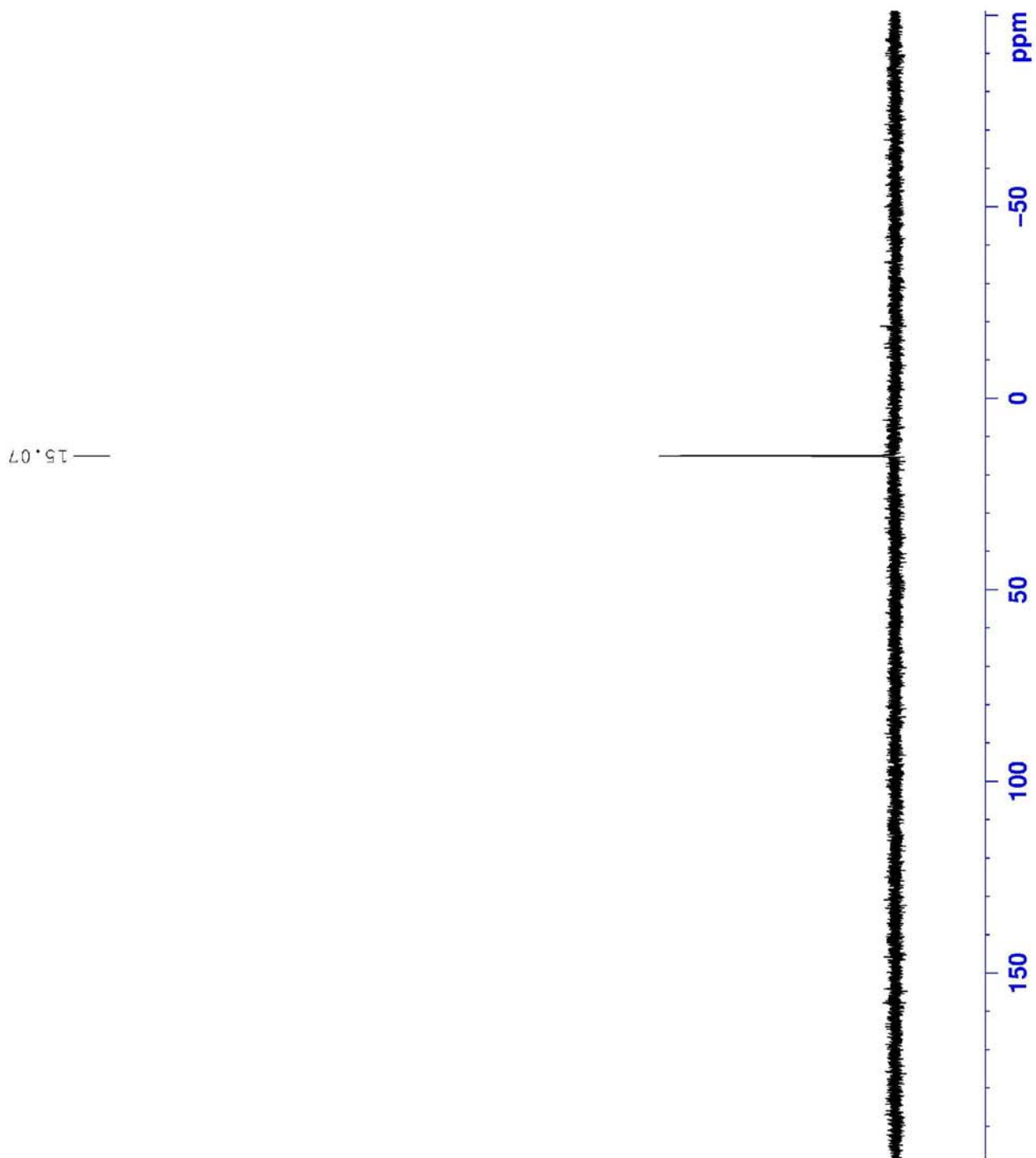


Figure 2.14 ^{29}Si NMR spectrum of $\text{TpRu}(\text{PPh}_3)(\eta^3\text{-HSiPhMe}_2\text{H})\text{-1c}$

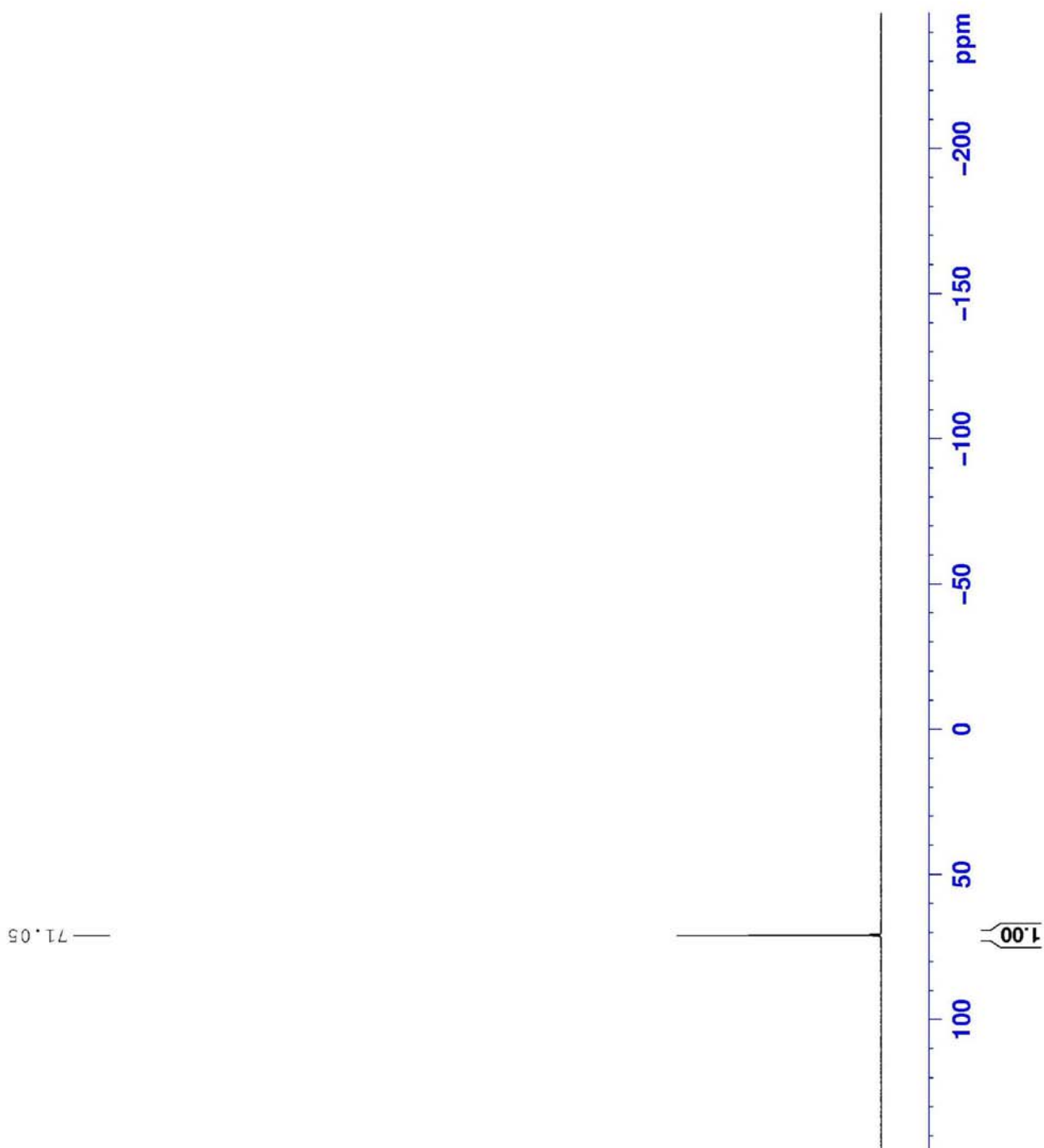


Figure 2.15 ^{31}P NMR spectrum of $\text{TpRu}(\text{PPh}_3)(\eta^3\text{-HSiPhMe}_2\text{H})\text{-1c}$

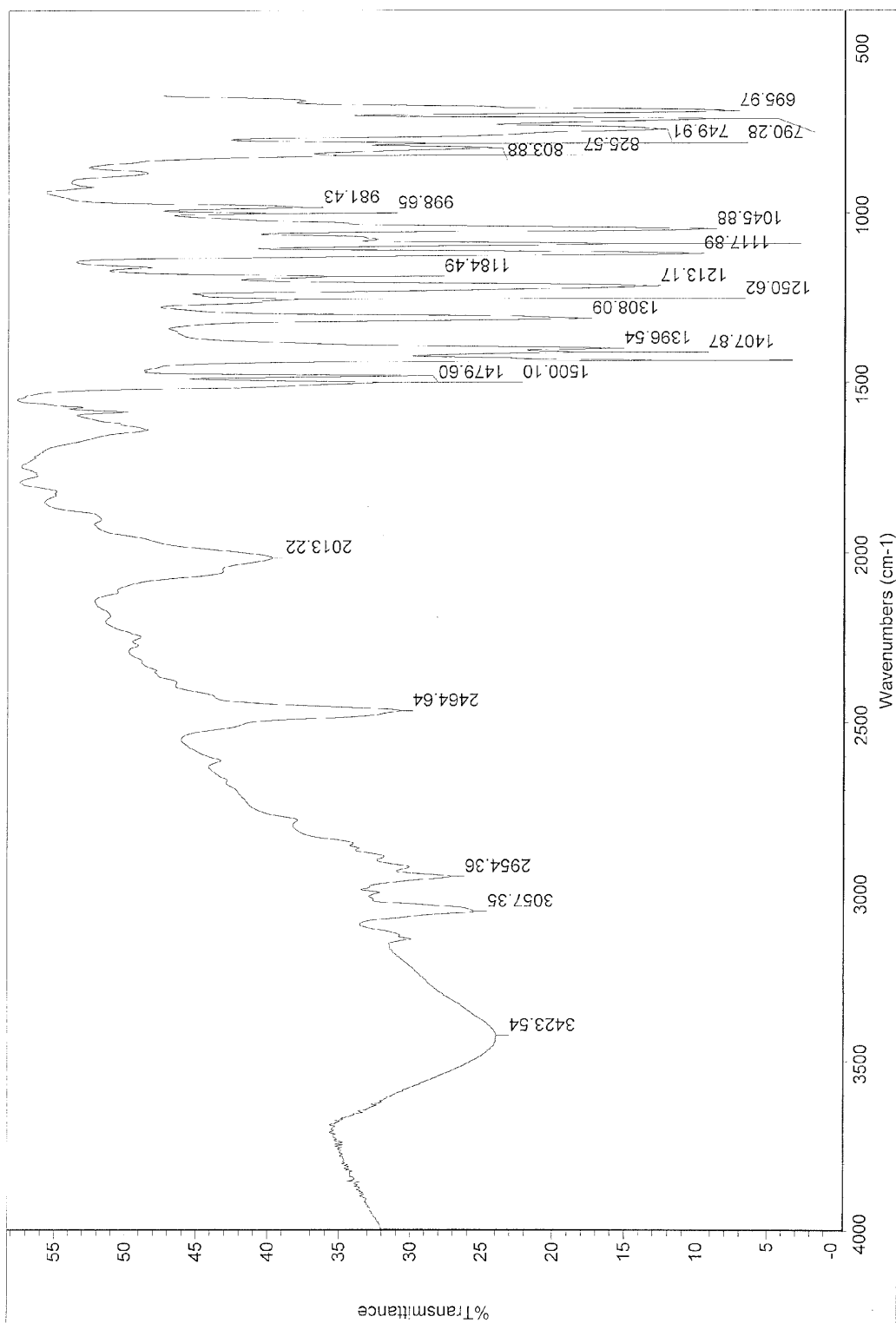


Figure 2.16 Infrared spectrum of $\text{TpRu}(\text{PPh}_3)(\eta^3\text{-HSiPhMe}_2\text{H})\text{-1c}$

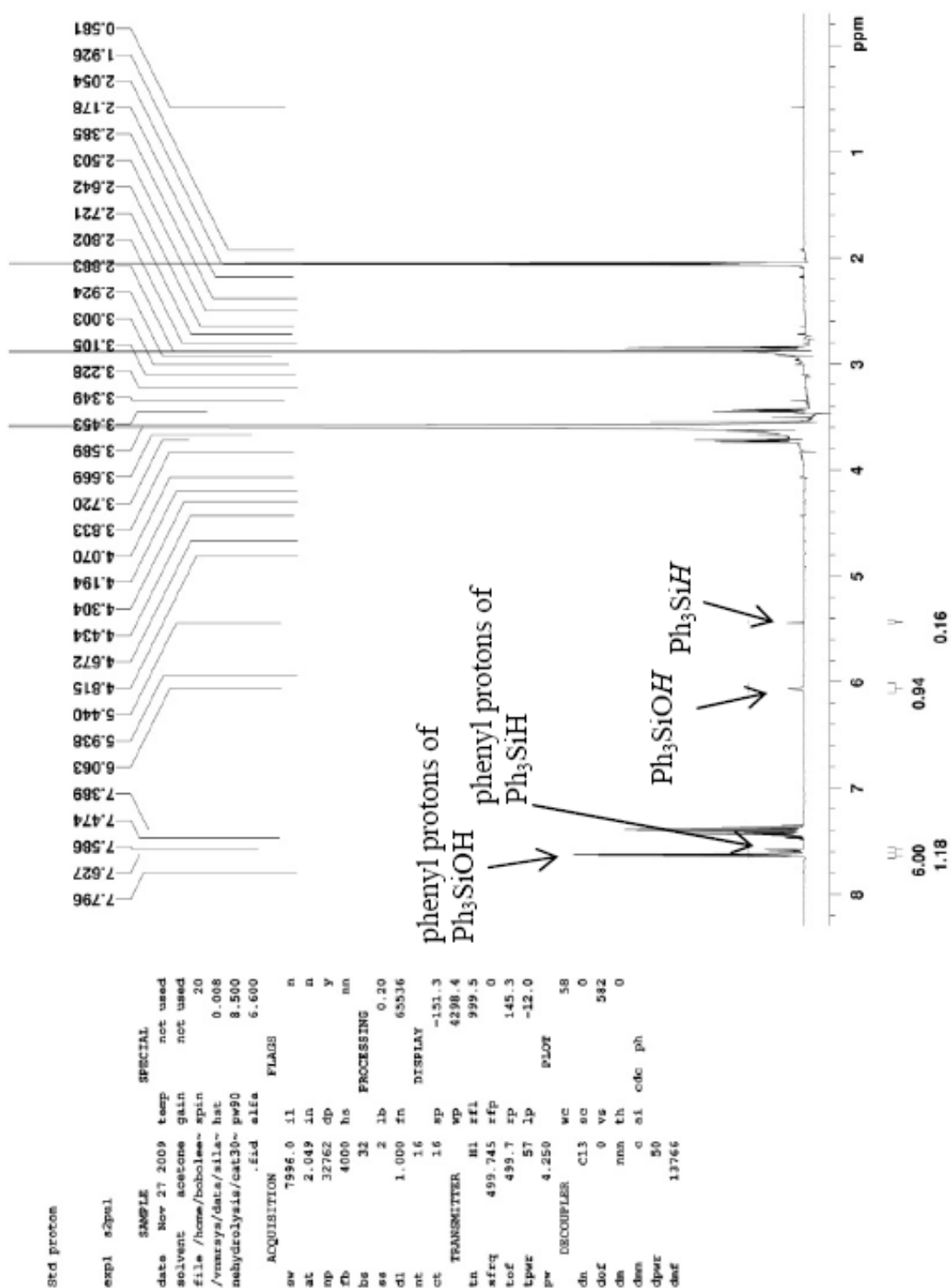


Figure 2.17 ^1H NMR spectrum of the reaction mixture of 1c-catalyzed hydrolytic oxidation of Ph_3SiH

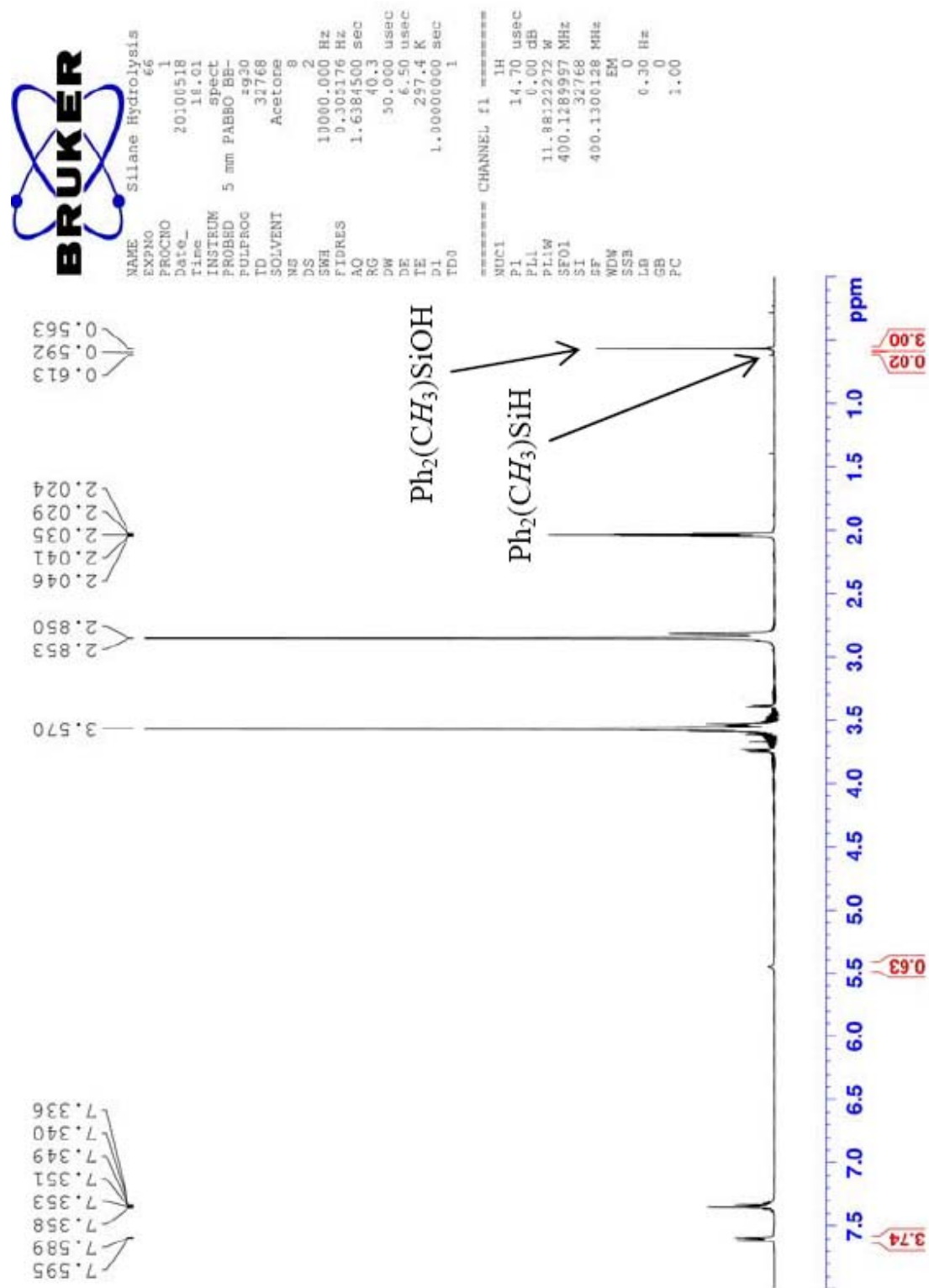


Figure 2.18 ¹H NMR spectrum of the reaction mixture of 1c-catalyzed hydrolytic oxidation of Ph₂MeSiH

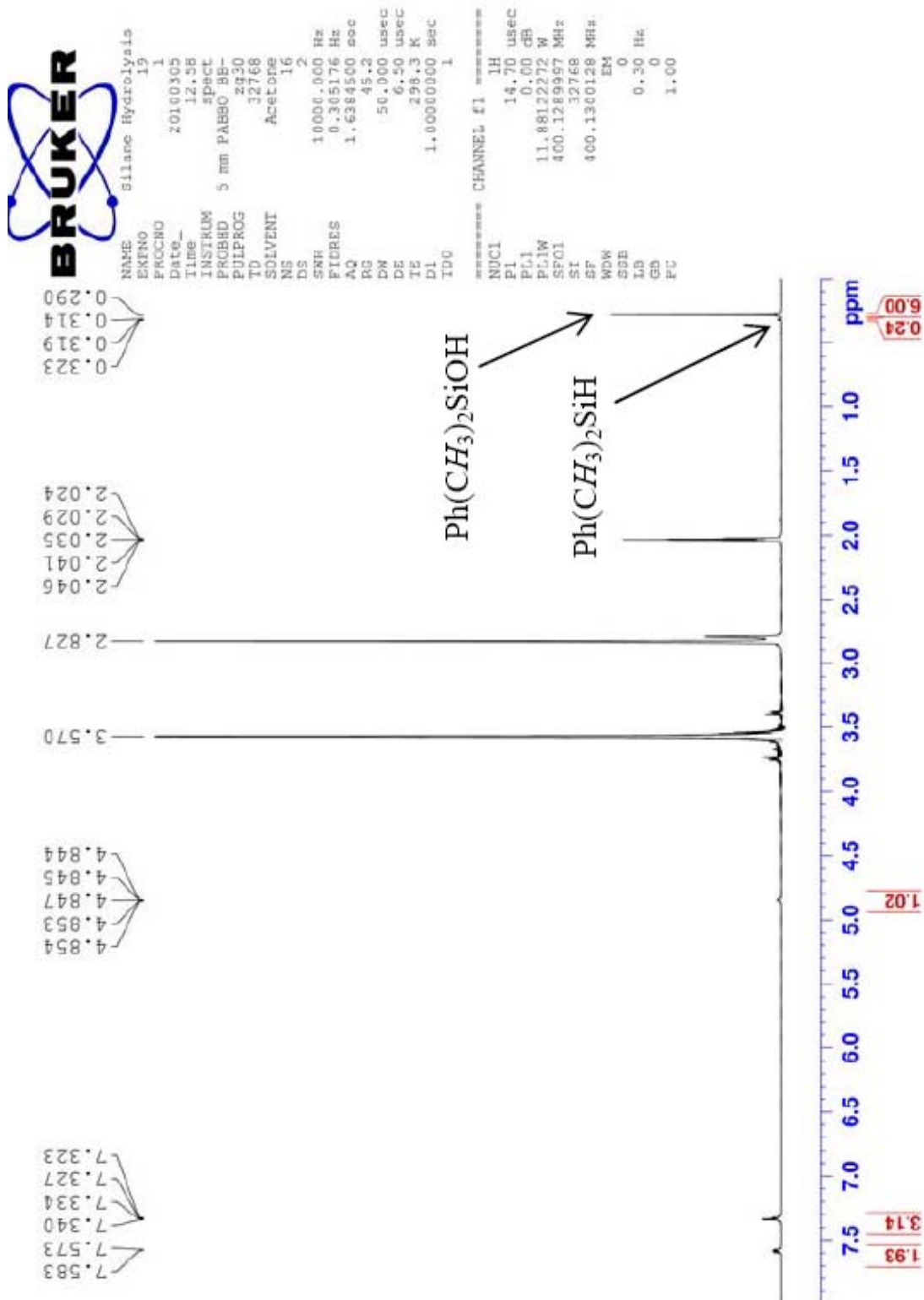


Figure 2.19 ¹H NMR spectrum of the reaction mixture of 1c-catalyzed hydrolytic oxidation of PhMe₂SiH

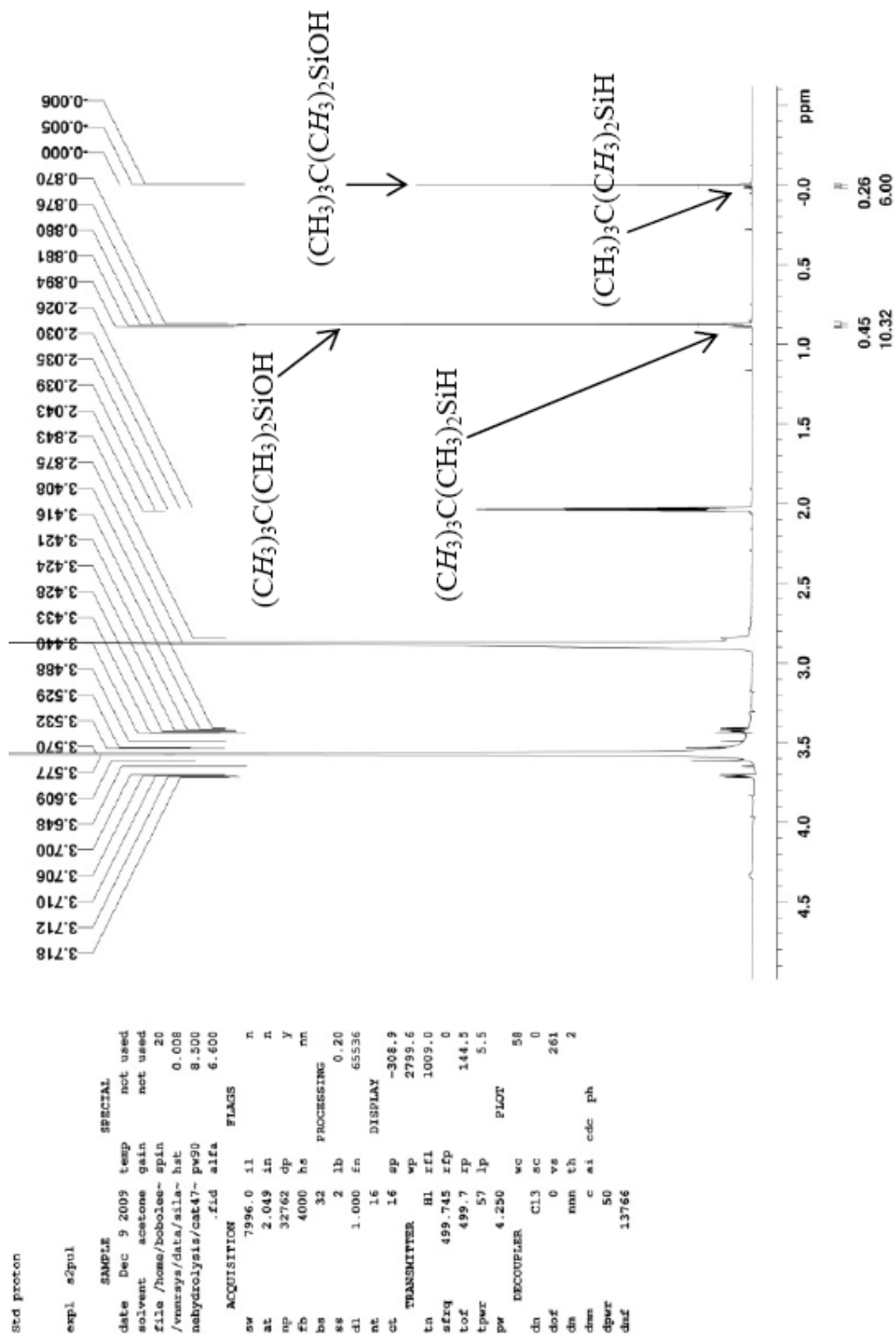


Figure 2.20 ^1H NMR spectrum of the reaction mixture of 1c-catalyzed hydrolytic oxidation of $t\text{BuMe}_2\text{SiH}$



Silane Hydrolysis

NAME
EXPNO 1
PROCNO 8
Date_ 20091229
Time 13.13
INSTRUM spect
PROBHD 5 mm PABBO BB-
PULPROG zg30
TD 32768
SOLVENT CD3CN
NS 16
DS 2
SWH 10000.000 Hz
FIDRES 0.305176 Hz
AQ 1.6384500 sec
RG 45.2
DW 50.000 usec
DE 6.50 usec
TE 292.7 K
D1 1.00000000 sec
TD0 1

CHANNEL f1

NUC1 1H
P1 14.70 usec
PL1 0.00 dB
PL1W 11.88122272 W
SFO1 400.1285997 MHz
SI 32768
SF 400.1300128 MHz
WDW EM
SSB 0
LB 0.30 Hz
GB 0
PC 1.00

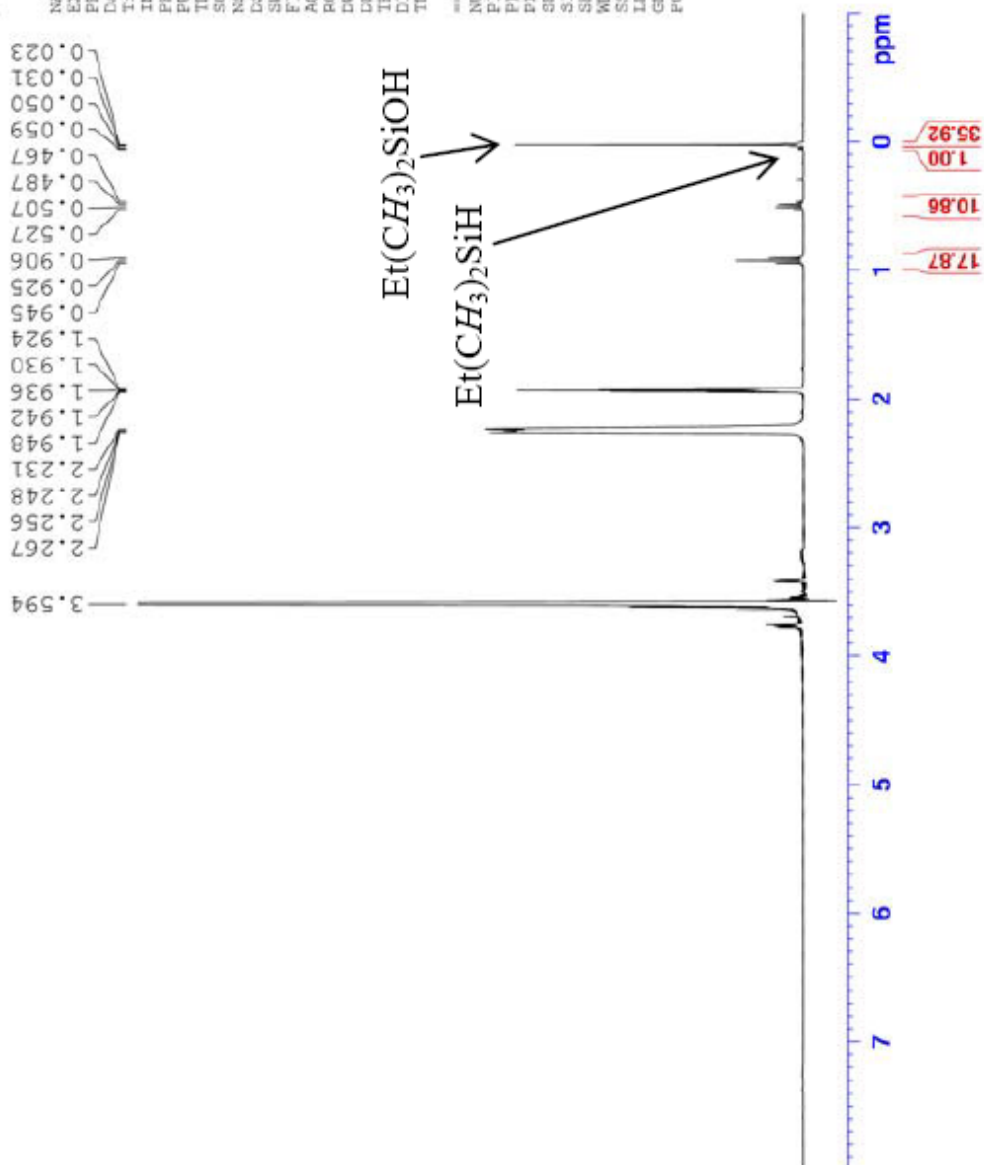


Figure 2.21 ¹H NMR spectrum of the reaction mixture of 1c-catalyzed hydrolytic oxidation of EtMe₂SiH



Silane Hydrolysis

NAME	EXPNO	16
PROCNO	1	
Date_	20100112	
Time	13.10	
INSTRUM	SPECT	
PROBHD	5 mm PABBO BB-	
PULPROG	zg30	
TD	32768	
SOLVENT	CD3CN	
NS	16	
DS	2	
SWH	10000.000 Hz	
FIDRES	0.305176 Hz	
AQ	1.6384500 sec	
RG	45.2	
DW	50.000 usec	
DE	6.50 usec	
TE	294.4 K	
D1	1.0000000 sec	
TD0	1	

===== CHANNEL f1 =====

NUC1	1H
PI	14.70 usec
PL1	0.00 dB
PL1W	11.88122272 W
SFO1	400.1289997 MHz
SI	32768
SF	400.1300128 MHz
WDW	EM
SSB	0
LB	0.30 Hz
GB	0
PC	1.00

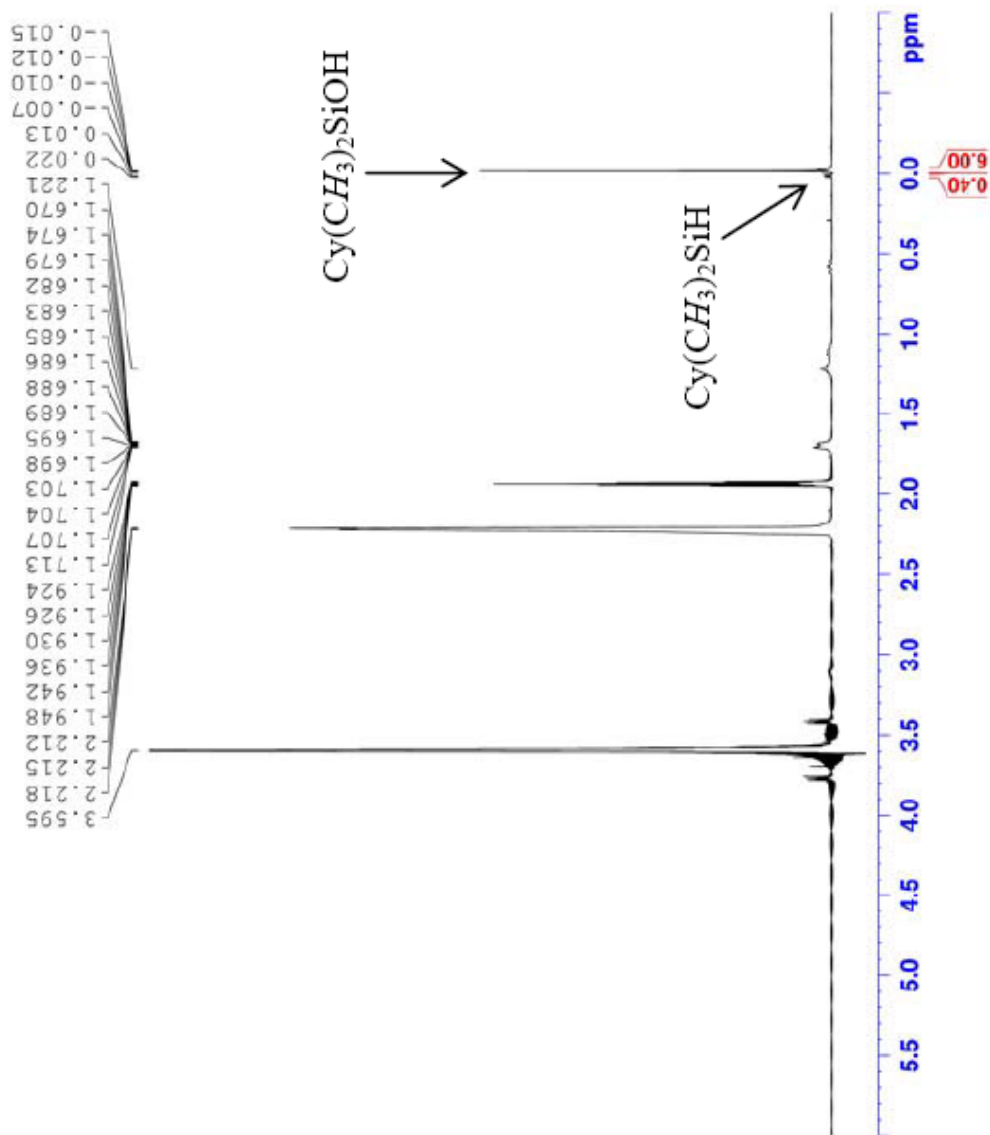


Figure 2.22 ^1H NMR spectrum of the reaction mixture of 1c-catalyzed hydrolytic oxidation of CyMe_2SiH

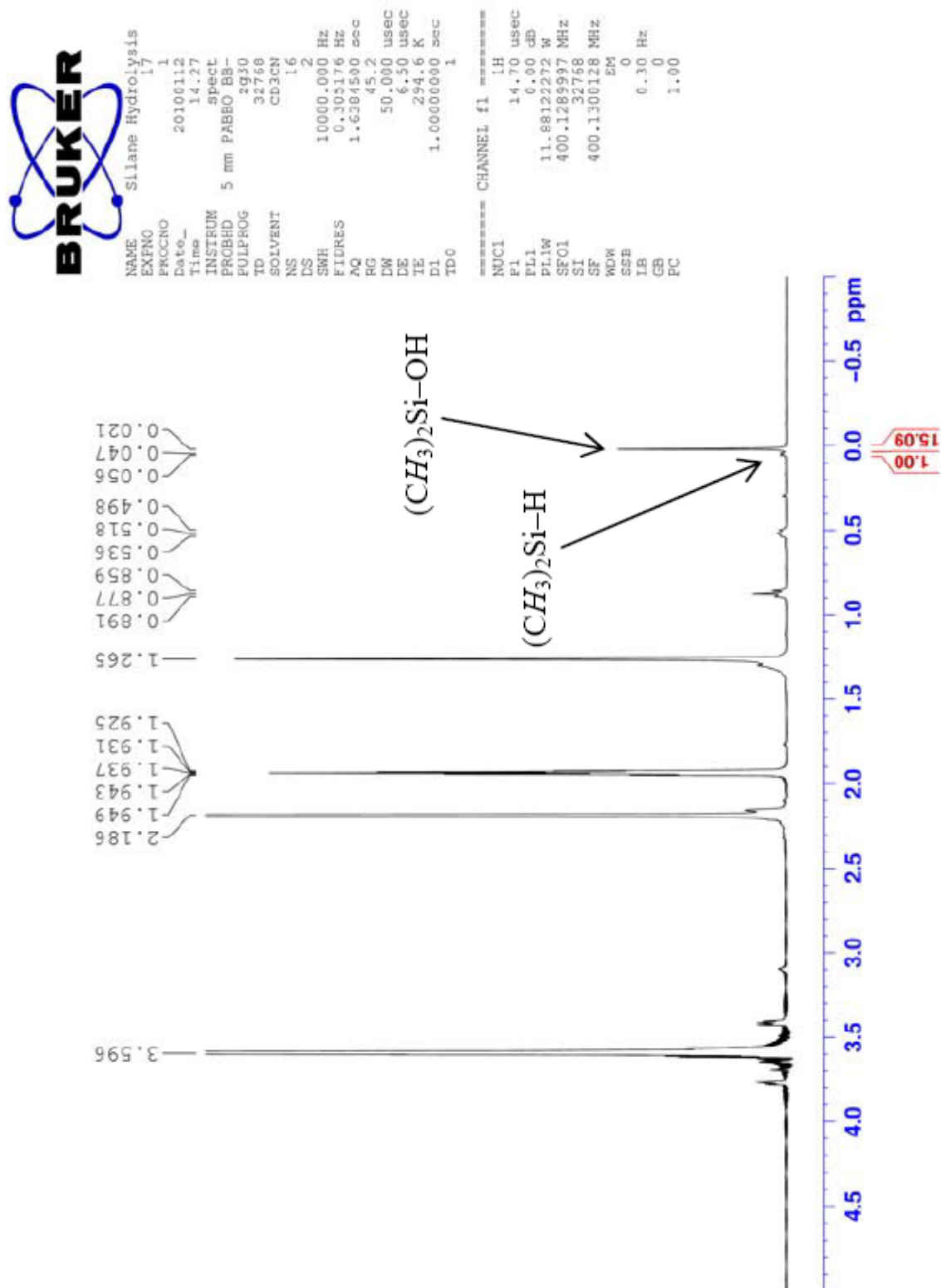


Figure 2.23 ¹H NMR spectrum of the reaction mixture of 1c-catalyzed hydrolytic oxidation of CH₃(CH₂)₁₆CH₂Me₂SiH

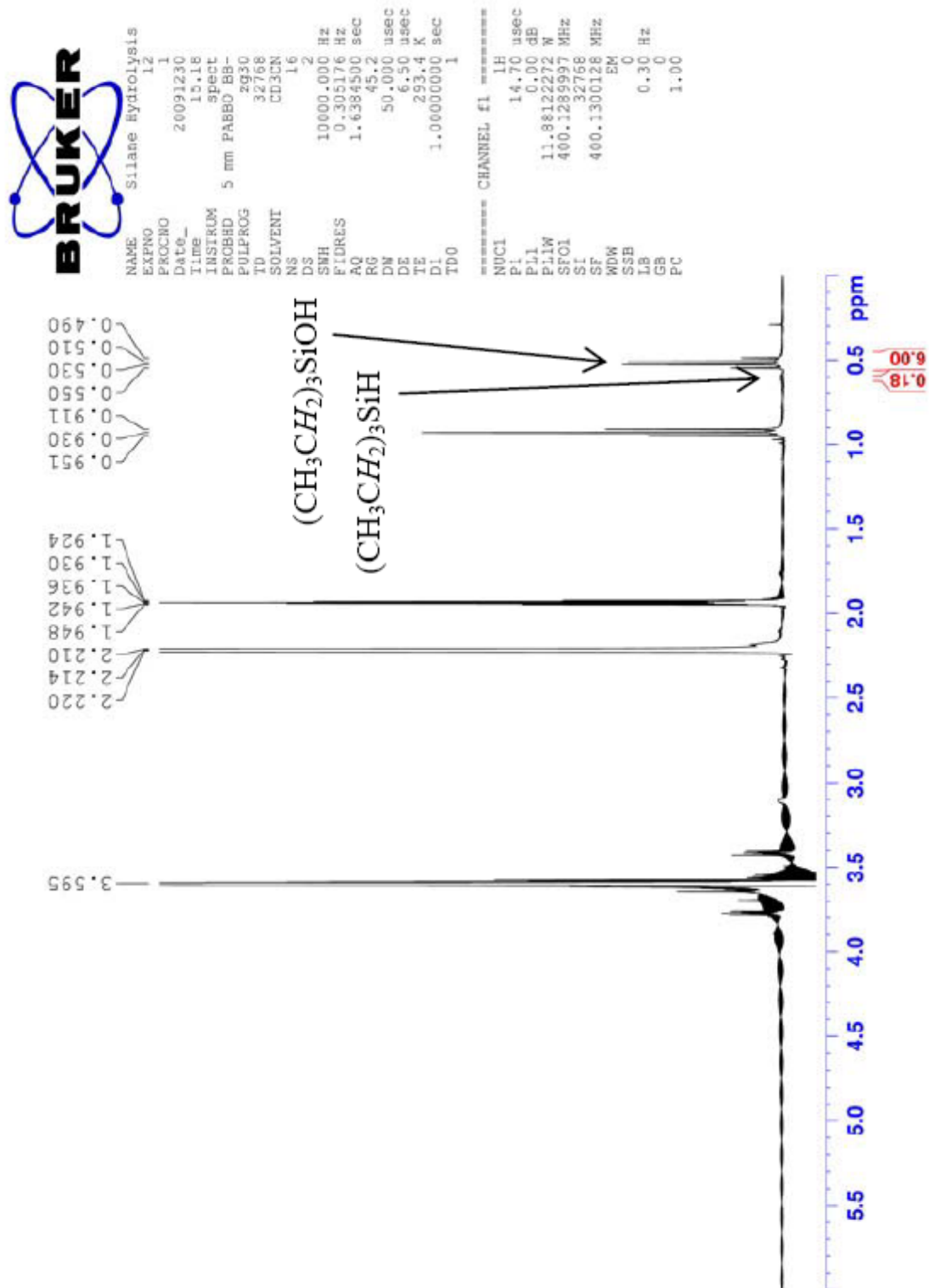


Figure 2.24 ¹H NMR spectrum of the reaction mixture of 1c-catalyzed hydrolytic oxidation of Et₃SiH

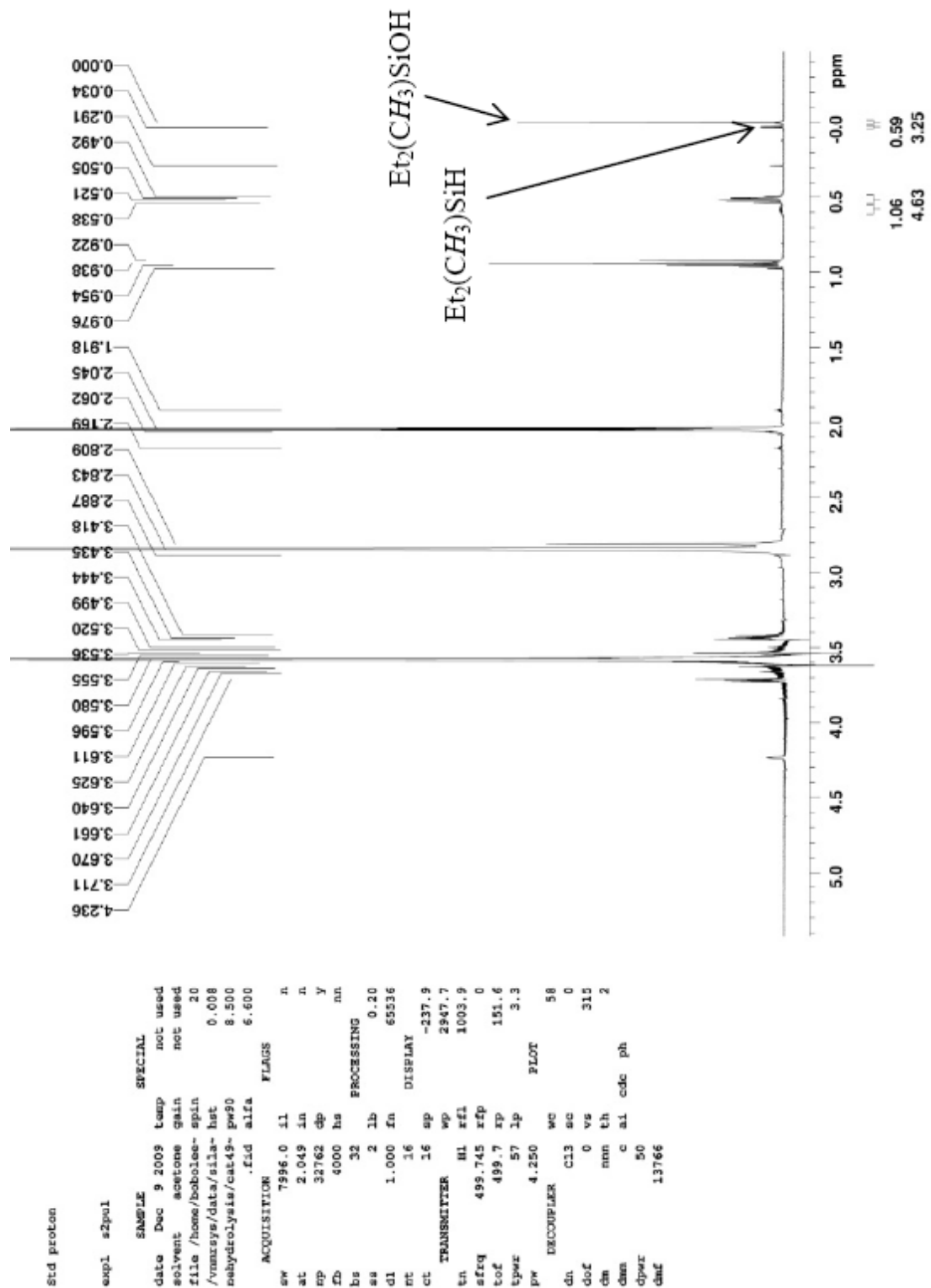


Figure 2.25 ¹H NMR spectrum of the reaction mixture of 1c-catalyzed hydrolytic oxidation of Et₂MeSiH

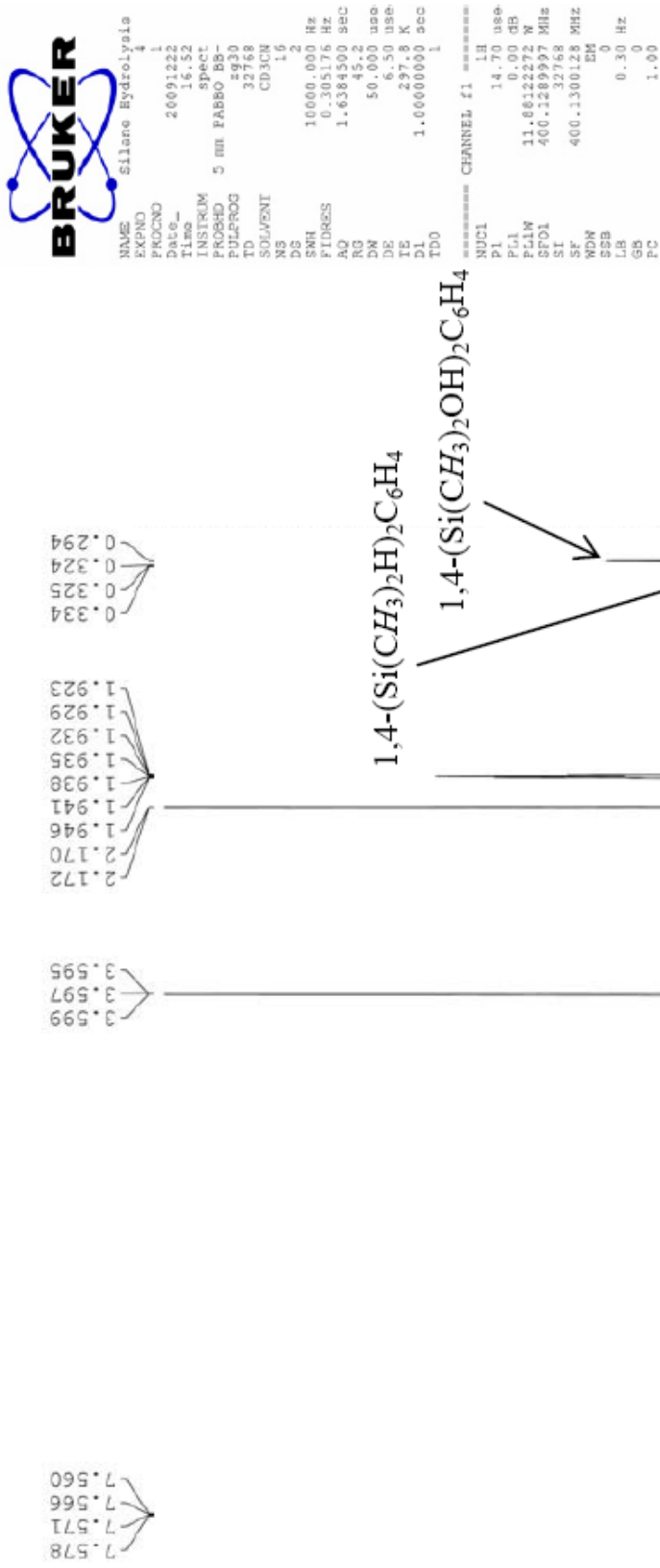


Figure 2.26 ¹H NMR spectrum of the reaction mixture of 1c-catalyzed hydrolytic oxidation of 1,4-(SiMe₂H)₂C₆H₄



```

NAME      Silane Hydrolysis
EXPNO    1
PROCNO   1
Date_    20100528
Time     12:36
INSTRUM  spect
PROBHD   5 mm F4BBO BB-
PULPROG  zg30
TD        32768
SOLVENT  Acetone
NS        16
DS        2
SWH       10000.000 Hz
FIDRES    0.305176 Hz
AQ         1.6384500 sec
RG         57
DW         50.000 usec
DE         6.50 usec
TE        297.1 K
D1         1.00000000 sec
TD0        1

===== CHANNEL f1 =====
NUC1      1H
P1         14.70 usec
PL1        0.00 dB
PL1W       11.68122272 W
SFOL       400.1289997 MHz
SI         32768
SF         400.1300128 MHz
WDW        EM
SSB        0
LB         0.30 Hz
GB         0
PC         1.00
  
```

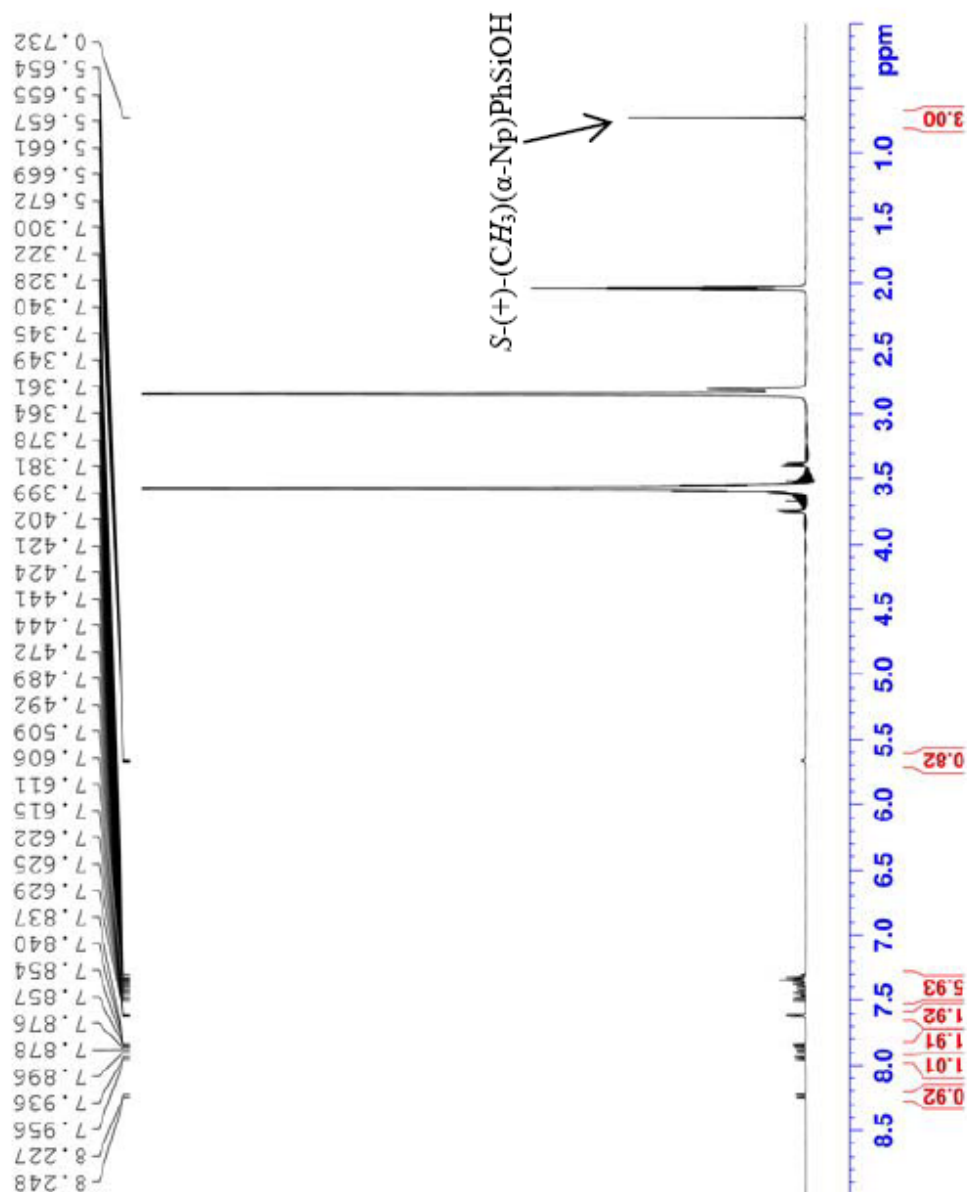


Figure 2.27 1H NMR spectrum of the reaction mixture of 1c-catalyzed hydrolytic oxidation of (+)-(R)-Me(α -Np)PhSiH

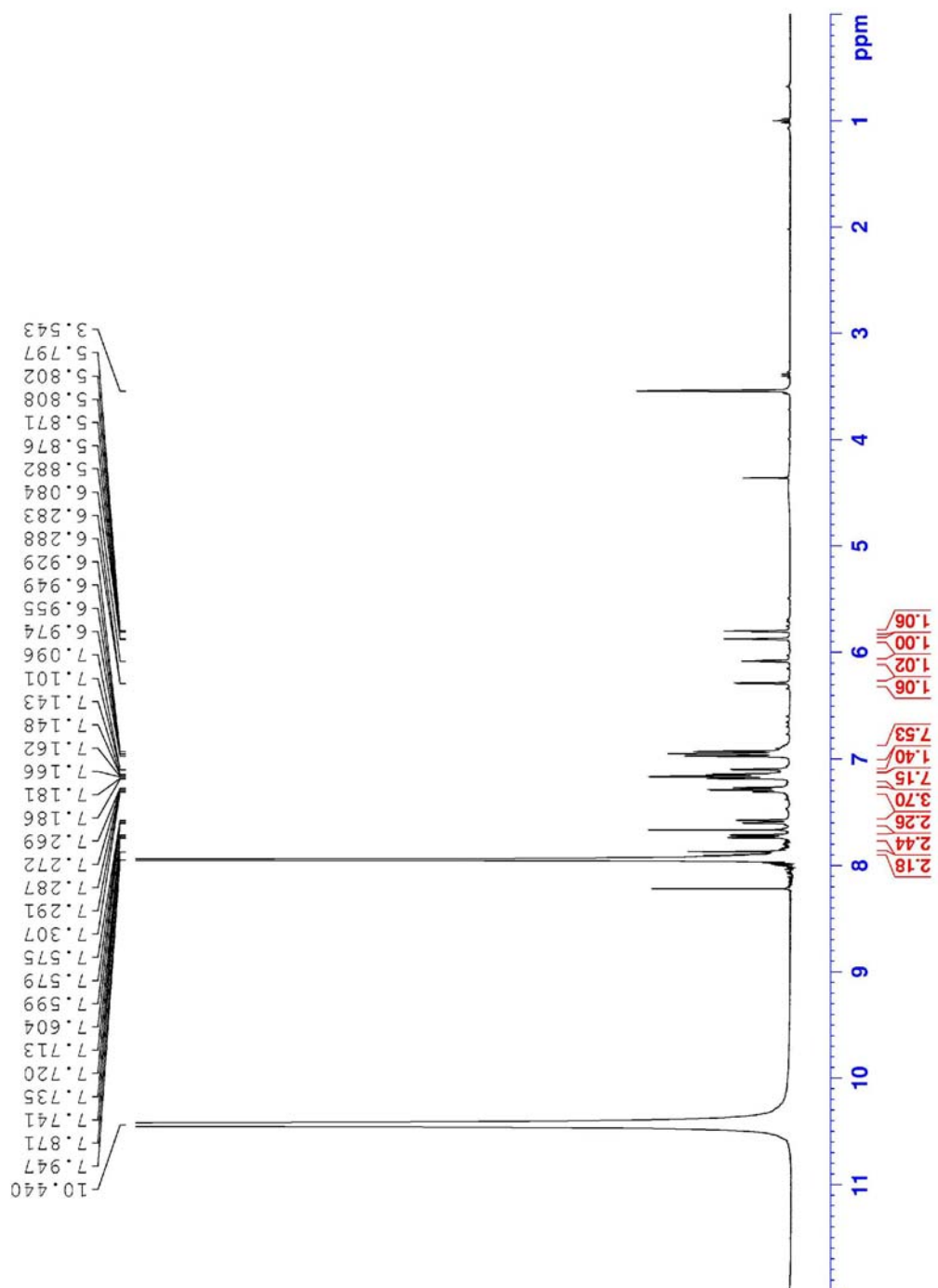


Figure 3.3 ^1H NMR spectrum of $\text{TpRu}(\text{PPh}_3)(\text{CO})(\eta^1\text{-OCHO})\text{-8}$ in 1:1 formic acid and dioxane

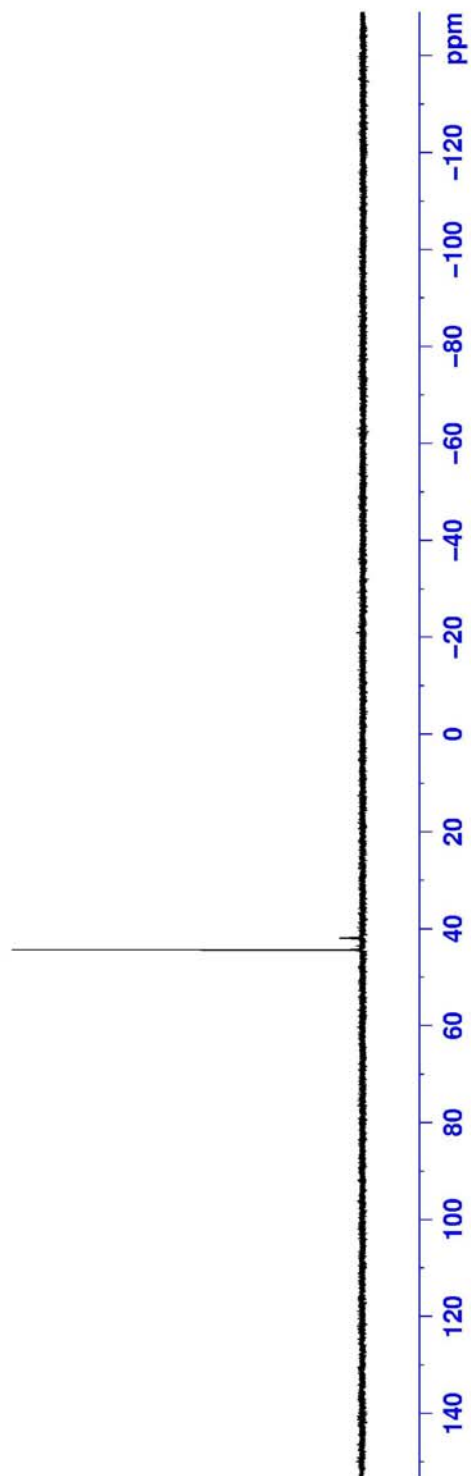


Figure 3.4 ^{31}P NMR spectrum of $\text{TpRu}(\text{PPh}_3)(\text{CO})(\eta^1\text{-OCHO})\text{-8}$ in 1:1 formic acid and dioxane


```

Current Data Parameters
NAME Ru(c12bpy) H2O
EXPNO 281
PROCNO 1

F2 - Acquisition Parameters
Date_ 20080522
Time 10.27
INSTRUM dbx400
PROBHD 5 mm QNP 1H
PULPROG zg30
TD 32768
SOLVENT CDCl3
NS 32
DS 0
SWH 16025.641 Hz
FIDRES 0.489064 Hz
AQ 1.0224116 sec
RG 64
DM 31.200 usec
DE 4.50 usec
TE 300.0 K
D1 2.50000000 sec

===== CHANNEL f1 =====
NUC1 1H
P1 10.00 usec
PL1 -6.00 dB
SF01 400.1279993 MHz

F2 - Processing parameters
SI 16384
SF 400.1300154 MHz
WDW EM
SSB 0
LB 0.00 Hz
GB 0
PC 1.00

1D NMR plot parameters
CX 20.00 cm
F1P 9.000 ppm
F4 3601.17 Hz
F2P 0.000 ppm
F2 0.00 Hz
PPMCM 0.45000 ppm/cm
HZCM 180.05848 Hz/cm

```

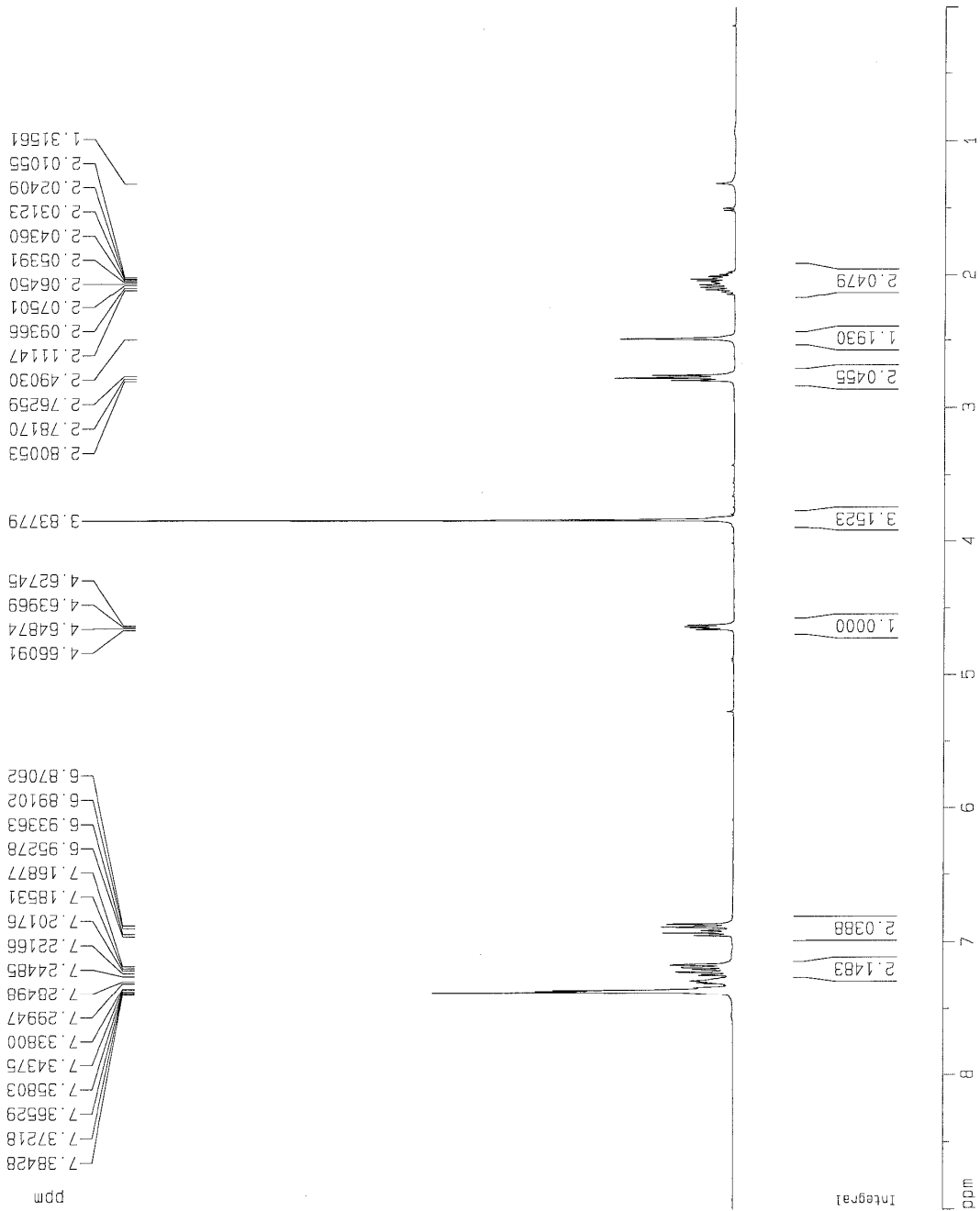


Figure 4.1 ^1H NMR spectrum of 3-(2-methoxyphenyl)-1-phenylpropan-1-ol

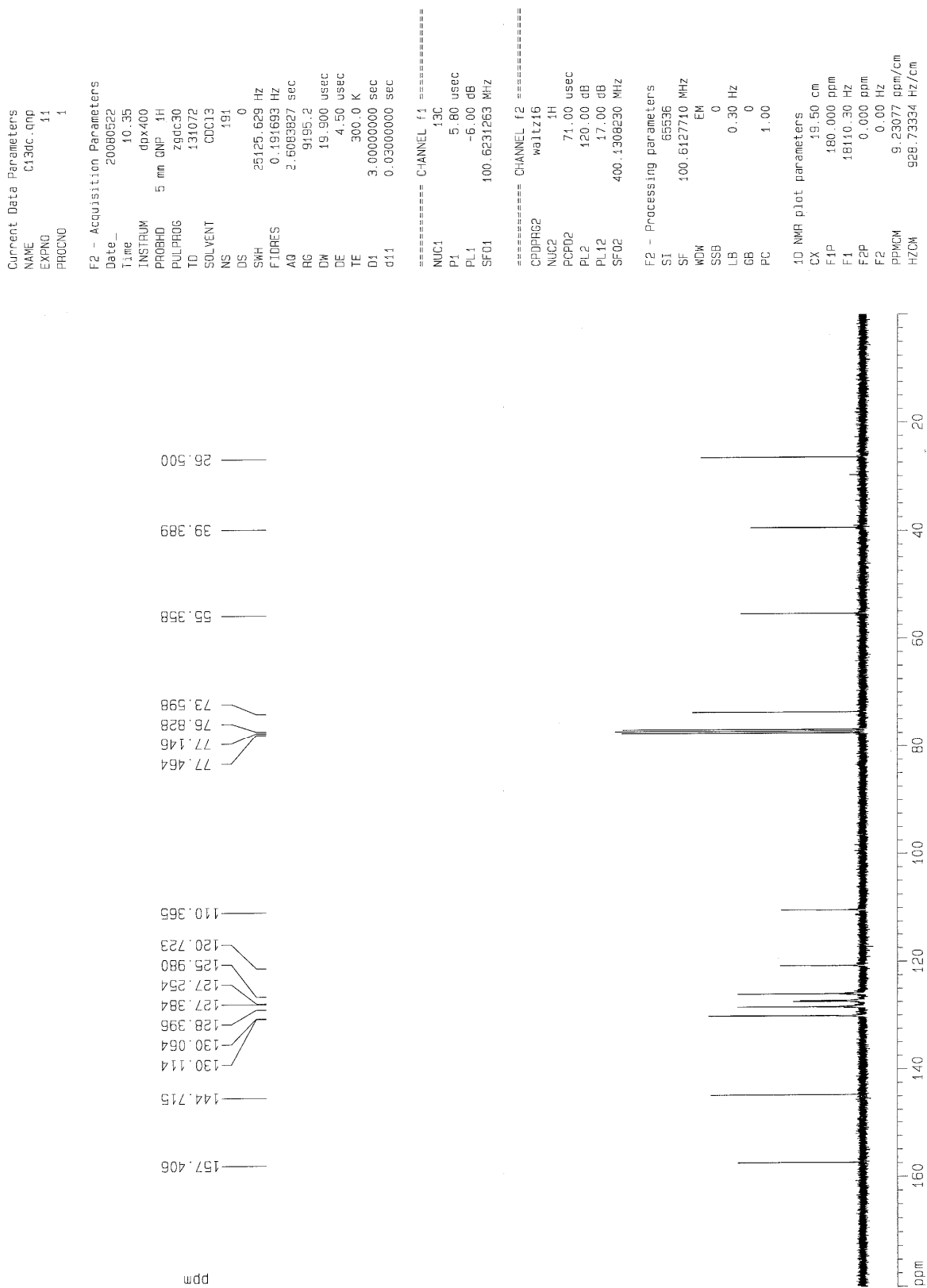


Figure 4.2 ^{13}C NMR spectrum of 3-(2-methoxyphenyl)-1-phenylpropan-1-ol

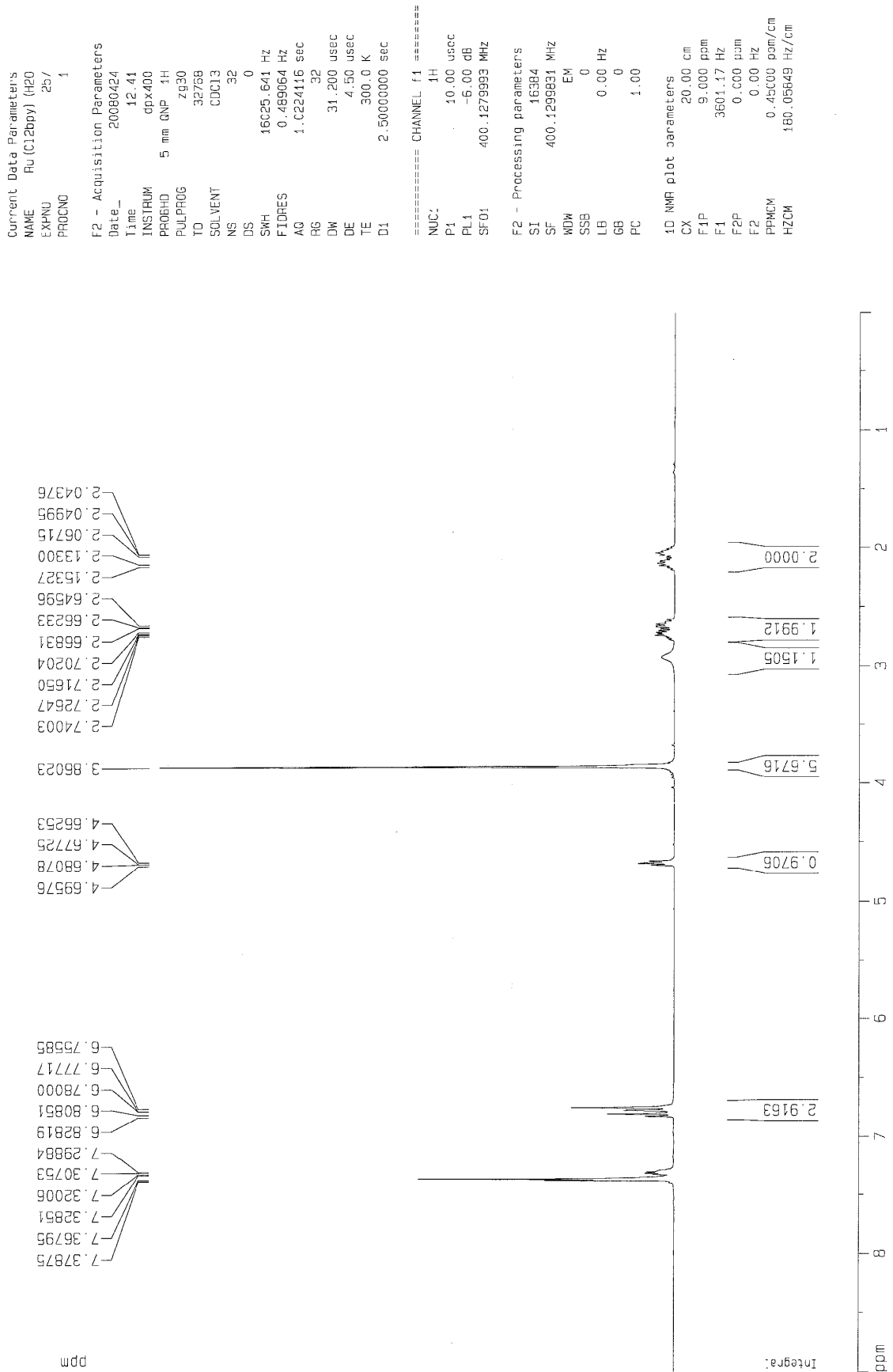


Figure 4.3 ^1H NMR spectrum of 3-(3,4-dimethoxyphenyl)-1-phenylpropan-1-ol

Current Data Parameters
 NAME C13dc.cnp
 EXPNO 8
 PROCNO 1

F2 - Acquisition Parameters

Date_ 20080424
 Time 12.47
 INSTRUM dpx400
 PROBHD 5 mm GNP 1H
 PULPROG zgpg30
 TD 131072
 SOLVENT CDCl3
 NS 159
 DS 0
 SWH 25125.629 Hz
 FIDRES 0.191693 Hz
 AQ 2.6083827 sec
 RG 9195.2
 DW 19.900 usec
 DE 4.50 usec
 TE 300.0 K
 D1 3.0000000 sec
 d11 0.0300000 sec

===== CHANNEL f1 =====
 NUC1 13C
 P1 5.80 usec
 PL1 -6.00 dB
 SF01 100.6231263 MHz

===== CHANNEL f2 =====
 CPDPRG2 waltz16
 NUC2 1H
 PCPD2 71.00 usec
 PL2 120.00 dB
 PL12 17.00 dB
 SF02 400.1308230 MHz

F2 - Processing parameters
 SI 65536
 SF 100.6127710 MHz
 WDW EM
 SSB 0
 LB 0.30 Hz
 GB 0
 PC 1.00

1D NMR plot parameters
 CX 19.50 cm
 F1P 180.000 ppm
 F1 18110.30 Hz
 F2P 0.000 ppm
 F2 0.00 Hz
 PPMCM 9.23077 ppm/cm
 HZCM 928.73334 Hz/cm

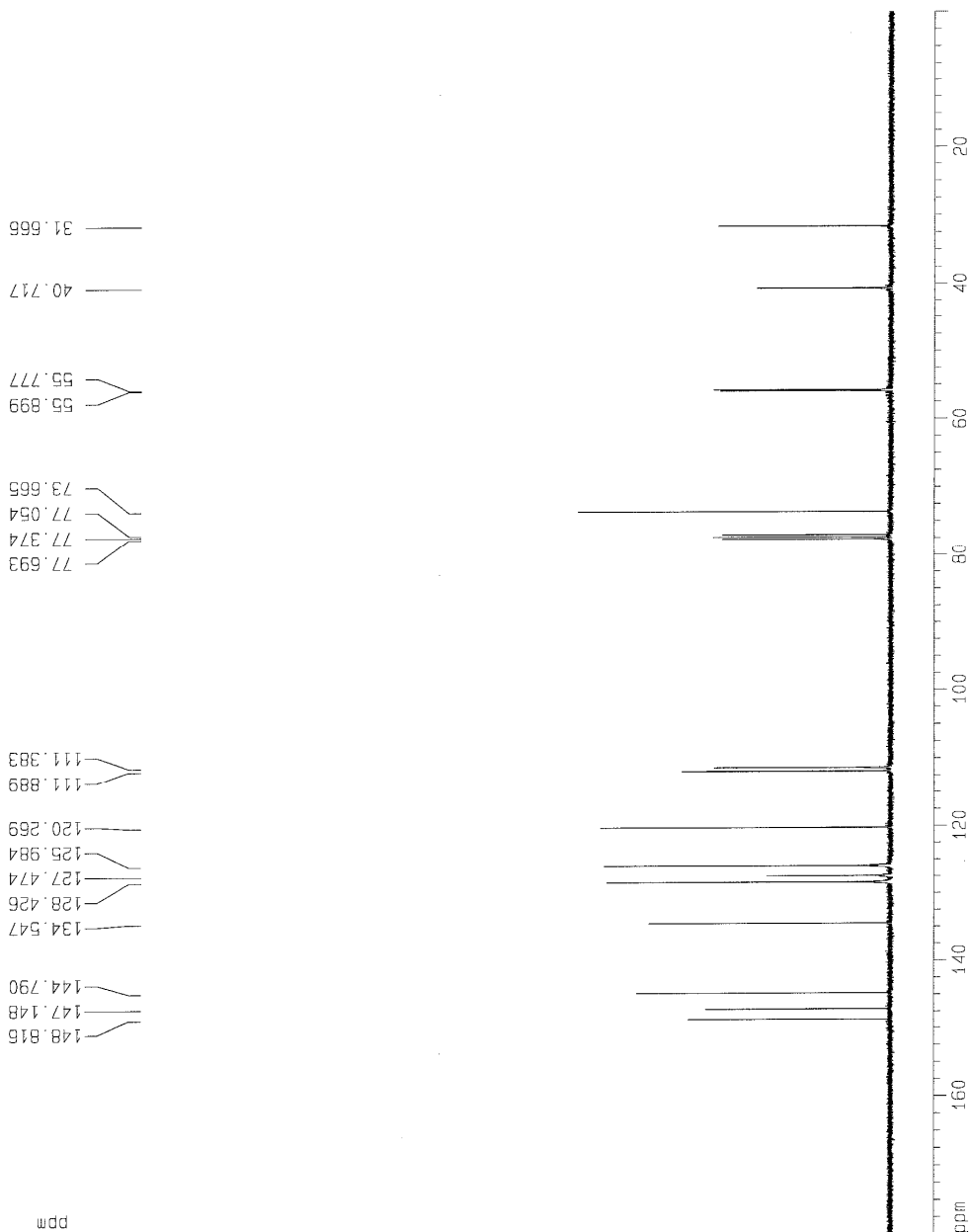


Figure 4.4 ^{13}C NMR spectrum of 3-(3,4-dimethoxyphenyl)-1-phenylpropan-1-ol

```

Current Data Parameters
NAME R1 (G12bp) (420
EXPNO 269
PROCNO 1

F2 - Acquisition Parameters
Date_ 20080502
Time 16:30
INSTRUM cpw400
PROBHD 5 mm QNP 1H
PULPROG zg30
TD 32768
SOLVENT CDCl3
NS 32
DS 0
SWH 16025.641 Hz
FIDRES 0.489064 Hz
AQ 1.0224116 sec
RG 32
DW 31.200 usec
DE 4.50 usec
TE 300.0 K
D1 2.50000000 sec

===== CHANNEL f1 =====
NUC1 1H
P1 10.00 usec
PL1 -6.00 dB
SF01 400.1279993 MHz

F2 - Processing parameters
SI 16384
SF 400.1300242 MHz
WDW EM
SSB 0
LB 0.00 Hz
GB 0
PC 1.00

1D NMR plot parameters
CX 20.00 cm
F1P 9.000 ppm
F1 3601.17 Hz
F2P 0.000 ppm
F2 0.00 Hz
PPMCM 0.45000 ppm/cm
HZCM 180.05650 Hz/cm

```

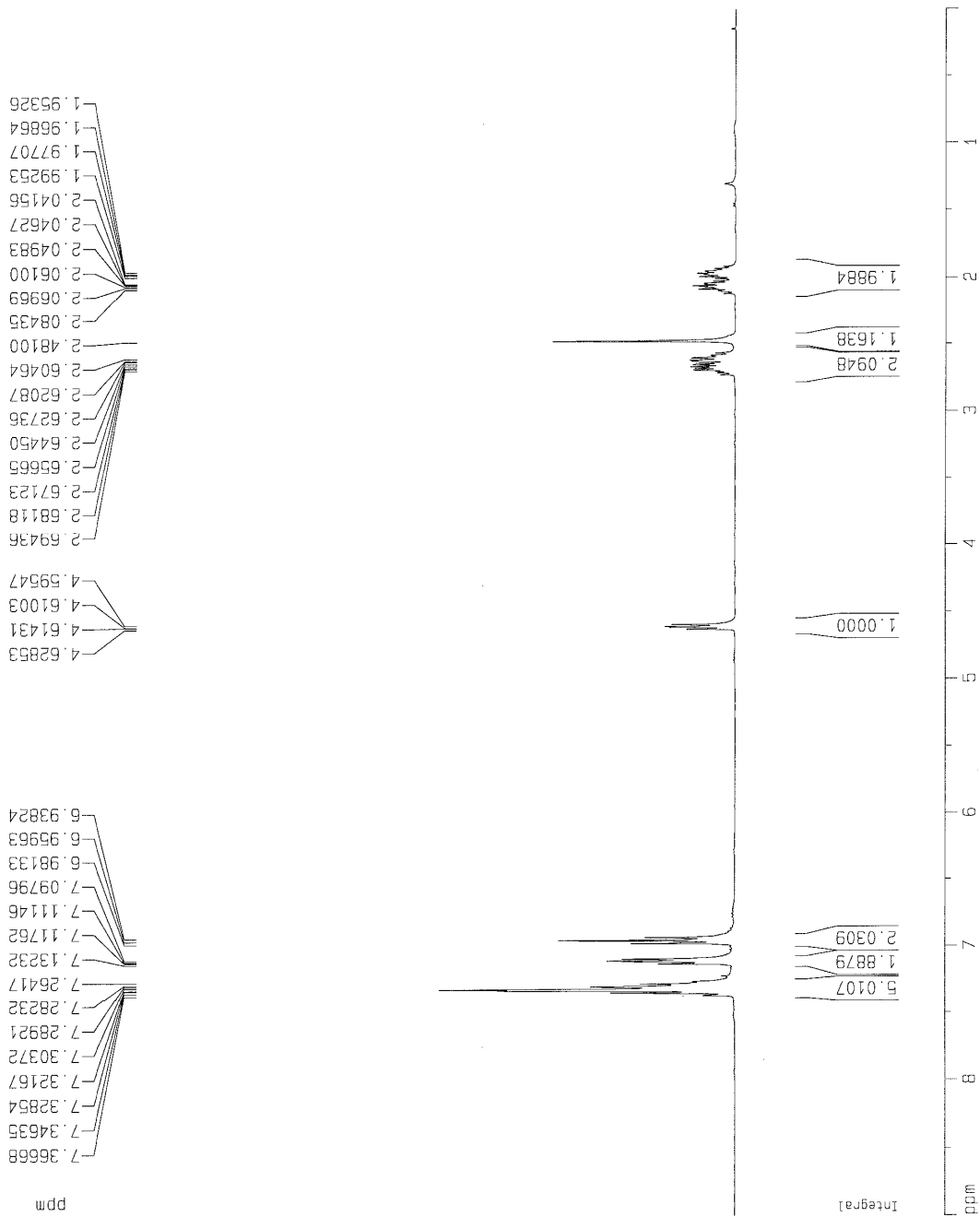


Figure 4.5 ^1H NMR spectrum of 3-(4-fluorophenyl)-1-phenylpropan-1-ol

Current Data Parameters
 NAME C13dc.qnp
 EXPNO 10
 PROCNO 1

F2 - Acquisition Parameters

Date_ 20080502
 Time 16.38
 INSTRUM dpx400
 PROBH0 5 mm QNP 1H
 PULPROG zgpg30
 TD 131072
 SOLVENT CDCl3
 NS 151
 DS 0
 SWH 25125.629 Hz
 FIDRES 0.191693 Hz
 AQ 2.6083827 sec
 RG 9195.2
 DW 19.900 usec
 DE 4.50 usec
 TE 300.0 K
 D1 3.0000000 sec
 d11 0.0300000 sec

===== CHANNEL f1 =====
 NUC1 13C
 P1 5.80 usec
 PL1 -6.00 dB
 SF01 100.6231263 MHz

===== CHANNEL f2 =====
 CPDPRG2 waltz16
 NUC2 1H
 PCPD2 71.00 usec
 PL2 120.00 dB
 PL12 17.00 dB
 SF02 400.1308230 MHz

F2 - Processing parameters
 SI 65536
 SF 100.6127710 MHz
 WDW EM
 SSB 0
 LB 0.30 Hz
 GB 0
 PC 1.00

1D NMR plot parameters
 CX 19.50 cm
 F1P 180.000 ppm
 F1 18110.30 Hz
 F2P 0.000 ppm
 F2 0.00 Hz
 PPMCM 9.23077 ppm/cm
 HZCM 928.73334 Hz/cm

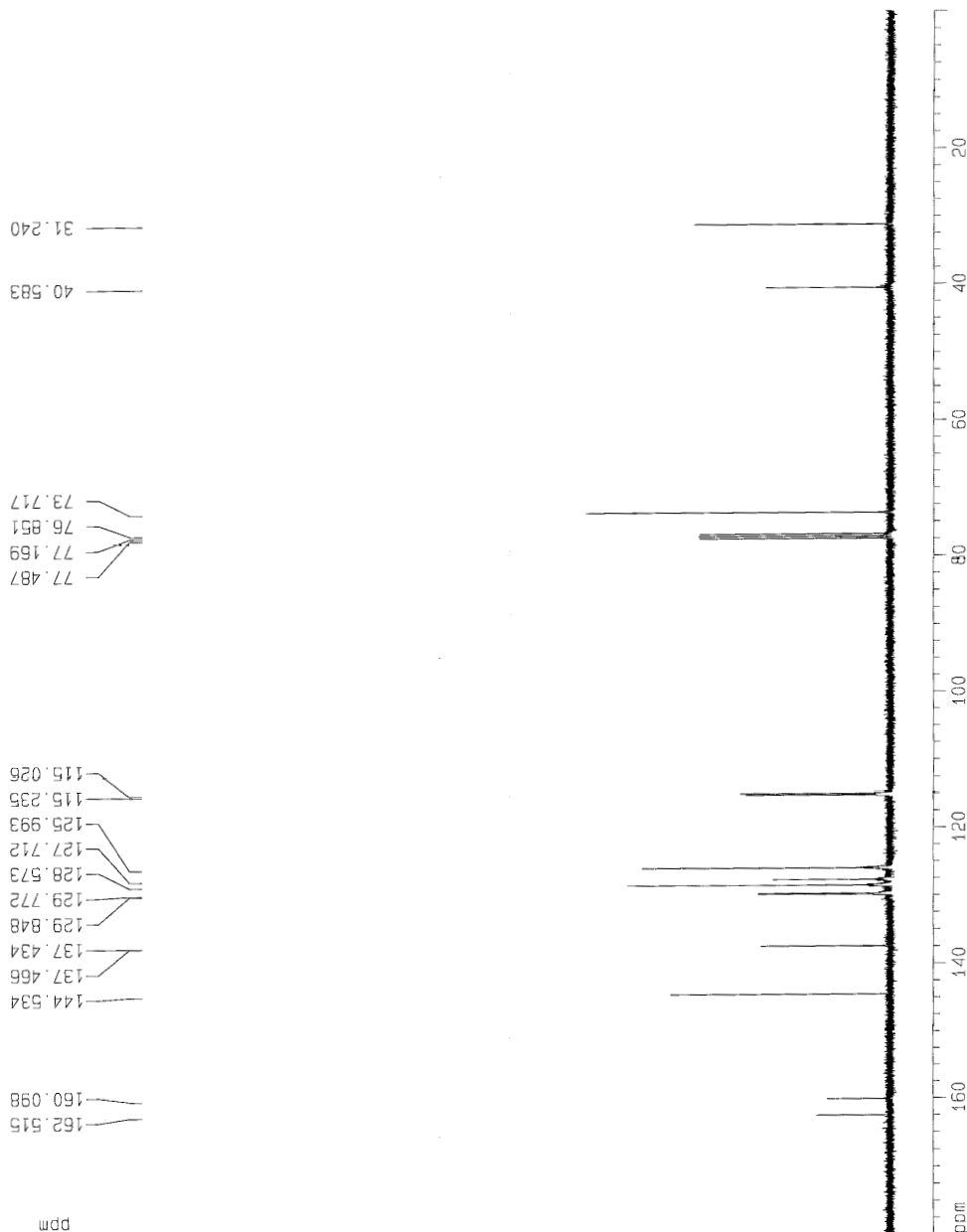


Figure 4.6 ¹³C NMR spectrum of 3-(4-fluorophenyl)-1-phenylpropan-1-ol

```

Current Data Parameters
NAME Ru (Cl2bpv) (H2O
EXPNO 280
PROCNO 1

F2 - Acquisition Parameters
Date_ 20080522
Time 9.28
INSTRUM dpx400
PROBHD 5 mm QNP 1H
PULPROG zg30
TD 32768
SOLVENT CDCl3
NS 32
DS 0
SWH 15025.541 Hz
FIDRES 0.489064 Hz
AQ 1.0224116 sec
RG 128
DM 31.200 usec
DE 4.50 usec
TE 300.0 K
D1 2.50000000 sec

===== CHANNEL f1 =====
NUC1 1H
P1 10.00 usec
PL1 -6.00 dB
SFO1 400.1279993 MHz

F2 - Processing parameters
SI 16384
SH 400.1300105 MHz
WDW EM
SSB 0
LB 0.00 Hz
GB 0
PC 1.00

1D NMR plot parameters
CX 20.00 cm
F1P 10.000 ppm
F1 4001.30 Hz
F2P 0.000 ppm
F2 0.00 Hz
PPMCM 0.50000 ppm/cm
HZCM 200.00000 Hz/cm

```

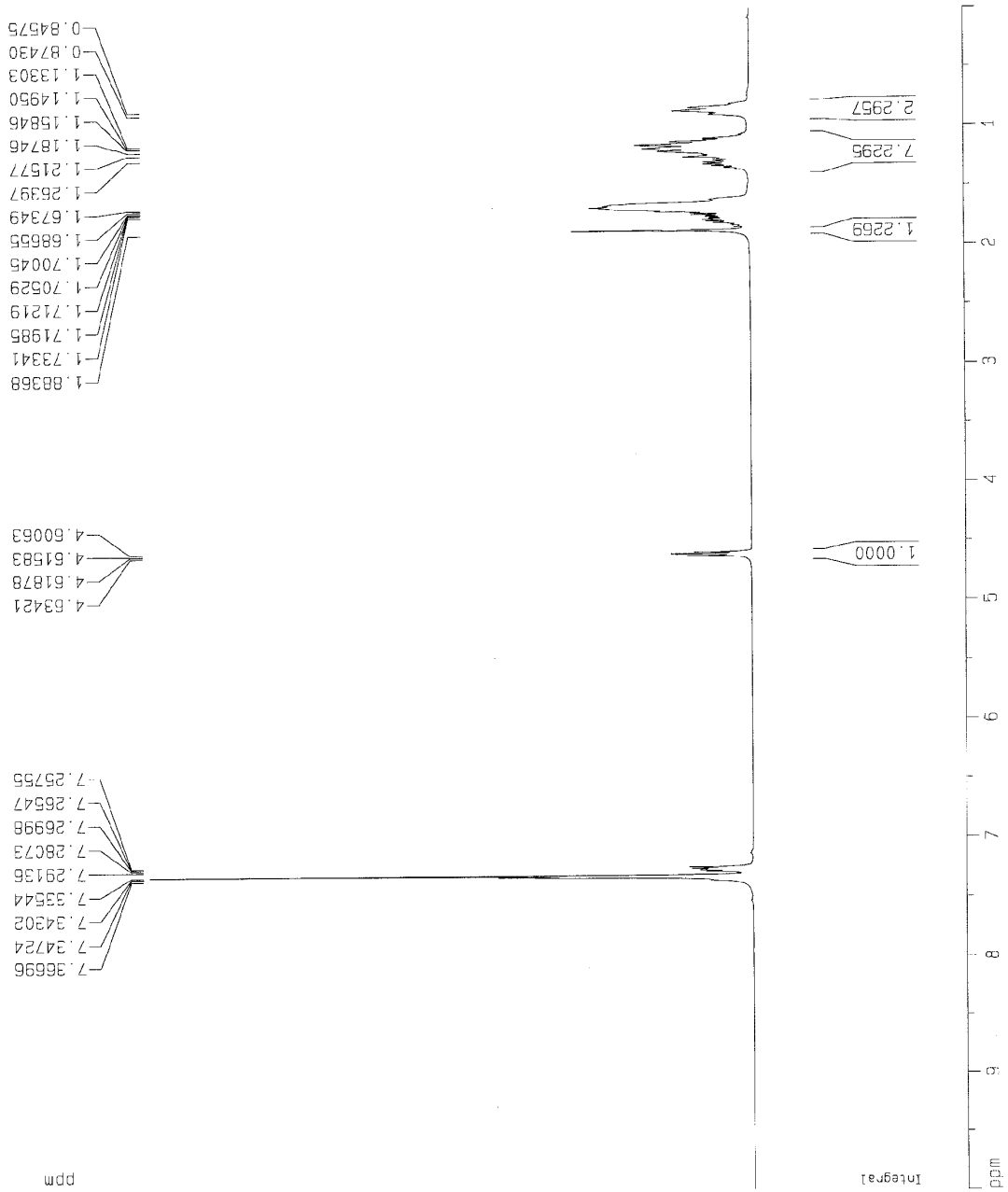


Figure 4.7 ^1H NMR spectrum of 1-cyclohexyl-1-phenylpropan-1-ol

Current Data Parameters
 NAME Cunknow
 EXPNO 49
 PROCNO 1

F2 - Acquisition Parameters
 Date_ 20080523
 Time 21.24
 INSTRUM dpx400
 PROBHD 5 mm QNP 4H
 PULPROG zgpg30
 TD 131072
 SOLVENT CDCl3
 NS 14876
 DS 0
 SWH 40404.039 Hz
 FIDRES 0.308258 Hz
 AQ 1.6220560 sec
 RG 7298.2
 UW 12.375 usec
 DE 4.50 usec
 TE 300.0 K
 D1 2.00000000 sec
 d11 0.03000000 sec

===== CHANNEL f1 =====
 NUC1 13C
 P1 5.80 usec
 PL1 -6.00 dB
 SFO1 100.6328515 MHz

===== CHANNEL f2 =====
 CPDPRG2 waltz16
 NUC2 1H
 PCPD2 71.00 usec
 PL2 120.00 dB
 PL12 17.00 dB
 SFO2 400.1506230 MHz

F2 - Processing parameters
 SI 65536
 SF 100.6127067 MHz
 WDM EM
 SSF 3
 LB 0.30 Hz
 GB 0
 PC 1.00

1D NMR plot parameters
 CX 20.00 cm
 FJP 180.000 ppm
 F1 18110.29 Hz
 F2 0.000 ppm
 F2 0.00 Hz
 PPMCM 9.00000 ppm/cm
 HZCM 905.51440 Hz/cm

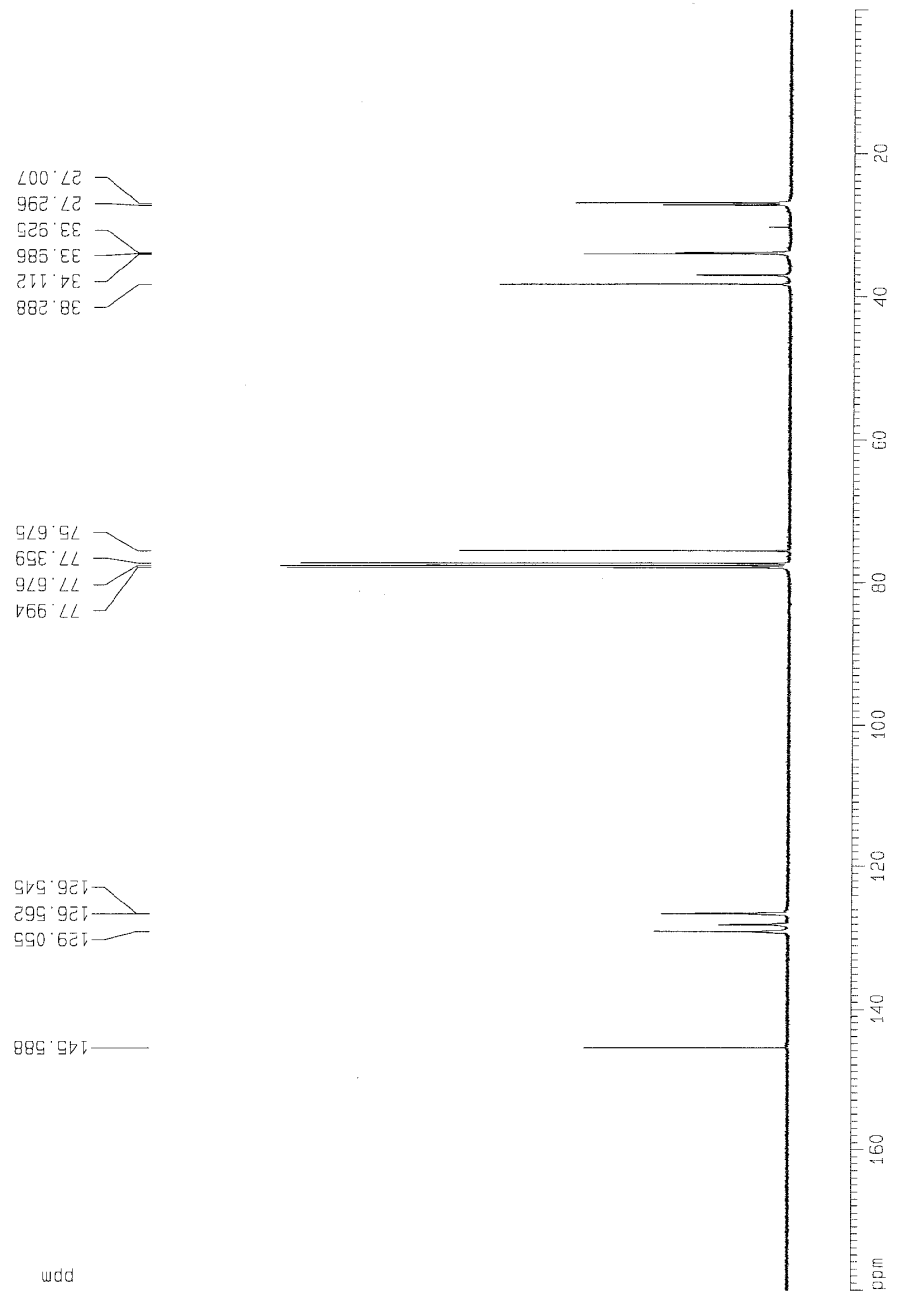


Figure 4.8 ¹³C NMR spectrum of 1-cyclohexyl-1-phenylpropan-1-ol


```

Current Data Parameters
NAME      Ru (C12bpv) (H2O)
EXPNO    197
PROCNO   1

F2 - Acquisition Parameters
Date_    20080313
Time     15:54
INSTRUM  ddx400
PROBHD   5 mm QNP 1H
PULPROG  zg30
TD        32768
SOLVENT  CDCl3
NS        32
DS        0
SWH       16025.641 Hz
FIDRES    0.489064 Hz
AQ        1.0224116 sec
RG         64
DW         31.200 usec
DE         4.50 usec
TE        300.0 K
TE        2.50000000 sec

===== CHANNEL f1 =====
NUC1      1H
P1        10.00 usec
PL1       -6.00 dB
SF01     400.1279993 MHz

F2 - Processing parameters
SI         16384
SF         400.1300232 MHz
WDW        EM
SSB        0
LB         0.00 Hz
GB         0
PC         1.00

1D NMR p1.c: parameters
CX         20.00 cm
F1P        9.000 ppm
F1         3601.17 Hz
F2P        0.000 ppm
F2         0.00 Hz
PPM0M      0.45000 ppm/cm
HZCM       180.05860 Hz/cm

```

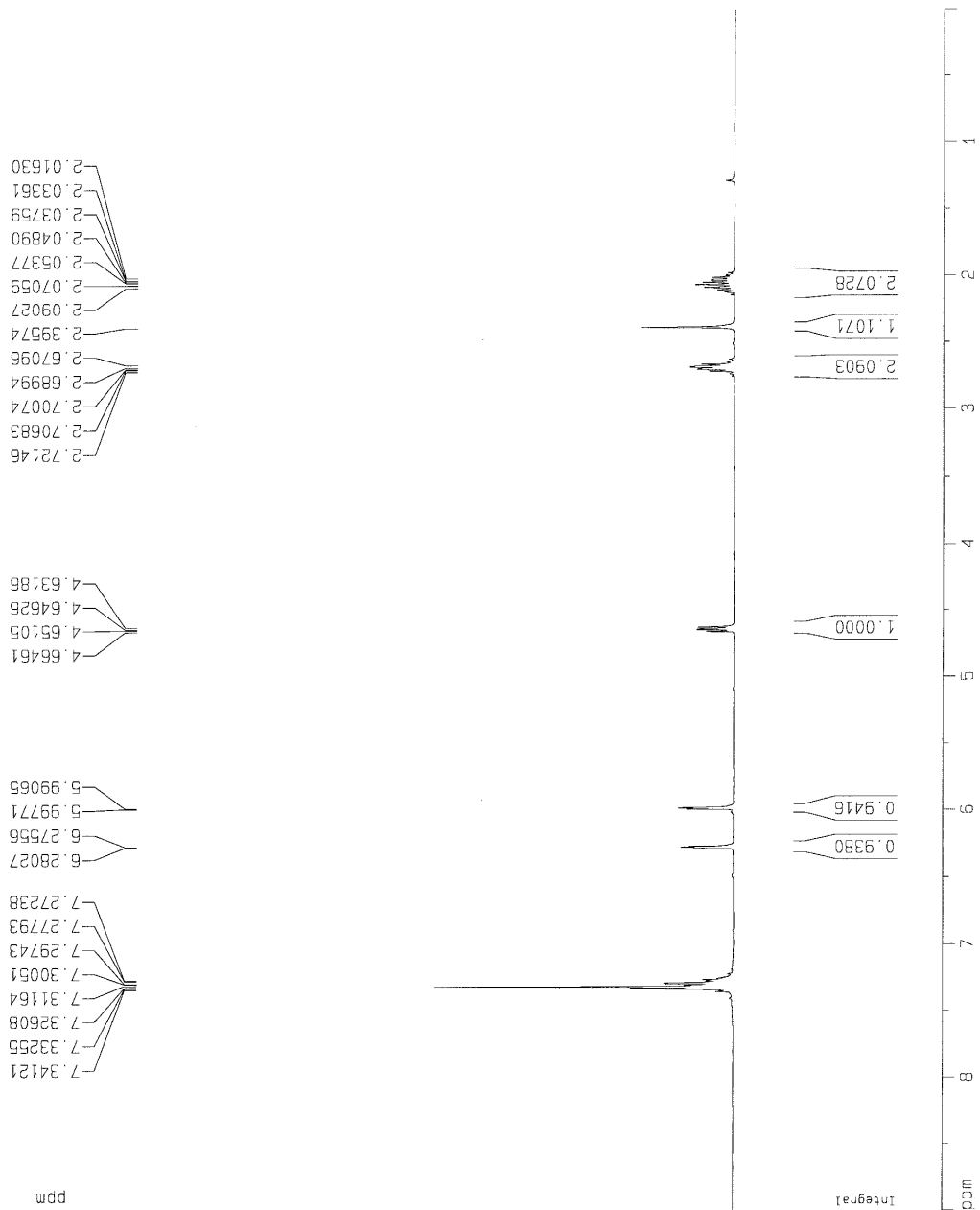


Figure 4.9 ^1H NMR spectrum of 3-(furan-2-yl)-1-phenylpropan-1-ol

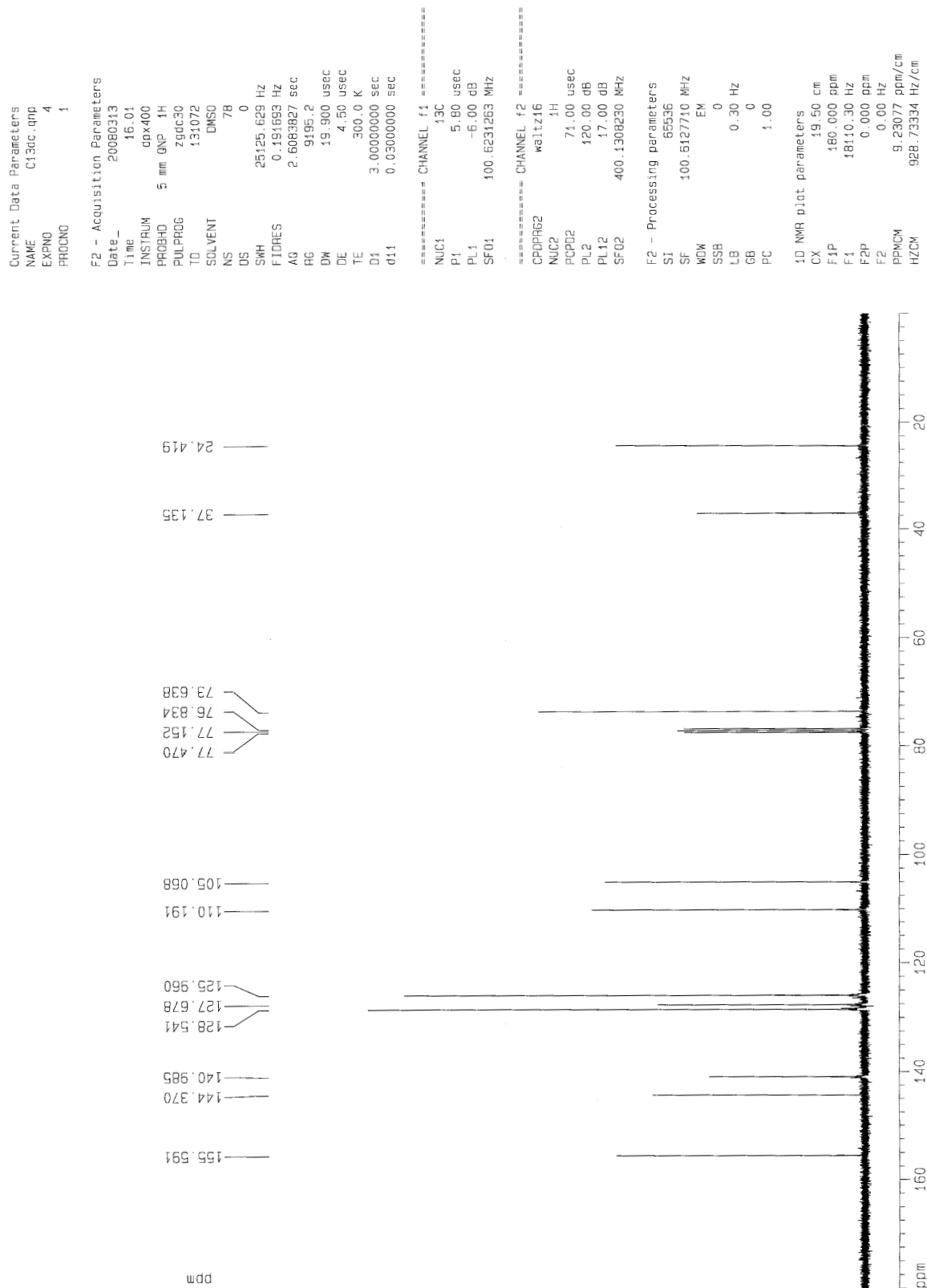


Figure 4.10 ^{13}C NMR spectrum of 3-(furan-2-yl)-1-phenylpropan-1-ol

```

Current Data Parameters
NAME Ru (12bpv) (H2O)
EXPNO 259
PROCNO 1

F2 - Acquisition Parameters
Date_ 20080429
Time 15.32
INSTRUM dx400
PROBHD 5 mm QNP 1H
PULPROG zg30
TD 32768
SOLVENT CDCl3
NS 32
DS 0
SWH 16025.641 Hz
FIDRES 0.483064 Hz
AQ 1.0224116 sec
RG 32
DM 31.200 usec
DE 4.50 usec
TE 300.0 K
D1 2.5000000 sec

===== CHANNEL f1 =====
NUC1 1H
P1 10.00 usec
PL1 -6.00 dB
SFO1 400.1278993 MHz

F2 - Processing parameters
SI 16384
SF 400.1300095 MHz
WDW EM
SSB 0
LB 0.00 Hz
GB 0
PC 1.00

1D NMR plot parameters
CX 20.00 cm
F1P 9.000 ppm
F1 3601.17 Hz
F2P 0.000 ppm
F2 0.00 Hz
PPMCM 0.75000 ppm/cm
HZCM 180.05849 Hz/cm

```

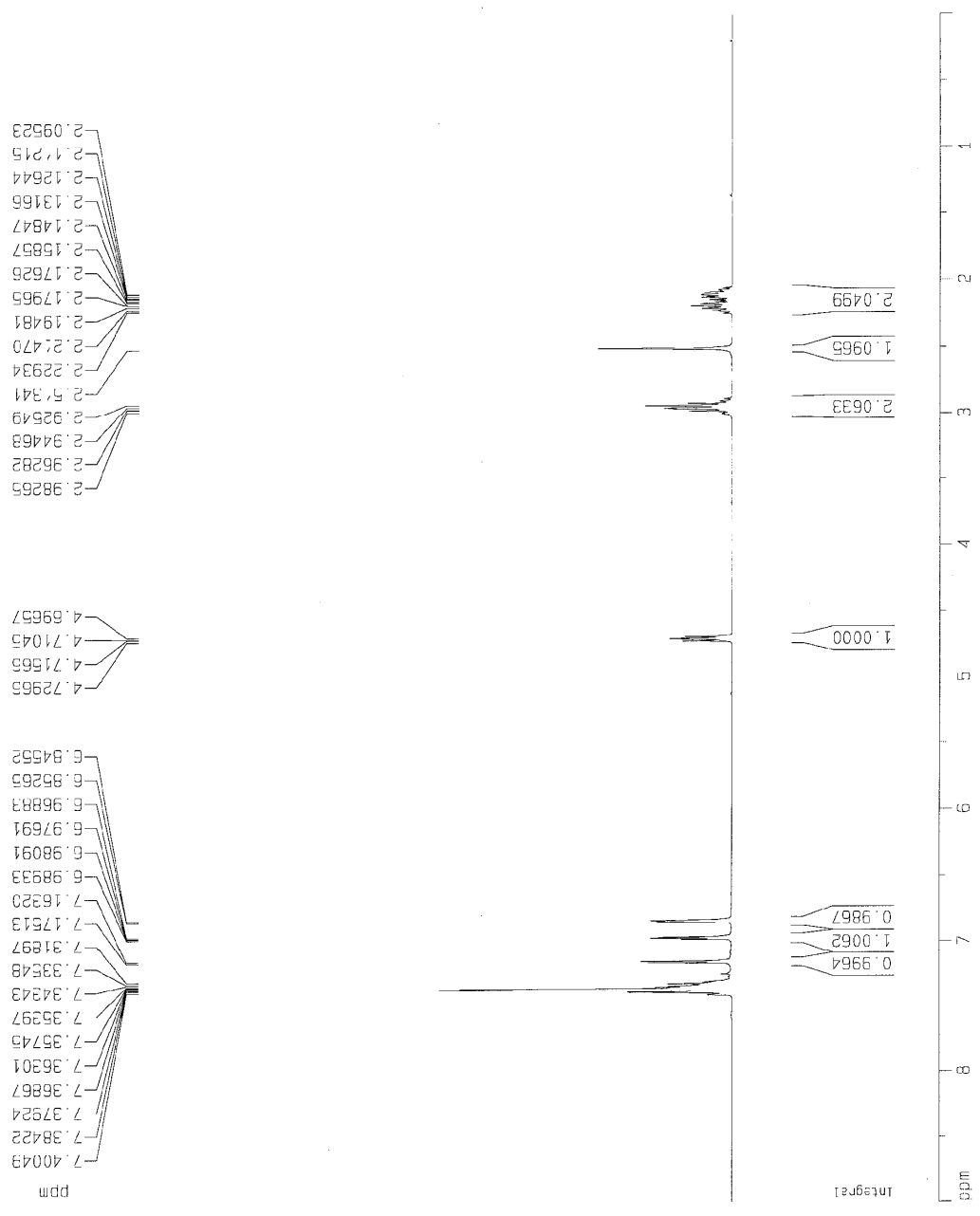


Figure 4.11 ¹H NMR spectrum of 1-phenyl-(3-thiophen-2-yl)-propan-1-ol

Current Data Parameters
 NAME C13dc.gnp
 FXPNG 9
 PROCNO 1

F2 - Acquisition Parameters

Date_ 20080425
 Time 15:37
 INSTRUM cp400
 PROBHD 5 mm GNP 1H
 PULPROG zgdc30
 TD 131072
 SOLVENT CDCl3
 NS 104
 DS 0
 SWH 25125.629 Hz
 FIDRES 0.191693 Hz
 AQ 2.6083827 sec
 TG 9195.2
 DW 19.900 usec
 DE 4.50 usec
 TE 300.0 K
 D1 3.00000000 sec
 d11 0.03000000 sec

==== CHANNEL f1 =====
 NUC1 13C
 P1 5.80 usec
 PL1 -6.00 dB
 SF01 100.6231263 MHz

==== CHANNEL f2 =====
 CPDPRG2 waltz16
 NUC2 1H
 PCPD2 71.00 usec
 PL2 120.00 dB
 PL12 17.00 dB
 SF02 400.1308230 MHz

F2 - Processing parameters
 SI 65536
 SF 100.6127710 MHz
 WDW EM
 SSB 0
 LB 0.30 Hz
 GB 0
 PC 1.00

1D NMR plot parameters
 CX 19.50 cm
 F1P 160.000 ppm
 F1 16098.04 Hz
 F2P 0.000 ppm
 F2 0.00 Hz
 PPMCM 8.20513 ppm/cm
 HZCM 825.54065 Hz/cm

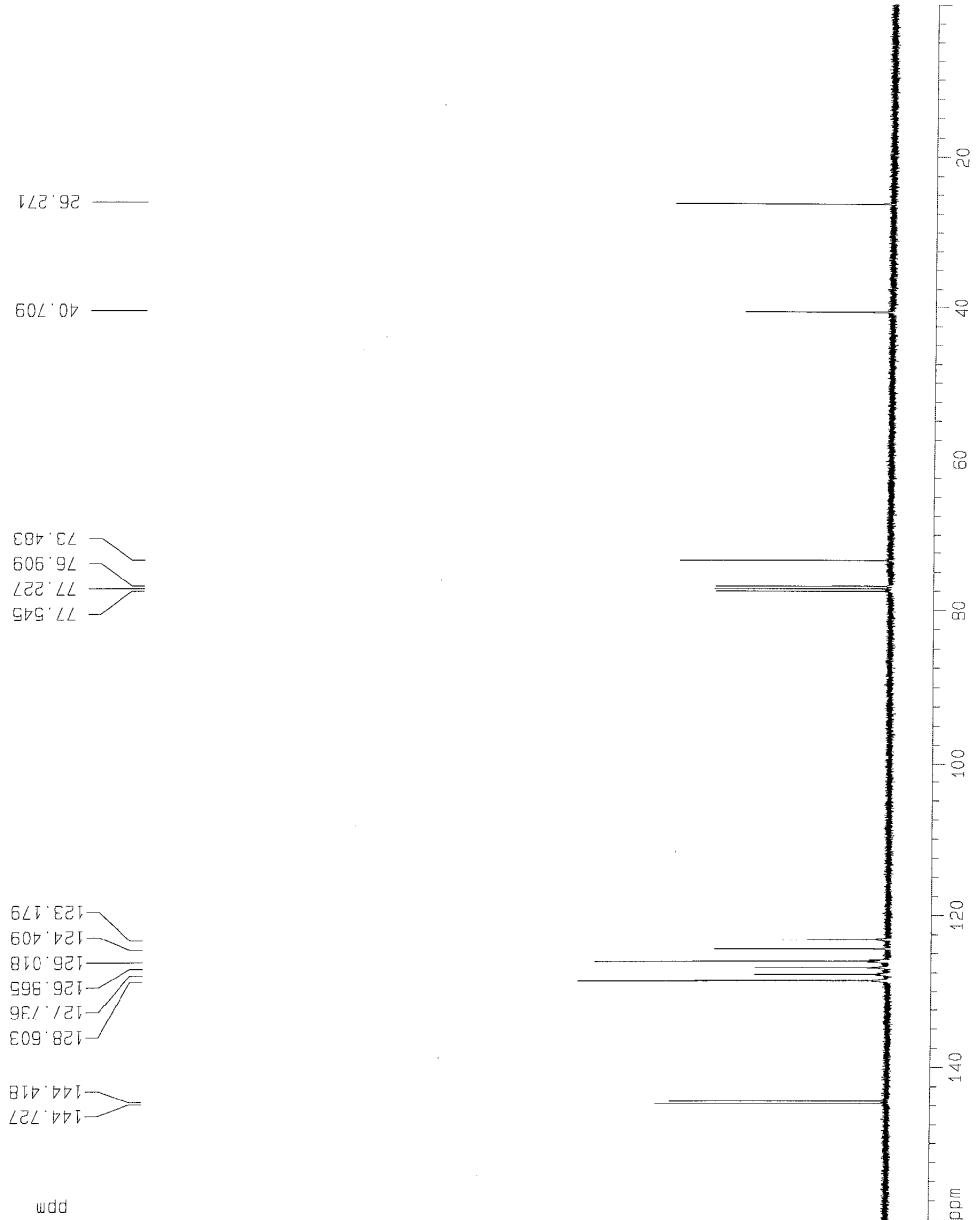


Figure 4.12 ¹³C NMR spectrum of 1-phenyl-(3-thiophen-2-yl)-propan-1-ol

References

1. G. J. Kubas, *Metal-Dihydrogen and σ -Bond Complexes: Structure, Bonding, and Reactivity*, Kluwer Academic/Plenum Publishers, New York, 2001.
2. McGrady, G. S.; Guilera, G., The multifarious world of transition metal hydrides. *Chemical Society Reviews* **2003**, 32, 383-392.
3. Kubas, G. J.; Ryan, R. R.; Swanson, B. I.; Vergamini, P. J.; Wasserman, H. J., Characterization of the 1st Examples of Isolable Molecular-Hydrogen Complexes, $\text{Mo}(\text{CO})_3(\text{PCy}_3)_2(\text{H}_2)$, $\text{W}(\text{CO})_3(\text{PCy}_3)_2(\text{H}_2)$, $\text{Mo}(\text{CO})_3(\text{P}^i\text{-Pr}_3)_2(\text{H}_2)$, $\text{W}(\text{CO})_3(\text{P}^i\text{-Pr}_3)_2(\text{H}_2)$ - Evidence for a Side-on Bonded η^{-2} Ligand. *Journal of the American Chemical Society* **1984**, 106, 451-452.
4. Kubas, G. J., Molecular-Hydrogen Complexes - Coordination of a Sigma-Bond to Transition-Metals. *Accounts of Chemical Research* **1988**, 21, 120-128.
5. Corey, J. Y.; Braddock-Wilking, J., Reactions of hydrosilanes with transition-metal complexes: Formation of stable transition-metal silyl

- compounds. *Chemical Reviews* **1999**, 99, 175-292.
6. Kubas, G. J., Metal-dihydrogen and sigma-bond coordination: the consummate extension of the Dewar-Chatt-Duncanson model for metal-olefin bonding. *Journal of Organometallic Chemistry* **2001**, 635, 37-68.
 7. Bader, R. F. W.; Matta, C. F.; Cortés-Guzmán, F., Where To Draw the Line in Defining a Molecular Structure. *Organometallics* **2004**, 23, 6253-6263.
 8. Lachaize, S.; Sabo-Etienne, S., Sigma-silane ruthenium complexes: The crucial role of secondary interactions. *European Journal of Inorganic Chemistry* **2006**, 2115-2127.
 9. Nikonov, G. I., Going beyond sigma complexation: Nonclassical interligand interactions of silyl groups with two and more hydrides. *Angewandte Chemie-International Edition* **2001**, 40, 3353-3355.
 10. Nikonov, G. I., New types of non-classical interligand interactions involving silicon based ligands. *Journal of Organometallic Chemistry* **2001**, 635, 24-36.

11. Koloski, T. S.; Pestana, D. C.; Carroll, P. J.; Berry, D. H., Monobis(Silyl) and Bis(Silyl) Complexes of Molybdenum and Tungsten - Synthesis, Structures, and Si-29 NMR Trends. *Organometallics* **1994**, 13, 489-499.
12. Luo, X. L.; Baudry, D.; Boydell, P.; Charpin, P.; Nierlich, M.; Ephritikhine, M.; Crabtree, R. H., Reaction of $\text{ReH}_7(\text{PPh}_3)_2$ with Silanes - Preparation and Characterization of the 1st Silyl Polyhydride Complexes, $\text{ReH}_6(\text{SiPh}_3)(\text{PPh}_3)_2$, $\text{ReH}_6(\text{SiEt}_3)(\text{PPh}_3)_2$, $\text{ReH}_6(\text{SiHEt}_2)(\text{PPh}_3)_2$. *Inorganic Chemistry* **1990**, 29, 1511-1517.
13. Luo, X. L.; Schulte, G. K.; Demou, P.; Crabtree, R. H., Unusual Stereochemical Rigidity in 7-Coordination - Synthesis and Structural Characterization of $\text{ReH}_2(\text{SiPh}_3)(\text{CO})(\text{PMe}_2\text{Ph})_3$, $\text{ReH}_2(\text{SiPh}_3)(\text{CO})(\text{PMe}_2\text{Ph})_3$. *Inorganic Chemistry* **1990**, 29, 4268-4273.
14. Hussein, K.; Marsden, C. J.; Barthelat, J. C.; Rodriguez, V.; Conejero, S.; Sabo-Etienne, S.; Donnadieu, B.; Chaudret, B., X-ray structure and theoretical studies of $\text{RuH}_2(\eta^2\text{-H}_2)(\eta^2\text{-HSiPh}_3)(\text{PCy}_3)_2$, a complex with two different η^2 -coordinated sigma bonds. *Chemical Communications* **1999**, 1315-1316.

15. Gutsulyak, D. V.; Kuzmina, L. G.; Howard, J. A. K.; Vyboishchikov, S. F.; Nikonov, G. I., Cp(ⁱPr₂MeP)FeH₂SiR₃: Nonclassical iron silyl dihydride. *Journal of the American Chemical Society* **2008**, *130*, 3732-3733.
16. Kubas, G. J., Catalytic processes involving dihydrogen complexes and other sigma-bond complexes. *Catalysis Letters* **2005**, *104*, 79-101.
17. Luo, X. L.; Crabtree, R. H., Homogeneous Catalysis of Silane Alcoholysis Via Nucleophilic-Attack by the Alcohol on an Ir(η^2 -HSiR₃) Intermediate Catalyzed by [IrH₂S₂(PPh₃)₂]SbF₆ (S=Solvent). *Journal of the American Chemical Society* **1989**, *111*, 2527-2535.
18. Chang, S.; Scharrer, E.; Brookhart, M., Catalytic silane alcoholysis based on the C₅H₅(CO)(PPh₃)Fe⁺ moiety. NMR spectroscopic identification of key intermediates. *Journal of Molecular Catalysis a-Chemical* **1998**, *130*, 107-119.
19. Buhl, M.; Mauschick, F. T., Density functional study of catalytic silane alcoholysis at a [Fe(Cp)(CO)(PR₃)]⁺ center. *Organometallics* **2003**, *22*, 1422-1431.

20. Fang, X. G.; Huhmann-Vincent, J.; Scott, B. L.; Kubas, G. J., H₂ binding to and silane alcoholysis on an electrophilic Mn(I) fragment with tied-back phosphite ligands. X-ray structure of a Mn-CH₂Cl₂ complex. *Journal of Organometallic Chemistry* **2000**, 609, 95-103.
21. Christ, M. L.; Saboetienne, S.; Chaudret, B., Highly Selective Dehydrogenative Silylation of Ethylene Using the Bis(Dihydrogen) Complex RuH₂(H₂)₂(PCy₃)₂ as Catalyst Precursor. *Organometallics* **1995**, 14, 1082-1084.
22. Lachaize, S.; Sabo-Etienne, S.; Donnadieu, B.; Chaudret, B., Mechanistic studies on ethylene silylation with chlorosilanes catalysed by ruthenium complexes. *Chemical Communications* **2003**, 214-215.
23. Yang, J.; Brookhart, M., Iridium-catalyzed reduction of alkyl halides by triethylsilane. *Journal of the American Chemical Society* **2007**, 129, 12656-12657.
24. Yang, J.; White, P. S.; Brookhart, M., Scope and Mechanism of the Iridium-Catalyzed Cleavage of Alkyl Ethers with Triethylsilane. *Journal of the*

American Chemical Society **2008**, 130, 17509-17518.

25. Gutsulyak, D. V.; Vyboishchikov, S. F.; Nikonov, G. I., Cationic Silane sigma-Complexes of Ruthenium with Relevance to Catalysis. *Journal of the American Chemical Society* **2010**, 132, 5950-5951.
26. I. Ojima, Z. Li, J. Zhu in *The Chemistry of Organic Silicon Compounds* (Eds.: S. Rappoport, Y. Apeloig), Wiley, New York, **1998**, Chap. 29.
27. E. W. Colvin, *Silicon Reagents in Organic Synthesis*, Academic Press, London, **1988**, p. 7.
28. Chandrasekhar, V.; Boomishankar, R.; Nagendran, S., Recent developments in the synthesis and structure of organosilanols. *Chemical Reviews* **2004**, 104, 5847-5910.
29. P. D. Lickiss, The Synthesis and Structure of Organosilanols. *Advances in Inorganic Chemistry* **1995**, 42, 147-262.

30. Hirabayashi, K.; Nishihara, Y.; Mori, A.; Hiyama, T., A novel C-C bond forming reaction of aryl- and alkenylsilanols. A halogen-free Mizoroki-Heck type reaction. *Tetrahedron Letters* **1998**, 39, 7893-7896.
31. Hirabayashi, K.; Kawashima, J.; Nishihara, Y.; Mori, A.; Hiyama, T., A new transformation of silanols. Palladium-catalyzed cross-coupling with organic halides in the presence of silver(I) oxide. *Organic Letters* **1999**, 299-301.
32. Denmark, S. E.; Wehrli, D., Highly stereospecific, palladium-catalyzed cross-coupling of alkenylsilanols. *Organic Letters* **2000**, 2, 565-568.
33. Hirabayashi, E.; Mori, A.; Kawashima, J.; Suguro, M.; Nishihara, Y.; Hiyama, T., Palladium-catalyzed cross-coupling of silanols, silanediols, and silanetriols promoted by silver(I) oxide. *Journal of Organic Chemistry* **2000**, 65, 5342-5349.
34. E. G. Rochow; W. F. Gilliam, Polymeric Methyl Silicon Oxides. *Journal of the American Chemical Society* **1941**, 63, 798-800.
35. R. O. Sana, Derivatives of the Methylchlorosilanes. I. Trimethylsilanol and its

Simple Ethers. *Journal of the American Chemical Society* **1944**, 66, 1707-1710.

36. Lickiss, P. D.; Lucas, R., Oxidation of sterically hindered organosilicon hydrides using potassium permanganate. *Journal of Organometallic Chemistry* **1995**, 521, 229-234.
37. Valliant-Saunders, K.; Gunn, E.; Shelton, G. R.; Hrovat, D. A.; Borden, W. T.; Mayer, J. M., Oxidation of tertiary silanes by osmium tetroxide. *Inorganic Chemistry* **2007**, 46, 5212-5219.
38. Adam, W.; Mello, R.; Curci, R., O-Atom insertion into Si-H Bonds by Dioxiranes; A Stereospecific and Direct Conversion of Silanes into Silanols. *Angewandte Chemie International Edition* **1990**, 29, 890-891.
39. Schubert, U.; Lorenz, C., Conversion of hydrosilanes to silanols and silyl esters catalyzed by $[\text{Ph}_3\text{CuH}]_6$ *Inorganic Chemistry* **1997**, 36, 1258-1259.
40. Lee, M.; Ko, S.; Chang, S., Highly selective and practical hydrolytic oxidation of organosilanes to silanols catalyzed by a ruthenium complex. *Journal of the*

American Chemical Society **2000**, 122, 12011-12012.

41. Lee, Y.; Seomoon, D.; Kim, S.; Han, H.; Chang, S.; Lee, P. H., Highly efficient iridium-catalyzed oxidation of organosilanes to silanols. *Journal of Organic Chemistry* **2004**, 69, 1741-1743.
42. Ison, E. A.; Corbin, R. A.; Abu-Omar, M. M., Hydrogen production from hydrolytic oxidation of organosilanes using a cationic oxorhenium catalyst. *Journal of the American Chemical Society* **2005**, 127, 11938-11939.
43. Corbin, R. A.; Ison, E. A.; Abu-Omar, M. M., Catalysis by cationic oxorhenium(v): hydrolysis and alcoholysis of organic silanes. *Dalton Transactions* **2009**, 2850-2855.
44. Mori, K.; Tano, M.; Mizugaki, T.; Ebitani, K.; Kaneda, K., Efficient heterogeneous oxidation of organosilanes to silanols catalysed by a hydroxyapatite-bound Ru complex in the presence of water and molecular oxygen. *New Journal of Chemistry* **2002**, 26, 1536-1538.

45. Choi, E.; Lee, C.; Na, Y.; Chang, S., [RuCl₂(p-cymene)]₂ on carbon: An efficient, selective, reusable, and environmentally versatile heterogeneous catalyst. *Organic Letters* **2002**, 4, 2369-2371.
46. Mitsudome, T.; Arita, S.; Mori, H.; Mizugaki, T.; Jitsukawa, K.; Kaneda, K., Supported silver-nanoparticle-catalyzed highly efficient aqueous oxidation of phenylsilanes to silanols. *Angewandte Chemie-International Edition* **2008**, 47, 7938-7940.
47. Sakakura, T.; Choi, J. C.; Yasuda, H., Transformation of carbon dioxide. *Chemical Reviews* **2007**, 107, 2365-2387.
48. Edited by Aresta, M., Carbon Dioxide as Chemical Feedstock. 2010 Wiley-VCH Verlag GmbH & Co. KGaA, Weinheim.
49. Tsai, J. C.; Nicholas, K. M., Rhodium-Catalyzed Hydrogenation of Carbon-Dioxide to Formic-Acid. *Journal of the American Chemical Society* **1992**, 114, 5117-5124.

50. Lau, C. P.; Chen, Y. Z., Hydrogenation of Carbon-Dioxide to Formic-Acid Using a 6,6'-Dichloro-2,2'-Bipyridine Complex of Ruthenium, Cis-[Ru(6,6'-Cl₂bpy)₂(H₂O)₂](CF₃SO₃)₂. *Journal of Molecular Catalysis a-Chemical* **1995**, 101, 33-36.
51. Yin, C. Q.; Xu, Z. T.; Yang, S. Y.; Ng, S. M.; Wong, K. Y.; Lin, Z. Y.; Lau, C. P., Promoting effect of water in ruthenium-catalyzed hydrogenation of carbon dioxide to formic acid. *Organometallics* **2001**, 20, 1216-1222.
52. Ng, S. M.; Yin, C. Q.; Yeung, C. H.; Chan, T. C.; Lau, C. P., Ruthenium-catalyzed hydrogenation of carbon dioxide to formic acid in alcohols. *European Journal of Inorganic Chemistry* **2004**, 1788-1793.
53. Ezhova, N. N.; Kolesnichenko, N. V.; Bulygin, A. V.; Kremleva, E. V.; Filatova, M. P.; Slivinskii, E. V., The specifics of carbon dioxide hydrogenation to formic acid in the presence of triphenylphosphine rhodium complexes. *Petroleum Chemistry* **2004**, 44, 24-27.
54. Ohnishi, Y. Y.; Matsunaga, T.; Nakao, Y.; Sato, H.; Sakaki, S.,

Ruthenium(II)-catalyzed hydrogenation of carbon dioxide to formic acid.

theoretical study of real catalyst, ligand effects, and solvation effects. *Journal of the American Chemical Society* **2005**, 127, 4021-4032.

55. Koinuma, H.; Kawakami, F.; Kato, H.; Hirai, H., Hydrosilylation of Carbon-Dioxide Catalyzed by Ruthenium Complexes. *Journal of the Chemical Society-Chemical Communications* **1981**, 213-214.

56. Sussfink, G.; Reiner, J., Anionic Ruthenium Clusters as Catalysts in the Hydrosilylation of Carbon-Dioxide. *Journal of Organometallic Chemistry* **1981**, 221, C36-C38.

57. Eisenschmid, T. C.; Eisenberg, R., The Iridium Complex Catalyzed Reduction of Carbon-Dioxide to Methoxide by Alkylsilanes. *Organometallics* **1989**, 8, 1822-1824.

58. Jansen, A.; Gorls, H.; Pitter, S., trans-[Ru^{II}Cl(MeCN)₅][Ru^{III}Cl₄(MeCN)₂]
: A reactive intermediate in the homogeneous catalyzed hydrosilylation of carbon dioxide. *Organometallics* 2000, 19, (2), 135-138.

59. Jansen, A.; Pitter, S., Homogeneously catalysed reduction of carbon dioxide with silanes: a study on solvent and ligand effects and catalyst recycling. *Journal of Molecular Catalysis a-Chemical* **2004**, 217, 41-45.
60. Matsuo, T.; Kawaguchi, H., From carbon dioxide to methane: Homogeneous reduction of carbon dioxide with hydrosilanes catalyzed by zirconium-borane complexes. *Journal of the American Chemical Society* **2006**, 128, 12362-12363.
61. Deglmann, P.; Ember, E.; Hofmann, P.; Pitter, S.; Walter, O., Experimental and theoretical investigations on the catalytic hydrosilylation of carbon dioxide with ruthenium nitrile complexes. *Chemistry-a European Journal* **2007**, 13, 2864-2879.
62. Riduan, S. N.; Zhang, Y. G.; Ying, J. Y., Conversion of Carbon Dioxide into Methanol with Silanes over N-Heterocyclic Carbene Catalysts. *Angewandte Chemie-International Edition* **2009**, 48, 3322-3325.
63. Berkefeld, A.; Piers, W. E.; Parvez, M., Tandem Frustrated Lewis Pair/Tris(pentafluorophenyl)borane-Catalyzed Deoxygenative Hydrosilylation of

- Carbon Dioxide. *Journal of the American Chemical Society* **2010**, 132, 10660-10661.
64. Fang Huang, G. L., Lili Zhao, Haixia Li, Zhi-Xiang Wang, The Catalytic Role of N-Heterocyclic Carbene in a Metal-Free Conversion of Carbon Dioxide into Methanol: A Computational Mechanism. *Journal of the American Chemical Society* **2010**, 132, 12388.
65. Huang, F.; Lu, G.; Zhao, L.; Li, H.; Wang, Z. X., The catalytic role of N-heterocyclic carbene in a metal-free conversion of carbon dioxide into methanol: a computational mechanism study. *Journal of the American Chemical Society* **2010**, 132, 12388-12396
66. Hahn, C., Enhancing Electrophilic Alkene Activation by Increasing the Positive Net Charge in Transition-Metal Complexes and Application in Homogeneous Catalysis. *Chemistry – A European Journal* **2004**, 10, 5888-5899.
67. Sen, A., Organometallic Chemistry of Electrophilic Transition and Lanthanide Metal-Ions - the Dominant Pathways for Reactions Involving C=C, C-C, and

C-H Bonds. *Accounts of Chemical Research* **1988**, 21, 421-428.

68. Landis, C. R.; Halpern, J., Cationic rhodium hydrogenation catalysts containing chelating diphosphine ligands: effect of chelate ring size. *Journal of Organometallic Chemistry* **1983**, 250, 485-490
69. Crabtree, R., Iridium Compounds in Catalysis. *Accounts of Chemical Research* **1979**, 12, 331-338.
70. Hansen, S. M.; Volland, M. A. O.; Rominger, F.; Eisentrager, F.; Hofmann, P., A new class of ruthenium carbene complexes: Synthesis and structures of highly efficient catalysts for olefin metathesis. *Angewandte Chemie-International Edition* **1999**, 38, 1273-1276.
71. Taube, R.; Sylvester, G., In Applied Homogeneous Catalysis with Organometallic Compounds, Cornils, B.; Hermann, W. A., Eds. Wiley-VCH, Weinheim, 2000, p.298.
72. Johnson, L. K.; Killian, C. M.; Brookhart, M., New Pd(II)-Based and

Ni(II)-Based Catalysts for Polymerization of Ethylene and Alpha-Olefins.

Journal of the American Chemical Society **1995**, 117, 6414-6415.

73. Tempel, D. J.; Johnson, L. K.; Huff, R. L.; White, P. S.; Brookhart, M.,

Mechanistic studies of Pd(II)-alpha-diimine-catalyzed olefin polymerizations.

Journal of the American Chemical Society **2000**, 122, 6686-6700.

74. Ittel, S. D.; Johnson, L. K.; Brookhart, M., Late-metal catalysts for ethylene

homo- and copolymerization. *Chemical Reviews* **2000**, 100, 1169-1203.

75. Jiang, Z.; Sen, A., Tailored cationic palladium(II) compounds as catalysts for

highly selective linear dimerization of styrene and linear polymerization of

p-divinylbenzene. *Journal of the American Chemical Society* **1990**, 112,

9655-9657

76. Sen, A., Organometallic Chemistry of Electrophilic Transition and Lanthanide

Metal-Ions - the Dominant Pathways for Reactions Involving C=C, C-C, and

C-H Bonds. *Accounts of Chemical Research* **1988**, 21, 421-428.

77. Zassinovich, G.; Mestroni, G.; Gladiali, S., Asymmetric Hydrogen Transfer-Reactions Promoted by Homogeneous Transition-Metal Catalysts. *Chemical Reviews* **1992**, 92, 1051-1069.
78. Noyori, R.; Hashiguchi, S., Asymmetric transfer hydrogenation catalyzed by chiral ruthenium complexes. *Accounts of Chemical Research* **1997**, 30, 97-102.
79. Backvall, J. E., Transition metal hydrides as active intermediates in hydrogen transfer reactions. *Journal of Organometallic Chemistry* **2002**, 652, 105-111.
80. Tang, W. J.; Zhang, X. M., New chiral phosphorus ligands for enantioselective hydrogenation. *Chemical Reviews* **2003**, 103, 3029-3069.
81. Dani, P.; Karlen, T.; Gossage, R. A.; Gladiali, S.; van Koten, C., Hydrogen-transfer catalysis with pincer-aryl ruthenium(II) complexes. *Angewandte Chemie-International Edition* **2000**, 39, 743-746.
82. Amoroso, D.; Jabri, A.; Yap, G. P. A.; Gusev, D. G.; dos Santos, E. N.; Fogg, D. E., The first Ru(η^3 -PCP) complexes of the electron-rich pincer ligand

- 1,3-bis((dicyclohexylphosphino)methyl)benzene: Structure and mechanism in transfer hydrogenation catalysis. *Organometallics* **2004**, 23, 4047-4054.
83. Medici, S.; Gagliardo, M.; Chase, P. A.; Williams, S. B.; Gladiali, S.; Lutz, M.; Speck, A. L.; van Klink, G. P. M.; van Koten, G., Novel P-Stereogenic PCP Pincer-Aryl Ruthenium(II) Complexes and Their Use in the Asymmetric Hydrogen Transfer Reaction of Acetophenone *Helvetica Chimica Acta* **2005**, 88, 694
84. Gagliardo, M.; Chase, P. A.; Brouwer, S.; van Klink, G. P. M.; van Koten, G., Electronic effects in PCP-pincer Ru(II)-based hydrogen transfer catalysis. *Organometallics* **2007**, 26, 2219-2227.
85. Baratta, W.; Chelucci, G.; Gladiali, S.; Siega, K.; Toniutti, M.; Zanette, M.; Zangrando, E.; Rigo, P., Ruthenium(II) terdentate CNN complexes: Superlative catalysts for the hydrogen-transfer reduction of ketones by reversible insertion of a carbonyl group into the Ru-H bond. *Angewandte Chemie-International Edition* **2005**, 44, 6214-6219.

86. Baratta, W.; Siega, K.; Rigo, P., Fast and chemoselective transfer hydrogenation of aldehydes catalyzed by a terdentate CNN ruthenium complex [RuCl(CNN)(dppb)]. *Advanced Synthesis & Catalysis* **2007**, 349, 1633-1636.
87. Zeng, F. L.; Yu, Z. K., Exceptionally efficient unsymmetrical ruthenium(II) NNN complex catalysts bearing a pyridyl-based pyrazolyl-imidazolyl ligand for transfer hydrogenation of ketones. *Organometallics* **2008**, 27, 2898-2901.
88. Zeng, F. L.; Yu, Z. K., Construction of Highly Active Ruthenium(II) NNN Complex Catalysts Bearing a Pyridyl-Supported Pyrazolyl-Imidazolyl Ligand for Transfer Hydrogenation of Ketones. *Organometallics* **2009**, 28, 1855-1862.
89. Baratta, W.; Da Ros, P.; Del Zotto, A.; Sechi, A.; Zangrando, E.; Rigo, P., Cyclometalated ruthenium(II) complexes as highly active transfer hydrogenation catalysts. *Angewandte Chemie-International Edition* **2004**, 43, 3584-3588.
90. Sortais, J. B.; Ritleng, V.; Voelklin, A.; Holuigue, A.; Smail, H.; Barloy, L.; Sirlin, C.; Verzijl, G. K. M.; Boogers, J. A. F.; de Vries, A. H. M.; de Vries, J. G.; Pfeffer, M., Cycloruthenated primary and secondary amines as efficient catalyst

- precursors for asymmetric transfer hydrogenation. *Organic Letters* **2005**, *7*, 1247-1250.
91. Sortais, J. B.; Barloy, L.; Sirlin, C.; de Vries, A. H. M.; de Vries, J. G.; Pfeffer, M., Cycloruthenated compounds as efficient catalyst for asymmetric hydride transfer reaction. *Pure and Applied Chemistry* **2006**, *78*, 457-462.
92. Baratta, W.; Herdtweck, E.; Siega, K.; Toniutti, M.; Rigo, P., 2-(Aminomethyl)pyridine-phosphine ruthenium(II) complexes: Novel highly active transfer hydrogenation catalysts. *Organometallics* **2005**, *24*, 1660-1669.
93. Laxmi, Y. R. S.; Backvall, J. E., Mechanistic studies on ruthenium-catalyzed hydrogen transfer reactions. *Chemical Communications* **2000**, 611-612.
94. Samec, J. S. M.; Backvall, J. E.; Andersson, P. G.; Brandt, P., Mechanistic aspects of transition metal-catalyzed hydrogen transfer reactions. *Chemical Society Reviews* **2006**, *35*, 237-248.
95. Sasson, Y.; Blum, J., Homogeneous Catalytic Transfer-Hydrogenation of

Dichlorotris(Triphenylphosphine)Ruthenium (II). *Tetrahedron Letters* **1971**, 12, 2167-2170.

96. Sasson, Y.; Blum, J.; Dunkelbl.E, $\text{RuCl}_2(\text{PPh}_3)_3$ - Catalyzed Transfer Hydrogenation of Cyclohexane-1,3-Diones. *Tetrahedron Letters* **1973**, 14, 3199-3202.

97. Sasson, Y.; Blum, J., Dichlorotris(Triphenylphosphine)Ruthenium-Catalyzed Hydrogen Transfer from Alcohols to Saturated and Alpha,Beta-Unsaturated Ketones. *Journal of Organic Chemistry* **1975**, 40, 1887-1896.

98. Wang, G. Z.; Backvall, J. E., Ruthenium-catalysed transfer hydrogenation of imines by propan-2-ol. *Journal of Chemical Society, Chemical Communications* **1992**, 980-982.

99. Chowdhury, R. L.; Backvall, J. E., Efficient Ruthenium-Catalyzed Transfer Hydrogenation of Ketones by Propan-2-ol. *Journal of the Chemical Society-Chemical Communications* **1991**, 1063-1064.

100. Aranyos, A.; Csjernyik, G.; Szabo, K. J.; Backvall, J. E., Evidence for a ruthenium dihydride species as the active catalyst in the RuCl₂(PPh₃)-catalyzed hydrogen transfer reaction in the presence of base. *Chemical Communications* **1999**, (4), 351-352.
101. Hashiguchi, S.; Fujii, A.; Takehara, J.; Ikariya, T.; Noyori, R., Asymmetric Transfer Hydrogenation of Aromatic Ketones Catalyzed by Chiral Ruthenium(II) Complexes. *Journal of the American Chemical Society* **1995**, 117, 7562-7563.
102. Haack, K. J.; Hashiguchi, S.; Fujii, A.; Ikariya, T.; Noyori, R., The catalyst precursor, catalyst, and intermediate in the Ru-II-promoted asymmetric hydrogen transfer between alcohols and ketones. *Angewandte Chemie-International Edition in English* **1997**, 36, 285-288.
103. Yamakawa, M.; Ito, H.; Noyori, R., The metal-ligand bifunctional catalysis: A theoretical study on the ruthenium(II)-catalyzed hydrogen transfer between alcohols and carbonyl compounds. *Journal of the American Chemical Society* **2000**, 122, 1466-1478.

104. Yi, C. S.; He, Z. J.; Guzei, I. A., Transfer hydrogenation of carbonyl compounds catalyzed by a ruthenium-acetamido complex: Evidence for a stepwise hydrogen transfer mechanism. *Organometallics* **2001**, 20, 3641-3643.
105. Blum, Y.; Czarkie, D.; Rahamim, Y.; Shvo, Y., (Cyclopentadienone)Ruthenium Carbonyl-Complexes - a New Class of Homogeneous Hydrogenation Catalysts. *Organometallics* **1985**, 4, 1459-1461.
106. Noyori, R.; Hashiguchi, S., Asymmetric transfer hydrogenation catalyzed by chiral ruthenium complexes. *Accounts of Chemical Research* **1997**, 30, 97-102.
107. Maytum, H. C.; Tavassoli, B.; Williams, J. M. J., Reduction of aldehydes and ketones by transfer hydrogenation with 1,4-butanediol. *Organic Letters* **2007**, 9, 4387-4389.
108. Maytum, H. C.; Francos, J.; Whatrup, D. J.; Williams, J. M. J., 1,4-Butanediol as a Reducing Agent in Transfer Hydrogenation Reactions. *Chemistry-an Asian Journal* **2010**, 5, 538-542.

109. Hamid, M. H. S. A.; Slatford, P. A.; Williams, J. M. J., Borrowing hydrogen in the activation of alcohols. *Advanced Synthesis & Catalysis* **2007**, 349, 1555-1575.
110. Guillena, G.; Ramon, D. J.; Yus, M., Alcohols as electrophiles in C-C bond-forming reactions: The hydrogen autotransfer process. *Angewandte Chemie-International Edition* **2007**, 46, 2358-2364.
111. Nixon, T. D.; Whittlesey, M. K.; Williams, J. M. J., Transition metal catalysed reactions of alcohols using borrowing hydrogen methodology. *Dalton Transactions* **2009**, 753-762.
112. Dobereiner, G. E.; Crabtree, R. H., Dehydrogenation as a Substrate-Activating Strategy in Homogeneous Transition-Metal Catalysis. *Chemical Reviews* **2010**, 110, 681-703.
113. Cami-Kobeci, G.; Williams, J. M. J., Substrate activation: Indirect beta-bromination of alcohols. *Synlett* **2003**, 124-126.

114. Cho, C. S.; Kim, B. T.; Kim, H. S.; Kim, T. J.; Shim, S. C., Ruthenium-catalyzed one-pot beta-alkylation of secondary alcohols with primary alcohols. *Organometallics* **2003**, *22*, 3608-3610.
115. Fujita, K.; Asai, C.; Yamaguchi, T.; Hanasaka, F.; Yamaguchi, R., Direct beta-alkylation of secondary alcohols with primary alcohols catalyzed by a Cp*Ir complex. *Organic Letters* **2005**, *7*, 4017-4019.
116. Martinez, R.; Ramon, D. J.; Yus, M., RuCl₂(DMSO)₄ catalyzes the beta-alkylation of secondary alcohols with primary alcohols through a hydrogen autotransfer process. *Tetrahedron* **2006**, *62*, 8982-8987.
117. Viciano, M.; Sanau, M.; Peris, E., Ruthenium Janus-head complexes with a triazolediylidene ligand. structural features and catalytic applications. *Organometallics* **2007**, *26*, 6050-6054.
118. Cheung, H. W.; Lee, T. Y.; Lui, H. Y.; Yeung, C. H.; Lau, C. P., Ruthenium-Catalyzed beta-Alkylation of Secondary Alcohols with Primary Alcohols. *Advanced Synthesis & Catalysis* **2008**, *350*, 2975-2983.

119. Gnanamgari, D.; Leung, C. H.; Schley, N. D.; Hilton, S. T.; Crabtree, R. H., Alcohol cross-coupling reactions catalyzed by Ru and Ir terpyridine complexes. *Organic & Biomolecular Chemistry* **2008**, 6, 4442-4445.
120. Gnanamgari, D.; Sauer, E. L. O.; Schley, N. D.; Butler, C.; Incarvito, C. D.; Crabtree, R. H., Iridium and Ruthenium Complexes with Chelating N-Heterocyclic Carbenes: Efficient Catalysts for Transfer Hydrogenation, beta-Alkylation of Alcohols, and N-Alkylation of Amines. *Organometallics* **2009**, 28, 321-325.
121. Ng, S. M.; Lau, C. P.; Fan, M. F.; Lin, Z. Y., Experimental and theoretical studies of highly fluxional $\text{TpRu}(\text{PPh}_3)_2\text{H}_2\text{SiR}_3$ complexes (Tp = hydridotris(pyrazolyl)borate). *Organometallics* **1999**, 18, (13), 2484-2490.
122. Sommer, L. H.; Frye, C. L.; Parker, G. A.; Michael, K. W., Stereochemistry of Asymmetric Silicon. I. Relative and Absolute Configurations of Optically Active α -Naphthylphenylmethylsilanes. *Journal of the American Chemical Society* **1964**, 86, 3271.

123. Chan, W. C.; Lau, C. P.; Chen, Y. Z.; Fang, Y. Q.; Ng, S. M.; Jia, G. C., Syntheses and characterization of hydrotris(1-pyrazolyl)borate dihydrogen complexes of ruthenium and their roles in catalytic hydrogenation reactions. *Organometallics* **1997**, 16, 34-44.
124. Lynch, B. J.; Fast, P. L.; Harris, M.; Truhlar, D. G., Adiabatic connection for kinetics. *Journal of Physical Chemistry A* **2000**, 104, 4811-4815.
125. Fukui, K., A Formulation of Reaction Coordinate. *Journal of Physical Chemistry* **1970**, 74, 4161-4163.
126. Fukui, K., The Path of Chemical-Reactions - the Irc Approach. *Accounts of Chemical Research* **1981**, 14, 363-368.
127. Hay, P. J.; Wadt, W. R., *Ab initio* effective core potentials for molecular calculations. Potentials for K to Au including the outermost core orbitals. *The Journal of Chemical Physics* **1995**, 82, 299.
128. Ehlers, A. W.; Bohme, M.; Dapprich, S.; Gobbi, A.; Hollwarth, A.; Jonas, V.;

- Kohler, K. F.; Stegmann, R.; Veldkamp, A.; Frenking, G., A Set of F-Polarization Functions for Pseudo-Potential Basis-Sets of the Transition-Metals Sc-Cu, Y-Ag and La-Au. *Chemical Physics Letters* **1993**, 208, 111-114.
129. Hollwarth, A.; Bohme, M.; Dapprich, S.; Ehlers, A. W.; Gobbi, A.; Jonas, V.; Kohler, K. F.; Stegmann, R.; Veldkamp, A.; Frenking, G., A Set of D-Polarization Functions for Pseudo-Potential Basis-Sets of the Main-Group Elements Al-Bi and F-Type Polarization Functions for Zn, Cd, Hg. *Chemical Physics Letters* **1993**, 208, 237-240.
130. Krishnan, R.; Binkley, J. S.; Seeger, R.; Pople, J. A., Self-Consistent Molecular-Orbital Methods .20. Basis Set for Correlated Wave-Functions. *Journal of Chemical Physics* **1980**, 72, 650-654.
131. Gordon, M. S., The Isomers of Silacyclopropane. *Chemical Physics Letters* **1980**, 76, 163-168.
132. Hariharapc; Pople, J. A., Influence of Polarization Functions on Molecular-Orbital Hydrogenation Energies. *Theoretica Chimica Acta* **1973**, 28,

213-222.

133. Binning, R. C.; Curtiss, L. A., Compact Contracted Basis-Sets for 3rd-Row Atoms - Ga-Kr. *Journal of Computational Chemistry* **1990**, 11, 1206-1216.
134. Frisch, M. J.; Trucks, G. W.; Schlegel, H. B.; Scuseria, G. E.; Robb, M. A.; Cheeseman, J. R.; Montgomery, J. A.; Vreven, Jr. T.; Kudin, K. N.; Burant, J. C.; Millam, J. M.; Iyengar, S. S.; Tomasi, J.; Barone, V.; Mennucci, B.; Cossi, M.; Scalmani, G.; Rega, N.; Petersson, G. A.; Nakatsuji, H.; Hada, M.; Ehara, M.; Toyota, K.; Fukuda, R.; Hasegawa, J.; Ishida, M.; Nakajima, T.; Honda, Y.; Kitao, O.; Nakai, H.; Klene, M.; Li, X.; Knox, J. E.; Hratchian, H. P.; Cross, J. B.; Adamo, C.; Jaramillo, J.; Gomperts, R.; Stratmann, R. E.; Yazyev, O.; Austin, A. J.; Cammi, R.; Pomelli, C.; Ochterski, J. W.; Ayala, P. Y.; Morokuma, K.; Voth, G. A.; Salvador, P.; Dannenberg, J. J.; Zakrzewski, V. G.; Dapprich, S.; Daniels, A. D.; Strain, M. C.; Farkas, O.; Malick, D. K.; Rabuck, A. D.; Raghavachari, K.; Foresman, J. B.; Ortiz, J. V.; Cui, Q.; Baboul, A. G.; Clifford, S.; Cioslowski, J.; Stefanov, B. B.; Liu, G.; Liashenko, A.; Piskorz, P.; Komaromi, I.; Martin, R. L.; Fox, D. J.; Keith, T.; Al-Laham, M. A.; Peng, C. Y.; Nanayakkara, A.; Challacombe, M.; Gill, P. M. W.; Johnson, B.; Chen, W.; M. Wong, W.; Gonzalez,

C.; Pople, J. A., Gaussian 03, revision B05; Gaussian, Inc.: Pittsburgh, PA, 2003.

135. Schubert, U., η^2 -Coordination of Si-H σ Bonds to Transition Metals. *Advances in Organometallic Chemistry* **1990**, 30, 151

136. Lin, Z. Y., Structural and bonding characteristics in transition metal-silane complexes. *Chemical Society Reviews* **2002**, 31, 239-245.

137. Chen, Y. Z.; Chan, W. C.; Lau, C. P.; Chu, H. S.; Lee, H. L.; Jia, G. C., Synthesis of alkyl- and aryl[hydrotris(pyrazolyl)borato]carbonylruthenium complexes by decarbonylation of alcohols. Synthesis of $\text{TpRuH}(\text{H}_2)(\text{PPh}_3)$ [Tp = hydrotris(pyrazolyl)borate], an observable intermediate in the decarbonylation reaction. *Organometallics* **1997**, 16, 1241-1246. We are in fact not sure of the exact structure of $\text{TpRuH}(\text{H}_2)(\text{PPh}_3)$; it might be analogous to those of $\text{TpRu}(\text{PPh}_3)(\eta^3\text{-HSiPh}_3\text{H})$, $\text{TpRu}(\text{PPh}_3)(\eta^3\text{-HSiPh}_2\text{MeH})$, and $\text{TpRu}(\text{PPh}_3)(\eta^3\text{-HSiPhMe}_2\text{H})$, containing a $[\eta^3\text{-H}_3]^-$ moiety instead of the hydride and $\eta^2\text{-H}_2$ ligand.

138. Vyboishchikov, S. F.; Nikonov, G. I., Unique $\{\text{H}(\text{SiR}_3)_2\}$, (H_2SiR_3) , $\text{H}(\text{HSiR}_3)$,

and $(\text{H}_2)\text{SiR}_3$ Ligand Sets Supported by the $\{\text{Fe}(\text{Cp})(\text{L})\}$ Platform ($\text{L}=\text{CO}, \text{PR}_3$)

Chemistry-a European Journal **2006**, 12, 8518-8533.

139. Leung, C. W.; Zheng, W. X.; Wang, D. X.; Ng, S. M.; Yeung, C. H.; Zhou, Z. Y.;

Lin, Z. Y.; Lau, C. P., Catalytic H/D exchange between organic compounds and

D_2O with $\text{TpRu}(\text{PPh}_3)(\text{CH}_3\text{CN})\text{H}$ (Tp = hydro(trispyrazolyl)borate). Reaction of

$\text{TpRu}(\text{PPh}_3)(\text{CH}_3\text{CN})\text{H}$ with water to form acetamido complex

$\text{TpRu}(\text{PPh}_3)(\text{H}_2\text{O})(\text{NHC}(\text{O})\text{CH}_3)$. *Organometallics* **2007**, 26, 1924-1933.

140. Fung, W. K.; Huang, X.; Man, M. L.; Ng, S. M.; Hung, M. Y.; Lin, Z. Y.; Lau, C.

P., Dihydrogen-bond-promoted catalysis: Catalytic hydration of nitriles with the

indenylruthenium hydride complex $(\eta^5\text{-C}_9\text{H}_7)\text{Ru}(\text{dppm})\text{H}$ (dppm =

bis(diphenylphosphino)methane). *Journal of the American Chemical Society*

2003, 125, 11539-11544.

141. Fan, M. F.; Jia, G. C.; Lin, Z. Y., Metal-silane interaction in the novel

pseudooctahedral silane complex $\text{cis-Mo}(\text{CO})(\text{PH}_3)_4(\text{H} \cdots \text{SiH}_3)$ and some related isomers: An ab initio study. *Journal of the*

American Chemical Society **1996**, 118, 9915-9921.

142. Fan, M. F.; Lin, Z. Y., Competing Metal- π -Acetylene and Metal- σ -(H-Si) Interactions in the Complex $\text{Ti}(\eta^5\text{-C}_5\text{H}_5)_2(\eta^2\text{-trans-RC} \equiv \text{CSiHR})$. *Organometallics* **1997**, 16, 494-496.
143. Fan, M. F.; Lin, Z. Y., Stability of the *trans*-Bis(H \cdots Si) Structure in the Complex $\text{RuH}_2(\text{PCy}_3)_2(\kappa\text{-}\eta^2\text{-H}\cdots\text{SiMe}_2\text{-}o\text{-C}_6\text{H}_4\text{-SiMe}_2\cdots\text{H})$, Studied by Density Functional Theory. *Organometallics* **1999**, 18, 286-289.
144. Hartwig, J. F.; Bhandari, S.; Rablen, P. R., Addition of Catecholborane to a Ruthenium-Alkyl - Evidence for Sigma-Bond Metathesis with a Low-Valent, Late Transition-Metal. *Journal of the American Chemical Society* **1994**, 116, 1839-1844.
145. Lee, J. C.; Peris, E.; Rheingold, A. L.; Crabtree, R. H., An Unusual Type of H \cdots H Interaction: Ir-H \cdots H-O and Ir-H \cdots H-N Hydrogen-Bonding and Its Involvement in Sigma-Bond Metathesis. *Journal of the American Chemical Society* **1994**, 116, 11014-11019.

146. Schlaf, M.; Morris, R. H., A Dihydrogen Complex, $[\text{Os}(\eta^2\text{-H}_2)(\text{CO})(\text{Qus})(\text{PPh}_3)_2]^+$, in Equilibrium with Its Coordinated Thiol Tautomer (Qus = Quinoline-8-Thiolate). *Journal of the Chemical Society-Chemical Communications* **1995**, 625-626.
147. Musaev, D. G.; Mebel, A. M.; Morokuma, K., An Ab-Initio Molecular-Orbital Study of the Mechanism of the Rhodium(I)-Catalyzed Olefin Hydroboration Reaction. *Journal of the American Chemical Society* **1994**, 116, 10693-10702.
148. Siegbahn, P. E. M.; Crabtree, R. H., Modeling the solvent sphere: Mechanism of the Shilov reaction. *Journal of the American Chemical Society* **1996**, 118, 4442-4450.
149. Hinderling, C.; Feichtinger, D.; Plattner, D. A.; Chen, P., A combined gas-phase, solution-phase, and computational study of C-H activation by cationic iridium(III) complexes. *Journal of the American Chemical Society* **1997**, 119, 10793-10804.
150. Milet, A.; Dedieu, A.; Kapteijn, G.; vanKoten, G., Sigma-bond metathesis reactions involving palladium(II) hydride and methyl complexes: A theoretical

- assessment. *Inorganic Chemistry* **1997**, 36, 3223-3231.
151. Yin, C. Q.; Xu, Z. T.; Yang, S. Y.; Ng, S. M.; Wong, K. Y.; Lin, Z. Y.; Lau, C. P.,
Promoting effect of water in ruthenium-catalyzed hydrogenation of carbon dioxide to formic acid. *Organometallics* **2001**, 20, (6), 1216-1222.
152. Ng, S. M.; Yin, C. Q.; Yeung, C. H.; Chan, T. C.; Lau, C. P.,
Ruthenium-catalyzed hydrogenation of carbon dioxide to formic acid in alcohols. *European Journal of Inorganic Chemistry* **2004**, (9), 1788-1793.
153. Sun, N. Y.; Simpson, S. J., [Tris(1-pyrazolyl)hydroborato]ruthenium chemistry: Preparation and reactions of $\{\text{Ru}(\eta^3\text{-HB}[1\text{-pyrazolyl}]_3)(\text{PPh}_3)(\text{CO})(\text{X})\}$ ($\text{X} = \text{H}, \text{Cl}$). The X-ray crystal structure of $\{\text{Ru}(\eta^3\text{-HB}[1\text{-pyrazolyl}]_3)(\text{PPh}_3)(\text{CO})(\text{PMe}_3)\}\text{PF}_6$. *Journal of Organometallic Chemistry* 1992, 434, 341-349.
154. Castarlenas, R.; Esteruelas, M. A.; Onate, E., Preparation, X-ray structure, and reactivity of an osmium-hydroxo complex stabilized by an N-heterocyclic carbene ligand: A base-free catalytic precursor for hydrogen transfer from

- 2-propanol to aldehydes. *Organometallics* **2008**, 27, 3240-3247.
155. Esteruelas, M. A.; Hernandez, Y. A.; Lopez, A. M.; Olivan, M.; Rubio, L.,
Reactions of a dihydride-osmium(IV) complex with aldehydes: Influence of the
substituent at the carbonyl group. *Organometallics* **2008**, 27, 799-802.
156. Zhao, J.; Hartwig, J. F., Acceptorless, neat, ruthenium-catalyzed dehydrogenative
cyclization of diols to lactones. *Organometallics* **2005**, 24, 2441-2446.
157. Portnoy, M.; Frolow, F.; Milstein, D., Methanol Reduces an Organopalladium(II)
Complex to a Palladium(I) Hydride - Crystallographic Characterization of a
Hydrido-Bridged Palladium Complex. *Organometallics* **1991**, 10, 3960-3962.
158. Dinger, M. B.; Mol, J. C., Degradation of the first-generation Grubbs metathesis
catalyst with primary alcohols, water, and oxygen. Formation and catalytic
activity of ruthenium(II) monocarbonyl species. *Organometallics* **2003**, 22,
1089-1095.
159. Murahashi, S. I.; Naota, T.; Ito, K.; Maeda, Y.; Taki, H., Ruthenium-Catalyzed

Oxidative Transformation of Alcohols and Aldehydes to Esters and Lactones.

Journal of Organic Chemistry **1987**, 52, 4319-4327.

160. Esteruelas, M. A.; Werner, H., 5-Coordinate and 6-Coordinate Hydrido(Carbonyl)-Ruthenium(II) and Osmium(II) Complexes Containing Triisopropylphosphine as Ligand. *Journal of Organometallic Chemistry* **1986**, 303, 221-231.

161. Gu, L. Q.; Zhang, Y. G., Unexpected CO₂ Splitting Reactions To Form CO with N-Heterocyclic Carbenes as Organocatalysts and Aromatic Aldehydes as Oxygen Acceptors. *Journal of the American Chemical Society* **2010**, 132, 914-915.

162. Itagaki, H.; Shinoda, S.; Saito, Y., Liquid-Phase Dehydrogenation of Methanol with Homogeneous Ruthenium Complex Catalysts. *Bulletin of the Chemical Society of Japan* **1988**, 61, 2291-2294.

163. Jung, C. W.; Garrou, P. E., Dehydrogenation of Alcohols and Hydrogenation of Aldehydes Using Homogeneous Ruthenium Catalysts. *Organometallics* **1982**, 1, 658-666.

164. Shinoda, S.; Itagaki, H.; Saito, Y., Dehydrogenation of Methanol in the Liquid-Phase with a Homogeneous Ruthenium Complex Catalyst. *Journal of the Chemical Society-Chemical Communications* **1985**, 860-861.
165. Halcrow, M. A.; Chaudret, B.; Trofimenko, S., Tris-Pyrazolyl-Borate Dihydrogen Complexes of Ruthenium. *Journal of the Chemical Society-Chemical Communications* **1993**, 465-467.
166. Ison, E. A.; Trivedi, E. R.; Corbin, R. A.; Abu-Omar, M. M., Mechanism for reduction catalysis by metal oxo: Hydrosilation of organic carbonyl groups catalyzed by a rhenium(V) oxo complex. *Journal of the American Chemical Society* **2005**, 127, 15374-15375.
167. Liu, G. B.; Zhao, H. Y.; Thiemann, T., Triphenylphosphine-catalyzed dehydrogenative coupling reaction of carboxylic acids with silanes - A convenient method for the preparation of silyl esters. *Advanced Synthesis & Catalysis* **2007**, 349, 807-811.
168. Wong, K. Y.; Lee, W. O.; Che, C. M.; Anson, F. C., Synthesis and

Electrocatalytic Properties of a Cis-Diaquo-Ruthenium(II) Complex with
6,6'-Dichloro-2,2'-Bipyridine. *Journal of Electroanalytical Chemistry* **1991**, 319,
207-216.